Aging Effects on the Relation between Liquefaction Resistance and Shear Wave Velocity in Sand Deposits

Roozbeh Safaeian Amoly

Submitted to the
Institute of Graduate Studies and Research
in partial fulfillment of the requirements for the degree of

Doctor of Philosophy
in
Civil Engineering

Eastern Mediterranean University
April 2016
Gazimagusa, North Cyprus

ABSTRACT

Although shear wave velocity as an index property can be measured in field at low cost without necessarily drilling boreholes, there are some concerns over its use, mainly because of the liquefaction being associated with medium to large shear strain in contrast to the infinitesimal shear strain involved in the propagation of the shear wave. In spite of such potential shortcoming, there has been a lot of work towards the use of shear wave velocity, attempting to establish some charts correlating the cyclic strength and shear wave velocity. Thus, if there is a link between small-strain shear-wave velocity and medium-to-large strain liquefaction, the use of the shear wave velocity will be justified as an effective tool to assess the liquefaction resistance of in-situ deposits of sandy soils, not only for uncemented soils of Holocene age, but also for cemented soils of Holocene and Pleistocene age. In view of this shortcoming, a newly introduced parameter “cyclic yield strain” is proposed to indicate that shear wave velocity can be used to differentiate between the cyclic resistance of fresh and aged sand deposits. This parameter is defined as the ratio of the cyclic stress ratio required to cause liquefaction in a specified number of cycles to the shear modulus at small strains which are determined by the velocity of shear wave propagation.

Large numbers of cyclic triaxial tests were performed on undisturbed and reconstituted samples of sand deposits obtained from areas of known liquefaction at the time of the 2011 Great East Japan Earthquake. In this test scheme, shear wave velocity was measured first in the laboratory, followed by the application of cyclic loads to determine the cyclic shear strength. The undisturbed samples were classified

into two groups, namely; old alluvial (or diluvial) deep deposits and near-surface shallow deposits which had apparently been disturbed by the liquefaction in the 2011 event. The data were plotted in terms of the cyclic stress ratio versus the shear wave velocity and a curve of equal cyclic yield strain was drawn through average points in the plot for the two groups of soils, that is, one for undisturbed and the other for liquefaction-disturbed soils. It was found that the cyclic yield strain was larger for the latter type of soils as compared to the undisturbed soils from the old aged deposits. Similar sets of laboratory tests were performed as well on several sand samples reconstituted with different relative densities. Similar plots for these reconstituted samples indicated the same average value of the cyclic yield strain as that of the liquefaction-disturbed soils.

In view of the fact that the larger the cyclic yield strain, the more ductile behavior the soils exhibit, and vice versa, it was concluded that the cyclic yield strain could be utilized as a yardstick parameter for taking into account the effect of aging or cementation of sand deposits. Accordingly, it is hypothesized that the cyclic yield strain will take larger values for ductile fresh sand deposits and smaller values for brittle aged sand deposits. It is suggested that two different curves pertaining to new and old sand deposits can be used to correlate the liquefaction resistance and the shear wave velocity in sites of natural deposits in order to consider the effect of aging or cementation.

Keywords: Aging, Cyclic yield strain, Liquefaction, Shear wave velocity.

ÖZ

Sismik aktivite olan bölgelerde sıvılaşma potansiyelinin tesbiti geoteknik mühendisleri için önemli bir konudur. Dolayısıyla kumlu zeminlerin çevrimsel kayma mukavemetlerinin tesbiti çok önemlidir. Yöntemlerden biri kayma dalga hızını arazide bazı pratik ve ucuz yöntemlerle sondaj kuyusu kazmadan da ölçmektir. Ancak bu yöntemlerin sıvılaşmanın kayma dalgasının yayılmasından kaynaklanan sonsuz küçük, orta ve büyük kayma gerilimleri ile ilişkili olmasından dolayı bazı dezavantajları vardır. Buna ragmen kayma dalgası hızının kullanılması yönünde, çevrimsel kayma mukavemeti ile kayma dalga hızını ilişkilendirmek amacıyla çok çalışma yapılmıştır. Böylece, kayma dalga hızı ve sıvılaşma arasında fiziksel bir ilişki bularak, kayma dalga hızının etkin bir araç olarak sadece Holocene döneme ait çimentolaşmamış kumlu zeminler değil, Holocene ve Pleistocene dönemlere ait çimentolaşmış kumların da sıvılaşma potansiyeli tesbitinde kullanılabileceği kanıtlanmaya çalışılmıştır. Bu amaç doğrultusunda "çevrimsel akma mukavemeti" adı altında yeni bir parametre önerilerek kayma dalga hızının genç ve yaşlı kum katmanların çevrimsel kayma mukavemetlerinin belirlenmesinde kullanılabileceği belirlenmiştir. Bu parametre sıvılaşmaya neden olan çevrimsel stresle kayma modülünün oranı olarak ifade edilir.

2011 Japon depremi esnasında sıvılaştığı bilinen kumlu zeminler üzerinde bir dizi çevrimsel üç eksenli deney yapılmıştır. Önce kayma dalga hızı ölçülmüş, sonra çevrimsel yükleme ile çevrimsel kayma mukavemeti elde edilmiştir. Örselenmemiş nümuneler eski alüvyonlu derin katmanlar ve yüzeye yakın önceden sıvılaştığı bilinen katmanlar olarak ikiye ayrılır. Elde edilen data çevrimsel kayma mukavemeti

ve kayma dalga hızı ilişkisi olarak çizilip, iki grup zemin için örselenmemiş ve sıvılaşarak örselenmiş, eşit çevrimsel akma gerilme noktalarından iki eğri çizilerek sunulmuştur. Çevrimsel akma gerilmesi örselenmiş zeminler için örselenmemiş katmanlara göre daha büyük olduğu gözlemlenmiştir. Bir dizi benzer deney tamamen örselenmiş durumdan yeniden oluşturulan nümuneler üzerinde de gerçekleştirilmiştir. Deney sonuçlarından elde edilen eğrilerin, sıvılaşarak örselenmiş nümunelerden elde edilen ortalama çevrimsel akma gerilme değerini verdiği gözlemlenmiştir. Çevrimsel akma gerilmesi arttıkça zeminin davranışı daha sünek olup, bu parametrenin kumlu zeminlerin yaşı ve çimentolanmasına bir ölçek olarak da kullanılabileceği sonucuna varılmıştır. Bu sonuçtan çevrimsel akma gerilmesinin sünek genç kum katmanlar için yüksek, kırılgan yaşlı katmanlar içinse düşük değerler olduğu varsayılabilir.

Anahtar kelimeler: Yaşlanma etkisi, çevrimsel akma gerilmesi, sıvılaşma mukavemeti, kayma dalga hızı.

ACKNOWLEDGMENT

Firstly, I would like to truly acknowledge God, the compassionate, the merciful, who never delays to help me and to instruct me in the right paths. Indeed, I am not able to really appreciate his doing everything for me in the past, present, and future, and also his placing a number of great people on the way of my life. Thus, I always feel that the hand of God intervenes in my life because of being among them. Although words fail me to express my gratitude to all of them, since I imagine them as gifts from God, the majority of these people who have had a profound impact on academic and social life are gratefully acknowledged as follows:

I wish to express my deep gratitude to my supervisor, Associate Professor Huriye Bilsel, for supporting and supervising me not only in the present dissertation but also in my whole PhD program. Without her support, this dissertation would not have been possible.

I would like to express my deep appreciation to Professor Kenji Ishihara for his excellent planning and management during 3 months when I was in Japan from first day to last day, and also for instructing and supervising me in all steps of laboratory tests and the present dissertation. Working with him is a unique experience not only throughout my career but also throughout my personal life.

Special thanks go to Professor Takaji Kokusho for allowing me to work in his laboratory in Chuo University, Tokyo.

I would like to gratefully thank the managers, Mr. Mitsuo Hayashi and Mr. Shinichi

Yamada, and the technicians, Mr. Mamoru Wakasugi and Mr. Takeshi Tanaka, in geotechnical laboratory of Kiso-jiban consultants Co. Ltd, Tokyo, for their help and experimentation advice.

I wish to express my deepest gratitude to my dear grandparents, Haj Aliosat Eshghi and Hajyeh Fatemeh Yousefi, for their invaluable love, kindness and impeccable manners towards me.

I would like to express my deepest appreciation to my parents, Kheyronnesa Eshghi and Mohammadyoosef Safaeian Amoly, for their invaluable love, full support, continuous encouragement, and patience towards me along my life.

Lastly, I am extremely grateful to my wife, Shokooh Shakeri Aski, for being my partner and best friend. Her encouragements and supports made me continue my study in PhD level. Also, I gratefully acknowledge my wife's parents for their support and encouragements.

TABLE OF CONTENTS

ABSTRACT iii

ÖZ…….. v

ACKNOWLEDGMENT vii

LIST OF TABLES xiii

LIST OF FIGURES xiv

LIST OF SYMBOLS xix

1 INTRODUCTION 1

1.1 Background Research 1

1.2 Aims and Scope 2

1.3 Outline of the Thesis 3

2 REVIEW OF PREVIOUS INVESTIGATIONS 5

2.1 Introduction 5

2.2 Effect of Aging on the Soil Liquefaction Resistance 5

2.3 Assessment of Soil Liquefaction Resistance versus Shear Wave Velocity 11

2.4 The Effect of Non-plastic Fines Content on the Liquefaction Potential 23

2.4.1 Field Studies 23

2.4.2 Laboratory Studies 25

2.5 Cyclic and Monotonic Behavior of Silty Sand 36

3 INTRODUCTION OF "CYCLIC REFERENCE STRAIN" AND "CYCLIC YIELD STRAIN" 45

3.1 Introduction 45

3.2 Relation between Cyclic Stress Ratio and Amplitude of Cyclic Strain 47

3.3 Factors Affecting the Ductility or Brittleness of Soils under Cyclic Loading . 51

3.4 Relationship between Cyclic Resistance and Shear Wave Velocity 52

4 FIELD INVESTIGATION AND RECOVERY OF UNDISTURBED SAMPLES 54
4.1 Introduction 54
4.2 Asahi Site 55
4.2.1 Geological Characteristics of Asahi Site 58
4.2.2 Correlation between Shear Wave Velocity and SPT N-value for Asahi Site 59
4.2.3 Recovery of Undisturbed Specimens 60
4.3 Kyakari Tailings Dam Site 65
5 MEASUREMENTS OF CYCLIC RESISTANCE AND SHEAR WAVE VELOCITY IN THE LABORATORY 69
5.1 Introduction 69
5.2 Sample Preparation and Required Equipment 70
5.2.1 Trimming of Undisturbed Frozen Soil Sample 70
5.2.2 Reconstituted Specimens 73
5.2.3 Setting-up the Specimen to Triaxial Cell 74
5.3 Cyclic Triaxial Test Apparatus and the Procedure of Test 75
5.3.1 Cyclic Triaxial Apparatus for Measuring Liquefaction Resistance 75
5.3.2 The Procedure of Cyclic Tiaxial Test for Measuring Liquefaction Resistance 79
5.4 The Procedure of the V_S and V_P Measurement 82
5.5 Results of Tests on the Undisturbed and Reconstituted Samples 84
5.5.1 Triaxial Liquefaction Curves 84
5.5.2 Deviator Axial Stress, Stress Path and Pore Water Pressure 96
5.5.3 V_S and V_P Measurements 98
5.5.4 Post-liquefaction Volume Change 99

6 RESULTS OF TESTS ON THE SAMPLES FROM ASAHI SITES, OHYA SITE, AND NAGOYA SAND 101
6.1 Test Results on Samples from Asahi Sites 101
6.2 Test Results on Samples from Ohya Site 103
6.3 Relation between the Cyclic Strength and Shear Wave Velocity for Undisturbed Samples 104
6.3.1 Plots of Cyclic Strength versus V_{S1} for Old Unliquefied Sands 104
6.3.2 Plots of Cyclic Strength versus V_{S1} for Fresh Fills or Liquefied Deposits 106
6.4 Cyclic Strength versus Shear Wave Velocity for Reconstituted Samples 108
6.4.1 Cyclic Strength versus V_{S1} for Reconstituted Samples from Asahi Sand 108
6.4.2 Cyclic Strength versus V_{S1} for Reconstituted Samples from Nagoya Sand 110
6.5 Summary of the R_L versus V_{S1} Relations for Undisturbed Samples from New Deposits and Reconstituted Samples 111
6.6 Discussion about the Cyclic Yield Strain as Related to the Liquefaction Resistance and Shear Wave Velocity 111
6.7 Discussions on the Relationship between Liquefaction Resistance and Shear Wave Velocity for Fresh and Old Deposits 114
7 CONCLUSION AND RECOMMENDATION 123
7.1 Conclusion 123
7.2 Recommendation 125
REFERENCES 126
APPENDICES 144
Appendix A: Axial and Deviator Stress, Stress Path and Pore Water Pressure of Undisturbed and Reconstituted Samples 145

Appendix B: V_S and V_P Measurements 193

Appendix C: Post-liquefaction Volume Change 223

LIST OF TABLES

Table 2.1: Some of the literature about the monotonic undrained behavior of sand–silt mixtures 40

Table 2.2: Some of the literature about the cyclic triaxial undrained behavior of sand–silt mixtures 43

Table 4.1: Asahi soil profiles with FC<10% and average depths<10m 60

Table 6.1: Undisturbed samples from Asahi 103

Table 6.2: Tailings dam at Ohya mine (Miyagi Prefecture) 104

Table 6.3: Reconstituted specimens from Asahi sand 109

Table 6.4: Reconstituted samples of Nagoya sand with different fines contents 110

LIST OF FIGURES

Figure 2.1: Field liquefaction resistance of old sand deposits (Arango et al, 2000).... 7

Figure 2.2: Recommended boundary curves for old sand deposits by Leon et al. (2006) 8

Figure 2.3: CRR-V_{S1} curves corrected for age for clean sand by Andrus et al. (2009) 10

Figure 2.4: Consecutive changes in liquefaction resistance envisaged chronologically by Ishihara et al. (2015) 11

Figure 2.5: Stress ratios versus normalized shear modulus by Tokimatsu and Uchida (1990) 12

Figure 2.6: Preliminary probabilistic V_{S1}-based liquefaction chart by Kayen et al. (2004) 14

Figure 2.7: Probabilistic V_{S1}-based liquefaction chart by Kayen et al. (2013)..... 15

Figure 2.8: Correlations between normalized shear-wave velocity and the CRR by Liu and Mitchell (2006) 16

Figure 2.9: Comparison between presheared and/or overconsolidated reconstituted specimens and intact specimens by Wang et al. (2006)..... 17

Figure 2.10: Comparison between the field-based correlations and the laboratory-based correlations by Baxter et al. (2008)..... 18

Figure 2.11: V_{S1}-basesd liquefaction curve for silica sand No. 8 by Zhou et al. (2010) 19

Figure 2.12: Comparison between various proposed V_{S1}-based liquefaction curves by Ahmadi and Paydar (2014) 20

Figure 2.13: Liquefiable, non – liquefiable, and suspected to liquefaction zones by

Ahmadi and Paydar (2014) 21

Figure 2.14: Proposed constant cyclic shear strain for NS category by Dobry et al. (2015) 22

Figure 2.15: Correlations between $(N_1)_{60}$-value and Stress ratios required to cause liquefaction with earthquake magnitude of 7.5 by Seed et al. (1985) 24

Figure 2.16: Liquefaction resistance change in various fines contents with identical relative density by Singh (1994) 27

Figure 2.17: Representative normalized stress-strain and stress paths curves of Lagunillas silty sand by Zlatovic and Ishihara (1997) 28

Figure 2.18: Position of steady-state line with various percentages of fines in sand Cubrinovski and Rees (2008) 29

Figure 2.19: Undrained triaxial tests on Neveda sand with 7% fines (a) stress paths (b) Principal stress difference by Yamamuro and Lade (1998) 30

Figure 2.20: Change in intergranular void ratio and relative density with liquefaction potential in various fines contents by Monkul and Yamamuro (2011) 31

Figure 2.21: Cyclic resistance ratios versus silt content with Monterey sand at constant void ratio by Polito (1999) 32

Figure 2.22: Interfine and intergranular contact indices by Thevanayagam (1998) .. 33

Figure 2.23: Equivalent granular state parameter by Baki et al. (2010) 35

Figure 2.24: Initial states different types of monotonic behavior by Rahman et al. (2014) 36

Figure 2.25: Initial conditions of the cyclic behavior by Rahman et al. (2014) 36

Figure 3.1: Implication of the yield strain in cyclic loading 49

Figure 3.2: Characteristic curves pertaining to ductile or brittle behaviour of soils .. 53

Figure 4.1: Location of two sites for undisturbed sampling 55

Figure 4.2: Location of undisturbed sampling at Asahi, Chiba 56

Figure 4.3: Soil profile at the site of sampling in Asahi (HG-S-1) 56

Figure 4.4: Soil profile at the site of sampling in Asahi (SN-S-1) 57

Figure 4.5: Soil profile at the site of sampling in Asahi (SN-S-2) 57

Figure 4.6: Sigle-tube sampler, Denison Sampler and Triple-tube sampler (International manual for the sampling of soft cohesive soils, Tokyo, 1981) 58

Figure 4.7: Correlation between V_{S1} and (N1)60 proposed by Andrus and Stokoe (2000) and the present study 59

Figure 4.8: Old map of Asahi site in 1770's 62

Figure 4.9: Current map of Asahi site 63

Figure 4.10: East-west cross section of Asahi sit 64

Figure 4.11: Plan view of the failed Kayakari tailings dam at Ohya mine 66

Figure 4.12: Cross section A-A' of the failed Kayakari tailings dam at Ohya mine . 66

Figure 4.13: Cross section of Kayakari tailings dam before the failure and after the earthquake 67

Figure 4.14: Soil profiles of B-2 and III-6 before the failure and after the earthquake 67

Figure 4.15: Soil profiles of B-1 and I-2 before the failure and after the earthquake. 68

Figure 5.1: Trimming of undisturbed frozen soil sample 71

Figure 5.2: Preparation of reconstituted samples 74

Figure 5.3: Setting-up the Specimen to Triaxial Cell 75

Figure 5.4: Hydraulic cyclic triaxial test apparatus used for reconstituted samples in The laboratory of Kiso-Jiban consultants Co. Ltd 76

Figure 5.5: Pneumatic cyclic triaxial test apparatus used for undisturbed samples in

the laboratory of Kiso-Jiban consultants Co. Ltd..... 77

Figure 5.6: Schematic diagrams of cyclic triaxial apparatus and V_S and VP measuring device..... 78

Figure 5.7: Grain size distributions of undisturbed specimens from Asahi site 81

Figure 5.8: The top cap and pedestal of triaxial cell..... 83

Figure 5.9: Compression and Shear Waves Generator 83

Figure 5.10: V_S and V_P measurement system 83

Figure 5.11: Triaxial liquefaction curves for No. 1, 9, 27 &29 [SN-S-2 (20.1m-20.8m)] by KJCC 85

Figure 5.12: Triaxial liquefaction curves for No. 1, 5, 9, 27 &29 [SN-S-2 (20.1m-20.8m)] by KJCC&CHEC 86

Figure 5.13: Triaxial liquefaction curves for No. 19 & 19-2 [SN-S-2 (13.0m-14.0m)] by KJCC&CHEC 87

Figure 5.14: Triaxial liquefaction curves for No. 24 [SN-S-1 (1.0m-2.0m)] by KJCC&CHEC 88

Figure 5.15: Triaxial liquefaction curves for No. 23 & 28 [SN-S-1 (24.0m-26.1m)] by KJCC&..... 89

Figure 5.16: Triaxial liquefaction curves for No. 3, 8 & 14 [HG-S-1 (2.0m-3.0m) & (4.0m-5.0m] by KJCC&CHEC 90

Figure 5.17: Triaxial liquefaction curves for No. 12 & 17 [HG-S-1 (18.0m-20.0m)] by KJCC&CHEC 91

Figure 5.18: Triaxial liquefaction curves for reconstituted samples from Asahi site 92

Figure 5.19: Triaxial liquefaction curves for Nagoya sand with nonplastic fines at relative density of 70%..... 95

Figure 5.20: Triaxial liquefaction curves for Nagoya sand with nonplastic fines at

relative density of 50%..... 95
Figure 5.21: Triaxial liquefaction curves for Nagoya sand with nonplastic fines and different relative densities..... 96
Figure 5.22: Pore water pressure, axial strain, deviator stress versus number of cycles 97
Figure 5.23: Shear wave velocity measurement in the laboratory..... 98
Figure 5.24: Compression wave velocity measurements in the laboratory 99
Figure 5.25: Post-liquefaction volume changes versus time..... 100
Figure 6.1: Relation between the cyclic resistance and shear wave velocity for old unliquefied deposits 107
Figure 6.2: Relation between the cyclic resistance and shear wave velocity for undisturbed samples from new fills and liquefied alluvium..... 107
Figure 6.3: Relation between the cyclic resistance and shear wave velocity..... 109

LIST OF SYMBOLS

γ_{cl}	Constant cyclic shear strain
ε_a	Single amplitude of axial strain
ε_{ay}	Cyclic yield strain
ρ	Unit bulk density of a soil
σ_d	Single amplitude of axial deviator stress
σ_v'	In-situ vertical effective overburden stress
σ_0'	Initial confining stress
CRR	Cyclic resistance ratio
CSR	Cyclic stress ratio
C_u	Coefficient of uniformity
D_{50}	Mean grain diameter
D_{50}-sand/d_{50}-silt	Mean grain diameter ratio between sand grains and fines
e	void ratio
$(e_c)_{eq}$	Equivalent intergranular contact void ratio
$(e_f)_{eq}$	Equivalent interfine contact void ratio
e_f	Interfine contact void ratio
e_s	Intergranular contact void ratio
e_{ss}^*	Equivalent granular void ratio at steady state line
e*	Equivalent granular void ratio
FC	Fines content
FC_{th}	A certain threshold fines content
g	Gravitational acceleration ($9.8 m/s^2$)

G_0	Initial shear modulus
G_{01}	Stress normalized intial shear modulus
K_{DR}	Aging correction factor or strength gain factor
M	Earthquake magnitude
MEVR	Measured to estimated shear-wave velocity ratio
Nc	Number of cycles
$(N_1)_{60}$	SPT energy-corrected and overburden stress-corrected blow count
P_a	Reference overburden stress (=100 kPa)
P_L	Liquefaction potential
q_{ss}	Deviatoric stress at steady state
R_L	Cyclic resistance ratio
S_{us}	Undrained shear strength
V_S	Small strain shear wave velocity
V_{S1}	Stress normalized shear wave velocity

Chapter 1

INTRODUCTION

1.1 Background Research

Practically the cyclic strength to liquefaction or the liquefaction resistance is expressed by the term "Cyclic Stress Ratio", CSR in field, or the term "Cyclic Resistance Ratio", CRR in laboratory. Simplified procedure originally developed by Seed and Idriss (1971) has established a sound basis for the existing empirical liquefaction charts estimating the CSR or the CRR versus the standard penetration test (SPT) blow count, the cone penetration test (CPT) tip resistance, and small-strain shear-wave velocity (V_S) which have recently been utilized. A restriction of these charts is that their field data were primarily obtained from uncemented soils dated back to only less than ten thousand years ago, namely, young Holocene sediments. Thus, the old aged sand deposits were not taken into account in these charts (Youd et al. 2001).

Noticeable increase in liquefaction resistance of sand deposits with geological age was first recognized in the late seventies by Youd and Hoose (1977) and Youd and Perkins (1978). In their investigation, according to field observation after earthquakes, the past few-hundred-year sediments are generally most likely to liquefy than older sediments which are belonged to Holocene epoch. As such, Pleistocene and particularly Pre-pleistocene are more resistant to liquefaction than young Holocene sediments. Based on their assessment, the liquefaction susceptibility

was qualitatively estimated in terms of age of deposit. In this view, the new age deposits (less than 500 years), Holocene sand sediments, Pleistocene sediments (between 10,000 and 1.8 million years) and Pre-pleistocene sediments were categorized as high-to-very high, moderate-to-high, very low-to-low, and very low for liquefaction susceptibility, respectively.

The studies quantitatively carried out concerning the aging effects on the CRR were conducted by Mori et al. (1978), Seed (1979), Kokusho et al. (1983), and Troncoso et al. (1988). Subsequently, these investigations have recently been carried out by Arango and Migues (1996), Lewis et al. (1999, 2004, and 2008), Hayati and Andrus (2008 and 2009), Heidari and Andrus (2010) and Ishihara et al. (2015), described further in Chapter 2.

Tokimatsu and Uchida (1990), Andrus and Stokoe (2000), Kayen et al. (2004 & 2013), Liu and Mitchell (2006), Wang et al. (2006), Baxter et al (2008), Zhou et al (2010), Ahmadi and Paydar (2014) and Dobry et al. (2015) have proposed V_S-based liquefaction charts to separate non-liquefaction and liquefaction occurrence based on field observations or laboratory results, described further in Chapter 2.

1.2 Aims and Scope

The scope of research presented in this dissertation is to introduce a new parameter termed “Cyclic Yield Strain” for providing a physical interpretation for showing that shear-wave velocity as an index property can be used to distinguish between the liquefaction resistance of unaged and aged sand deposits.

To achieve this aim, a large number of cyclic traixial tests along with laboratory and field V_S-measurements have been conducted on the undisturbed samples obtained

from Asahi sites and Ohya mine tailings dam, and the reconstituted samples from Asahi and Nagoya sites. Based on the test results, two curves are proposed by two different equal cyclic yield strains. One of them can be representative of new sand deposits, whereas the other curve can pertain to old sand deposits.

1.3 Outline of the Thesis

This dissertation consists of seven chapters described as follows:

Chapter 2 includes a review of literature on the effect of aging on liquefaction resistance, V_S-based liquefaction curves, the effect of nonplastic fines on liquefaction resistance, and the monotonic and cyclic behavior of silty sand.

Chapter 3 introduces a new parameter termed “Cyclic Yield Strain”. This parameter is defined as the ratio of liquefaction resistance to initial shear modulus in cyclic loading condition. It also is illustrated that the larger value of cyclic yield strain can indicate the ductile behavior of new sand deposits, whereas the smaller value of that can exhibit the brittle behavior of old sand deposits.

Chapter 4 includes field studies and recovery of undisturbed samples by means of particular samplers. Field studies include Asahi sites and Ohya mine tailings dam, both of which were affected by the 2011 Great East Japan Earthquake. The correlation between shear-wave velocity and SPT N-value is proposed for Asahi sites. The geological characteristics of Asahi sites are examined as well.

Presented in Chapter 5 are the results of cyclic resistance and shear-wave velocity measurements in the laboratory. Equipment and test procedures conducted are described in detail.

The two different curves are proposed in Chapter 6 from collected data. One of them is representative of new sand deposits based on the results of undisturbed samples extracted from liquefied depths of Asahi sites and Kayakari tailings dam, and the reconstituted samples from the soils of tested undisturbed samples from Asahi and Nagoya sites. The other curve pertains to old sand deposits based on the results of undisturbed samples extracted from nonliquified depths of Asahi sites and Kayakari tailings dam. Moreover, a comparison is drawn between the cyclic yield strain in the simple shear mode and the volumetric cyclic threshold shear strain proposed by Dobry et al. (1980), and a comparison between the V_S-based liquefaction curves and the other published curves is drawn in literature.

Finally, the conclusions and recommendations are summarized in Chapter 7.

Chapter 2

REVIEW OF PREVIOUS INVESTIGATIONS

2.1 Introduction

Section 2.2 of this chapter the studies conducted on sand deposits in order to examine the aging effects on the liquefaction resistance. The Section 2.3 reviews the correlations between the shear wave velocity and the CSR or the CRR proposed in the literature. Since pure sands have rarely been found in sand deposits and the existence of the fines in sandy soils has mainly impact on soil liquefaction and cyclic mobility, the Section 2.4 will be assigned to the effect of fines content on the liquefaction potential in terms of field and laboratory studies. Multiple studies are listed in the Section 2.5 in order to examine the monotonic and cyclic behavior of silty sand on the basis of various amounts of fines contents and confining pressures with different methods of specimen preparation.

2.2 Effect of Aging on the Soil Liquefaction Resistance

Mori et al. (1978) noted that the probability of increase in the cyclic resistance of aged sand deposits to liquefaction over that of freshly deposited specimens in laboratory is on the order of 100%.

Seed (1979) revealed outcomes from laboratory tests carried out on identical specimens (Monterey No. 0) subjected to sustained pressure for a limited period, from 0.1 to 100 days after sample preparation. These specimens under longer periods of sustained pressure indicated an increase in cyclic resistance to liquefaction of

about 25% over those under shorter periods. He also presented results of laboratory cyclic tiaxial tests carried out on undisturbed specimens of sand deposits with geological age about 10,000 years. The aged specimens showed about 75% increase in liquefaction resistance over freshly deposited specimens.

Kokusho et al. (1983) indicated that the cyclic strength of undisturbed Narita sand over that of freshly reconstituted laboratory samples reaches up to 80%.

Troncoso et al. (1988) reported about 100-250% increase in cyclic resistance of undisturbed sandy specimens, with 25% fines content and void ratio ranging from 0.80 to 0.92 in various ages of 1, 5, 30 years, as compared to freshly deposited specimen in laboratory. Those specimens were obtained from two tailings dams (No.1 & No.4) located at El Cobre in Chile, which were recovered by block sampling.

Arango and Migues (1996) further examined the significance of aging on the cyclic resistance to initial liquefaction in sand deposits. In their investigation, laboratory experiments were conducted on undisturbed and reconstituted samples obtained from Gillibrand Quarry site at Tapo Canyon (about 2 million years old). A procedure of freezing and thawing of undisturbed samples was utilized to minimize the level of sample disturbance. Cyclic strength of aged field of Tapo Canyon sand increased by a factor of 1.6-2.7 as compared to commonly used empirical chart (SPT-values versus CRR).

Lewis et al. (1999) investigated the cyclic strength of old deposits (85000 to 200000 years of age) of Charleston at South Carolina by means of field performance data. In

their study, the peak ground accelerations of meizoseismal area were assumed 0.5g and 0.3g in order to evaluate the occurred CSR. Then, the specific boundary curves proposed by Lewis et al. (1999) that showed that the cyclic resistance are 1.3-3 times greater than those suggested by Holocene aged, empirical chart.

Arango et al. (2000) displayed that age has a profound impact on the field cyclic resistance of sand deposits by taking into consideration outcomes of previous studies and data from Savannah River Site (SRS), South Carolina. Based on gathered all data, they proposed the correlation between age and the strength gain factor by means of an update on the relation suggested by Kramer and Arango (1998) which are consistent with the outcomes of previous investigations by Seed (1979), Arango and Migues (1996) and Lewis et al. (1999) considered as upper boundary, and by Skempton (1986) and Kulhawy and Mayne (1990) considered as lower boundary as shown in Figure 2.1.

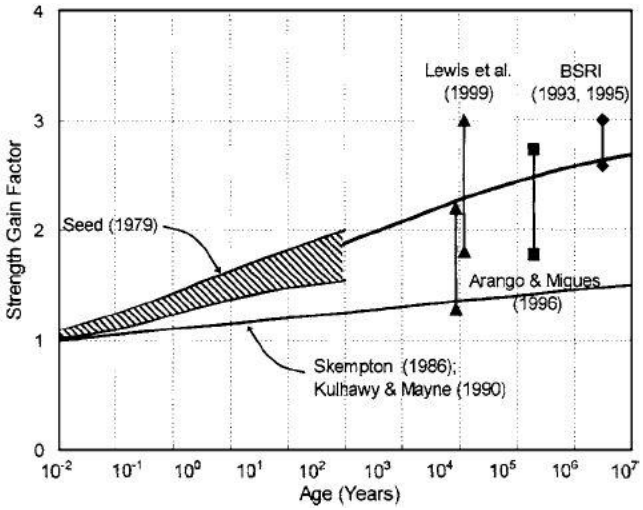

Figure 2.1: Field liquefaction resistance of old sand deposits (Arango et al, 2000)

Since commonly used empirical boundary curves are based on different in-situ soil indices, i.e. SPT, CPT and V_S, associated with young Holocene age deposits, Leon et

al. (2006) proposed new boundary curves which account for the aging effect on in-situ soil parameters of four sites, ranging in age from 200,000 to 450,000 years, in the South Carolina Coastal Plain (SCCP). In this research, current geotechnical data and correction factors illustrated in the literature were utilized by four-step procedure to recommend boundary curves for semi-empirical liquefaction charts. Figure 2.2 illustrates the V_{S1}-based liquefaction chart along with the existing boundary curves of Andrus and Stokoe (2000). They also estimated that minimum peak ground acceleration causing liquefaction in old sandy deposits of the SCCP tends to increase about 1.6 times greater than the case in which soil aging was not considered. Thus, an increase of about 60% in the cyclic shear strength to liquefaction for old sand deposits over current cyclic resistance of existing empirical chart was suggested.

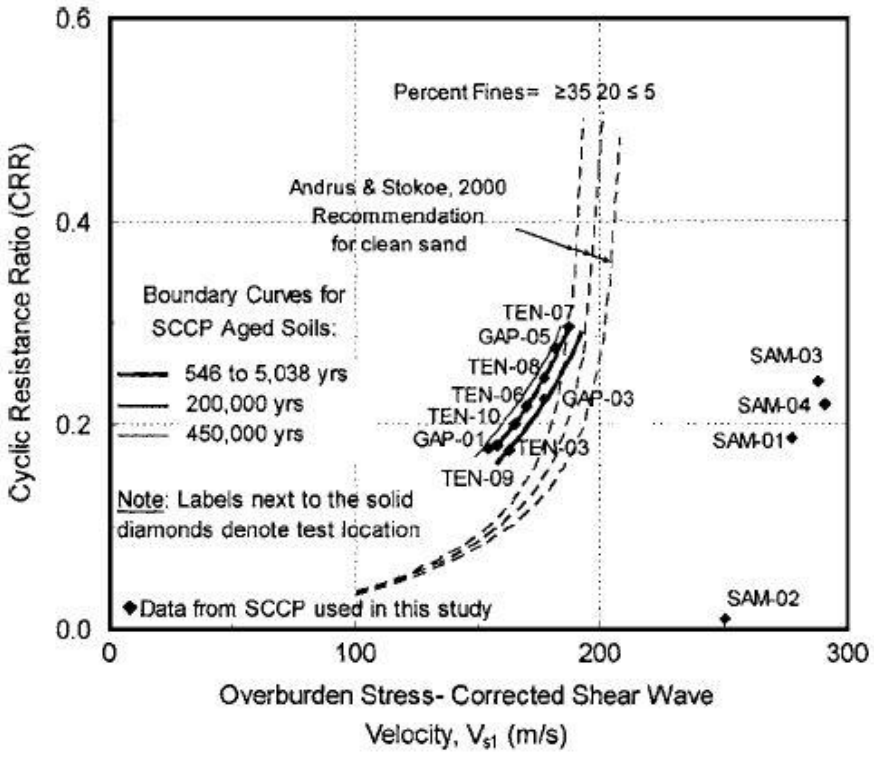

Figure 2.2: Recommended boundary curves for old sand deposits by Leon et al. (2006)

Hayati and Andrus (2009) updated the relationship of the factor correcting liquefaction resistance of sand deposits, K_{DR}, in terms of "aging", previously

proposed by Hayati et al. (2008), and the relationship between K_{DR} and MEVR, Measured to Estimated shear wave Velocity Ratio, previously proposed by Andrus et al. (2009). Outcomes of over 30 sites in 5 countries for 24 cases, along with those of cyclic laboratory experiments on undisturbed and reconstituted samples for 13 cases, were examined to improve those relationships. In this research, it is perceived that K_{DR} increases by a factor of 0.12 per log cycle of time with a reference age of 2 days for reconstituted samples, and by a factor of 0.13 per log cycle of time with a reference age of 23 years for field and laboratory experiment outcomes.

Andrus et al. (2009) proposed that measured to estimated shear-wave velocity ratio (MEVR) would be promising alternative to quantify age of sand deposits, defined as the ratio of measured V_S to V_S quantified from SPT or CPT measurements. 91 data pairs of penetration resistance -V_S were utilized to quantify shear wave velocity for this aim. Accordingly, a relationship was developed between K_{DR} and MEVR to yield CRR curves modified for aging effect. Those curves based on V_{S1}, CPT and SPT were produced for clean sands using MEVR to consider the effect of age as shown in Figure 2.3.

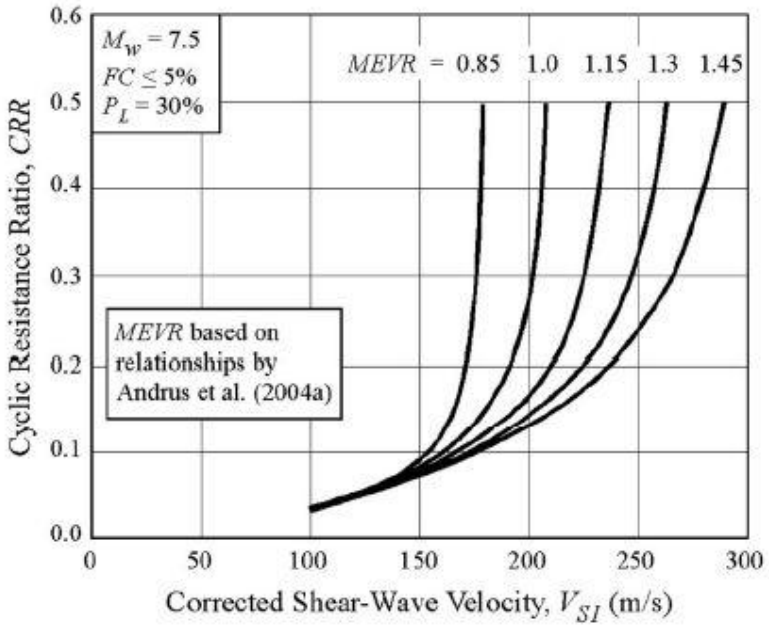

Figure 2.3: CRR-V_{S1} curves corrected for age for clean sand by Andrus et al. (2009)

In order to recognize the reasons why only one of the two tailings dams in Ohya mine failed, Ishihara et al. (2015) examined those embankments with regard to field and laboratory investigations conducted in 1979 and 2011. Kayakari dam underwent a breach during the 2011 earthquake. However, Takasega-mori dam did not experience dam failures. In this research, a scenario was envisaged consecutive changes in liquefaction resistance of slime in two dams during about 50 years, from 1960 to 2011, based on “aging”. Since those dams have experienced two earthquakes in this period, the scenario indicated a gradual increase in cyclic strength from the time of the filling to the time of Sanriku-minami earthquake (2003). The cyclic strength decreased dramatically when the 2003 earthquake occurred, whereas those dams then experienced a slight increase in cyclic strength between 2003 and 2011 as shown in Figure 2.4.

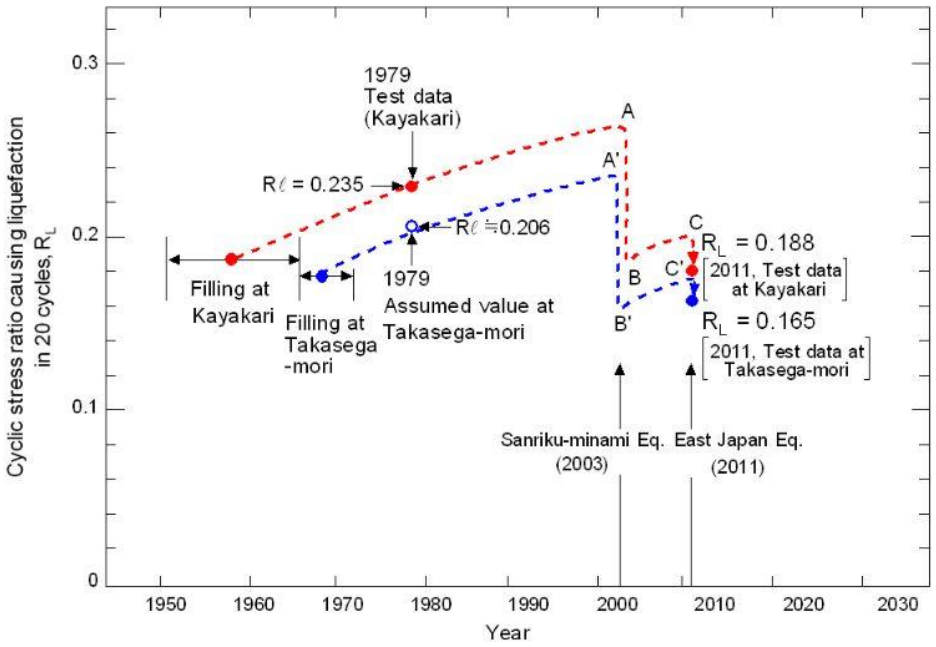

Figure 2.4: Consecutive changes in liquefaction resistance envisaged chronologically by Ishihara et al. (2015)

2.3 Assessment of Soil Liquefaction Resistance versus Shear Wave Velocity

Tokimatsu and Uchida (1990) proposed a simplified method estimating liquefaction resistance by means of shear wave velocity. To develop a relationship between shear wave velocity (elastic shear modulus) and liquefaction resistance, a multiple series of undrained cyclic triaxial tests was carried out on different types of sands with various confining pressures. Tokimatsu et al. (1986) showed a reasonable correlation between normalized shear modulus and liquefaction resistance for a given soil and confining pressure by which a correlation was developed between liquefaction resistance and shear wave velocity, using the well-known correlation between shear wave velocity and shear modulus.

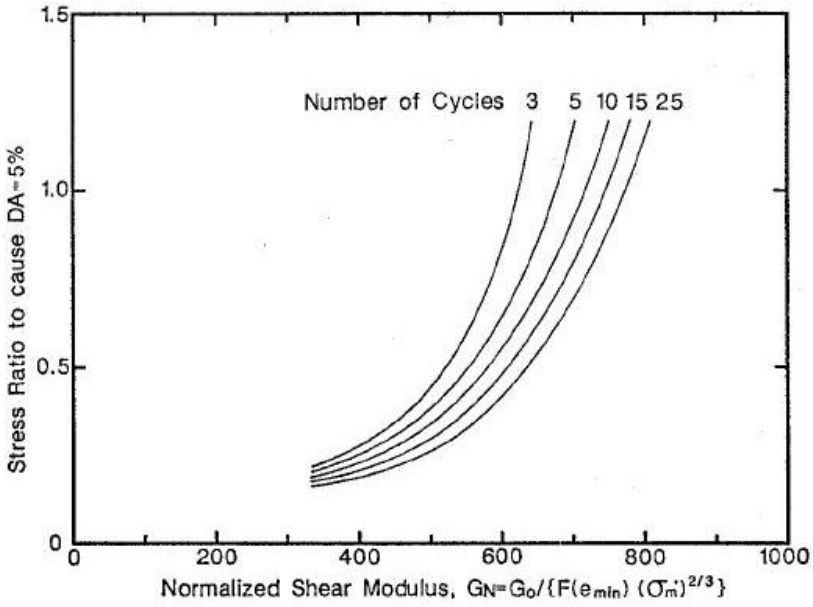

Figure 2.5: Stress ratios versus normalized shear modulus by Tokimatsu and Uchida (1990)

In this method, elastic shear modulus is determined by in-situ measurements of shear wave velocity by means of well-known equation ($G_0 = \rho V_s^2$). After assessing normalized shear modulus with respect to minimum void ratio of soil and effective overburden pressure, the stress ratio causing liquefaction is determined by the chart as shown in Figure 2.5. This chart presented representative correlation between cyclic strength ratios causing double amplitude of 5% and normalized shear modulus at various number of cycles in triaxial test conditions. Then the stress ratio is converted to field conditions by the equation suggested by Seed (1979).

Andrus and Stokoe (2000) presented a simplified procedure for assessing liquefaction resistance of sand deposits by means of measuring shear wave velocity. It conforms to a general framework of Seed-Idriss simplified procedure with respect to SPT N-values. In order to establish relations between CSR or CRR and V_{S1}, the data related to 225 case histories for 26 earthquakes and field performances for

almost 70 sites were utilized for a wide range of soil types prone to liquefaction. Consequently, CSR or CRR-V_{S1} Chart was developed in three particular curves based on the percentage of fines content, i.e. FC<5%, 5%<FC<35%, FC>35%, for earthquakes with magnitude of 7.5. These curves can reasonably separate non-liquefaction and liquefaction occurrences. With regard to the critical points, the chart and the collected data are associated with the average depths of site investigation less than 10m, uncemented deposits of Holocene age, and the depths of groundwater table between 0.5m and 6m. Therefore, a cautious engineering judgment is required when this procedure is employed to sites where conditions are not the same as the database.

Kayen et al. (2004) presented a probabilistic evaluation of the onset of seismic liquefaction based on global V_S-data collections compiled from all over the world, including United States, India, China, Taiwan, and Japan. Since V_S-CSR or CRR charts have suffered from a scarcity of revealed shear-wave velocity profiles in terms of average depths of soil profiles (more than 10 m) and cyclic stress ratios (more than 0.3), it is necessary to compile more V_S-data sets because of better estimation of probabilistic evaluation of cyclic resistance of soil to liquefaction. Accordingly, microtremor and CSS-SASW-or-MASW, continuous swept-sine wave (spectral or multichannel) analysis of surface wave, methods utilized to obtain new field performance data for the sites where the profiles of penetration resistance and a few velocity profiles were published in the literature. In this regard, almost 300 liquefaction-assessment sites have been investigated to obtain new shear-wave velocity profiles. In order to develop a correlation between worldwide shear-wave velocity data set and probability of the onset of the seismic liquefaction, high-order probabilistic designs concerning Bayesian updating interpretation were applied along

with structural reliability analysis of data. In this effort, a preliminary probabilistic V_S-based liquefaction chart was proposed with respect to different liquefaction potentials, P_L, i.e. 5%, 20%, 50%, 80%, and 95%, for about 60% of worldwide V_{S1} dataset, as shown in Figure 2.6.

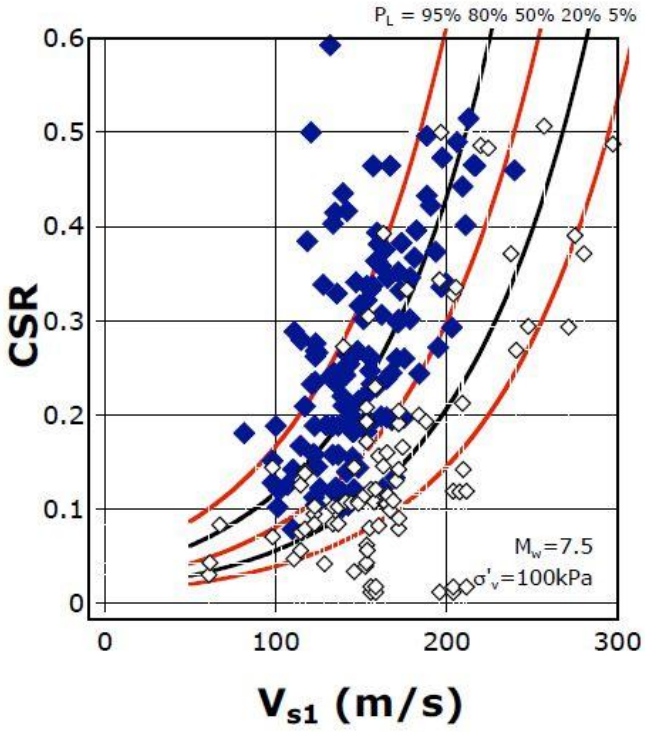

Figure 2.6: Preliminary probabilistic V_{S1}-based liquefaction chart by Kayen et al. (2004)

Moreover, Kayen et al. (2013) also revealed deterministic and probabilistic boundaries based on shear-wave velocity and evaluation of liquefaction susceptibility. In this procedure, an almost 10-year project has been implemented to collect new V_S-field data in order to improve correlations for seismically-induced liquefaction occurrence on the basis of shear wave velocity. To achieve this objective, in-situ V_S-measurements by means of non-invasive methods were performed for almost 300 new case histories of field liquefaction in United States, Greece, Taiwan, Japan, and China.

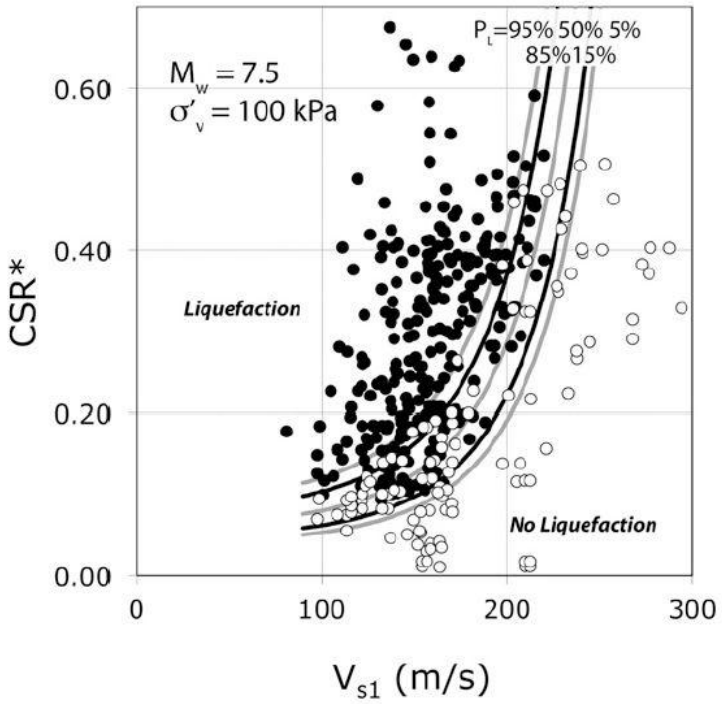

Figure 2.7: Probabilistic V_{S1}-based liquefaction chart by Kayen et al. (2013)

Most of the new case histories are associated with those formerly examined by penetration tests. These data were merged with formerly released case histories to make worldwide catalog of 400 case histories concerning field performance in order to evaluate shear wave velocity versus liquefaction resistance. To employ the V_S catalog probabilistically for engineering applications, two methods of Bayesian regression and structural reliability were applied. Thus, new global correlations have been presented relative to preceding study (Kayen et al. 2004), in which uncertainties of variables consisting mainly of the soil capacity (CRR) and the seismic demand (CSR) were estimated and considered in the analyses, causing reduced overall model error. Consequently, a set of probabilistic boundary curves was suggested with various liquefaction probabilities, P_L, of 5%, 15%, 50%, 85%, and 95%, among which the boundary curve with P_L=15% and FS=1.17 was suggested as the deterministic curve for separating non-liquefaction and liquefaction occurrence as shown in Figure 2.7.

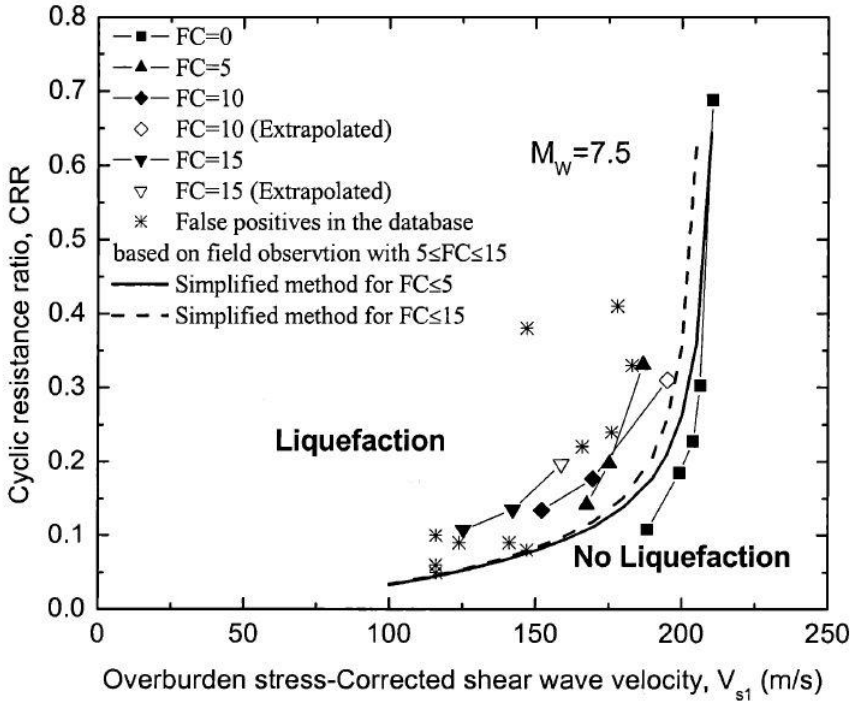

Figure 2.8: Correlations between normalized shear-wave velocity and the CRR by Liu and Mitchell (2006)

Liu and Mitchell (2006) were focused on the 46 false positives (no liquefaction detected when the V_{S1}-CSR plot proposed by Andrus and Stokoe (2000) indicated that it should have been liquefiable.) out of 156 cases classified as being in liquefaction zone. Approximately 67% of those are associated with sands containing less than 35% of fines content. In this investigation, the effect of non-plastic fines was examined on the shear wave velocity and the cyclic resistance of silty sands to liquefaction. In comparison with the semi-empirical curves in the simplified procedure for liquefaction assessment, the theoretical CRR-V_{S1} curves established for various fines contents of silty sand based on laboratory tests are altogether situated left and above those curves as shown in Figure 2.8. Thus, the outcomes proposed that the commonly used V_{S1}- based liquefaction chart may be overly conservative while applying sands with various non-plastic fines contents.

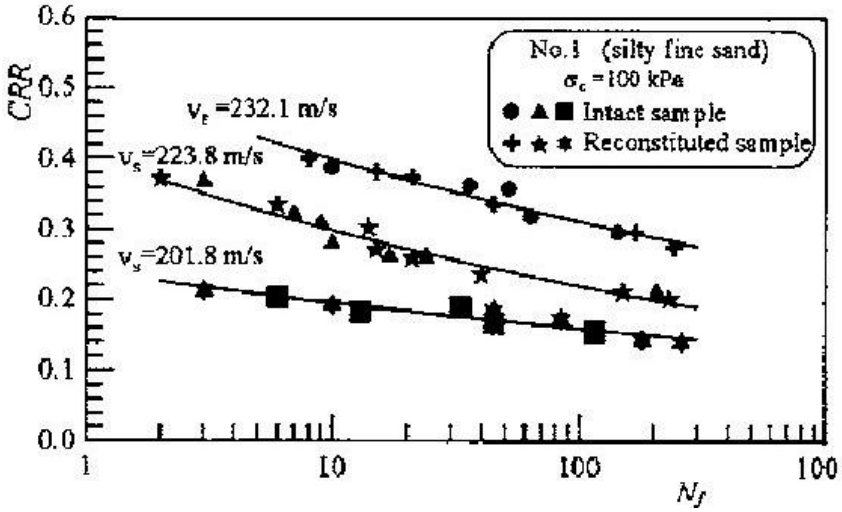

Figure 2.9: Comparison between presheared and/or overconsolidated reconstituted specimens and intact specimens by Wang et al. (2006)

Wang et al. (2006) studied the liquefaction resistance of undisturbed specimens in comparison with that of reconstituted ones if their shear wave velocities are similar to each other. They applied the combination of preshearing and overconsolidation for matching the shear-wave velocity of reconstituted specimens to that of undisturbed ones. They indicated that there was a good consistency between the liquefaction resistance of undisturbed and reconstituted specimens if the liquefaction triggering was defined as less than 6% double amplitude axial strain in cyclic loading as shown in Figure 2.9. Indeed, the outcomes can endorse the hypothesis that specimens reconstituted to in-situ value of shear wave velocity may yield the same liquefaction resistance as the undisturbed ones.

Baxter et al. (2008) developed a new V_{S1}- CRR correlation for two types of non-plastic silt from Providence, Rhode Island, by means of cyclic triaxial apparatus equipped with bender element. The specimens of natural silt were secured by block sampling, and were also provided by geotechnical borings. The results showed that the correlation is not dependent of the stress history and sample preparation. The

laboratory outcomes indicated that the liquefaction resistances of Providence silts are significantly overestimated by the existing field-based (V_{S1}-CRR) correlation. Figure 2.10 depicts the dependence of the V_{S1}-CRR correlation on soil type. Thus it is suggested that the silt-specific (V_{S1}-CRR) curves are necessary to develop from the outcomes of reconstituted specimens on which cyclic traxial tests are conducted, since V_{S1}-CRR correlations from laboratory results can be suitable alternatives to these established by field performance data.

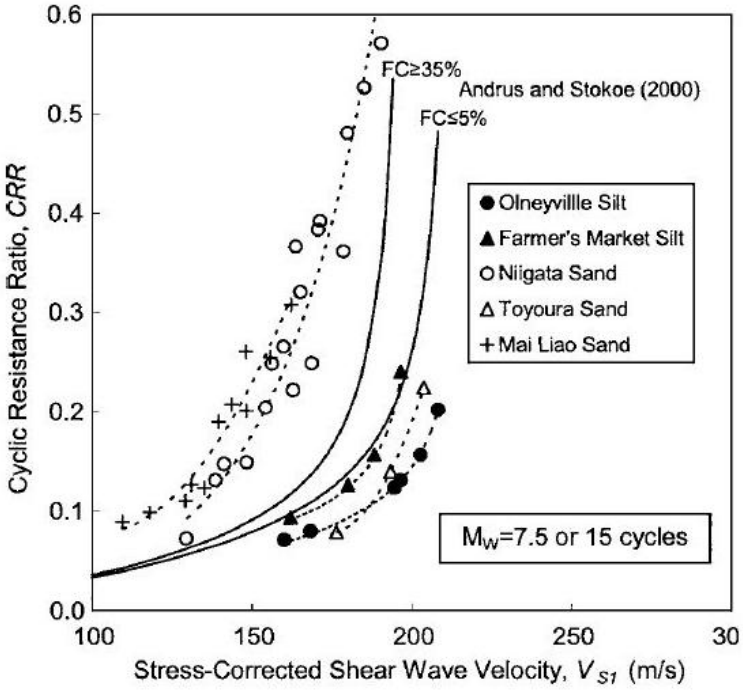

Figure 2.10: Comparison between the field-based correlations and the laboratory-based correlations by Baxter et al. (2008)

Zhou et al. (2010) addressed the reliability of soil-type correlation relating shear-wave velocity to liquefaction resistance in practices. Dynamic centrifuge model and cyclic laboratory tests were conducted on saturated silica sand No. 8 using bender element for V_S measurements. The outcomes indicated that the semi-empirical V_{S1}-CRR curve obtained from laboratory cyclic tests can accurately separate liquefaction and non-liquefaction zones from the (V_{S1}, CRR) data sets produced by dynamic

centrifuge tests; whereas, the liquefaction resistance of silica sand are significantly over- or under- estimated by the existing curves based on different silty sands as shown in Figure 2.11. These results also verified that V_{S1}-CRR correlation for liquefaction evaluation is strongly dependent on soil type, implies the necessary of establishing site-specific V_{S1}- CRR curves from laboratory cyclic tests for engineering practices.

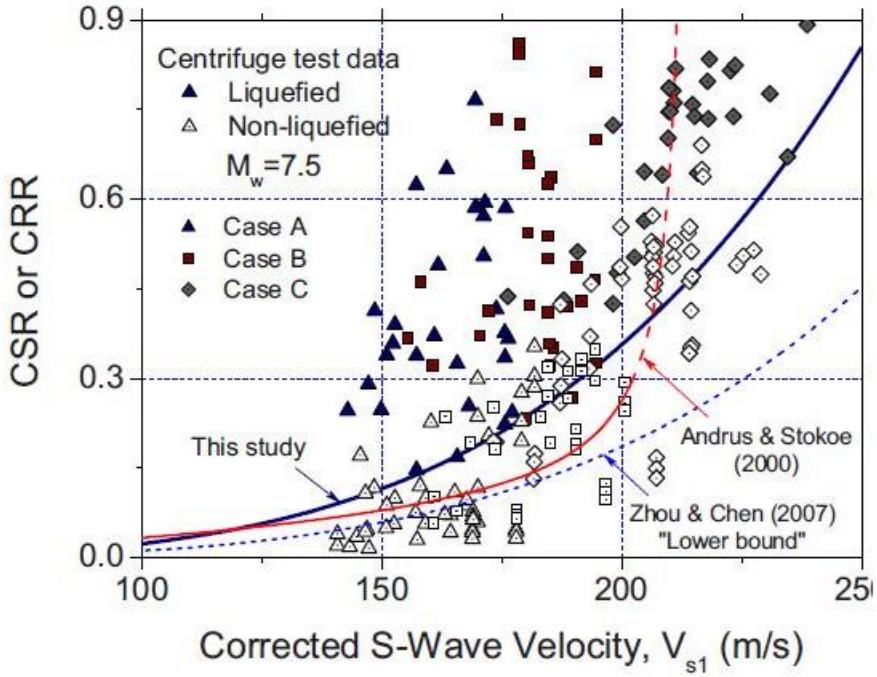

Figure 2.11: V_{S1}-basesd liquefaction curve for silica sand No. 8 by Zhou et al. (2010)

Ahmadi and Paydar (2014) investigated whether the V_{S1}-CRR correlation is unique, or soil – specific correlation is necessary to develop. In this research, a new semi-empirical method was suggested to develop soil-specific V_{S1}-CRR curve. In order to verify the suggested method, a number of laboratory liquefaction and bender element tests were conducted on two types of sand from Babolsar and Firozkoh. Figure 2.12 depicts the V_{S1}-CRR curves proposed by other researchers based on either field performance data or laboratory test, along with two curves of this research. It is indicated the correlations of various types of sand are not unique, and the boundary

curves developed by simplified procedure can only be used for an initial estimation of cyclic resistance to liquefaction. They also proposed the mapped area as shown in Figure 2.13, classified by liquefiable, non – liquefiable, and suspected to liquefaction zones, in order to estimate liquefaction potential microzonation by means of V_S measurements.

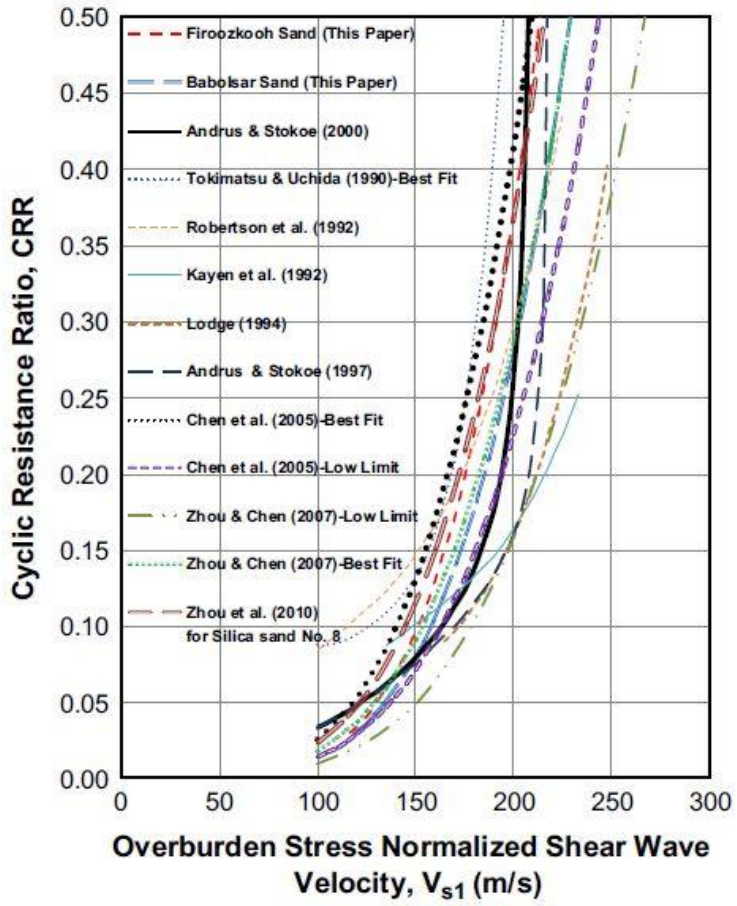

Figure 2.12: Comparison between various proposed V_{S1}-based liquefaction curves by Ahmadi and Paydar (2014)

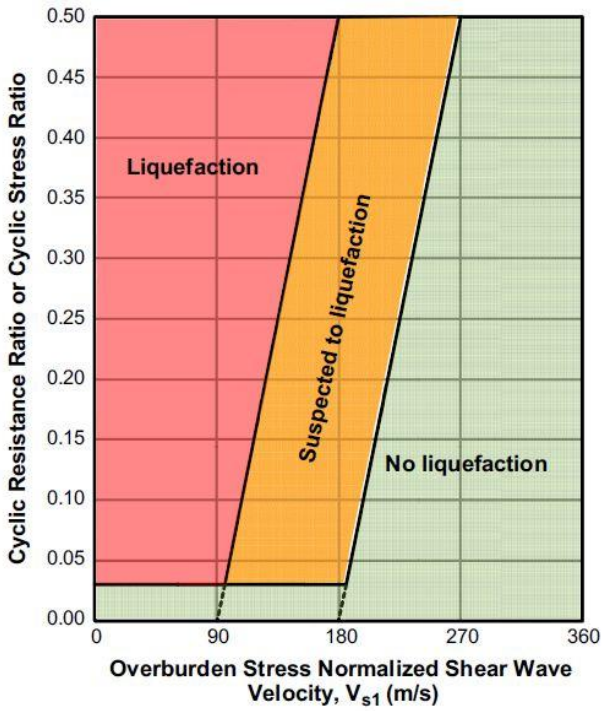

Figure 2.13: Liquefiable, non – liquefiable, and suspected to liquefaction zones by Ahmadi and Paydar (2014)

Dobry et al. (2015) pointed out the cyclic strain approach to examine the liquefaction susceptibility of clean and silty sands based on in-situ measurements of shear wave velocity by means of constant cyclic shear strain. In this study, 110 case histories were considered among 225 case histories endorsing Andrus-Stokoe shear-wave velocity-based chart for gravels, silts, and sands. Selected case histories consisting of clean sands and silty sands containing non-plastic fines were divided into three major categories, i.e. UF (Uncompacted Fill), CF (Compacted Fill), and NS (Natural Soils). The dumped fill, hydraulic fill, original fill, and uncompacted fill sub-categories were considered under UF category. CF category comprises the dunes, fluvial/alluvial, and original alluvial categories. Eventually, NS category were composed of sites belonged to Holocene age based on Andrus et al. (2003). The data of case histories were plotted with Andrus-Stokoe curve for clean sand, the curve of Kayen et al. (2013) with P_L=0.15, and two curves of different constant cyclic shear

strains, $\gamma_{cl} = 0.03\%$ and $\gamma_{cl} = 0.1 - 0.2\%$, in order to distinguish liquefiable and non-liquefiable points in V_S-based liquefaction chart based on field observations in various categories. In this regard, Andrus-Stokoe curve, along with the former line of constant cyclic strain recommended in this research may be a good indicator of liquefaction and non-liquefaction occurrence for UF category. Both Andrus and Stokoe (2000) and Kayen et al. (2013) curves can indicate the non-liquefaction occurrence in CF category. Eventually, since both such curves cannot predict reasonably well the liquefaction occurrence in NS category, the latter line of constant cyclic strain recommended in this research may be a good predictor of increased cyclic strength only in sites of the Imperial Valley as shown in Figure 2.14. In recent category, the 13 data points were recognized as false positive which means that they are not liquefiable soils, but are placed upper than separating curve of Andrus and Stokoe (2000) as liquefiable soils.

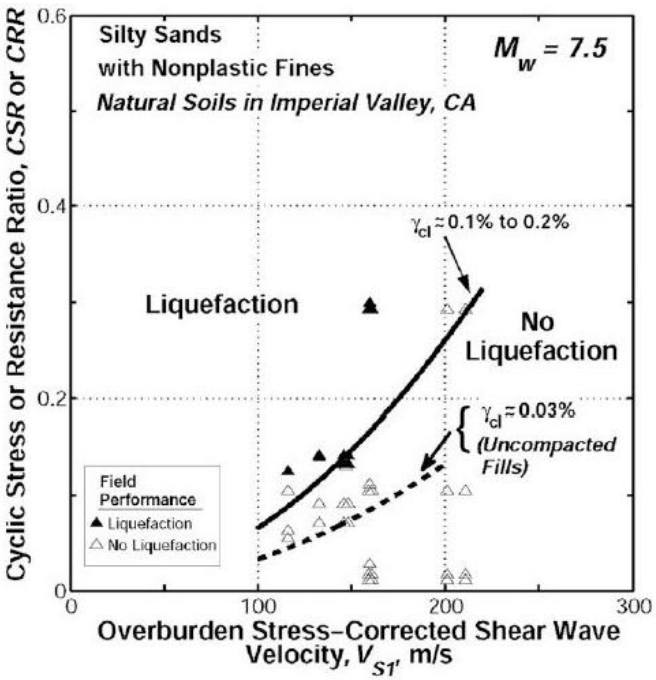

Figure 2.14: Proposed constant cyclic shear strain for NS category by Dobry et al. (2015)

Also, they believed that the increased cyclic strength of the Imperial Valley is due to preshaking of natural sand deposits of the sites in the high seismic activity zones, not due to geologic age.

2.4 The Effect of Non-plastic Fines Content on the Liquefaction Potential

2.4.1 Field Studies

Although some of the studies indicate that the liquefaction resistance is inversely proportional to the silt content of sand, some historical cases reported do not confirm this trend.

Okashi (1970) detected that the sands with fines content of 10% are less prone to liquefaction than clean sands in the famous Niigata earthquake in Japan. Fei (1991) observed that increasing fines content increases the liquefaction resistance of silty sands as observed in Tangshan earthquake in China. Moreover, on examination of 17 worldwide earthquakes, Tokimatso and Yoshimi (1983) realized that 50% of soil liquefaction occurred in sands with fines content less than 5%. They also found that the clean sands have less liquefaction resistance than sands with fines content more than 10 % at the same SPT $(N_1)_{60}$-value.

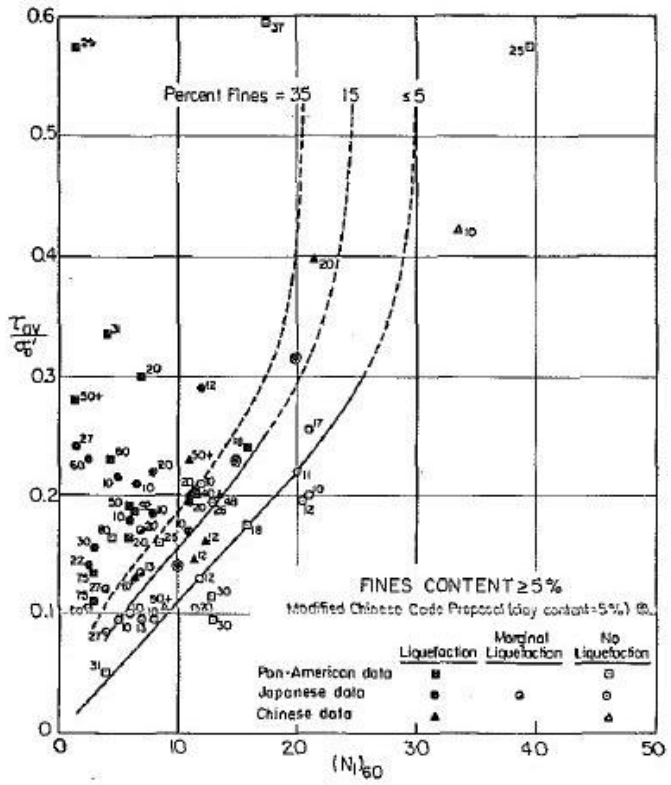

Figure 2.15: Correlations between $(N_1)_{60}$-value and Stress ratios required to cause liquefaction with earthquake magnitude of 7.5 by Seed et al. (1985)

Furthermore, Seed et al. (1985) proposed relationship between N_1-value and cyclic stress ratio leading to liquefaction for silty sands in M=7.5 earthquakes. In this regard, three boundary curves suggested with different fines contents (FC), FC < 5, 15% < FC < 35% and FC > 35%, indicate that cyclic stress ratio (CSR) causing liquefaction increases with increase in the percentage of fines content at a given N_1-value, $(N_1)_{60}$, as shown in Figure 2.15.

However, Garga and Mckay (1984) and Okusa et al. (1980) reported that some cases of liquefaction in the mine tailing dams containing fines (slimes) contents from 0 to 100% occurred in different earthquakes in Japan and Chile. Moreover, Troncoso and Verdugo (1985) realized that the mine tailing dams containing high percentage of fines (slimes) contents are more prone to liquefaction than the same dams containing sand and they are absolutely weak in earthquake-induced liquefaction.

2.4.2 Laboratory Studies

The dynamic behavior of silt-sand mixtures is not completely related to the percentage of fines content based on recent research on such soils. Consequently, different or even contradictory results can be observed in the literature. Thus there is need to consider other terms along with fines content or new approaches. Even though there are numerous studies about the effect of non-plastic fines content on the various silt-sand mixtures, it seems that they can personally be categorized in three major groups named as traditional, partially microstructural, and microstructural approaches by author.

All investigations have been implemented in "traditional approach", which are based on commonly used comparison bases, i.e. void ratio, relative density and steady state line [Kuerbis et al., 1988; Finn, 1991; Zaltovic and Ishihara, 1995 and 1997; Pradhan et al., 1995; Yamamuro and Lade, 1998; Yamamuro and Covert, 2001; Shapiro and Yamamuro, 2003; Yamamuro and Wood, 2004; Cubrinovski and Rees, 2008; Monkul and Yamamuro, 2011; and Monkul, 2012].

The second one is called "partially microstructural approach" which has partially been considered as the concept of microstructure in the silty-sand soils and defines a new comparison basis, i.e. limiting silt content and "soil special relative density" [Polito, 1999; Polito and Martin, 2001; and Polito et al., 2008].

The third approach is termed "microstructural approach" which has considerably been regarded for the conceptual framework of microstructure with new comparison bases, i.e. equivalent intergranular contact void ratio, interfine contact void ratio and equivalent steady state line [Thevayaganam, 2000; Thevayaganam and Martin, 2002;

Thevayaganam et al., 2002, Xenaki and Athanasopoulos , 2003; Rahman and Lo, 2007; Baki et al., 2010; and Rahman et al., 2013].

2.4.2.1 Traditional Approach

Kuerbis et al. (1988) considered the concept of sand skeleton as the rationale behind the specific behavior of the silty sands and proposed that silt merely plays the role of filler in the sand skeleton up to 20%.

Koester (1994) reported that there is a fluctuation of the cyclic resistance with increasing fines content in experimental results. In other words, the cyclic resistance of silt-sand mixtures decreases up to less than one-quarter of that of clean sand at silt content of 20%. Then beyond that percentage, the cyclic resistance of those increases up to one-third of that of clean sand at silt content of 60%.

Singh (1994) studied that the liquefaction resistant of silt-sand mixture decreases with increasing fines content up to 30% , beyond which increases with increasing fines content in the same void ratio or relative density as shown in Figure 2.16. It is shown that relative density and void ratio cannot be reliable criteria to account for the liquefaction potential of sandy silt sand and silty sands.

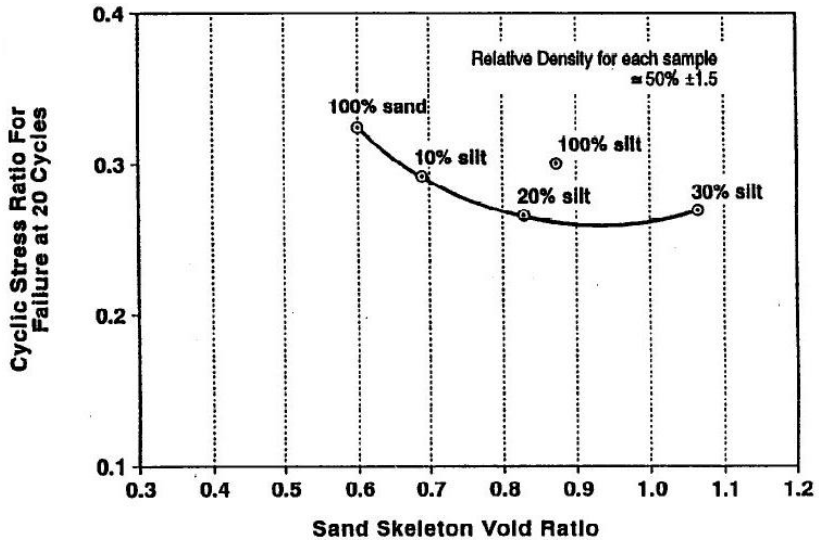

Figure 2.16: Liquefaction resistance change in various fines contents with identical relative density by Singh (1994)

Pardhan (1995) implemented laboratory experiments on silty sand to examine the effect of fines content on the liquefaction potential. It was found that presence of fines up to about 15% does not influence liquefaction potential significantly.

Zlatovic and Ishihara (1995) indicate that silt content affects strongly the peak, residual strength, and also the position of the steady state line or quasi-steady state line, though the slopes of those are practically independent of the presence of nonplastic fines in sands using various methods of sample preparations. Using moist placement method, for instance, the contractiveness of specimens increases with increasing silt content in Toyora sand up to the fines content of 30%, beyond which that of specimens decreases. However, the peak and residual strength decrease up to that specified fines content, beyond which those increase.

Zlatovic and Ishihara (1997) studied the behavior of loose silty sands and sandy silts in terms of the effects of soil fabric by means of monotonic triaxial tests. Specimens were prepared in the three distinctively methods to prepare very loose structure using

dry depositition, moist placement, and water sedimentation methods. In order to provide a reasonable interpretation of the soil behavior, the stress paths and stress-strain curves were normalized to the applied confining pressure. It was discovered that the effects of fabric on the undrained behavior are insignificant up to peak strength, beyond which the fabric, however, becomes a significant factor controlling the undrained response of such soils, including minimal and residual strength, as shown in Figure 2.17.

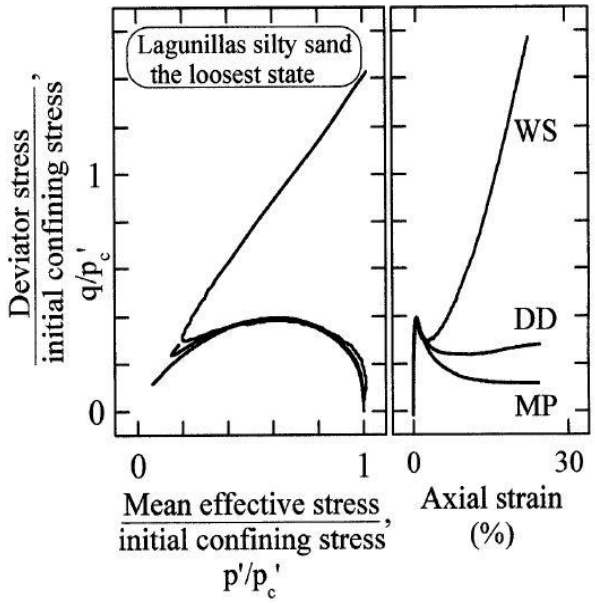

Figure 2.17: Representative normalized stress-strain and stress paths curves of Lagunillas silty sand by Zlatovic and Ishihara (1997)

Cubrinovski and Rees (2008) perceived two comparison bases, i.e. relative density and steady state line, in order to evaluate the effects of fines on sands. It is shown that the steady state line moves downwards in the e-$p^{'}$ (D_r -$p^{'}$) curve with increasing fines in clean sand base as shown in Figure 2.18. This implies that the flow potential of silty sand effectively increases due to exposing contractive behavior affiliated with strain softening. At a given relative density, the liquefaction resistance of sand with 30% fines is much less than that of the clean sand. If initial state relative to the

steady state line serve a basis for comparison, liquefaction resistance of such soils can increase with increase in silt content.

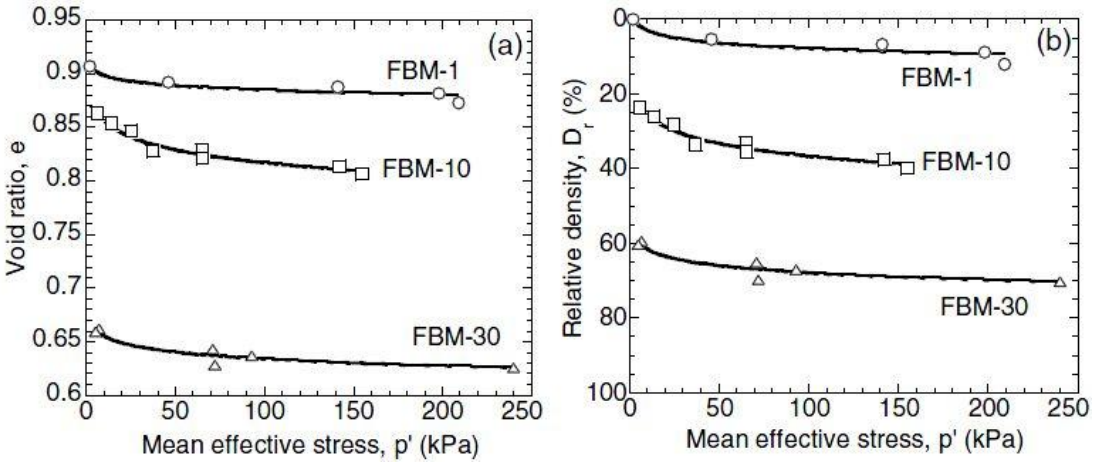

Figure 2.18: Position of steady-state line with various percentages of fines in sand Cubrinovski and Rees (2008)

Yamamuro and Lade (1998) studied the behavior of very loose Nevada sand with 7% fines at 30% relative density in terms of steady state line in drained as well as undrained compression tests using dry depositional method. In this study, steady state lines were obtained from these experiments at three different low relative densities of 12, 22 and 31%. A unique steady state line is not observed in this condition. Moreover, they have observed that specimens with greater density at lower pressures are more susceptible to statically liquefy than those with lower density at high pressures. Therefore, the void ratio cannot be the establishing parameter to identify the behavior of loose silty sands due to "reverse" behavior of such soils as shown in Figure 2.19, as opposed to the expected behavior of clean sands. Thus, volumetric compressibility was suggested to provide a reliable criterion for differentiating between non-liquefaction and liquefaction behavior.

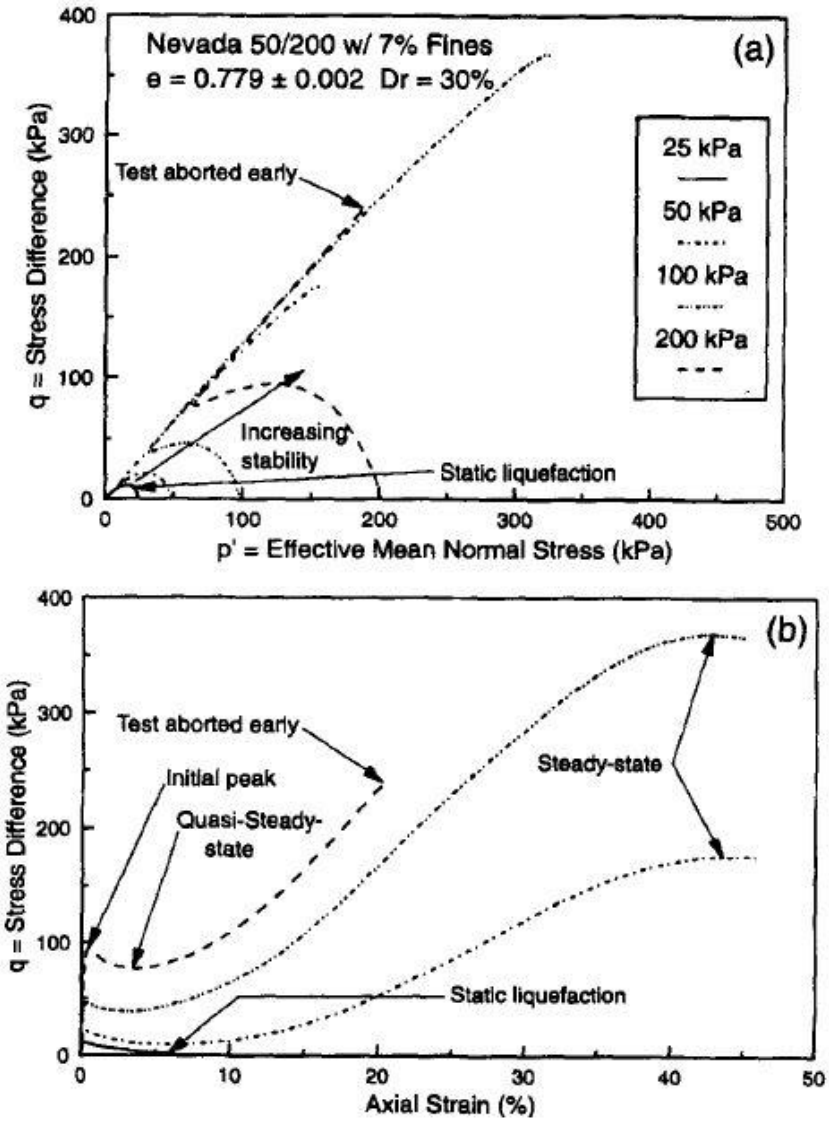

Figure 2.19: Undrained triaxial tests on Neveda sand with 7% fines (a) stress paths (b) Principal stress difference by Yamamuro and Lade (1998)

Yamamuro and Covert (2001) examined the behavior of loose Nevada sands with 40% silt content using undrained cyclic and monotonic triaxial tests. They showed that the outcomes are somewhat different from the behavior of sand with lower silt content. The more fines content can provide a more volumetrically contractive response throughout the whole strain-stress behavior. Monkul and Yamamuro (2011) found that the mean grain diameter ratio (D_{50}-sand/d_{50}-silt) between the sand grains and the fines grains plays significant role on the liquefaction potential. If it is adequately small, the liquefaction potential of sand increases gradually with increase

in fines content ranging from 0 to 20%; otherwise, the potential liquefaction of clean sand may actually be more than the potential liquefaction of silty sand. This study has also disclosed that current comparison criteria, i.e. void ratio, intergranular void ratio and relative densities, are not adequate to evaluate the effect of fines on the liquefaction potential of such soils as shown in Figure 2.20. It is suggested that the relative size of grains, along with content and plasticity, should also be regarded to characterize the effects of silt on the liquefaction potential of sands in practical applications.

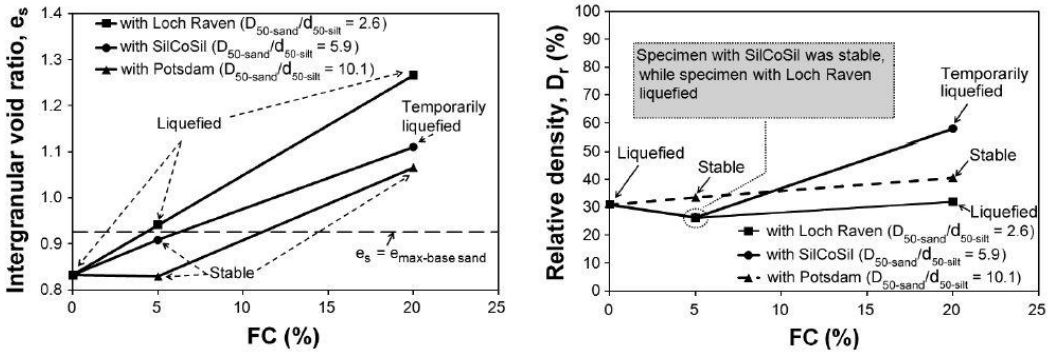

Figure 2.20: Change in intergranular void ratio and relative density with liquefaction potential in various fines contents by Monkul and Yamamuro (2011)

2.4.2.2 Partially Microstructural Approach

Polito (1999) and Polito and Martin (2001) implemented a laboratory parametric study using cyclic triaxial tests conducted to characterize the influence of non-plastic fines on the liquefaction resistance of sands. In this regard, the amount of limiting silt content was estimated between 25% and 45% for most silt-sand mixtures, in which silt is accommodated in the voids made by the sand skeleton without damaging the sand structure. In this light, two distinct behaviors can be considered by the limiting silt content and soil specific relative density. If the fines content become below the limiting silt content, there is enough space in the voids made by the sand skeleton containing the silt. Consequently, the liquefaction resistance is governed mainly by

soil specific relative density, and increasing soil specific relative density leads increase in liquefaction resistance of silty sands. However, if the fines content becomes higher than the limiting silt content, the structure of specimens comprise sand grains surrounded dominantly by silt matrix with little contacts between sand grains. Consequently, the soil specific relative density is weakly dependent on the liquefaction resistance, and the liquefaction resistance is governed by the silt fraction void ratio of such soils. Figure 2.21 depicts that the liquefaction resistance of such soil decreases with increasing fines content up to the limiting silt content at constant void ratio, beyond which that gradually increases by about 0.4 with increasing silt content up to 100% as shown in Figure 2.21.

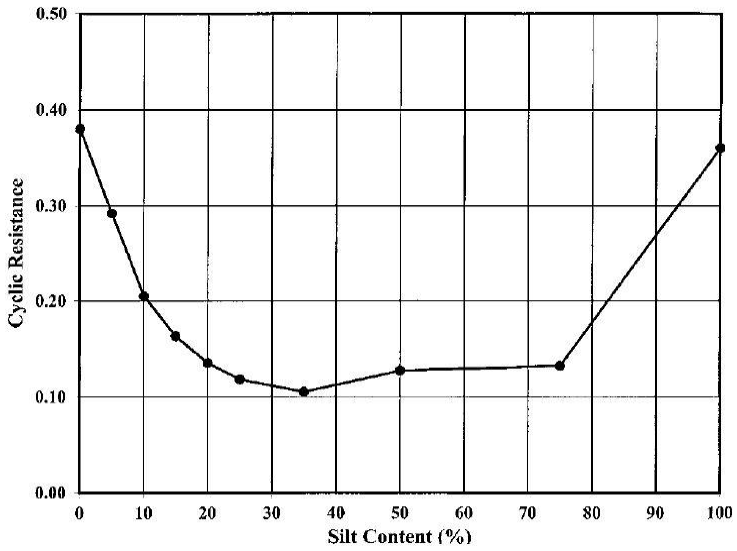

Figure 2.21: Cyclic resistance ratios versus silt content with Monterey sand at constant void ratio by Polito (1999)

2.4.2.3 Microstructural Approach

Based on such controversial outcomes in the behavior of silty sands, it is complicated to account for this behavior only in terms of common comparison bases. Thevanayagam (1998) proposed that the influence of silt and sand on silt-sand mixtures should be separately considered as a delicate composite matrix. In this

regard, the intergranular contact void ratio (e_s) and interfine contact void ratio (e_f) were newly introduced as shown in Figure 2.22. They play a key role on undrained shear strength (S_{us}) of silty sand. When S_{us} is compared at identical e_s, intergranular void ratio is less than $e_{max,HS}$ (maximum void ratio of host sand), both of the host sand and silty sand indicate same S_{us} that is not dependent on initial confining pressure. For fines content higher than about 30%, the behavior of the sandy silts and silty sand is similar to nonplastic fines determined by interfine void ratio, unless such soils are very dense.

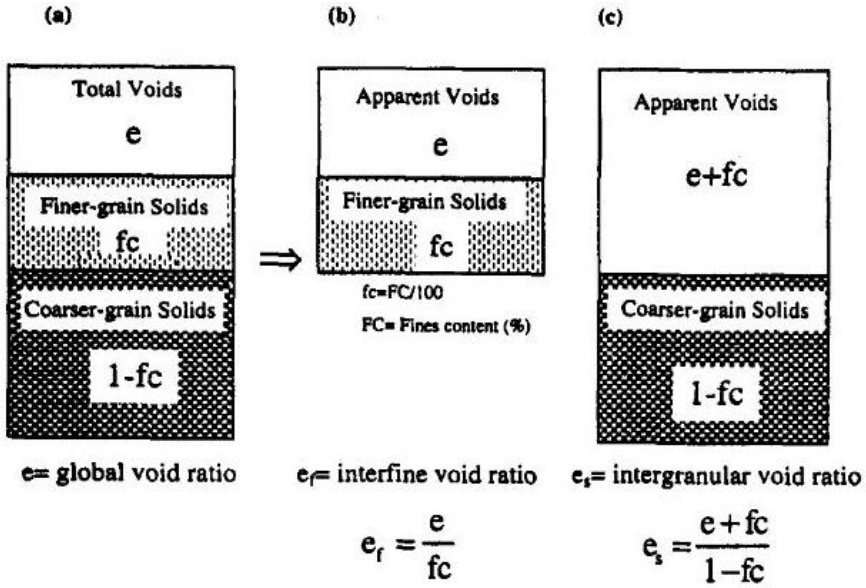

Figure 2.22: Interfine and intergranular contact indices by Thevanayagam (1998)

Thevanayagam et al. (2000) investigated the evaluation of cyclic strength behavior of silty sand based on interfine and intergranular contact indices. In this regard, undrained cyclic triaxial tests were carried out on various specimens containing sand with different percentages of silt, including 0, 15, 25, and 60%, prepared by dry air deposition method or moist tamping method. Also, the effective confining pressure of 100 kPa and the cyclic stress ratio of 0.2 remain constant in these cyclic tests. It is found that at the low fines content (FC) (less than FC_{th} – a certain threshold fines

content), the cyclic strength increases with increase in finer grains content, when compared at a given e_c (intergranular coarse grains contact void ratio); otherwise, at high FC (more than FC_{th}) the cyclic strength decreases with increase in finer grains content, when compared at a given e_f. Thevanayagam et al. (2002) considered the intergranular and interfine void ratio and confining pressures as criteria to characterize the behavior of silt-sand mixtures. In this regard, new equivalent intergranular contact void ratio, $(e_c)_{eq} = [e + (1-b)f_c]/[1-(1-b)f_c]$, and new equivalent interfine contact void ratio, $(e_f)_{eq} = e/[f_c + (1-f_c)/(R_d)^m]$, are defined to classify the behavior of these soils at below and beyond FC_{th}. It is shown that if the fines content is less than FC_{th}, the mechanical response of silty sands is dominated by inter coarse-grain friction. When they are compared at identical $(e_c)_{eq}$, the behavior of all specimens is akin to that of host sand at $e = (e_c)_{eq}$. However, if the fines content is higher than FC_{th}, the shear response is dominated by interfine contact density and friction. When they are compared at identical $(e_f)_{eq}$, the behavior of all specimens is akin to that of host silt at $e = (e_f)_{eq}$.

Rahaman and Lo (2007) found that the liquefaction behavior of fines-sand mixtures is dependent on the host sand gradation (i.e. C_u = coefficient of uniformity). Generally speaking, the deviatoric stress at steady state (q_{ss}) increases with increasing C_u for the identical fines type and contents. Moreover, angularity and plasticity of fines play a significant role in the liquefaction behavior and steady state strength; whereas, the effect of angularity is greater than plasticity on q_{ss} in such soils.

Baki et al. (2010) considered the equivalent granular state parameter (ψ*) and equivalent granular void ratio (e*) to characterize three different behavior of sand-fines mixtures, i.e. cyclic instability, cyclic mobility and transition behavior. This parameter is determined by this relation, $\psi^* = e^* - e_{ss}{}^*$, where $e_{ss}{}^*$ is equivalent granular void ratio at steady state line, as shown in Figure 2.23. When ψ* is positive, cyclic instability in loose silty sand with 15-30% fines occurs. On the other hand, cyclic mobility is found in specimens if ψ* is negative. However, transition behavior is observed in specimens at about zero value of ψ*.

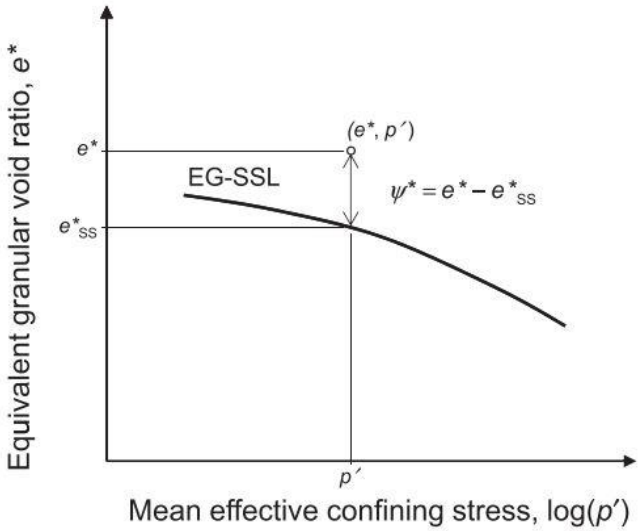

Figure 2.23: Equivalent granular state parameter by Baki et al. (2010)

Rahman et al. (2014) defined equivalent granular state parameter to predict cyclic liquefaction behavior of sand with fines ranging from 0 to 30%. A single equivalent granular steady state line (EG-SSL) can be utilized as the reference curve due to defining ψ*. Irrespective of fines content, ψ*(0) were considered to classify the flow, non-flow and limited flow based on the undrained behavior under monotonic loading as shown in Figure 2.24, and to classify cyclic instability, transient, and cyclic mobility based on undrained behavior under cyclic loading as shown in Figure 2.25.

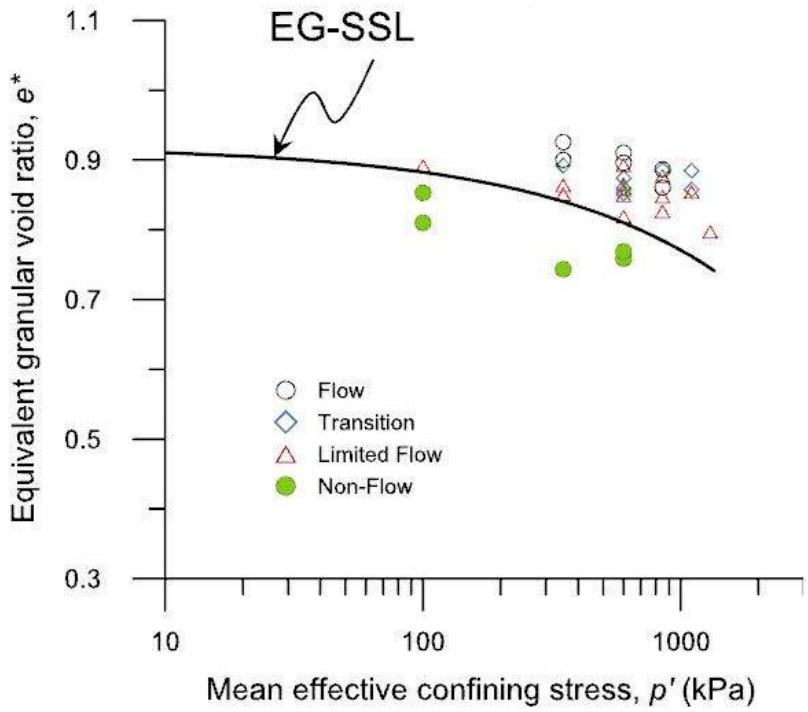

Figure 2.24: Initial states different types of monotonic behavior by Rahman et al. (2014)

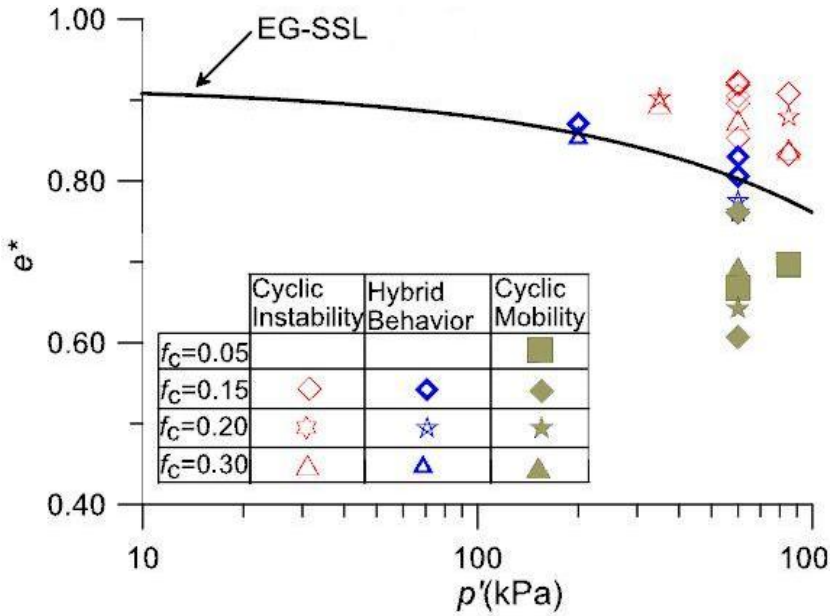

Figure 2.25: Initial conditions of the cyclic behavior by Rahman et al. (2014)

2.5 Cyclic and Monotonic Behavior of Silty Sand

Table 2.1 and Table 2.2 demonstrate that a number of studies have been implemented on the monotonic and cyclic behavior of silty sands in various fines contents,

confining pressures, specimen preparation methods and comparison bases. In accordance with these investigations, three major aspects, i.e. fines content, confining pressure and specimen preparations method, which are examined to assess the peak and residual shear strength, or the liquefaction resistance of such soils.

As illustrated by those tables, the effect of fines content is considered by Kuerbis et al. (1988), Pitman et al. (1994), Zlatovic and Ishihara (1995), Lade and Yamamuro (1997), Thavayaganam et al. (2000), Polito and Martin (2001), Xenaki and Athanasopoulus (2003), Naeini and Baziar (2004), Georgiano (2007), Yang et al. (2006), Sitharam and Dash (2008), Belkhatir et al. (2010) and Dash and Sitharam (2011).

The effect of confining pressure is considered by Zlatovic and Ishihara (1995), Andrianopoulos et al. (2001), sitharam et al. (2004), Naeini and Baziar (2004), Yang et al. (2006), Murthy et al. (2007), Bobe et al. (2009) and Stamatopoluos (2011).

The specimen preparation method is regarded by Zlatovic and Ishihara (1995), Naeini and Baziar (2004) and Murthy et al. (2007). Among three aspects, the effect of non-plastic fines on the liquefaction resistance leads to somewhat contradictory outcomes. Some results of laboratory studies show increase in liquefaction resistance or dilatancy of silty sands with increasing fines content [Shen et al. 1977; Kuerbis et al. 1988; Pitman et al. 1994; Ni et al. 2004; Georgiannou 2006], while results of some other laboratory studies indicate increasing fines content decreases the liquefaction resistance or contractiveness of silty sand [Erten and Maher 1995; Zlatovic and Ishihara 1995; Lade and Yamamuro 1997; Thevanayagam and Mohan 2000; Naeini and Baziar 2004; Yang et al. 2006; Murthy et al. 2007; Rees 2010;

Belkhatir et al. 2010; Stamatopoulous 2011; Dash and Sitharam 2011]. Generally speaking, some of experimental outcomes reveal that liquefaction resistance can decrease with increasing fines content until particular percentage of fines content, which has different values in each type of sand and silt, is reached. Then the liquefaction resistance increases slowly with increase in fines content [Thavanayagam, Fiorillo and Liang 2000; Polito and Martin 2001; Xenki and Athanasopoulus 2002; Naeini and Baziar 2004; Sitharam and Dash 2008; Dash and Sitharam, 2011], though the liquefaction resistance of pure silt is less than that of pure sand under any condition.

With regard to the tables, there is no consensus on particular relationship between fines content and liquefaction resistance, since other characteristics of fines, i.e. plasticity, mineral content, particle shape and size, and gradation, are rather imperative than the amount of fines (Ishihara 1993); moreover, sedimentation history, aging effect and stress history are not considered in these experiments.

Furthermore, literature has disclosed generally some aspects of sands containing silt, such as gradation, particle size and fines content, having effect on the liquefaction potential in field and experimental studies.

Grain size affects the cyclic resistance more than grain size distribution or grain shape (Lee and Fitton 1968). The influence of gradation is less than that of mean grain diameter of silty sand (D_{50}). Further, the effects of D_{50} and C_u get less important to cyclic resistance when the number of cycles to failure increases (Chang et al. 1982). Monkul and Yamamuro (2011) have recently considered the ratio between mean grain size of sand and silt (D_{50}/d_{50}) as another major factor in

examining the effect of fines content on liquefaction potential.

According to data from the 1964 Niigata Earthquake, soils were prone to liquefaction when C_u was less than 5, and fines content was less than 10% (Ohsaki 1970 as repoted by Tokimatsu and Yoshimi 1983). Moreover, during the 2011 Great East Japan earthquake, preliminary investigation indicate that the majority of liquefaction occurred in the reclaimed silty sand deposits of Tokyo Bay area with distinguishable fines content as much as 30% to 40% (Lee et al. 2013).

Table 2.1: Some of the literature about the monotonic undrained behavior of sand–silt mixtures

Reference	**Sand type**	**D_{50} sand (mm)**	**Silt type**	**D_{50} fines (mm)**	**D_{50}/d_{50}**	**Sample preparation method[b]**	**Confining pressures - σ_{3c} (kPa)**	**Comparison basis**	**Fines contents (%)**	**Effect of increasing FC on liquefaction resistance**
Kuerbis et al.,1988	Brenda mine tailings sand (20/200) (angular)	0.25	Kamloops silt	0.012	20.8	SD	350	Similar intergranular void ratio	0, 4, 7.5, 14, 22%	Increase
Pitman et al., 1994	Ottawa sand (subrounded)	0.39	Crushed silica	-	-	MP	350	Similar initial void ratio	0, 10, 20, 30, 40%	Increase
Zlatovic and Ishihara, 1995	Toyoura sand	0.17	Toyoura silt	0.01	17	DD, MP, WS	50-500	Loosest possible density after deposition	0, 5, 10, 15, 25, 30, 40, 100%	Decrease
Lade and Yamamuro, 1997	Nevada sand (50/200) (angular)	0.16	Nevada fines	0.05	3.2	DD	25	Loosest possible density after deposition	0, 10, 20, 30%	Decrease
	Ottawa sand (50/ 200) (angular)	0.2			4				0, 10, 20, 30, 50%	
Thevanayagam and Mohan, 2000	Sand	0.25	Kaolin silt	0.009	27.8	DP	100	Same void ratio	0-27	Decrease
Ni et al., 2004	Old alluvium sand	0.73[a]	Crushed quartz	0.04[a]	18.3	MP	215	Same intergranular void ratio	0-9	Increase
Naeini and Baziar, 2004	Ardebil sand	0.19	Ardebil silt	0.025	7.6	WS, UM	150, 300, 500	Void ratio (PS)	0, 10, 15,20, 25, 30, 35, 50, 100%	Decrease until 35% of silt content then increase

Georgiannou, 2006	Ham River sand (subangular)	0.27[a]	HPF4 silt	0.04[a]	6.8	DP	49	Loosest possible density after deposition (anisotropic)	0, 1, 2.5, 10, 20, 40%	Increase
			Silt-size mica	0.01[a]	27				0, 1, 2.5, 5, 10%	Decrease
Yang et al., 2006	Hokksund (sharp edge and cubical)	0.44	Chengbei (angular &subangular)	0.032	13.75	MP	50, 100, 150	Interfine and intergranular void ratio and void ratio	0, 5, 10, 15, 20, 30, 50, 70, 94%	Decrease
Murthy et al., 2007	Ottawa sand (rounded)	0.39	SilCoSil 106	0.02[a]	19.5	SD, MP, WS	148 - 653	Void ratio	0, 5, 10, 15%	Decrease
Bobe et al., 2009	Sydney		Non-plastic silt			MP	30, 100, 300, 400, 600, 1115		10%	
Rees, 2010	Chrsitchurch silty sand	-	-	-	-	MP	100, 200	Void ratio and intergranular void ratio	0, 1, 10, 20, 25, 30	Decrease
Belkhatir et al.,2010	Chlef Sand	0.4	Chlef	0.04	10	MP	100	Relative density (RS)	0, 10, 20, 30, 40, 50%	Decrease
Stamatopoulous, 2011	Egyptian desert	0.35	Assirou	0.02	17.5	DR, MP	50, 100, 150, 200, 250	Void ratio and Intergranular void ratio	0, 15, 25%	-
Dash & Sitharam, 2011	Ahmedabad sand	0.375	Quarry dust	0.037	10.1	DD	100	Void ratio (PS)	0, 5, 10, 15, 20, 25, 30, 35, 40, 45, 50, 60, 75, 100%	Decrease until the limiting silt content (LSC) then increase
								Relative density (PS)		Decrease until LSC then relatively constant
								Sand skeleton void ratio (PS)		Constant then Increase

Monkul and Yamamuro, 2011	Nevada Sand-B (angular)	0.14	Loch Raven	0.055	2.6	DD	30	Loosest possible density after deposition	0, 5, 20%	Decrease
			SilCoSil 125	0.024	5.9					First increase then relative decrease
			Potsdam	0.014	10.1					First increase then relative decrease

[a]They were not expressed in the documents precisely, then they were read off from the gradation curve (D_{50}: mean grain diameter of sand and d_{50}: mean grain diameter).
[b]DR: Dry rodding; MP: Moist placement; DD: Dry deposition; SD: Slurry deposition; WS: Water sedimentation; DP: Dry air pluviation; MU: Moist undercompaction technique PS: Peak Strength; RS: Residual shear strength.

Table 2.2: Some of the literature about the cyclic triaxial undrained behavior of sand–silt mixtures

Reference	Sand type	D_{50} sand (mm)	Silt type	D_{50} fines (mm)	D_{50}/d_{50}	Sample preparation method	Confining pressures - σ_{3c} (kPa)	Comparison basis	Fines contents (%)	Effect of increasing FC on liquefaction resistance
Shen et al., 1977	Ottawa sand	0.4	silt	-	-	MP	-	Same intergranular void ratio	0-20	Increase
Erten and Maher, 1995	Ottawa sand (rounded)	0.6	SilCo Sil 125	0.017	35.3	MU	98	Same void ratio (Pore water generation)	0, 10, 20, 30%	Decrease
Thavanayagam, Fiorillo and Liang, 2000	Foundry Sand	0.24	Sil co sil	0.007	34.28	DD, MP	100	Void ratio, Intergranular void ratio	0, 10, 15, 25, 60%	Decrease /Increase
Polito and Martin, 2001	Monterey sand (0/30) (subangular to subrounded)	0.43	Yatesville silt	0.03	14.3	MU	100	Relative density	0, 5, 10, 15, 20, 35, 50, 75, 100%	Decrease / Increase (depending on relative density)
	Yatesville sand (subangular to subrounded)	0.18			6					
Andrianopoulos, Bouckovalas, and Papadimitriou, 2001	Clean sand	-	-	-	-	MU	50, 200	Same void ratio	0, 5, 10, 20, 30%	Increase (if confining pressure is lower than mean effective consolidation stress,P0)/ Decrease (if confining pressure is greater than P0)
Xenaki and	From natural soil of Shinias-	0.12	From natur	0.02	6	DD	200	Void ratio	0, 10, 30, 42, 55%	Decrease until 42% of silt content then increase

Athanasopoulus, 2003	Marathon		al soil					intergranular and interfine void ratio		Monotonically increased or decreased
Sitharam, Raju and Murthy, 2004	Two natural soils	0.12[a]	-	Natural one	-	DD	25, 50, 100, 200, 300	Relative density	13,20%	-
Sitharam and Dash, 2008	Ahmadabad sand (sub-angular to sub-rounded)	0.3	-	Quarry dust	-	DD	100	same void ratio	0, 10, 20, 30, 40, 50, 75, 100%	Decrease until 20% of silt content (the limiting silt content) then increase
Belkhatir et al., 2010	Chlef Sand	0.4	Chlef	0.04	10	MP	100	Relative density (RS)	0, 10, 20, 30, 40%	Decrease

[a]They were not expressed in the documents precisely, then they were read off from the gradation curve (D_{50}: mean grain diameter of sand and d_{50}: mean grain diameter).
[b]DR: Dry rodding; MP: Moist placement; DD: Dry deposition; SD: Slurry deposition; WS: Water sedimentation; DP: Dry air pluviation; MU: Moist undercompaction technique PS: Peak Strength; RS: Residual shear strength.

Chapter 3

INTRODUCTION OF "CYCLIC REFERENCE STRAIN" AND "CYCLIC YIELD STRAIN"

3.1 Introduction

Evaluation of liquefaction potential during earthquakes has been an important subject for geotechnical engineers in seismically active regions of the world. In this task, the assessment of cyclic resistance of sandy soil deposits is of critical importance in the field.

One of the methods to this aim would be to secure undisturbed samples of soils from in-situ deposits in question and to test them in the laboratory under cyclic loading condition. This method is considered to give sufficiently accurate information regarding the cyclic strength of in-situ soils reflecting their inherent characteristics formed during depositional processes under their own environments. However, some of shortcomings of this method are the difficulty in evaluating levels of sample disturbance and the high cost incurred in the sampling and testing.

The other method would be to assess the cyclic resistance of in-situ soils via the use of some empirical formulae or charts correlating the cyclic strength with the resistance of penetration tests such as the Standard Penetration Test (SPT) and the cone penetration resistance (CPT). Some of the shortcomings of these methodologies are accuracy and reliability of the empirical formulae correlating the cyclic strength with the penetration resistance, which may be changed by the quality of the field

investigations constituting the liquefaction database.

Another method would be to make use of shear wave velocity which can be measured in-situ at low cost by means of several procedures, e.g. downhole, crosshole and SASW technique, without necessarily drilling boreholes. However, there are some concerns over its use, mainly because of the liquefaction being associated with medium to large shear strain in contrast to the infinitesimal shear strain involved in the propagation of the shear wave (Jamiolkowski and Lo Presti 1990; Teachavorasinskun et al. 1994 and Roy et al. 1996). Since the small strain measurements of shear wave velocity are extremely sensitive to weak inter-particle bonds eliminated at medium and large strains, this concern can also be important for cemented soils (Andrus and Stokoe 2000). In spite of such potential shortcomings, there has been a lot of work towards the use of shear wave velocity, attempting to establish some charts correlating the cyclic strength and shear wave velocity. Typical papers dealing with this subject include Dobry et al. (1980), Stokoe et al. (1988), Tokimatsu and Uchida (1990) and Andrus and Stokoe (2000), Liu and Mitchell (2006), Baxter et al. (2008), Andrus et al. (2009) and Kayen et al. (2004 and 2013). Thus, if there is some physical interpretation provided for a link between small strain (shear wave velocity) and medium-to-large strain behaviour of soils (liquefaction), the use of the shear wave velocity will be justified as an effective tool to assess the liquefaction resistance of in-situ sand deposits, not only for uncemented soils of Holocene age, but also for cemented soils of Holocene and Pleistocene age.

It is an objective of the present study to propose a new parameter, i.e. “cyclic yield strain”, to indicate that shear wave velocity can be used to differentiate between the cyclic resistance of unaged and aged sand deposits.

3.2 Relation between Cyclic Stress Ratio and Amplitude of Cyclic Strain

In order to determine the resistance of a sandy soil to liquefaction, the cyclic triaxial tests are normally performed a few times by changing the cyclic stress ratio, $R_L = \sigma_d/(2\sigma_0')$, where σ_0' is the initial confining stress and σ_d denotes a single amplitude of axial deviator stress in the cyclic triaxial tests. Typical results of the tests are schematically illustrated in Figure 3.1(a). Suppose the cyclic stress ratio, $R_{c'}=0.20$, is applied to a sample, amplitude of the single amplitude of axial strain, ε_a, successively increases as indicated by a', b', c' and d' on the plot of the cyclic stress ratio versus the number of cycles. By repeating similar tests with different cyclic stress ratios, a series of points can be obtained similarly for each of the axial strain amplitude. By connecting the points of equal axial strain amplitude, a set of curved lines can be obtained as indicated in Figure 3.1(a).

It has been well-known that the cyclic stress ratio causing liquefaction with 100% pore water pressure build-up takes place almost concurrently with the development of an axial strain of 2.5% in the single amplitude. Thus, it is common practice to consider the cyclic stress ratio causing a single-amplitude axial strain of ε_a =2.5% as a state where liquefaction is triggered. However, since the line of equal axial strain, ε_a =2.5%, does depend upon the number of cycles as shown in the plot of Figure 3.1(a), it is necessary to specify the number of cycles to determine a value of cyclic stress ratio at liquefaction. The number of cycles is a key factor to be determined by counting the significant numbers of pulses in time histories of recorded motions during earthquakes. It has been customary to adopt 15 or 20 cycles of uniform loading as being the number representative of those typically experienced by large

earthquakes with a magnitude of the order M=7.5. In the present study, the number of cycles Nc = 20 will be taken up for determining the cyclic stress ratio, R_L, at liquefaction. Based on this presumption, the cyclic stress ratio causing liquefaction is read off as R_L=0.15, for instance, in the illustrative diagram shown in Figure 3.1(a).

When the equivalent number of cycles is fixed at Nc=20, it becomes possible to read off values of axial strain, ε_a, as a function of the applied cyclic stress ratio, R, as illustrated by points a→b→ c→ d in Figure 3.1(a). It is then possible to establish a plot of R versus ε_a as displayed by points a→b→ c→d in Figure 3.1(b). This curve indicating the growing amplitude of axial strain with the increase of cyclic stress ratio can be considered as non-linear stress-strain relationship in general term.

In the theory of elasto-plasticity, it is customary to represent the non-linear stress-strain relation approximately by bi-linear lines. In this case, one line is a tangent at zero point representing the elastic behaviour and another line is an asymptote towards a large strain bounded by an upper limit of stress, that is, the strength.

The same idea may be applied in the present study to represent the relation between the cyclic stress ratio, Rc, and amplitude of axial strain, ε_a, as indicated in Figure 3.1(b). Note that the upper limit is now chosen as the cyclic strength, R_L, defined as the cyclic stress ratio required to cause 2.5% single-amplitude axial strain in 20 cycles of load application. The tangent line at zero point is taken as a straight line with a slope, G_0, indicating the elastic behaviour at very small strain which is believed to take the same value , no matter how many cycles may be applied. These two lines are indicated by segment BC and segment AB, respectively, in Figure 3.1(b).

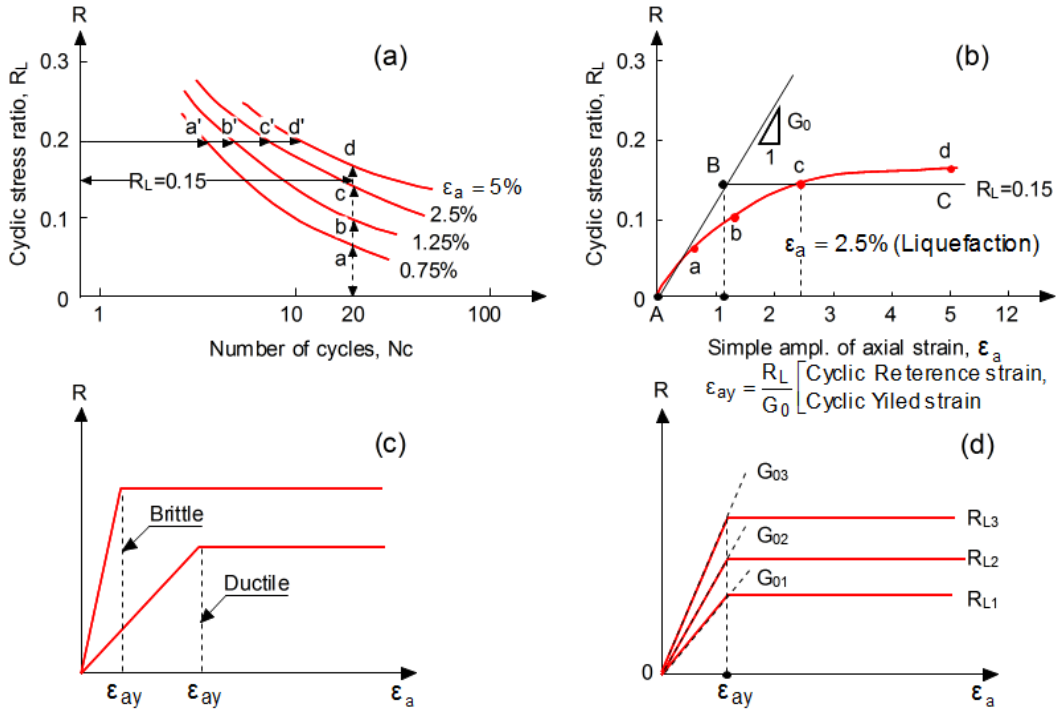

Figure 3.1: Implication of the yield strain in cyclic loading

Suppose the cyclic stress-strain curve of a sandy soil under cyclic loading is enclosed by the two straight lines as above, it is now possible to determine the axial strain corresponding to the point B which is the intersection of the two lines in Figure 3.1(b). This strain may be deemed as "reference strain" or "yield strain" in cyclic loading. In order to define this strain in non-dimensional format, the cyclic stress ratio multiplied by the atmospheric pressure P_a = 98 kN/ m^2, will be used. In view of the fact that the shear modulus, G_0, practically remains unchanged irrespective of whether the loading is monotonic or cyclic, the G_0-value obtained from shear wave can be considered as the shear modulus also in the cyclic loading conditions. Therefore, both G_0 and cyclic stress at liquefaction, $R_L \cdot P_a$, are deemed as the variables under cyclic loading conditions. In this context, the ratio between them will be referred to as "cyclic yield strain" hereafter.

It has been known that the shear modulus, G_0, increases in proportion to square root

of the confining stress σ_0' or effective overburden pressure σ_v' (Harden and Richart, 1963). Thus, the shear modulus G_o was normalized through the square root of the confining stress as follows:

$$G_{01} = G_0 \times \left(\frac{P_a}{\sigma_0'} \right)^{1/2} \tag{3.1}$$

Given the fact that the value of G_0 at the atmospheric pressure of P_a = 98 kN/m^2 is donated by G_{01}, the cyclic yield strain, ε_{ay}, can be defined as:

$$\varepsilon_{ay} = \frac{R_L \cdot P_a}{G_{01}} \tag{3.2}$$

Note that, if the value ε_{ay} in the triaxial mode is required to be converted to the cyclic yield strain, γ_y , in the simple shear mode, the relation $\gamma_y = 1.5\varepsilon_{ay}$ can be used.

The physical implication of the yield strain in cyclic loading, ε_{ay}, is illustrated in Figure 3.1(c). If the value of ε_{ay} is large, the soil is deemed as a material exhibiting "ductile" or "soft" behaviour. In contrast, if the yield strain, ε_{ay}, is small, the soil is considered as "brittle" or "stiff". Thus, the cyclic yield strain defined by Equation 3.2 can be used as an index property to indicate levels of ductility (softness) or brittleness (stiffness) of sandy soils under cyclic loading. It is well-known that the cyclic strength, R_L, of a soil from a given deposit tends to increase with increasing relative density, the initial shear modulus, G_{01}, also increases simultaneously. However, the rate of increase in $R_L \cdot P_a$, and G_{01} would be in such a way that the ratio between them, that is, the yield strain, ε_{ay}, stays at a constant value, if the level of ductility or brittleness of a given sand is identical. The idea of constant cyclic yield strain while changing R_L and G_{01} is illustrated in Figure 3.1(d).

The idea of using a certain level of strain as an index property was first introduced by

Dobry et al. (1980) who proposed the presence of a threshold strain separating occurrence and no occurrence of dilatancy-induced volume change or pore water pressure build-up in cyclic loading. The cyclic strain has been defined above in similar vein to that introduced by Dobry, but its interpretation and manner in which it is used would be different.

3.3 Factors Affecting the Ductility or Brittleness of Soils under Cyclic Loading

Several factors may exert influence on the ductility or brittleness of soils as defined above. As one of the factors, aging of soil deposits indicates that in-situ soils having a long history of deposition may show brittle behaviour, as opposed to ductile response of soils with a short history of deposition. Thus, the effect of aging of soil deposits may be reflected in the cyclic yield strain, ε_{ay}.

On the other hand, the brittleness or the stiffness of old sand deposits may be due to an increase in resistance to cyclic loading. Additional cyclic triaxial tests suggested that the higher resistance was not due to cementation; instead, it is postulated that the high resistance can be attributed to the interlocked particles and infilling associated with deposits of an old age (Kramer and Arango, 1998).

It is known that, for a given soil at a given state with identical density and stress history, the value of G_0 remains unchanged, whereas the cyclic strength tends to alter significantly with the number of cycles in question. Therefore, the cyclic yield strain, ε_{ay}, could also be a function of the number of load cycles, which is to be specified properly reflecting the duration of shaking during earthquakes.

Another conceivable factor influencing on the reference strain, ε_{ay}, would be the amount of fines, Fc, contained in sands in question. Sandy soils containing larger amount of fines are envisaged to exhibit more ductile behaviour, as compared to more brittle characteristics exhibited by the soils with lesser amount of fines. The reasoning similar to the above may, thus, be applicable to provide a physical interpretation for the R_L versus G_0 relationship for soils with varying content of fines.

3.4 Relationship between Cyclic Resistance and Shear Wave Velocity

The initial shear modulus, G_0, can be obtained from the shear wave velocity, V_S (m/s), as follows:

$$G_0 = \frac{\gamma_t}{g} V_s^{\,2} \tag{3.3}$$

where γ_t is the total unit weight of a soil and g ($9.8 m/s^2$) denotes the gravity acceleration. Since the shear wave velocity is a parameter of soils that can be measured either in the field or in the laboratory tests, the value of V_S has been used frequently to establish charts to estimate liquefiability of given soil deposits as summarized by Andrus and Stokoe (2000). Given the fact that the shear modulus, G_0, tends to increase in proportion to quarter root of the overburden pressure, the shear wave velocity, V_S, can be normalized to the velocity V_{S1} corresponding to the atmospheric pressure $P_a = 98$ kN/m^2 as follows:

$$V_{S1} = V_S \times \left(\frac{P_a}{\sigma_0'} \right)^{1/4} \tag{3.4}$$

where the law of normalization through the quarter root is the one proposed by Hardin and Richart (1963) based on the comprehensive test results. According to their work, the shear wave velocity was shown also to be a function of void ratio.

However, its dependence upon void ratio is deemed to be small particularly for clean sand, as compared to that upon the confining stress. Thus, only the effect of confining stress is considered in present study for normalization of the measured shear wave velocity as well as shear modulus.

Thus, through the use of ε_{ay} defined by Equation 3.2 the relation between R_L and V_{S1} can be expressed as,

$$R_L \cdot P_a = \frac{\gamma_t}{g} \varepsilon_{ay} \cdot V_{s1}^{\ 2} \tag{3.5}$$

With the relation of Equation 3.5, two characteristic curves are obtained at two different equal cyclic yield strains as displayed schematically in Figure 3.2. Generally speaking, ductile (or brittle) behaviour of soils would yield larger (or smaller) value of cyclic yield strain.

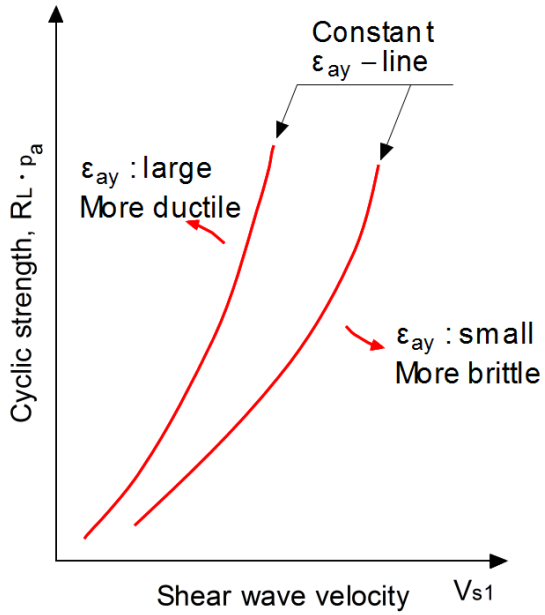

Figure 3.2: Characteristic curves pertaining to ductile or brittle behaviour of soils

Chapter 4

FIELD INVESTIGATION AND RECOVERY OF UNDISTURBED SAMPLES

4.1 Introduction

With the aim of estimating the value of ε_{ay}, large numbers of tests were conducted in the field and also in the laboratory using the cyclic triaxial test apparatus for undisturbed and disturbed samples of sandy soils. To this end, two important sites encountered the liquefaction in 2011 Great East Japan earthquake were considered in the present study. The 2011 earthquake with the earthquake magnitude (M_w) of 9.0 off the Pacific coast of Tohoku occurred on March 11, 2011, with the epicenter of the order of 70 kilometers from east of the Oshika Peninsula of Tohoku and the hypocenter at an underwater depth of the order of 30 km. The earthquake is often referred to in Japan as the Great East Japan earthquake.

One site is located at Asahi city in northern of Chiba Prefecture, Japan, along the coastal line of the Pacific Ocean. Half of specimens extracted from Asahi site were tested in Chiba Engineering Co. without Vs-measurement in laboratory, the results of which were obtained from its report, whereas cyclic triaxial tests along with laboratory Vs-measurement were conducted on the rest of the specimens in Kiso-Jiban Consultants Co. in this research. The other site is Kayakari tailings dam site at south of Kesenuma in Miyagi Prefecture, Japan, which did suffer from breach and release of liquefied tailings. The results of the cyclic triaxial tests conducted on the undisturbed specimens extracted in 1979 and 2011 were obtained from the paper by

Ishihara et al. (2015). The locations of both sites are shown in Figure 4.1. Furthermore, undisturbed samples were extracted and secured from man-made fills of the tailings dam and alluvial deposits of Asahi city using single-tube sampler, Denison sampler, or triple-tube sampler.

4.2 Asahi Site

Man-made fills and alluvial (Holocene) deposits near the surface suffered from ground settlement and tilt of private houses due to liquefaction at the time of the 2011 earthquake. Individual locations of sampling are indicated in Figure 4.2. The area of ground destruction is a broad flat plain surrounded by hills in the north and west. Soil borings were conducted at six places as indicated in Figure 4.2. More detailed soil profiles at three selected locations are shown in Figure 4.3 -4.5, where SPT N-values, shear wave velocity V_S, and depths of sampling are also indicated.

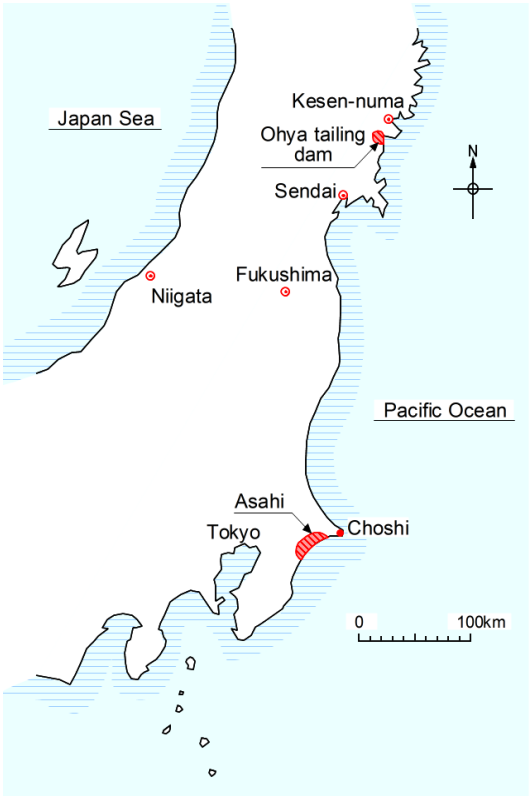

Figure 4.1: Location of two sites for undisturbed sampling

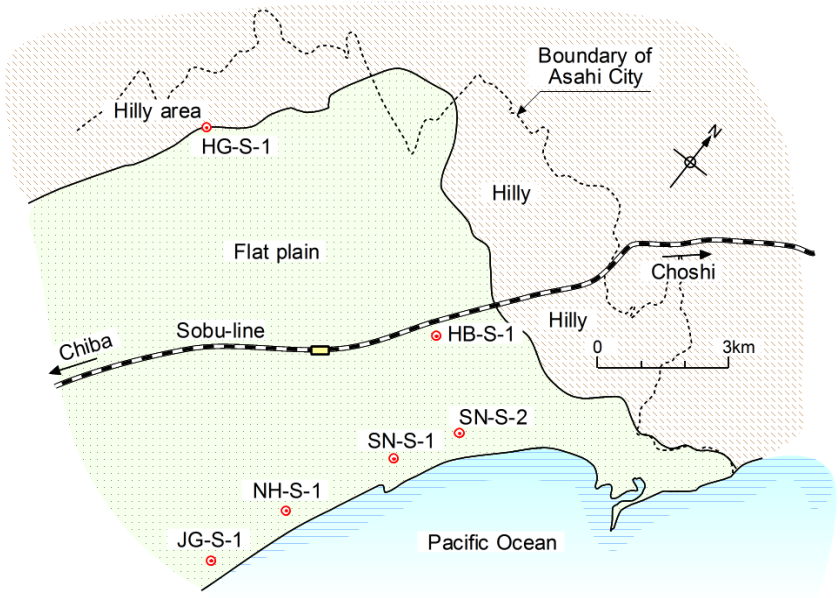

Figure 4.2: Location of undisturbed sampling at Asahi, Chiba

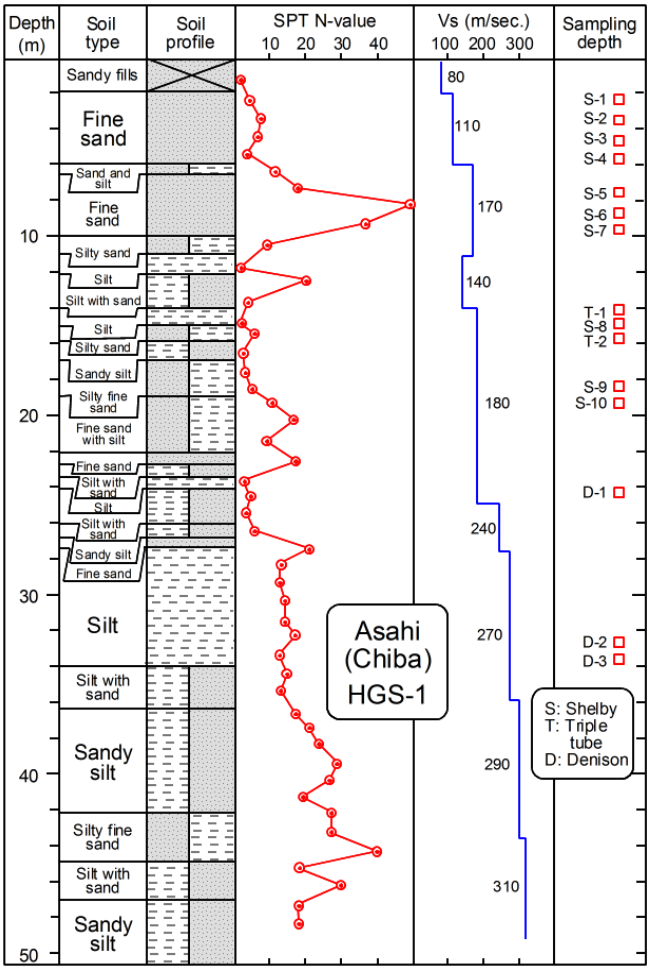

Figure 4.3: Soil profile at the site of sampling in Asahi (HG-S-1)

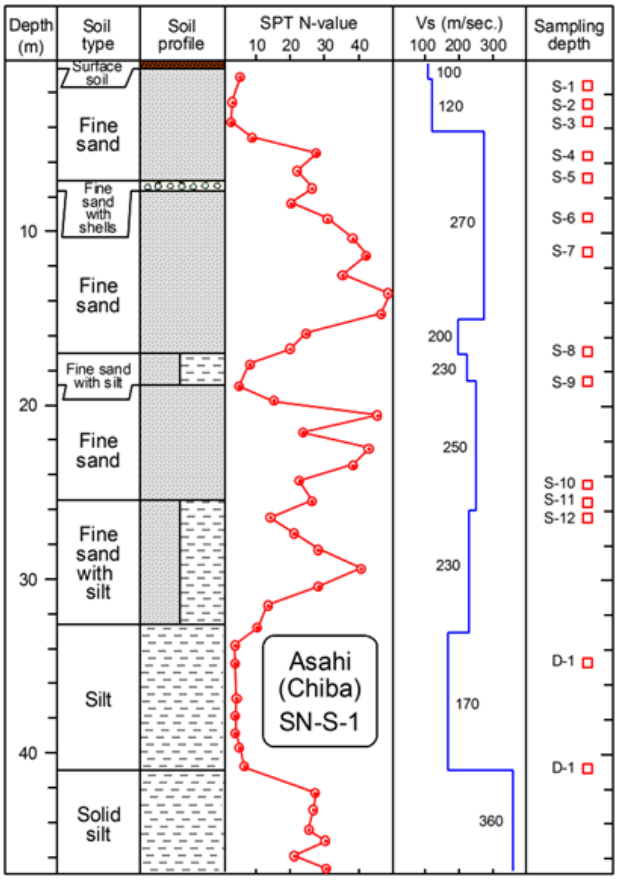

Figure 4.4: Soil profile at the site of sampling in Asahi (SN-S-1)

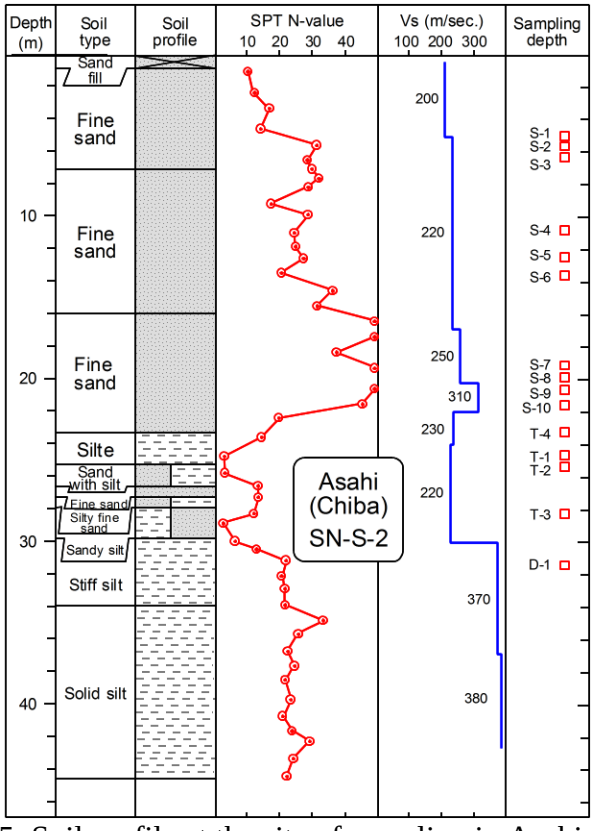

Figure 4.5: Soil profile at the site of sampling in Asahi (SN-S-2)

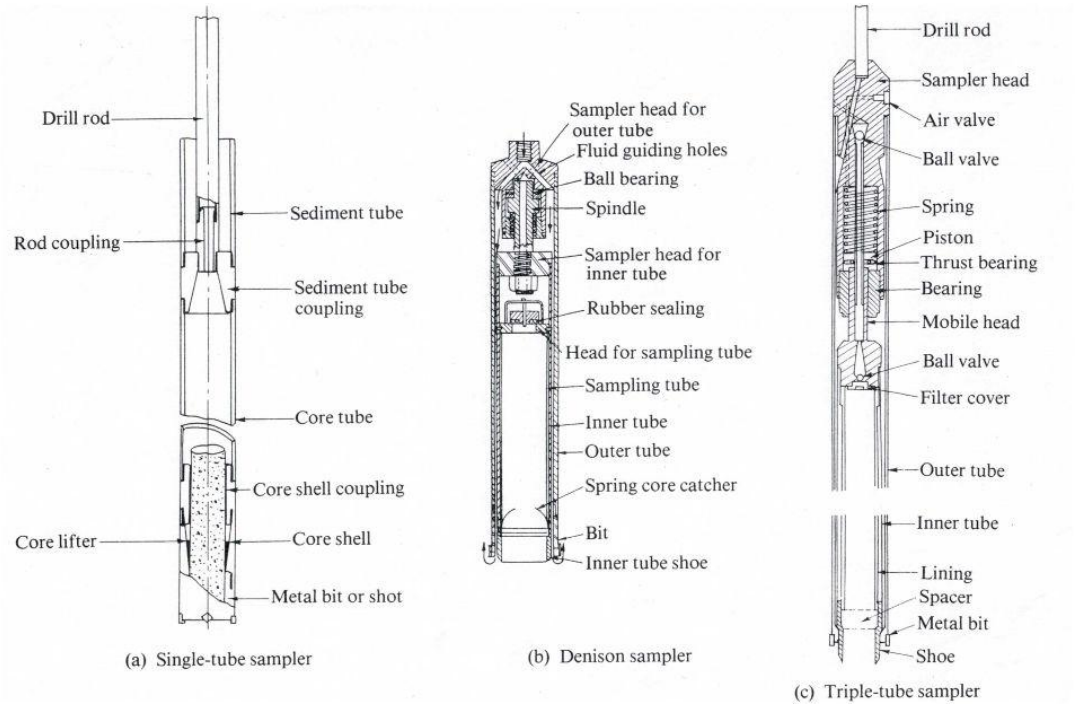

Figure 4.6: Sigle-tube sampler, Denison Sampler and Triple-tube sampler (International manual for the sampling of soft cohesive soils, Tokyo, 1981)

4.2.1 Geological Characteristics of Asahi Site

As the geological history of Asahi site, it is known that it used to be under a huge lake of 4 km × 6 km dimentions. As depicted in Figure 4.8. The shallow-depth lake was drained by constructing water channels and transformed into rice fields. Then, the land was covered by fill material of 1~3m height before buildings houses. Thus, it appears that the surface soils dumped and the near-surface soils of alluvial origin (AS1, AS2, etc.) have developed liquefaction. Figure 4.9 depicts the current map indicating strips of sand dune deposits of different ages in parallel to the coastal line. One of the cross section in East-West direction indicates several soil profiles as shown in Figure 4.10. The age of each old deposit is not exactly known, but alluvium is purported to have deposited during the last several thousand years. Diluvium is older and said to have more than 10 thousand-year history. This is in good agreement with the characteristics of the curve proposed in the present study for Asahi site as indicated in section 4.2.2.

4.2.2 Correlation between Shear Wave Velocity and SPT N-value for Asahi Site

Based on the correlation between normalized shear wave velocity and SPT N-value proposed by Andrus and Stokoe (2000) which is indicative of uncemented, Holocene sands with less than 10% fines content and average depths less than 10 m, the data of identical characteristics were obtained from some soil profiles of Asahi site as shown in Table 4.1. In order to compare two sets of data, N_{80} (energy ratio of 80%) related to Japanese SPT should be converted to N_{60} (energy ratio of 60%) of American SPT. The correlation of the present study indicated in Figure 4.2 is compared with the curve proposed by Andrus and Stokoe (2000). As such, the curve passed through the average points is placed higher than Andrus and Stokoe's curve because of using cemented, undisturbed samples. It seems to be reasonable to consider the curve of the present study as the representative of old aged deposits, and Andrus and Stokoe's curve as the representative of freshly deposited soils.

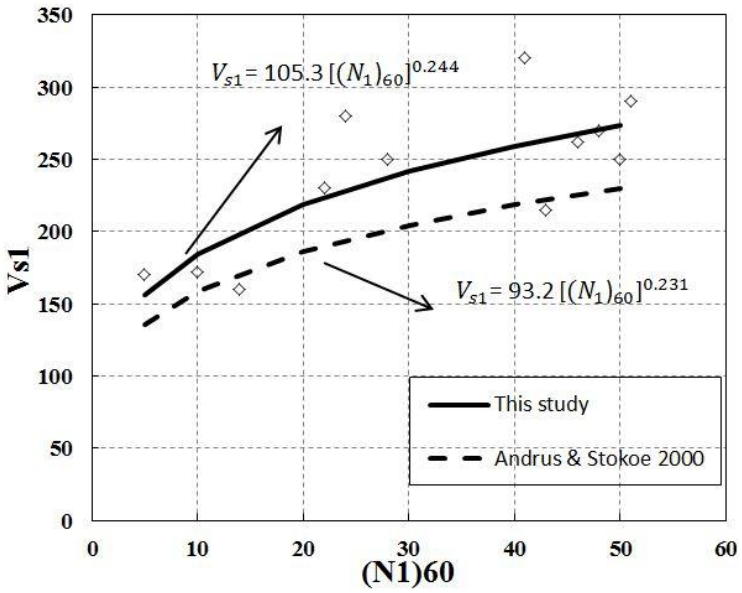

Figure 4.7: Correlation between V_{S1} and (N1)60 proposed by Andrus and Stokoe (2000) and the present study

Table 4.1: Asahi soil profiles with FC<10% and average depths<10m

SN-S-1	Vs (m/s)	N_{80} => N_{60}	σ_v(kPa)	V_{S1} (m/s)	$(N_1)_{60}$
Depth = 2m (FC=4.3%)	120	2 => 3	22	170	5
10m (7.0%)	270	35 => 45	78	290	51
6m (5.6%)	270	22 => 29	50	320	41
SN-S-2	Vs	N_{80} => N_{60}	σ_v	V_{S1}	$(N_1)_{60}$
2 (10%)	200	11 => 14	26	280	24
7 (9%)	220	30 => 39	61	250	50
HB-S-1	Vs	N_{80} => N_{60}	σ_v	V_{S1}	$(N_1)_{60}$
3 (1%)	190	13 => 17	34	250	28
8 (1%)	240	30 => 39	70	262	46
JG-S-1	Vs	N_{80} => N_{60}	σ_v	V_{S1}	$(N_1)_{60}$
2.5 (3%)	170	10 => 13	31	230	22
5.0 (2.2%)	180	23 => 30	49	215	43
9 (7%)	150	10 => 13	77	160	14
NH-S-1	Vs	N_{80} => N_{60}	σ_v	V_{S1}	$(N_1)_{60}$
4 (6.3%)	140	5 => 6.5	43	172	10
10 (9.6%)	260	35 => 45	85	270	48

4.2.3 Recovery of Undisturbed Specimens

Recovery of undisturbed samples was conducted by means of the single-tube sampler at mediumly shallow depths denoted by S-1, S-2, etc., by the triple tube sampler at mediumly soft soil deposits (T-1, T-2, etc.), and using the Denison sampler at stiff old deposits (D-1, D-2, etc.) as shown in Figure 4.6. The type of the samplers used is indicated on the right side column in each of the plots in Figure 4.3, Figure 4.4, Figure 4.5.

In the practice of site investigation in Japan, it is common to make use of these sampling techniques. The degree of disturbance during sampling is difficult to quantify accurately. It is believed that, despite some degree of disturbance, the intact samples recovered can still retain inherent structures such as thinly stratified complex matrix which was formed under respective depositional environments. These structures in intact soils are conceived to have more significant influence on the soil

response in the cyclic loading, as compared to some changes in the density during sampling and sample handling. Although the term “intact samples” can be conceptually relevant term for such samples, the term “undisturbed samples” has been commonly used in geotechnical society even for cohesionless soils. Thus, the term “undisturbed samples” is used hereafter in this thesis.

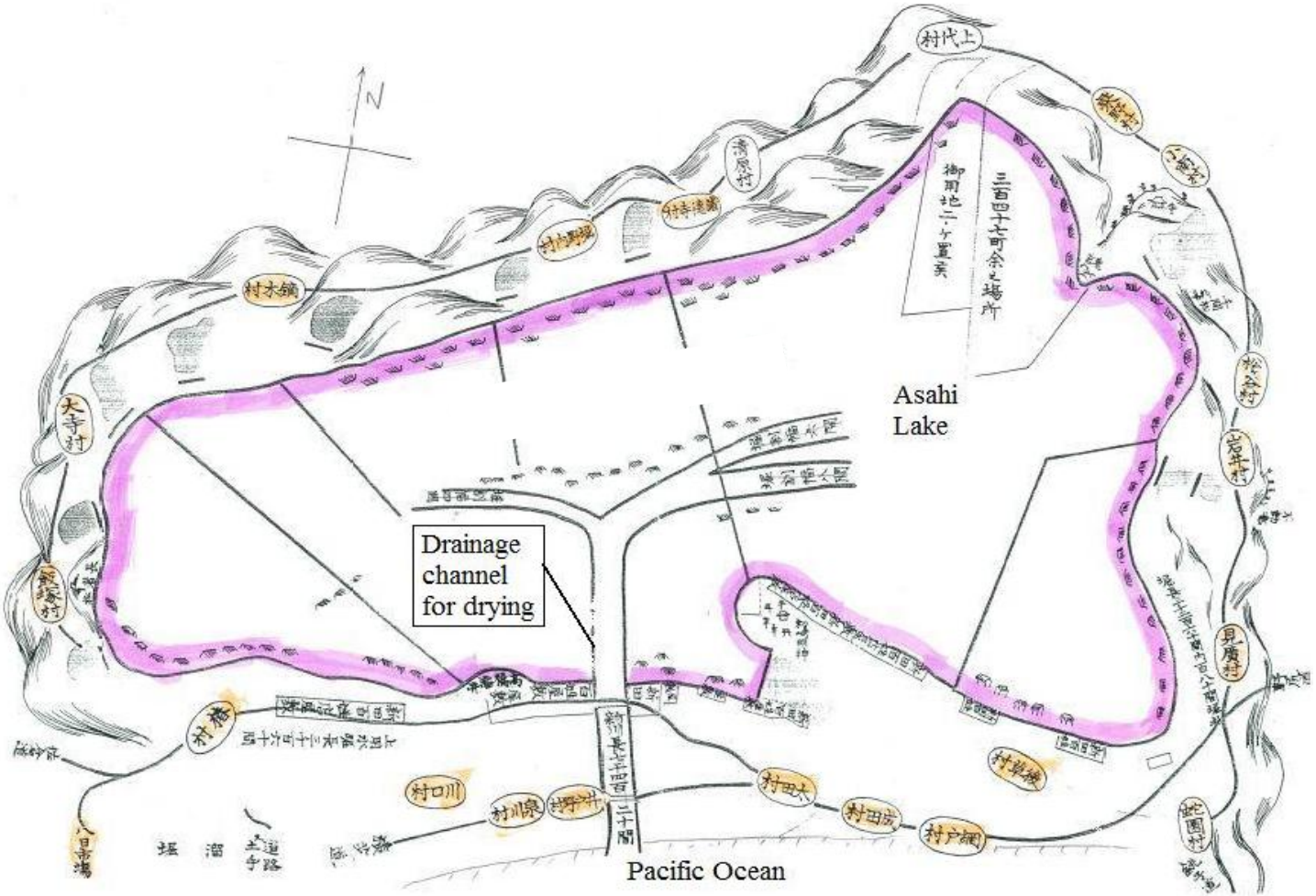

Figure 4.8: Old map of Asahi site in 1770's

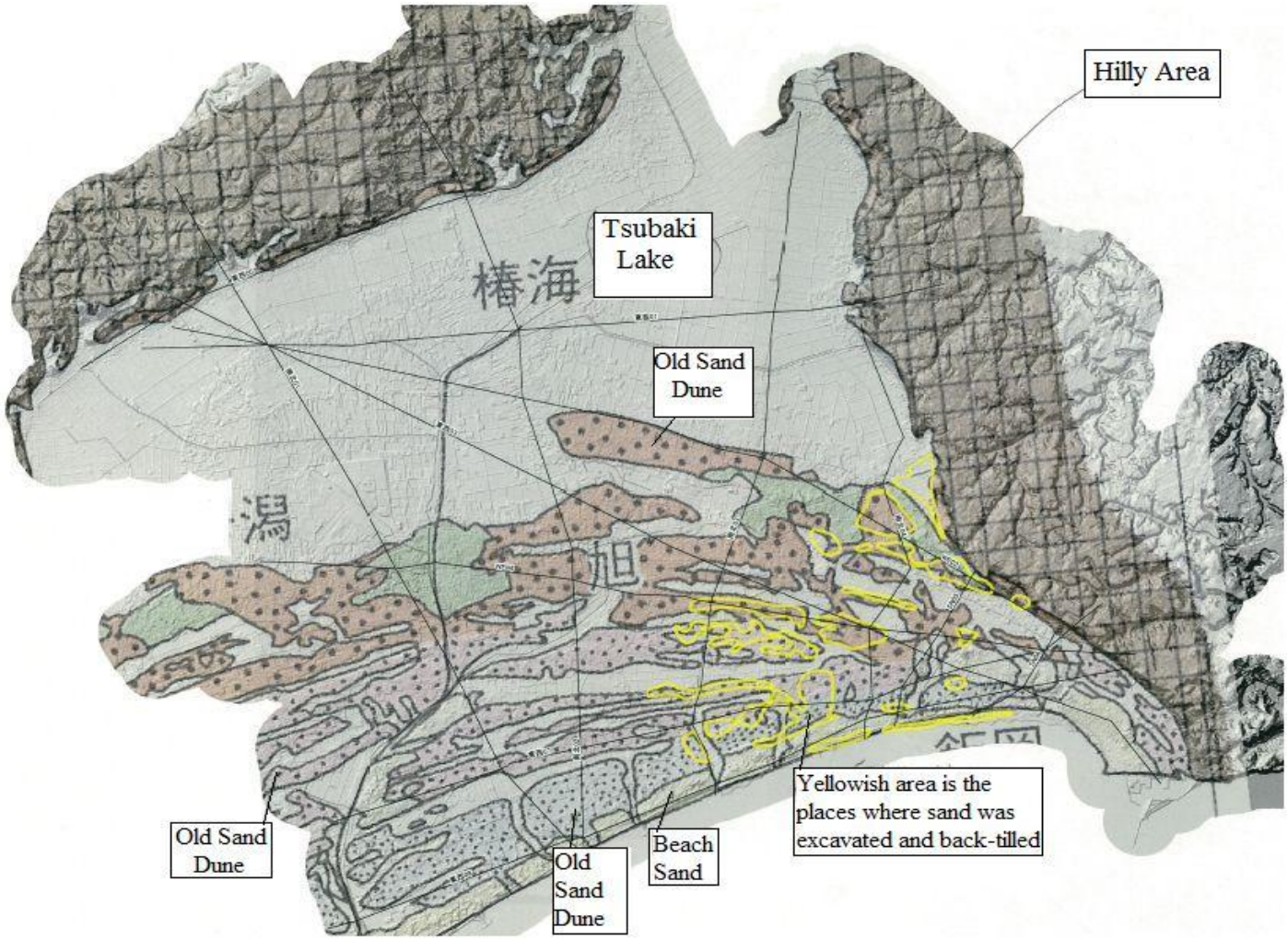

Figure 4.9: Current map of Asahi site

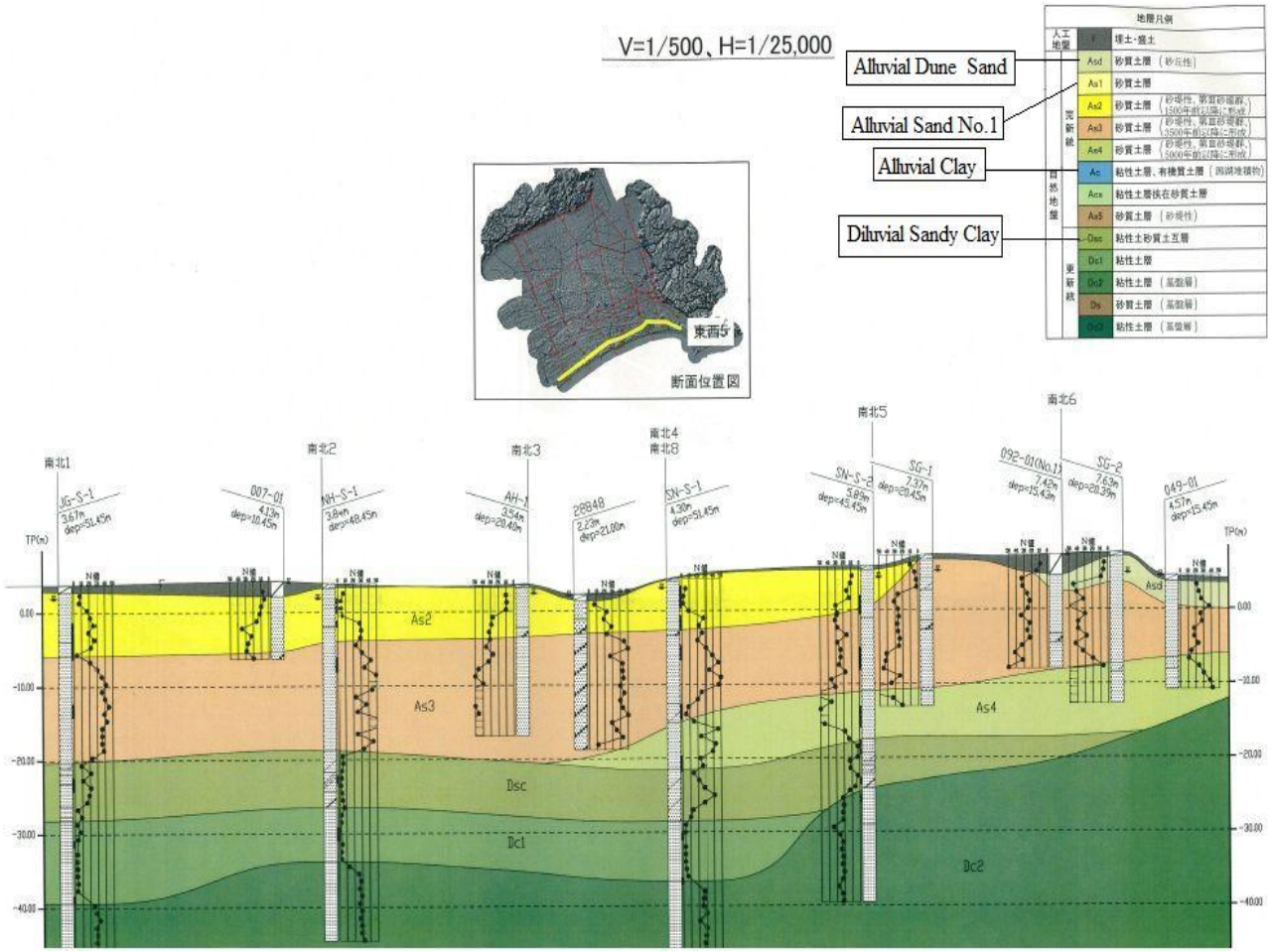

Figure 4.10: East-west cross section of Asahi sit

4.3 Kyakari Tailings Dam Site

The location of Kyakari tailings dam at Ohya mine site which failed during the 2011 earthquake is indicated on the map of Figure 4.1. The site, about 60 km from north of Sendai, was shaken strongly with a peak acceleration of 454 gal which was recorded at a nearby station. A plan view of the failed tailings pond is shown in Figure 4.11. Detailed account of soil conditions and features of failure is described in a paper by Ishihara et al (2015).

Because of assessing the level of liquefaction susceptibility of Kayakari pond during earthquake shaking, the geotechnical studies had been carried out in 1979, including recovery undisturbed specimens, velocity loggings, and SPT. A large number of cyclic triaxial experiments had been conducted to determine the liquefaction resistance of specimens extracted from the slime deposit of tailings dam. Undisturbed samples were secured by means of the triple tube sampler which is said to be suitable to obtain fairly good-quality samples from silty sand deposits of low to medium density. Same sets of experiments were carried out after the 2011 Great East Japan earthquake.

Two locations designated by B-1 and B-2 were selected for the field study at Kayakari disposal pond in 1979 as indicated in Figure 4.11 and Figure 4.12. The study after breach in the 2011 earthquake was carried out in three alignments designated by I, II and III at different points. Six boreholes were accomplished along the line A-A' in the alignment III after the earthquake as shown in Figure 4.11 and Figure 4.12. In order to compare between soil properties of before failure and after the earthquake, the soil profiles at B-2 and III-6 were considered in Figure 4.14. As

illustrated in Figure 4.13 and Figure 4.14, the surface soil up to the depth of 4m was uncovered by flow failure at III-6. Thus, only the portion below the depth of 4m is indicated at the soil profile after failure.

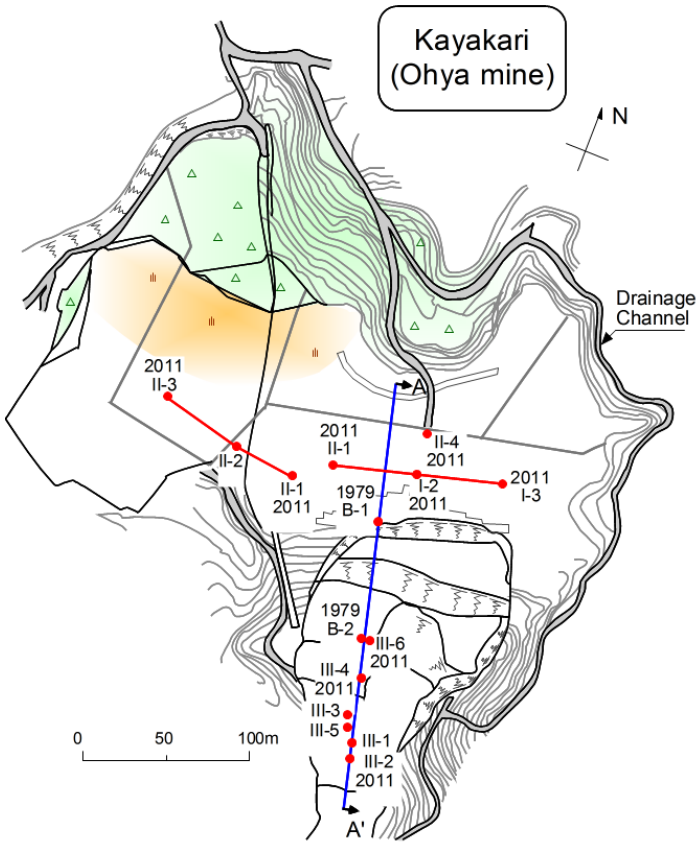

Figure 4.11: Plan view of the failed Kayakari tailings dam at Ohya mine

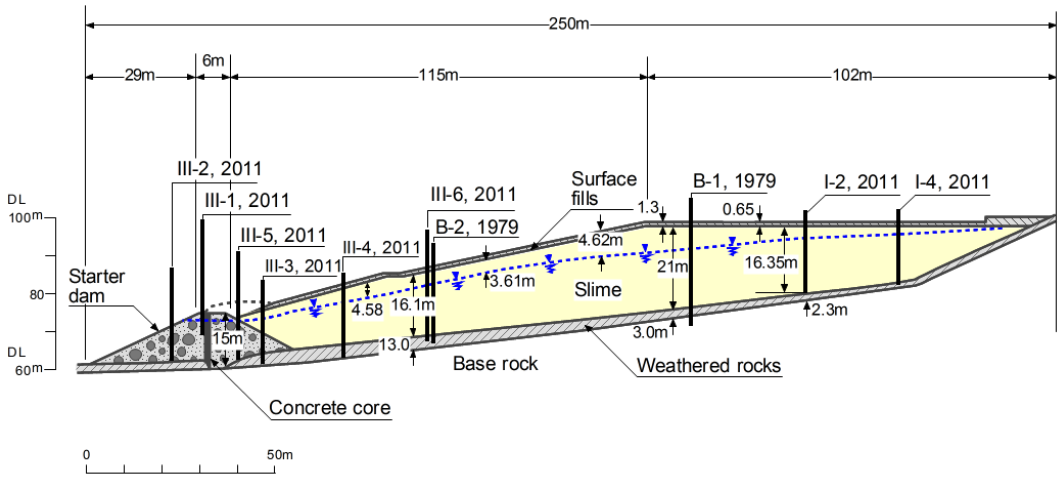

Figure 4.12: Cross section A-A' of the failed Kayakari tailings dam at Ohya mine showing the locations of boring logs in 1979 and 2011

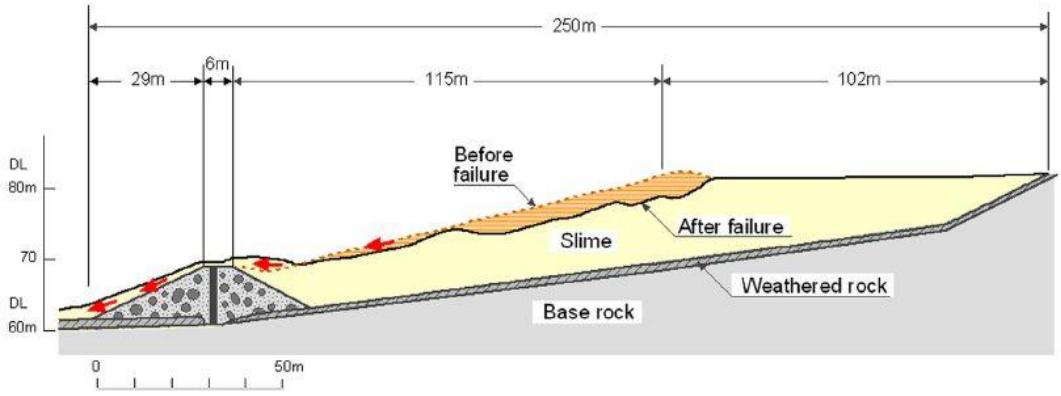

Figure 4.13: Cross section of Kayakari tailings dam before the failure and after the earthquake

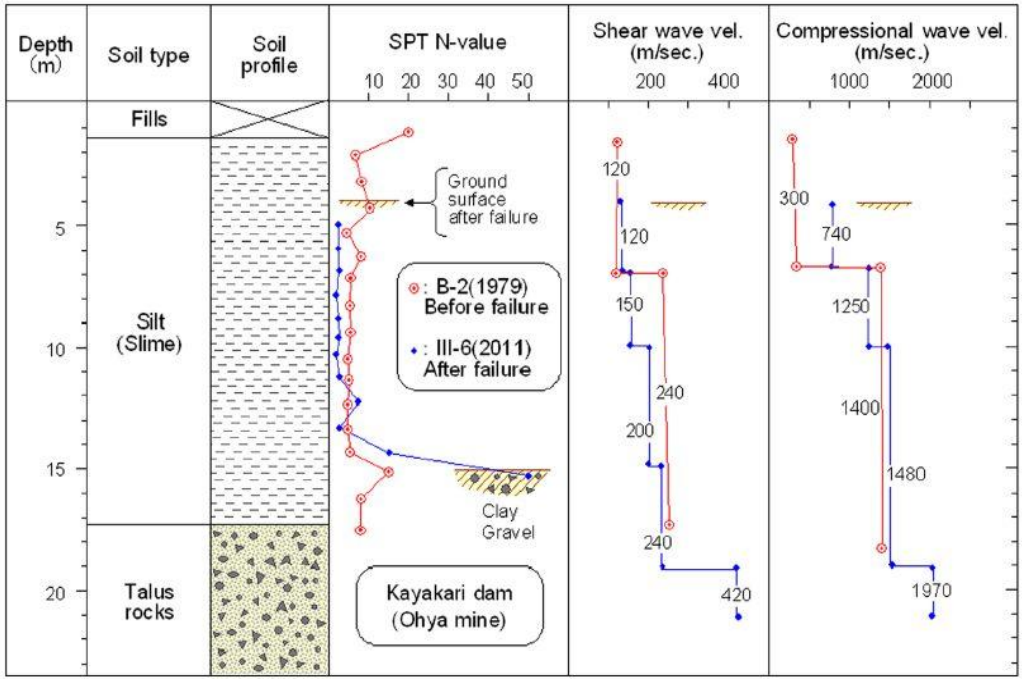

Figure 4.14: Soil profiles of B-2 and III-6 before the failure and after the earthquake

Figure 4.14 depicts that the N-values of SPT in 1979 study are greater than those after the failure. The shear wave velocity values also show the same trend as SPT N-values for before and after failure. The soil profiles at unchanged portions of dam, I-2 and B-1, are shown altogether in Figure 4.15 to draw a comparison between 2011 and 1979 data. The Figure 4.15 depicts a significant decrease in SPT N-value and shear wave velocity value after liquefaction occurrence.

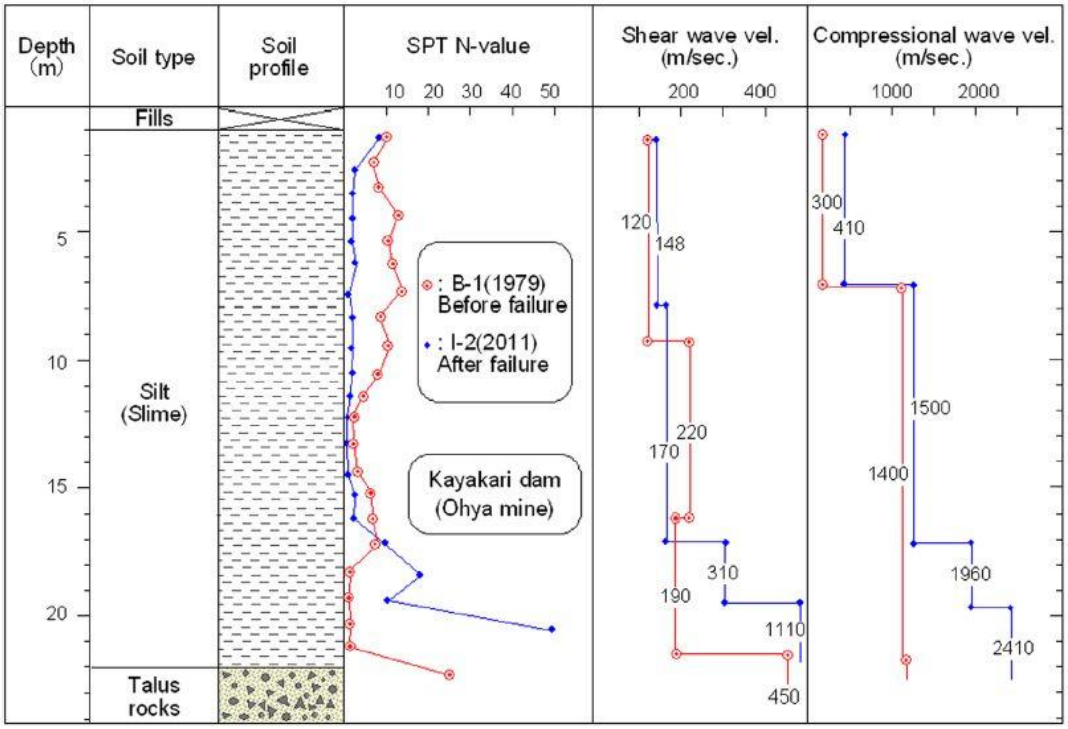

Figure 4.15: Soil profiles of B-1 and I-2 before the failure and after the earthquake

Chapter 5

MEASUREMENTS OF CYCLIC RESISTANCE AND SHEAR WAVE VELOCITY IN THE LABORATORY

5.1 Introduction

Undisturbed samples from the tailings disposal pond contained fairy large amount of non-plastic fines up to a maximum of 90%. The sampling tubes were transported directly to the laboratory and the vinyl chloride tubes were cut crosswise and test specimens extruded. The specimens were trimmed carefully to a cylindrical shape with 5 cm in diameter and 10 cm in height. After consolidating the specimens to a confining pressure circa 1.1 times the in-situ effective overburden pressure, the tests were performed using the cyclic triaxial test apparatus. The reason of choosing 1.1 times was simply to bring the samples to normally consolidated state as it was in situ. In this test scheme on samples from the tailing dam, shear wave measurement was not carried out in the laboratory.

Tube samples from Asahi site contained fines about 30% and thus were hung vertically overnight at the site to drain excess water. The partially saturated sands in the tubes were frozen in the field and then transported to the laboratory of the Chiba Engineering Co., Ltd. About half of the samples were tested there, but V_S measurements were not performed in the laboratory tests. Thus, only the V_S-values measured in situ by the method of the downhole logger were used for data processing. The remaining half of the undisturbed samples was transported to the laboratory of Kiso-Jiban Consultants Co., Ltd. and tested there. Details of the tests

for measuring liquefaction resistance and shear wave velocity are described in the following sections.

5.2 Sample Preparation and Required Equipment

5.2.1 Trimming of Undisturbed Frozen Soil Sample

The frozen soil from long tube were vertically extruded by means of a hydraulic sample extruder, and were cut off at 150-170 mm in height by hacksaw. Then, the specimens were trimmed off 50 mm in diameter using trimmer and straight edge, and cut into 100 mm long using miter box and straight edge or knife as well. After wrapping them up in plastic wrap, they were stored in the freezer of the laboratory. Details of trimming are illustrated in Figure 5.1 as follows:

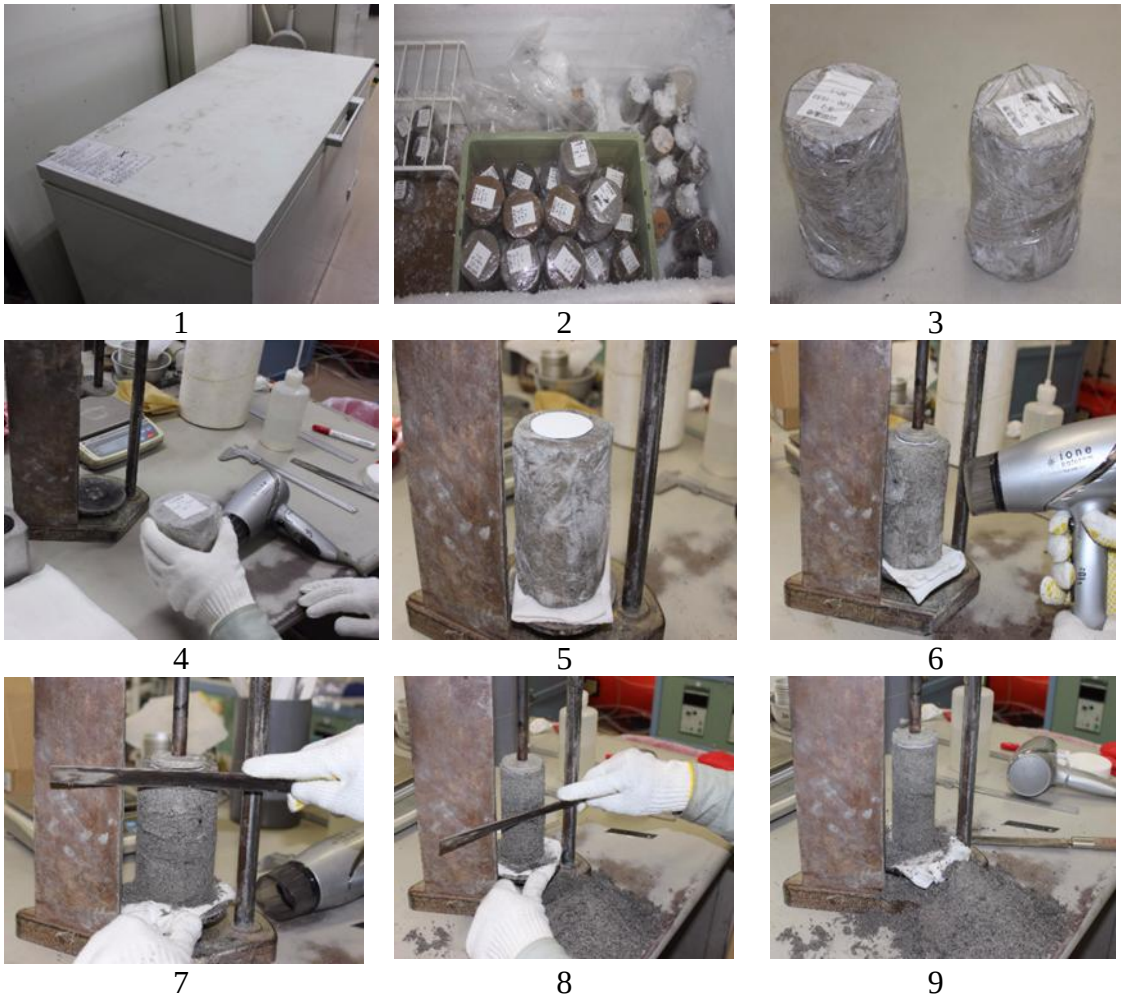

1 2 3

4 5 6

7 8 9

Figure 5.1: Trimming of undisturbed frozen soil sample

1) The extruded frozen specimens shall be cut off from the long tube into specified height, and shall then be kept in freezer after being wrapped in plastic wrap as shown in Figures 5.1.1-5.1.3.

2) The specimen shall be taken out from freezer after wearing industrial safety

gloves as shown in Figures 5.1.3-5.1.4.

3) The specimen shall be set on the trimmer after placing tissue paper on the top and the bottom of the sample as shown Figure 5.1.5.

4) Trimming of the specimen should be carried out carefully while the surface of the specimen is melting by a hot-air blower (a hair dryer) as shown in Figures 5.1.6-5.1.8.

5) A diameter of the specimen shall be made as designated size as shown in Figure 5.1.9.

6) The specimen shall be taken from trimmer, supported by miter box, as shown Figures 5.1.10-5.1.11.

7) The both ends of the specimen shall be made flat by miter box and special knife as shown in Figure 5.1.12.

8) The specimen after trimming with approximately 50 mm in diameter and 100 mm in height is shown in Figures 5.1.13-5.1.14.

9) The specimen shall be frozen in the freezer for 1 hour as shown in Figure 5.1.15.

10) The diameter and the height of the test specimen shall be measured by Vernier Caliper as shown in Figure 5.1.16.

11) The diameter and the height of the test specimen shall be measured by Vernier Caliper as shown in Figure 5.1.16.

12) The weight of the specimen shall be measured as shown in Figure 5.1.17.

13) The specimen shall be kept in a freezer so that it is prepared for using in the cyclic triaxial test as shown in Figures 5.1.18-5.1.20.

5.2.2 Reconstituted Specimens

The reconstituted specimens are required to have the same dry density and water content as undisturbed ones using a kind of moist placement method, in order to draw a rational comparison between undisturbed and disturbed samples. In the case of sample preparation, the soil of undisturbed samples was first separated from crushed shells. Based on specified density obtained from cyclic triaxial tests on undisturbed samples, weighed water is secondly added to air-dried soil sample to approach determined water content, and then they are homogenously mixed together. Next, the weighed wet soil samples were thirdly divided into 5 equal segments which were gently temped layer by layer, i.e. 5 layers, in “external” split forming mold, that is, this mold is not joined triaxial chamber and a 2.81-kg cylindrical weight on which circular lines are carved 20 mm away from each other to help experimenters to tamp soils accurately in 20-mm layers, as shown in Figure 5.2.1-5.2.9 in detail, respectively.

However, sample preparation is not easy while the density is too low, or the water content is too high because of membrane penetration or water bleeding from the mold. Under certain circumstances, low water content, e.g. 15% as well as the same void ratio as the corresponding undisturbed sample are selected to prepare the

reconstituted sample because it is known that the same void ratio with various water content yields the identical liquefaction resistance.

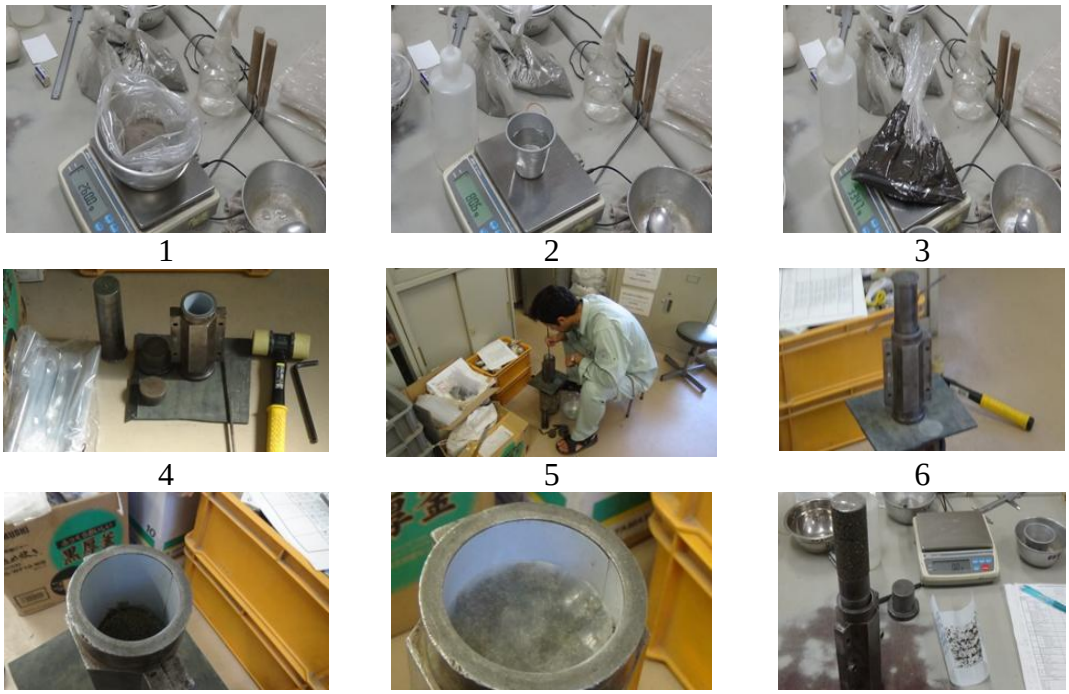

1 2 3 4 5 6 7 8 9

Figure 5.2: Preparation of reconstituted samples

5.2.3 Setting-up the Specimen to Triaxial Cell

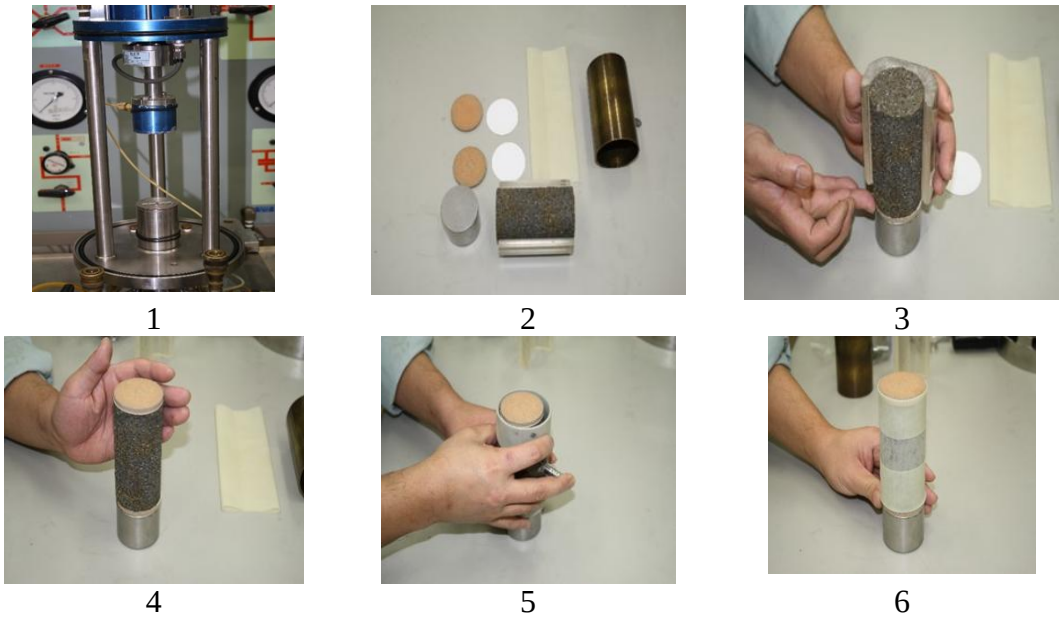

1 2 3 4 5 6



7 8 9

Figure 5.3: Setting-up the Specimen to Triaxial Cell

depicts the setting-up processes of sample in the tiaxial cell, described as follows:

1) Triaxial Cell used is shown in Figure 5.3.1
2) Specimen, porous stones, rubber membrane, and filter papers used are shown in Figure 5.1.2
3) After setting the porous stone on a base, the specimen shall be placed on the cylindrical base, and the porous stone shall be placed on the top of the specimen as shown in Figures 5.1.3-5.1.4
4) The specimen shall gently be covered by the rubber membrane without knocking the side of the specimen. The rubber membrane is folded at the top and the bottom of the specimen as shown in Figures 5.1.5-5.1.6
5) After setting the specimen in a cell for the triaxial test, the rubber membrane shall be unfolded and extended over the pedestal and the top cap as shown in Figures 5.1.7-5.1.8
6) O-rings shall be placed for sealing as shown in Figure 5.1.9

5.3 Cyclic Triaxial Test Apparatus and the Procedure of Test

5.3.1 Cyclic Triaxial Apparatus for Measuring Liquefaction Resistance

The cyclic triaxial testing apparatus illustrated in Figures 5.4 -5.6 include as follows:

1) Triaxial cell: top cap and pedestal for sample dimensions of 50 mm × 100 mm

2) Loading equipment (hydraulic or pneumatic control equipment): shaft load (about 1kN) varies slightly depending on Frequency 0.1 ~ 0.5Hz

3) Lateral pressure: 500 kPa (200 kPa back pressure at the same time)

4) Computer: Windows7, VBasic6.0

5) Controller and data acquisition

Figure 5.4: Hydraulic cyclic triaxial test apparatus used for reconstituted samples in The laboratory of Kiso-Jiban consultants Co. Ltd

Figure 5.5: Pneumatic cyclic triaxial test apparatus used for undisturbed samples in the laboratory of Kiso-Jiban consultants Co. Ltd

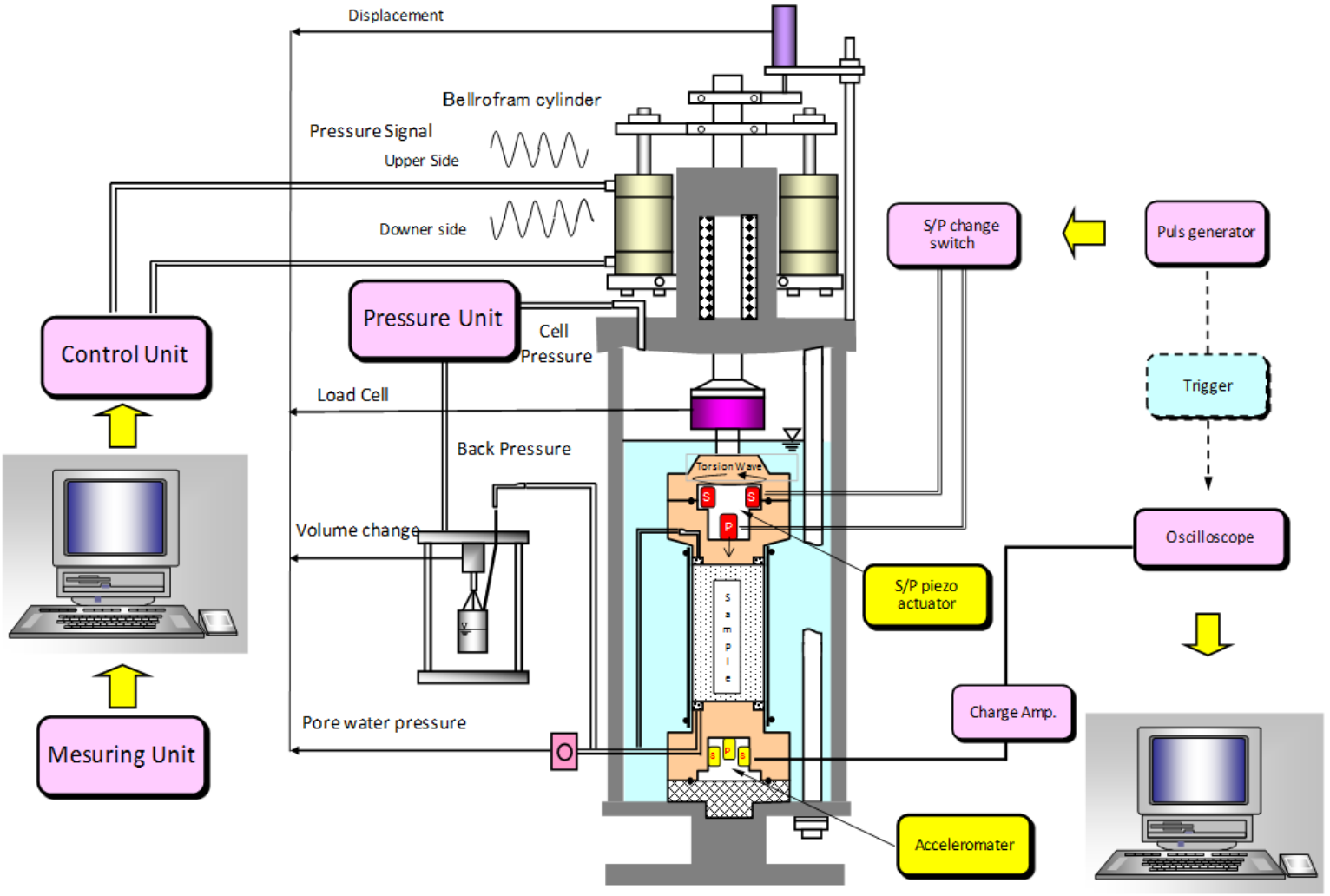

Figure 5.6: Schematic diagrams of cyclic triaxial apparatus and V_S and VP measuring device

5.3.2 The Procedure of Cyclic Tiaxial Test for Measuring Liquefaction Resistance

The tests were carried out in accordance with the Testing Standard of Japanese Geotechnical Society (Designation: JGS 0541-2000), which is termed "Method for Cyclic Undrained Triaxial Test on Soils". The procedure of this test is described step by step as follows:

For the sample set-up: the frozen sample was enclosed in rubber membrane as illustrated above, and was vertically placed between the pedestal and top cap in the triaxial cell after measuring the weight, the length (twice), and the diameter (6 times), i.e. twice on the bottom, the middle and the top, of the sample.

For thawing: the sample was allowed to thaw for approximately 1-2 hours while a slight 20 kN/m^2 vacuum was previously employed to keep the sample shape constant. After having completely thawed, the diameter and the height of the sample were measured for 6 times and twice, respectively, with Vernier Caliper. Next, the triaxial cell was set up around the sample and the water was then let to enter into it. In this step, the vacuum was slowly decreased to zero while the cell pressure was simultaneously increased to the value of 20 kN/m^2.

For carbon dioxide percolation: CO_2 gas was allowed to percolate slowly into the sample for 30-60 minutes, which is dependent on the amount of fine content, by openning the drainage valves of the pedestal and the top cap, in order to release the air bubbles entrapped in the water, and to replace carbon dioxide instead in the voids of sample.

For saturation and checking B-value: the de-aired water was allowed to flow slowly into the sample for approximately 30-60 minutes, or the 300 mls of that were run through it, in order to fill up all voids and let the sample well-saturated. Next, a 200 kN/m^2 back pressure was gradually employed while the cell pressure was automatically increased with 20 kN/m^2 difference. Applying the back pressure was lasted approximately 10 minutes at constant differential head because of better saturation. Then, the B-value of the sample, the ratio of the pore water pressure to cell pressure, was determined by increasing the cell pressure up to 50 kN/m^2, and measuring the change of the pore water pressure from the bottom drainage line connected to a pore water transducer. This procedure shall be repeated until a B-value of 0.95 or more is achieved.

For consolidation and cyclic triaxial test: the sample was isotropically consolidated to a specified effective confining pressure resulting from the difference between the cell pressure and back pressure after the saturation had been achieved. The effective confining pressure is dependent on the depth at which the undisturbed sample was extracted from the field.

Furthermore, as soon as the consolidation of the sample was fully accomplished in a drained condition for approximately 30-90 minutes, the sample was subjected to cyclic axial load in the form of 0.2 Hz sinusoidal wave in un-drained condition until the axial deformation of the sample reached up to 10%. Throughout cyclic loading, the values of axial deformation and load, and change in pore water pressure were automatically recorded with time at the constant cell pressure. the cyclic axial load is applied as many times as necessary to produce a state of liquefaction and continued further on until progressive development of axial strain was achieved up to about 10% in

double-amplitude. The tests as above were repeated 2~4 times by employing different cyclic stress ratios to determine the cyclic strength, R_L, for each of the specimens from the same depth which are conceived to have identical mechanical characteristics.

Post-liquefaction volume change: After finishing the cyclic loading tests as above, the valve of the pore water drainage line in the apparatus was opened and the volume of drained water measured about 30-60 minutes drainage by an electronic balance or a graduated burette. The amount of drained water divided by the specimen's volume was defined as the post-liquefaction volumetric strain, which can be used to estimate the settlement of the ground surface due to liquefaction. Following cyclic triaxial tests, index property tests were conducted on all undisturbed specimens to determine density, limiting void ratios and specific gravity, the values of which will be shown in next chapter. The grain size distribution curves of all undisturbed samples form Asahi site are shown in Figure 5.7.

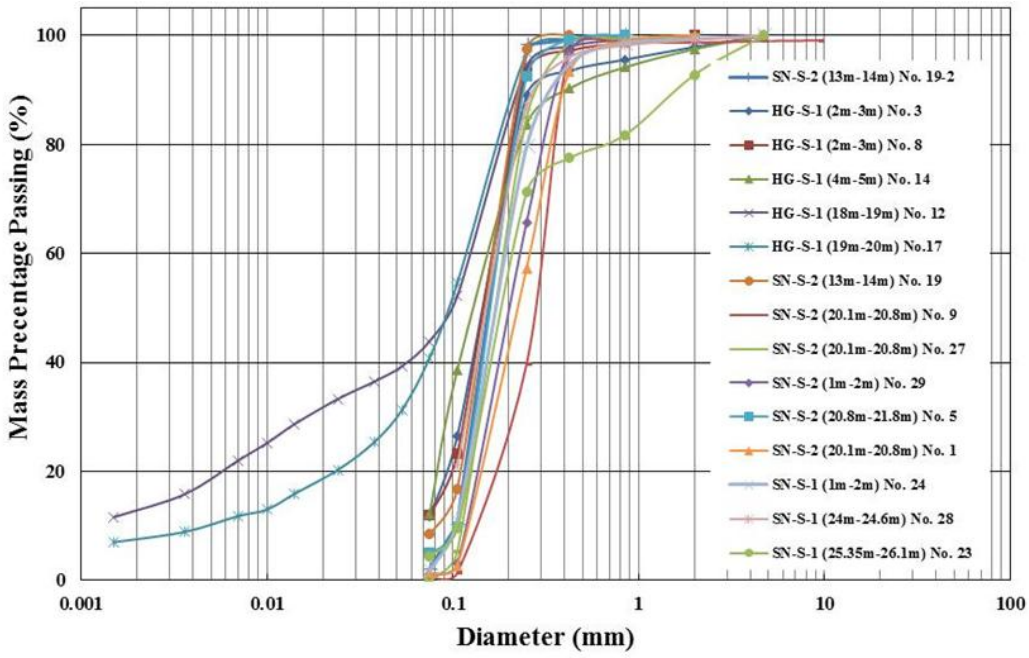

Figure 5.7: Grain size distributions of undisturbed specimens from Asahi site

5.4 The Procedure of the V_S and V_P Measurement

The triaxial test apparatus is equipped with a device to apply torsional impulse (step signal) at its top cap and to pick up the impulse transmitted through the specimen from a receiver at the pedestal. By dividing the length of the specimen by the time of transmission of the impulse, which was calculated by first arrival method, the shear wave velocity, V_S, was obtained. It is to be noted that the impulse produces only an infinitesimal strain in the specimen. Then, the phase of this test can be considered as non-destructive. In this experiment, the V_S and V_P were measured twice after these steps, i.e. consolidation, liquefaction in un-drained condition and approximately 30-60 minutes after opening the drainage value.

The applicability of this device is somewhat the same as bender element in practice. However, it generates torsional movement to send an impulse through the sample without any disturbance by entering small tools into the bottom and top of the sample as shown in Figure 5.8.

Figure 5.9 and figure 5.10 show that the system generally consists of (1) P and S Wave Generator and Driving Unit, (2) Receiver Accelerometer and Receiving Unit and (3) P/S Switching Unit. The P and S wave generators are built-in to the top cap and the receiver accelerometer is built-in to the pedestal.

Figure 5.8: The top cap and pedestal of triaxial cell

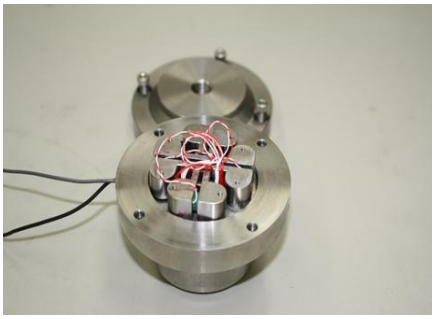

Figure 5.9: Compression and Shear Waves Generator

Figure 5.10: V_S and V_P measurement system

5.5 Results of Tests on the Undisturbed and Reconstituted Samples

Based on the laboratory tests on the undisturbed and reconstituted samples from Asahi and Nagoya sand deposits, multiple series of results were obtained from cyclic triaxial tests and shear-wave velocity measurement system. Details of these results are described as follows:

5.5.1 Triaxial Liquefaction Curves

For the purpose of determining the liquefaction resistance, one of the most significant results from cyclic triaxial tests is the plot of cyclic resistance ratios versus number of cycles. The results of this section are related to the undisturbed samples from Asahi, and reconstituted samples from Asahi and Nagoya.

5.5.1.1 Triaxial Liquefaction Curves of Undisturbed Samples from Asahi Site

Since about half of the undisturbed samples extracted from the Asahi field were delivered to Kisi-Jiban consultants Co. (KJCC), there was not enough number of samples (3 or 4) for plotting triaxial liquefaction curves at some of depths. Thus, the results of Chiba Engineering Co. (CHEC) were used at those depths so that the reasonable estimates of liquefaction resistance were made for undisturbed soil samples. In this case, these plots are shown from Figure 5.11 to Figure 5.17. The red color means that the undisturbed samples were tested by Kisi-Jiban consultants Co., whereas black color indicates the results of Chiba Engineering Co. the shapes of the circle, the rectangle, triangle, diamond, solid circle are indicative of 1%, 2%, 5%, 10% double-amplitude axial strains, and 95% pore water pressure build-up.

5.5.1.2 Triaxial Liquefaction Curves of Reconstituted Samples from Asahi Site

In the Figure 5.18, all the results related to reconstituted samples, made from the undisturbed samples of Asahi site, are gathered by connecting the points showing cyclic stress ratio in 20 cycles at 5% Double Amplitude of axial strain.

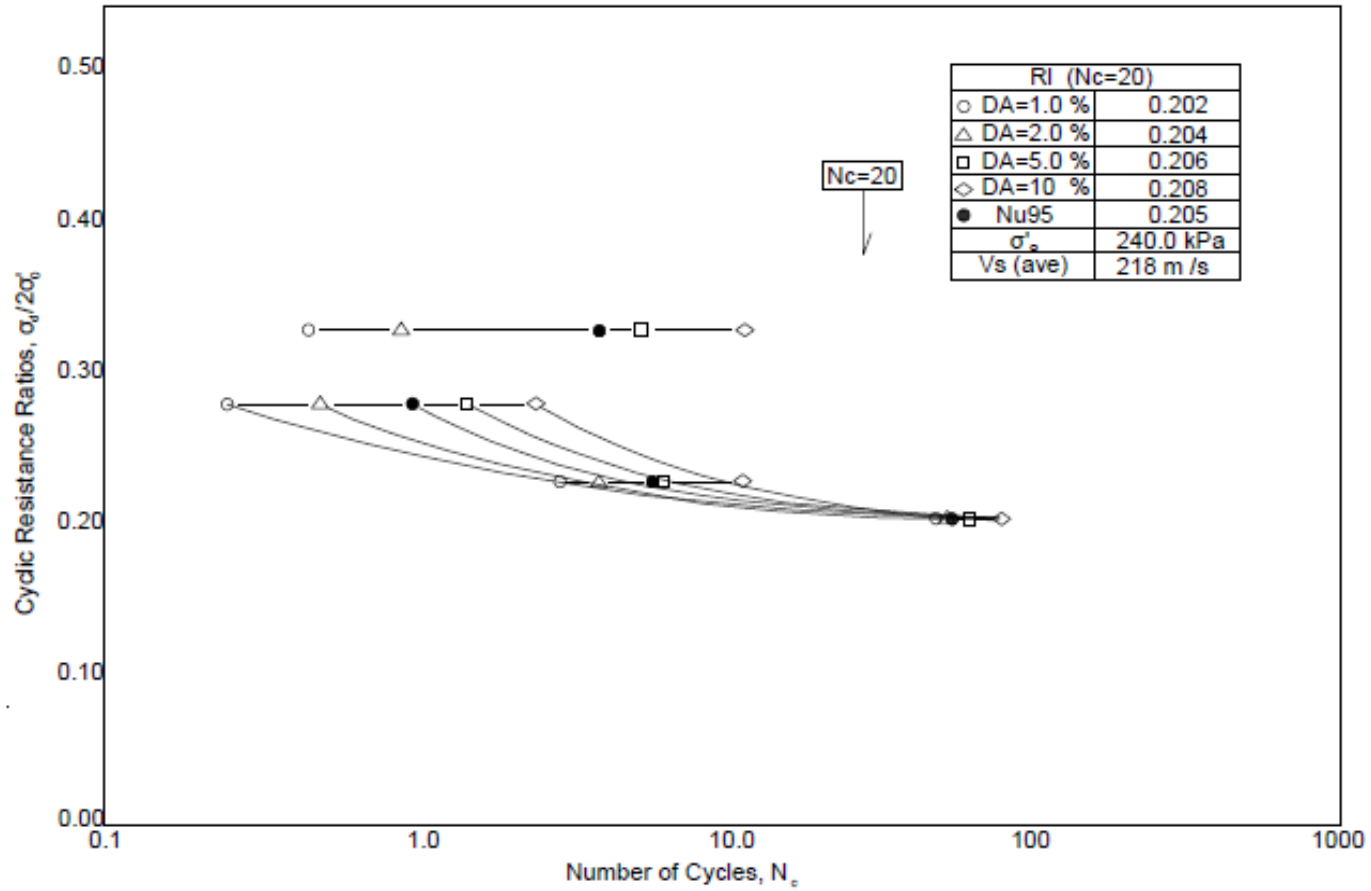

Figure 5.11: Triaxial liquefaction curves for No. 1, 9, 27 &29 [SN-S-2 (20.1m-20.8m)] by KJCC

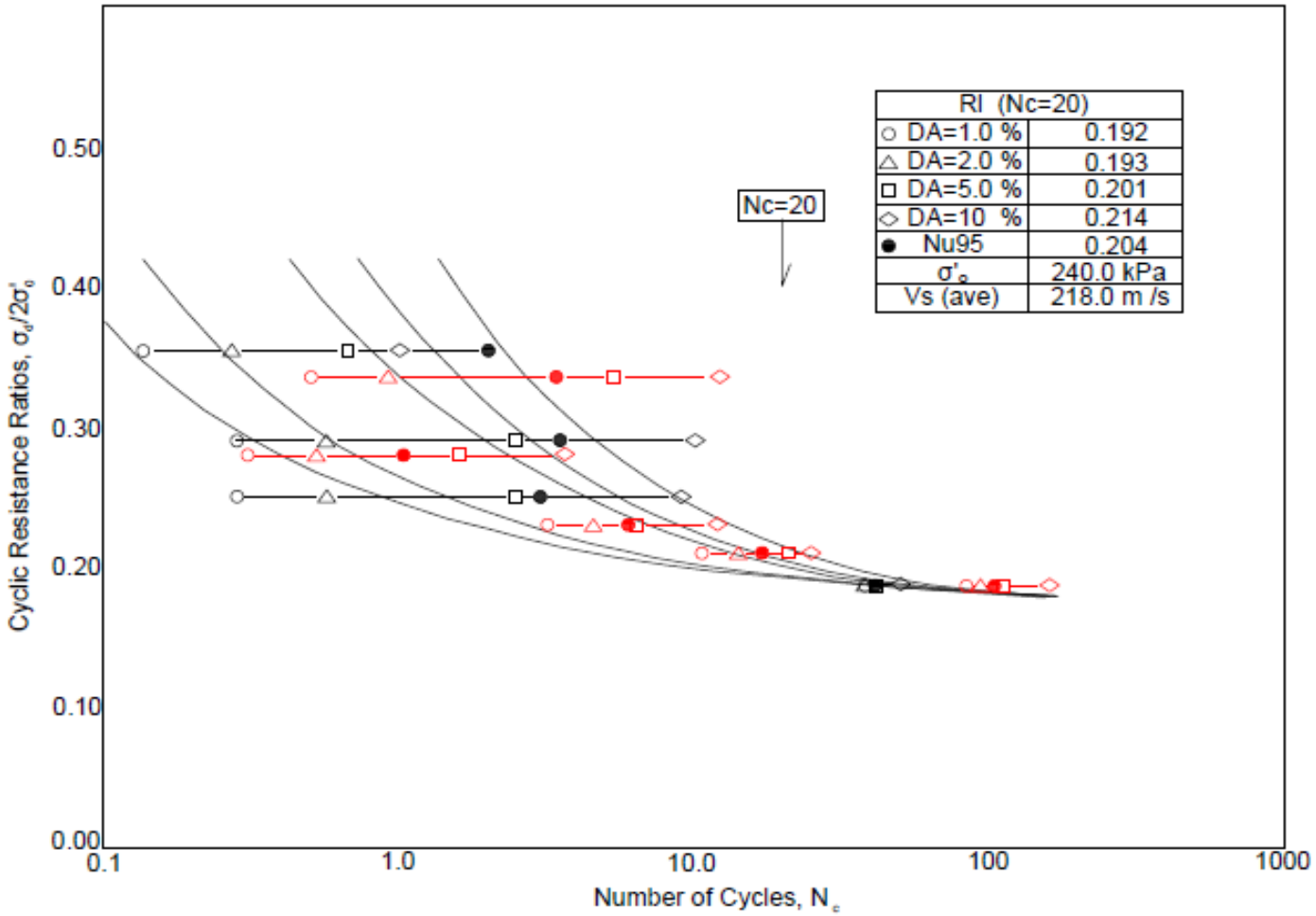

Figure 5.12: Triaxial liquefaction curves for No. 1, 5, 9, 27 &29 [SN-S-2 (20.1m-20.8m)] by KJCC&CHEC

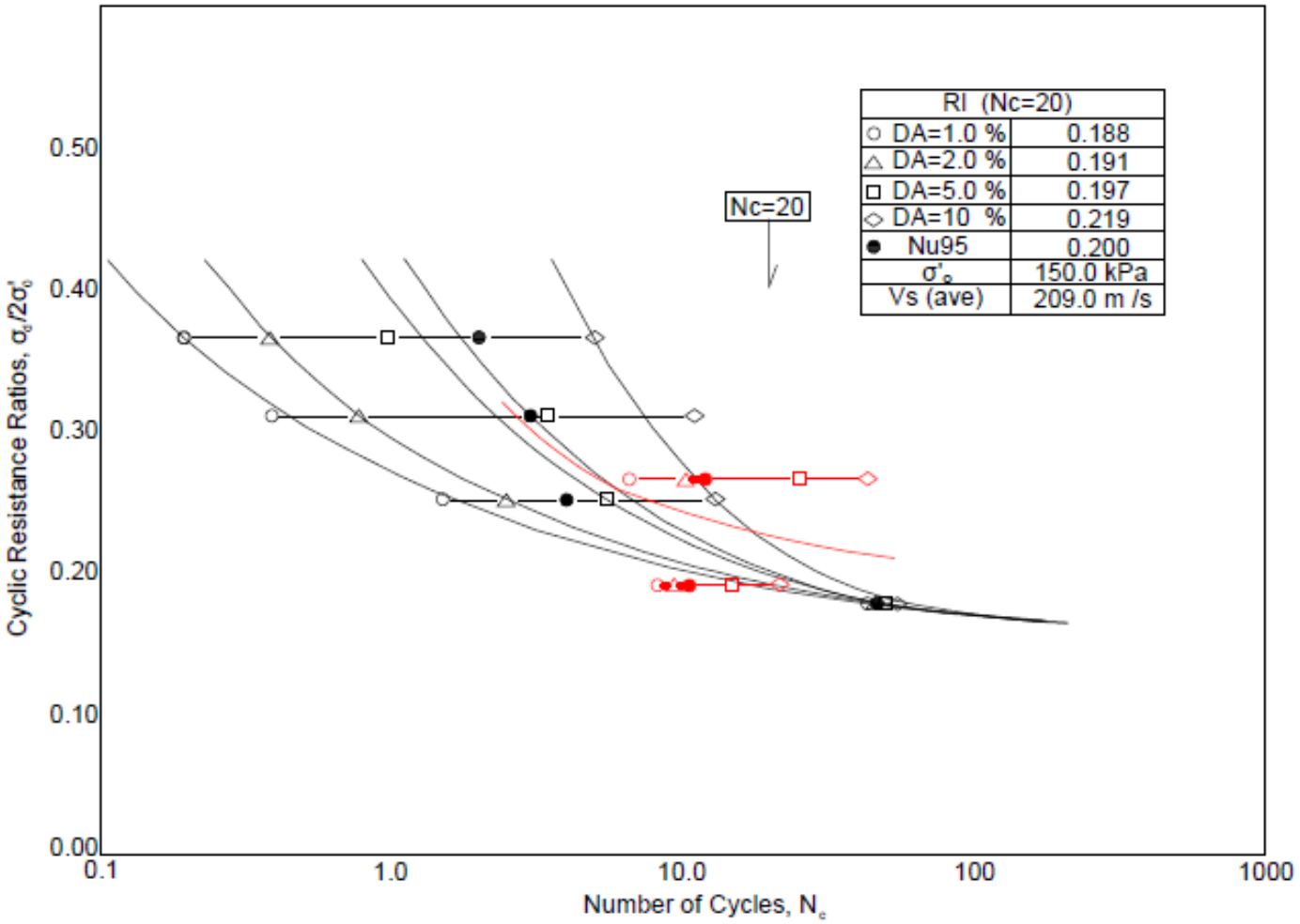

Figure 5.13: Triaxial liquefaction curves for No. 19 & 19-2 [SN-S-2 (13.0m-14.0m)] by KJCC&CHEC

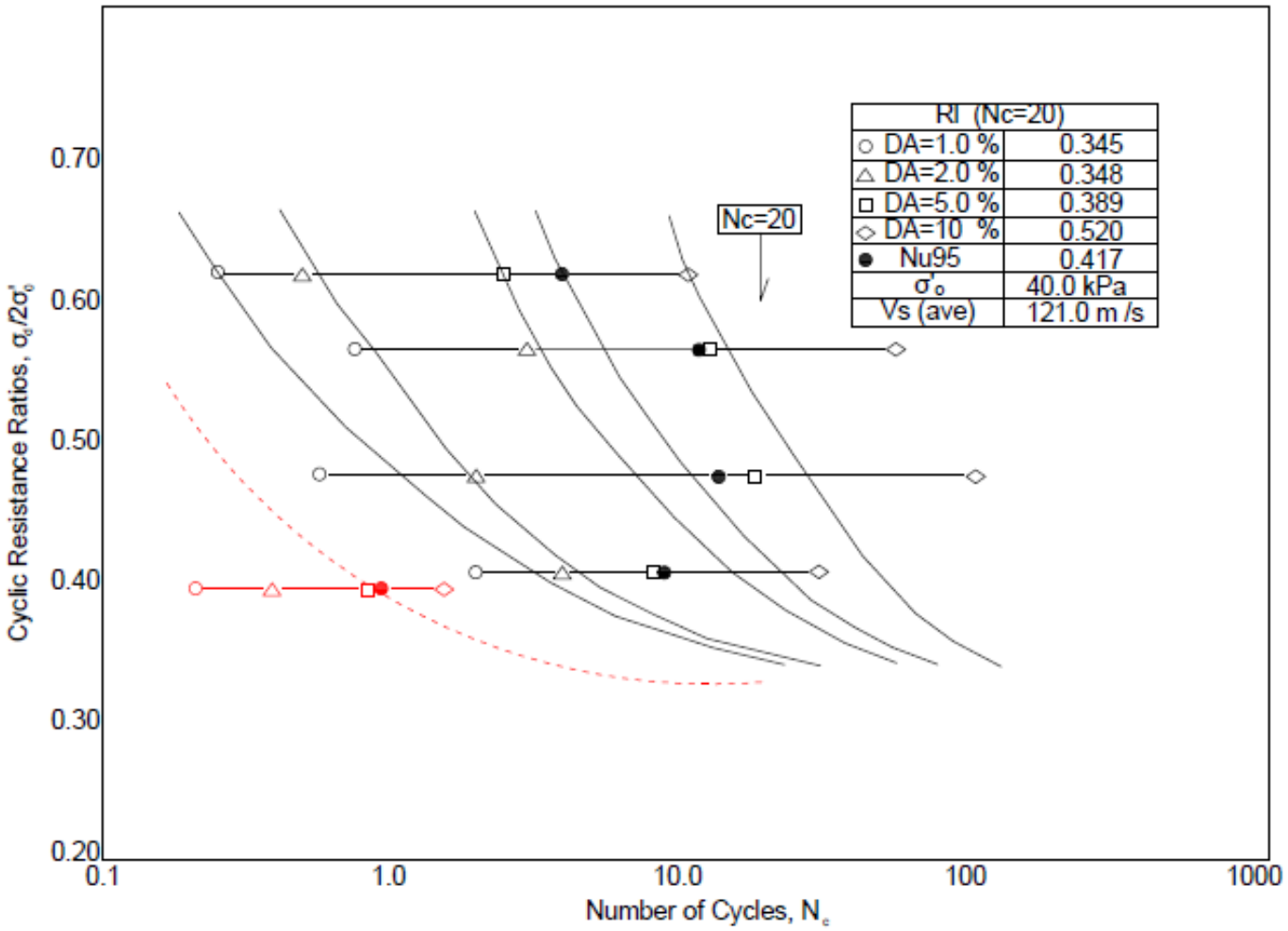

Figure 5.14: Triaxial liquefaction curves for No. 24 [SN-S-1 (1.0m-2.0m)] by KJCC&CHEC

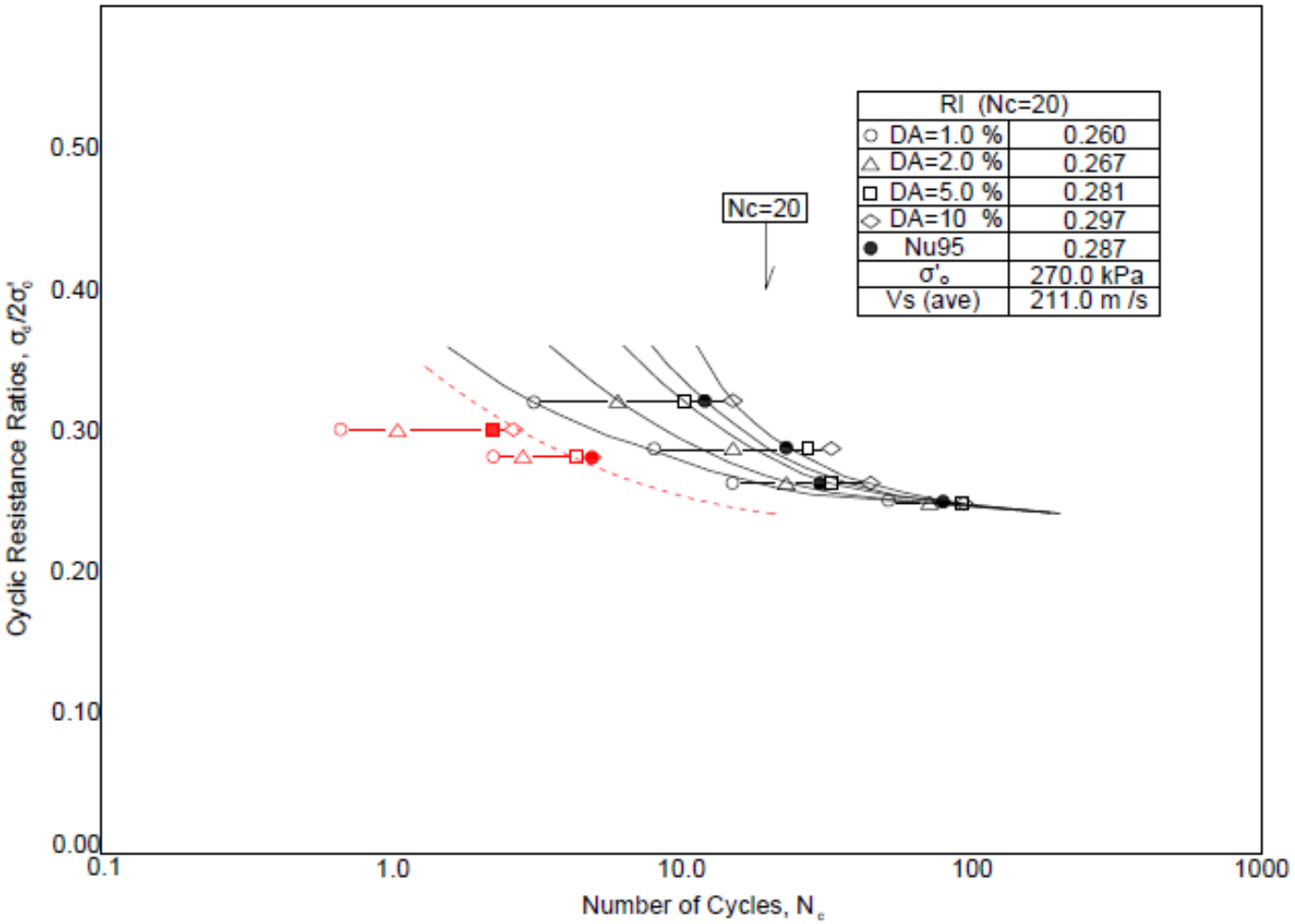

Figure 5.15: Triaxial liquefaction curves for No. 23 & 28 [SN-S-1 (24.0m-26.1m)] by KJCC&

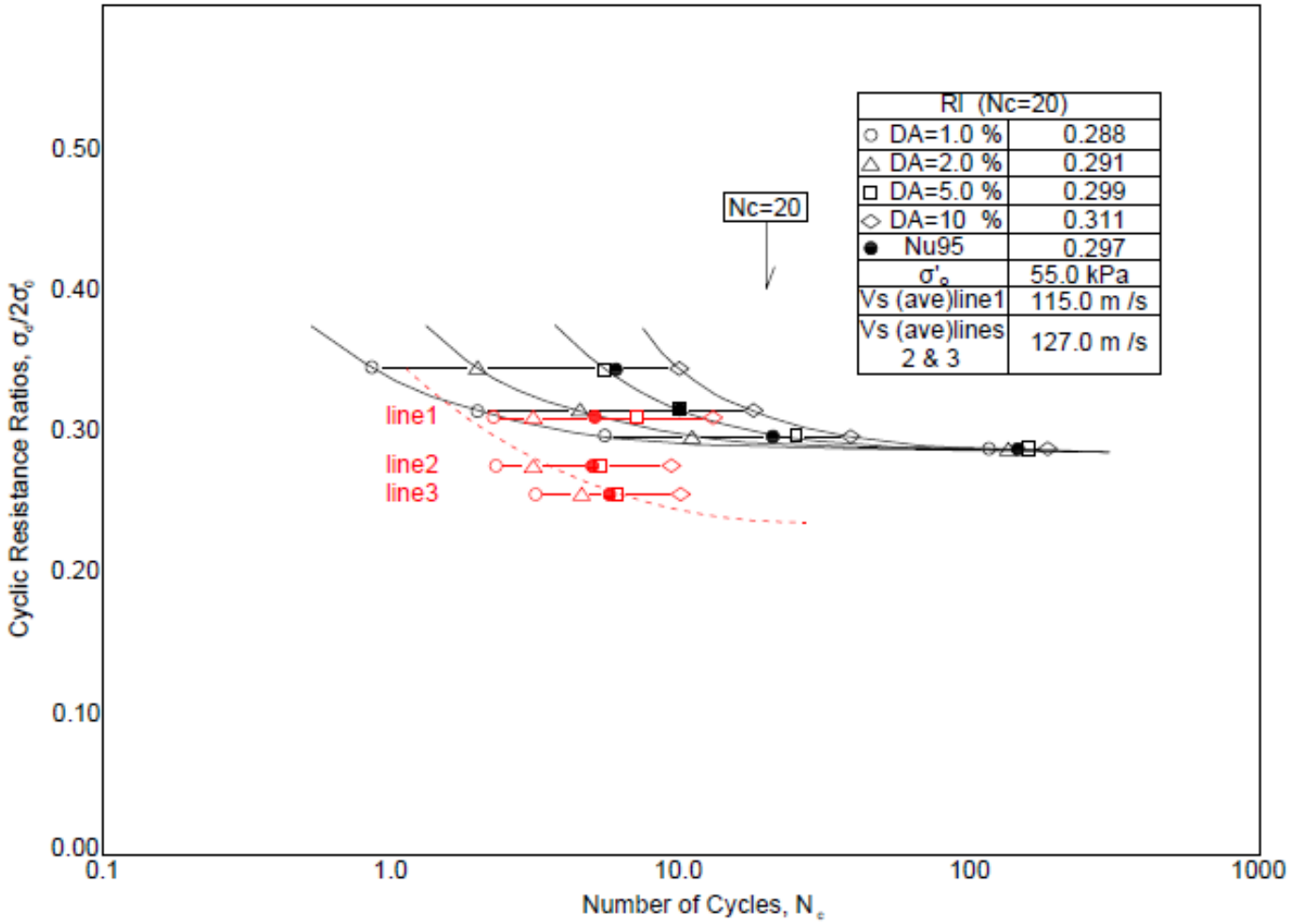

Figure 5.16: Triaxial liquefaction curves for No. 3, 8 & 14 [HG-S-1 (2.0m-3.0m) & (4.0m-5.0m] by KJCC&CHEC

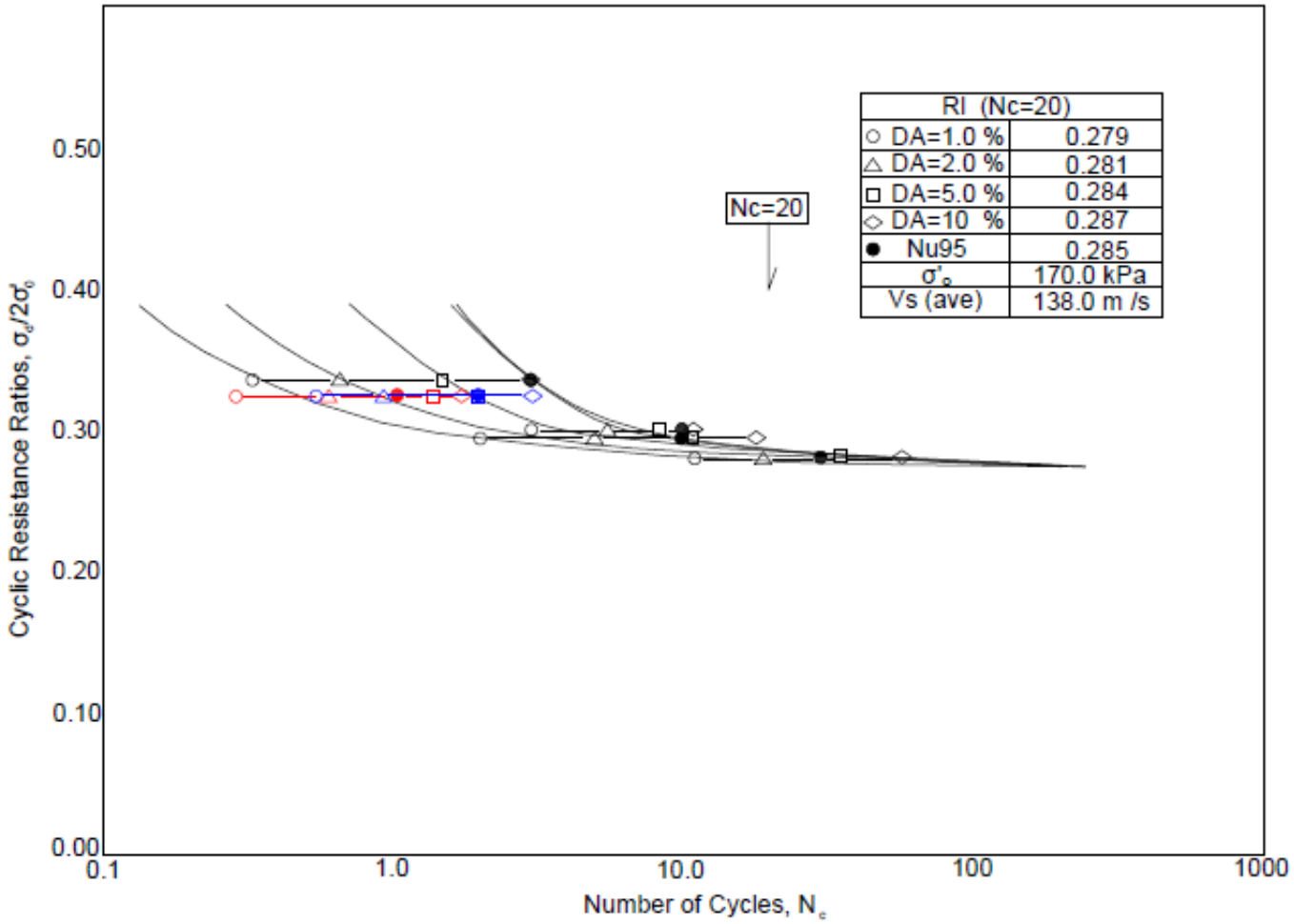

Figure 5.17: Triaxial liquefaction curves for No. 12 & 17 [HG-S-1 (18.0m-20.0m)] by KJCC&CHEC

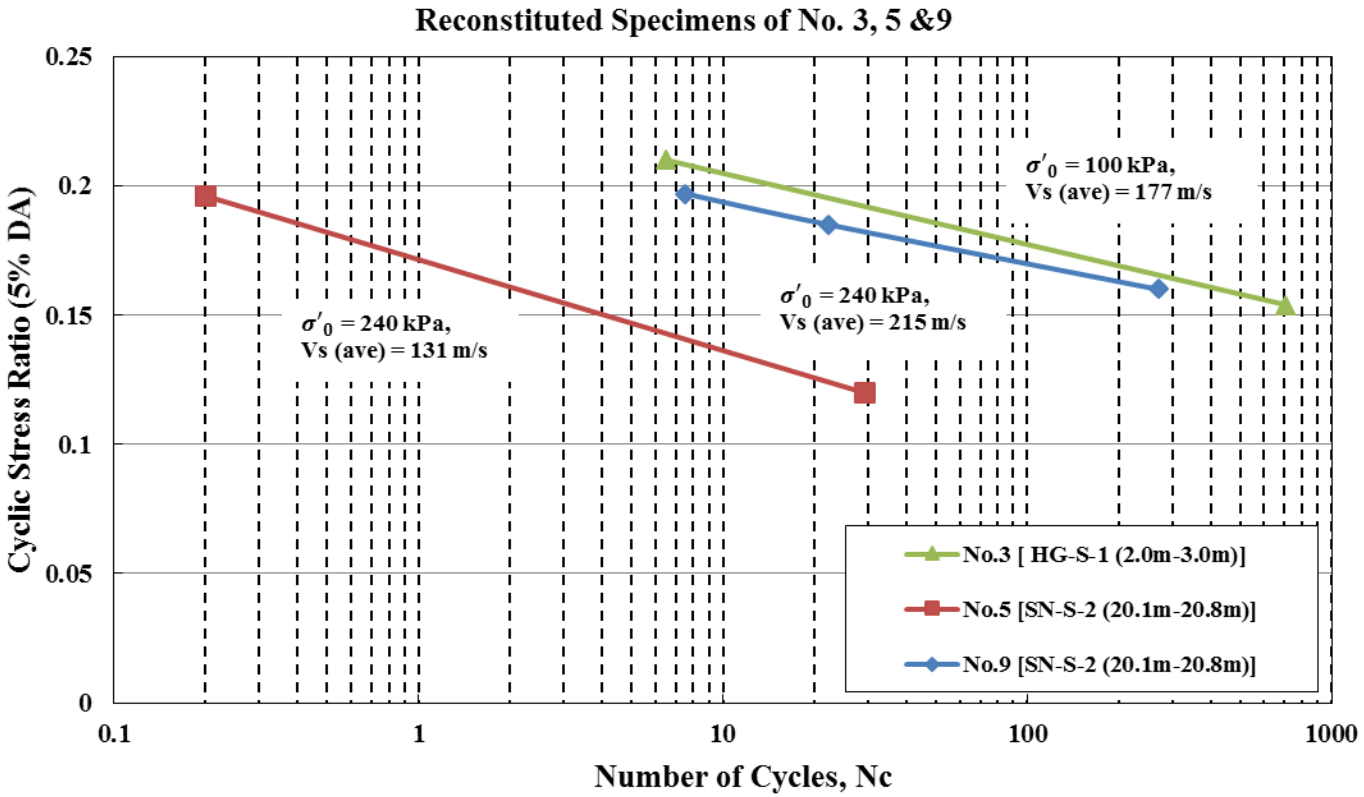

Figure 5.18: Triaxial liquefaction curves for reconstituted samples from Asahi site

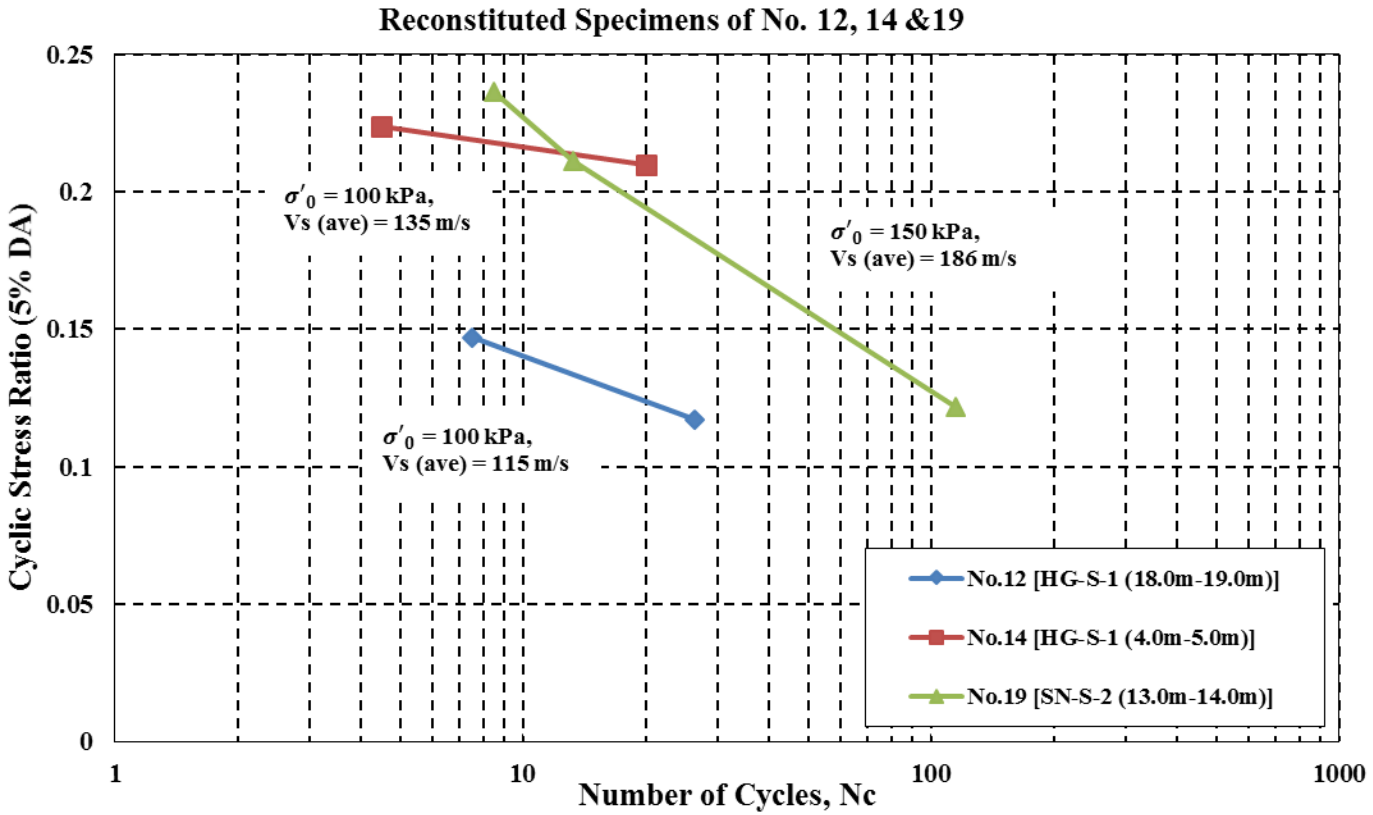

Figure 5.18: Triaxial liquefaction curves for reconstituted samples from Asahi site (Continued)

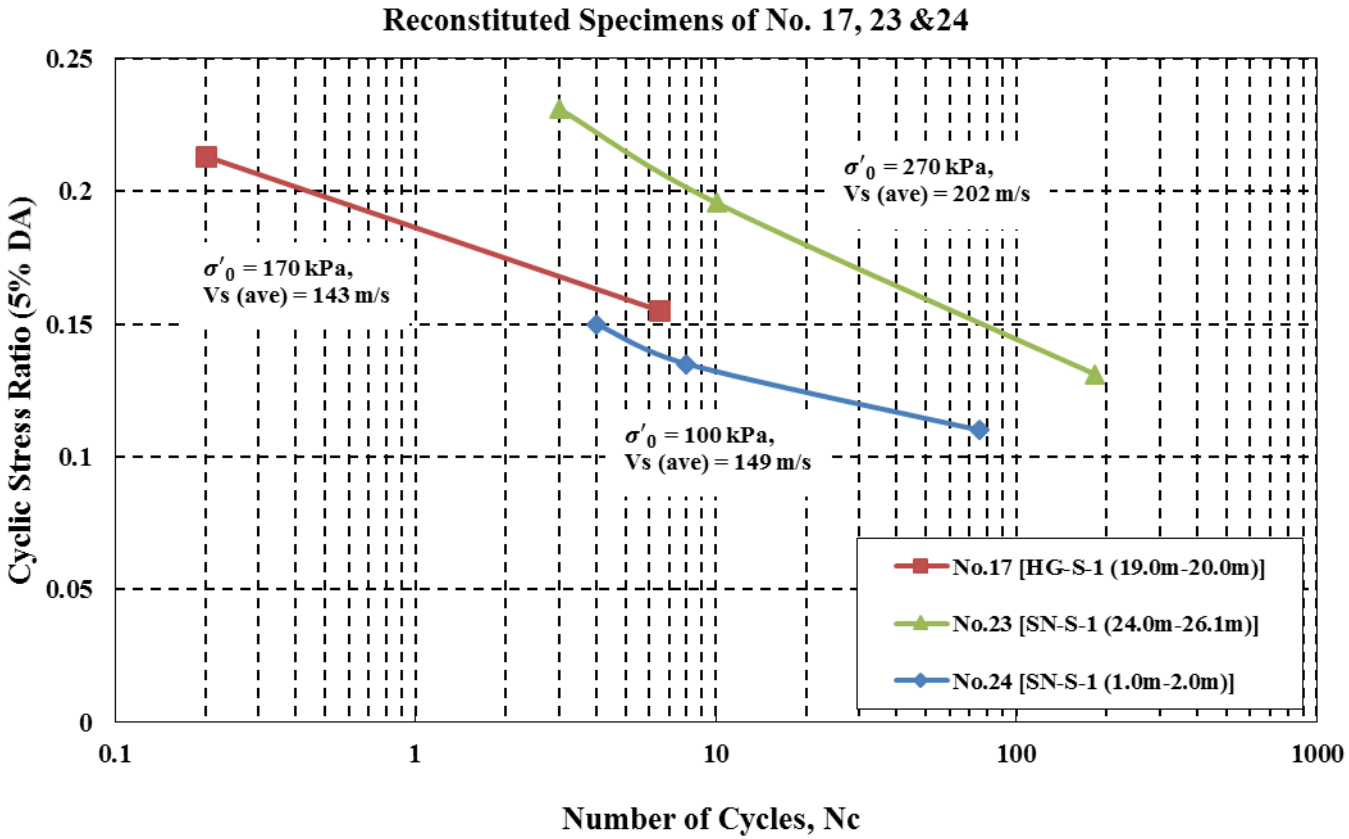

Figure 5.18: Triaxial liquefaction curves for reconstituted samples from Asahi site (Continued)

5.5.1.3 Triaxial Liquefaction Curves of Reconstituted Samples from Nagoya Sand

For supplementary tests, a number of cyclic triaxial tests were conducted on Nagoya sand with relative densities of 50% and 70% in three different fines contents of 0%, 10% and 30% as shown in Figure 5.19 and Figure 5.20 six curves were passed through the points obtained from cyclic stress ratio in 20 cycles at 5% Double Amplitude as shown Figure 5.21.

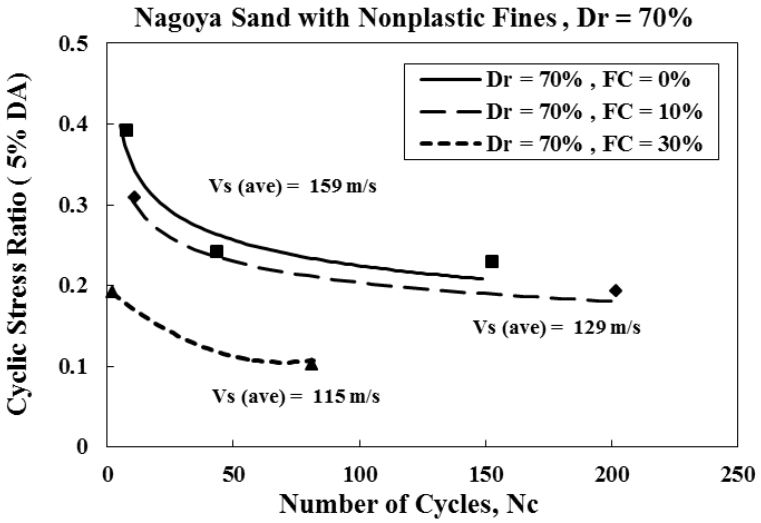

Figure 5.19: Triaxial liquefaction curves for Nagoya sand with nonplastic fines at relative density of 70%

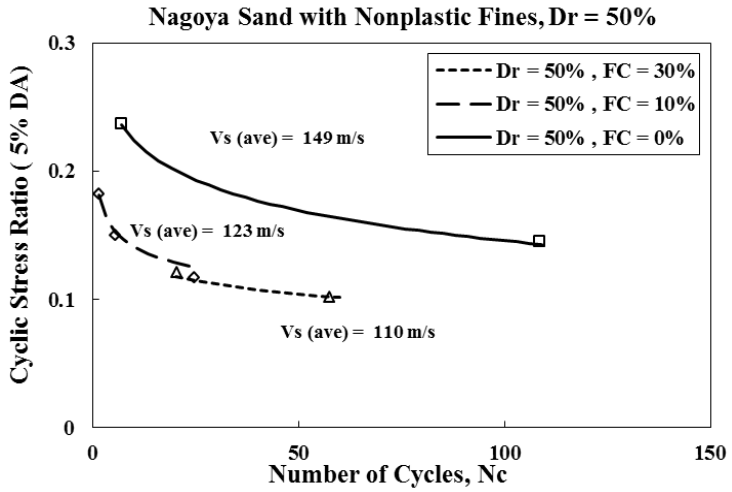

Figure 5.20: Triaxial liquefaction curves for Nagoya sand with nonplastic fines at

relative density of 50%

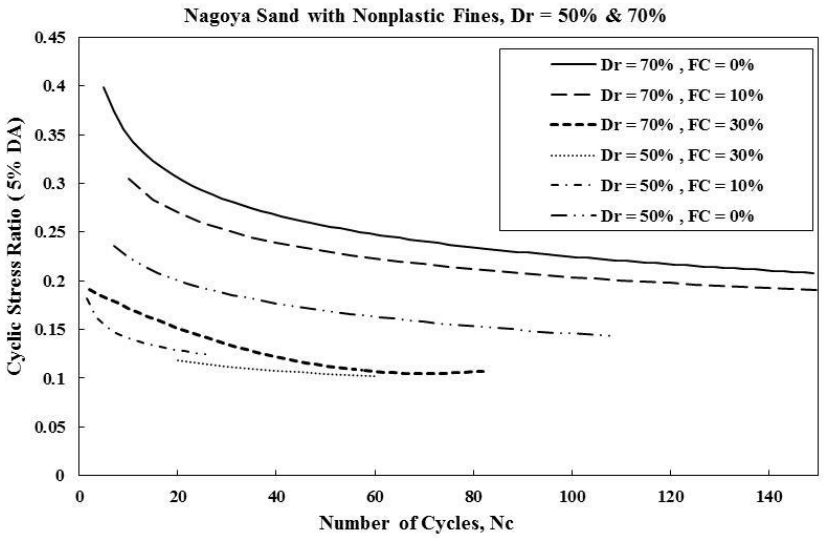

Figure 5.21: Triaxial liquefaction curves for Nagoya sand with nonplastic fines and different relative densities

5.5.2 Deviator Axial Stress, Stress Path and Pore Water Pressure

Figure 5.22 depicts deviator axial stress versus axial strain, stress path, and pore water pressure, axial strain and deviator stress versus number of cycles of the undisturbed sample [No.1, SN-S-2(20.10m-20.08m)]. The entire results of these plots are illustrated in Appendix A.

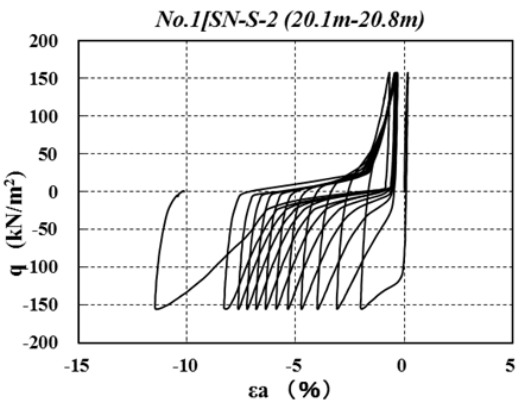

(a). Deviator stress versus axial strain.

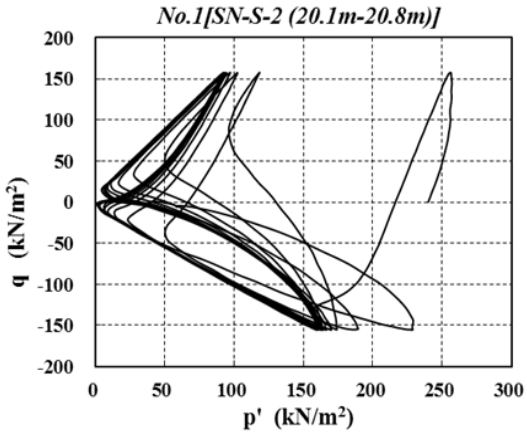

(b). Stress path during the undrained condition.

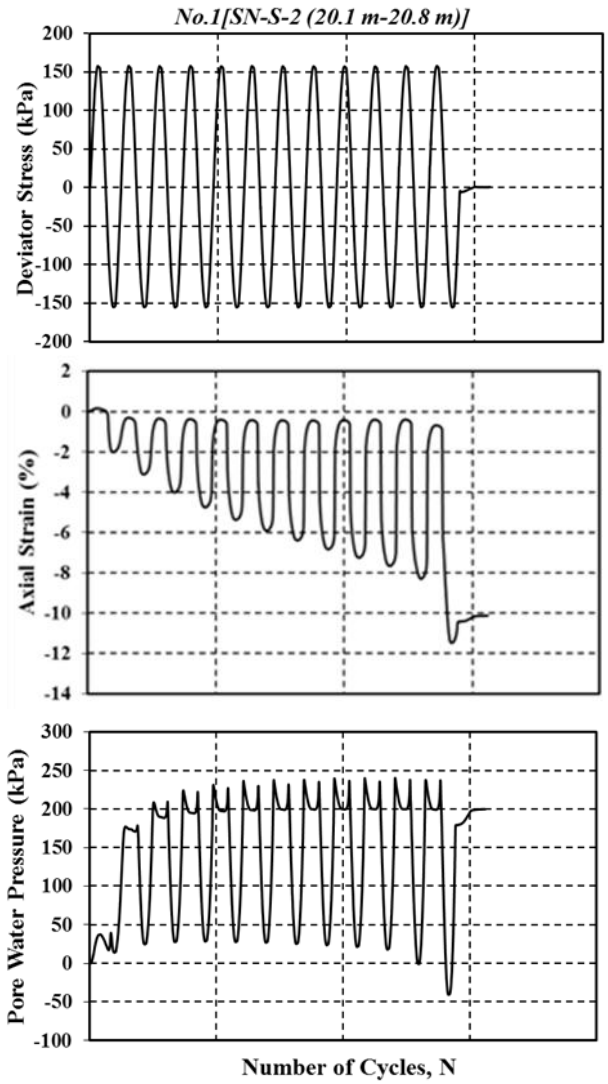

Figure 5.22: Pore water pressure, axial strain, deviator stress versus number of cycles

5.5.3 V_S and V_P Measurements

Figure 5.23 and Figure 5.24 indicate the shear-wave velocity measurement and compression wave velocity measurement of the undisturbed sample [No.1, SN-S-2(20.10m-20.08m)], respectively. The entire results of these plots are illustrated in Appendix B.

Vs	σh kN/m²	t1(▲) msec	t2(△) msec	δt msec	Vs m/sec
test 1	240.0	0.345	0.795	0.45	221
test 2	240.0	0.345	0.815	0.47	212
Average					216

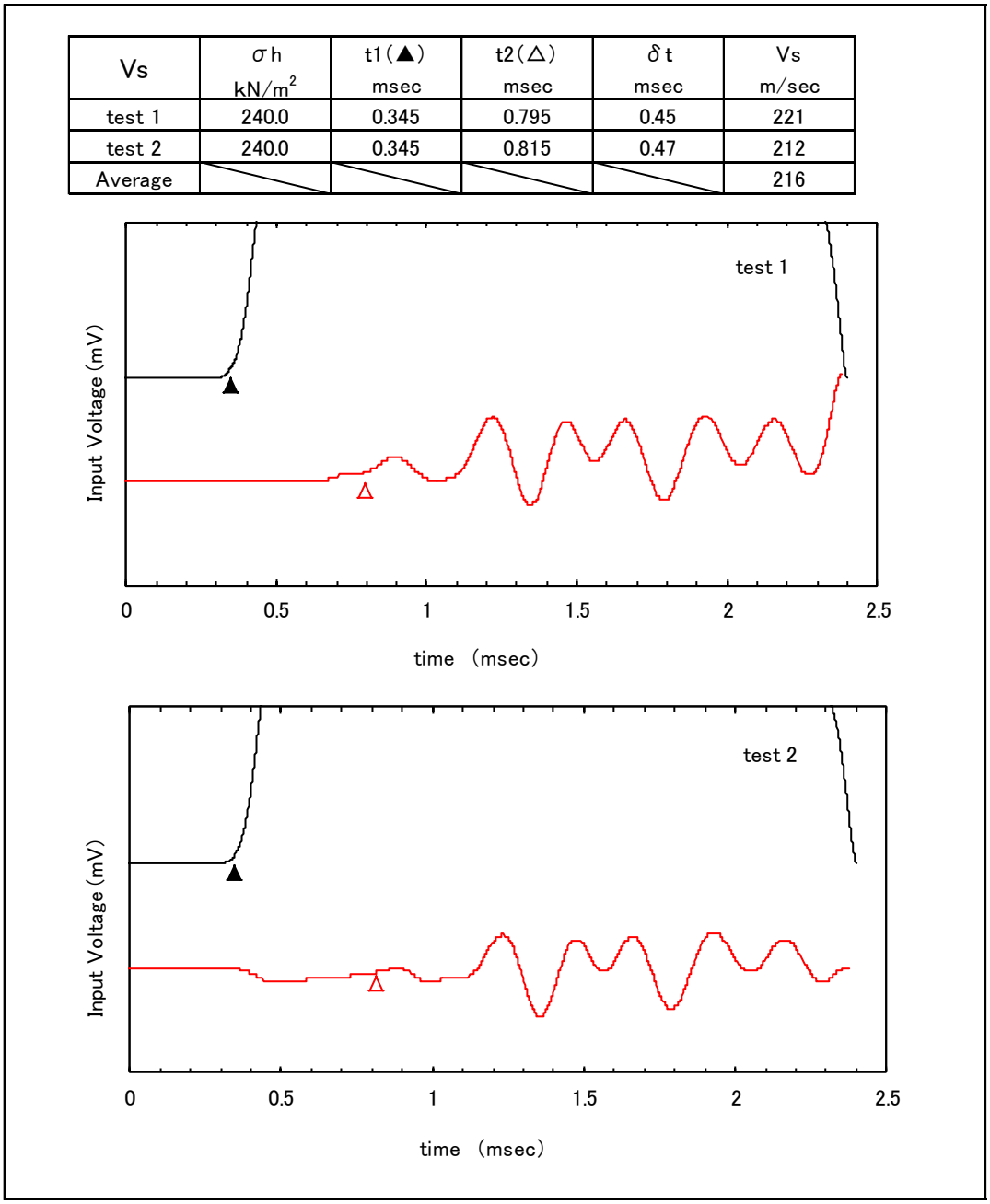

Figure 5.23: Shear wave velocity measurement in the laboratory

Vp	σh kN/m^2	t1(▲) msec	t2(△) msec	δt msec	Vp m/sec
test 1	240.0	0.205	0.260	0.055	1809
test 2	240.0	0.205	0.260	0.055	1809
Average					1809

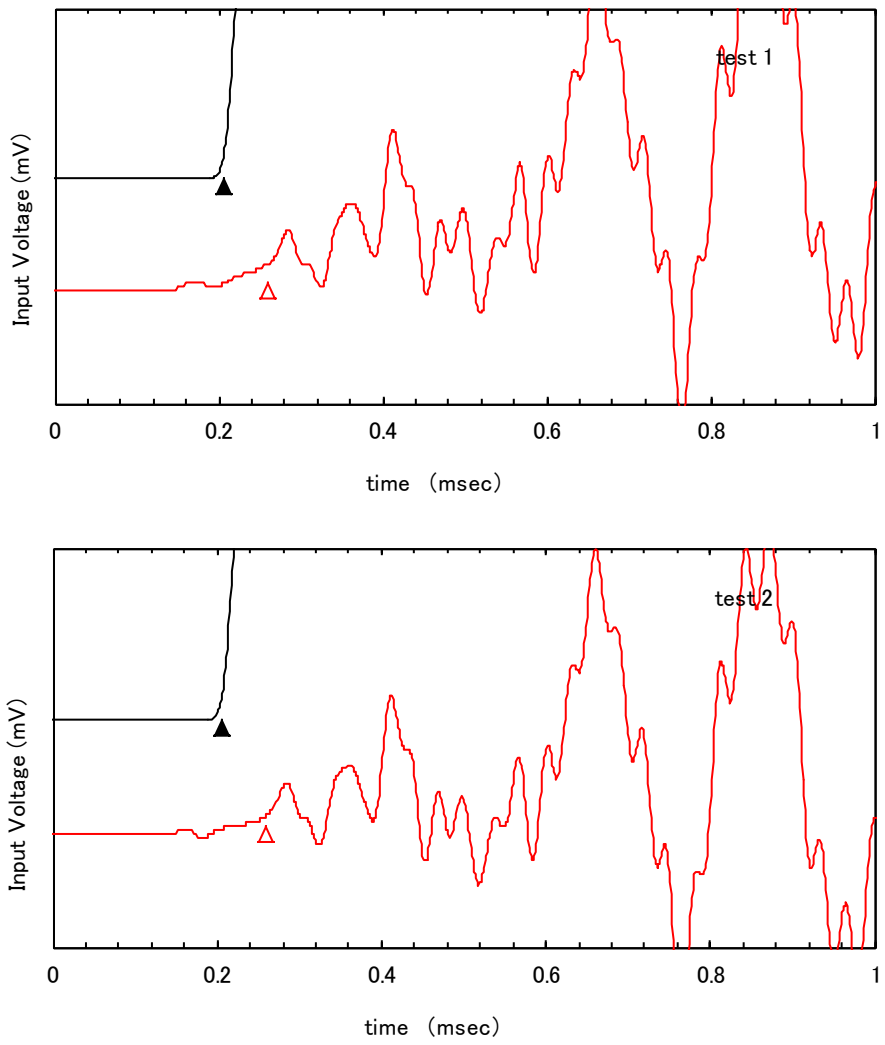

Figure 5.24: Compression wave velocity measurements in the laboratory

5.5.4 Post-liquefaction Volume Change

Figure 5.25 indicates the post-liquefaction volume change versus time of the undisturbed sample [No.12, HG-S-1 (20.10m-20.08m)]. The entire results of such plots are illustrated in Appendix C.

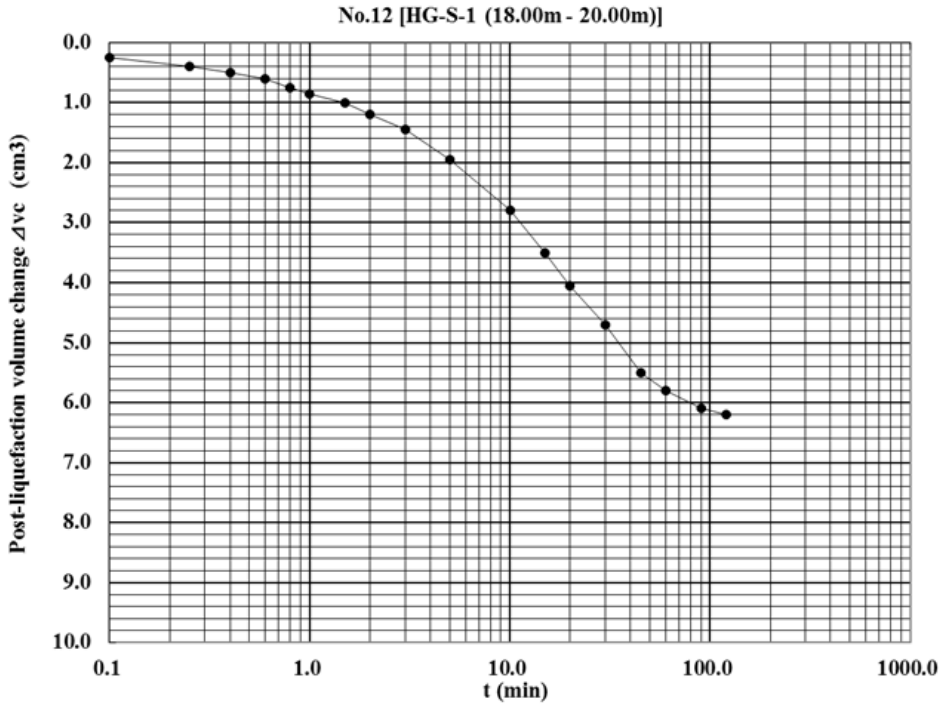

Figure 5.25: Post-liquefaction volume changes versus time

Chapter 6

RESULTS OF TESTS ON THE SAMPLES FROM ASAHI SITES, OHYA SITE, AND NAGOYA SAND

6.1 Test Results on Samples from Asahi Sites

The results of cyclic loading tests on the undisturbed samples from Asahi sites are shown in Table 6.1 together with several associated key parameters. The tests on samples denoted by S-1, S-4, S-6, S-7, S-8 and S-9 from the site HB-S-1, JG-S-1 and NH-S-1 were conducted at the laboratory of Chiba Engineering Co.. The shear wave measurement was not performed in this laboratory tests and therefore only the V_S-values obtained in the field by the downhole method are shown in the columns, V_S and V_{S1}. The cyclic stress ratio causing 2.5% single amplitude axial strain in 20 cycles, R_L, is shown in the second -from- the last column in Table 6.1. Since the value of R_L is the ratio of the amplitude of shear stress $\sigma_d/2$ to the confining stress σ_0', the value of R_L is multiplied by the atmospheric pressure P_a = 98 kN/m^2 and then divided by the normalized initial shear modulus G_{01}. Thus, the cyclic yield strain ε_{ay} indicated in the last column is non-dimensional. Note that the value of V_{S1} is the shear wave velocity normalized to the confining stress of 98 kN/m^2, where σ_v' is in-situ vertical effective overburden stress at a particular depth (kN/m^2), using the Equation 3.4.

The outcomes of the other majority of cyclic loading tests on undisturbed samples conducted at Laboratory of Kiso-Jiban Consultants Co. Ltd. are shown in Table 6.1. The tests were performed by first monitoring the shear wave velocity, V_S, and then

applying the cyclic load to the same sample. Thus, in the column V_S and V_{S1}, the results are indicated with prescript, "L". The cyclic loading tests to determine the cyclic strength, R_L, were performed 2~4 times by varying the amplitude of cyclic axial stress. Each time, the measured V_S-values were different. Thus, the average value among the 2~4 samples is indicated in the column of V_S and V_{S1} with the symbol "L" in Table 6.1. The cyclic yield strain was also calculated using the same value of R_L but with the V_{S1} values obtained in the field and in the laboratory as well. These are shown in Table 6.1 with the symbol "F" and "L", respectively.

On the basis of the soil profiles as shown in from Figure 4.3 to Figure 4.5, simple analyses of liquefaction were made using the method stipulated in the Japanese design code for bridge design. The analyses indicated that the recent man-made fills and alluvial deposits near the surface as new sand deposits designated by the geological symbol Fill and As, respectively, did develop liquefaction at the time of the 2011 earthquake. Therefore, these deposits are deemed to have been disturbed by the strong shaking. The undisturbed samples recovered from such deposits are denoted by "ℓ" in the third column of Table 6.1. The data of the other samples from deeper deposits as old sand deposits are considered not to have liquefied and are labelled as "n" in Table 6.1.

Table 6.1: Undisturbed samples from Asahi

Site	Sample number	Age	Depth (m)	Void Ratio (e)	σ_v' (kPa)	N-value	N1-value	FC (%)	Vs (m/s)	Vs_1 (m/s)	G_{01} (MPa)	R_L	$\varepsilon_{ay} = R_L pa / G_{01}$
HB-S-1	HB-S-1 (S-1)	Fill$^{\ell}$	1.0-3.8	0.673	30	7	9	0.9	F160	L168 F216	L52.2 F86.3	0.304	L** 5.82×10^{-4} F* 4.48×10^{-4}
	HB-S-1 (S-4)	As^{n}	7.0-10.9	1.409	87	25	27	1	F240	L189 F248	L65.7 F116.0	0.282	L 4.29×10^{-4} F 2.43×10^{-4}
	HB-S-1 (S-7)	As^{n}	15.0-16.9	1.094	150	21	26	10.7	F190	L201 F172	L76.4 F55.8	0.276	L 3.61×10^{-4} F 4.95×10^{-4}
	HB-S-1 (S-9)	As^{n}	22.0-23.7	1.166	215	12	8	9.6	F190	L208 F157	L81.8 F46.5	0.276	L 3.37×10^{-4} F 5.94×10^{-4}
JG-S-1	JG-S-1 (S-1)	As^{n}	5.0-8.0	1.068	74	25	29	2.2	F180	L150 F194	L42.9 F71.1	0.176	L 4.10×10^{-4} F 2.48×10^{-4}
	JG-S-1 (S-4)	As^{n}	8.0-9.9	1.134	91	22	23	6.6	F150	L168 F154	L53.1 F44.5	0.268	L 5.05×10^{-4} F 6.02×10^{-4}
	JG-S-1 (S-6)	As^{n}	16.0-17.8	0.843	163	45	35	5.7	F270	L192 F239	L69.6 F108.0	0.28	L 4.02×10^{-4} F 2.59×10^{-4}
	JG-S-1 (S-8)	Ds^{n}	26.0-27.8	0.959	248	11	7	28.7	F250	L179 F199	L73.4 F74.8	0.229	L 3.12×10^{-4} F 3.06×10^{-4}
NH-S-1	NH-S-1 (S-1)	Fill$^{\ell}$	2.0-5.8	0.884	53	4	6	20.5	F140	L121 F164	L27.3 F50.1	0.295	L 10.8×10^{-4} F 5.89×10^{-4}
	NH-S-1 (S-4)	As^{n}	10.0-11.9	0.874	112	31	30	9.6	F260	L199 F253	L75.3 F122.0	0.206	L 2.73×10^{-4} F 1.69×10^{-4}
	NH-S-1 (S-6)	Ds^{n}	26.0-27.0	1.258	244	4	3	84	F150	L165 F120	L51.4 F27.2	0.246	L 4.78×10^{-4} F 9.04×10^{-4}

$N_1=1.7/(\sigma_v' +0.7)$

L: Laboratory, F; Field, ℓ : Liquefied Alluviumu or Fills, □
n: non-liquefied, As: Alluvial sand, Ds: Diluvial sand

Table 6.1: Undisturbed samples from Asahi (Continued)

Site	Sample number	Age	Depth (m)	Void ratio (e)	σ_v' (kPa)	N-value	N1-value	FC (%)	Vs (m/s)	V5 (m/s)	G_{01} (MPa)	R_L	$\varepsilon_{ay} = R_L pa / G_{01}$
HG-S-1	HG-S-(S-1)	As$^{\ell}$	2.0-3.0	0.967	25	4	6	11.8	L 127 F 110	L 180 F 156	L 59.5 F 47.6	0.23	L 3.86×10^{-4} F 4.83×10^{-4}
	HG-S-(S-4)	As$^{\ell}$	4.0-5.0	1.02	60	6	8	12.1	L 115 F 115	L 131 F 131	L 31.5 F 31.5	0.3	L 9.52×10^{-4} F 9.52×10^{-4}
	HG-S-(S-1)	As^{n}	4.0-6.0	1.07	60	6	8	25.4	F 110	F 125	F 28.7	0.299	F 10.4×10^{-4}
	HG-S-(S-5)	As^{n}	7.0-10.0	0.653	87	18	19	26.2	F 170	F 176	F 45.4	0.281	F 4.80×10^{-4}
	HG-S-(S-11)	Ds^{n}	18.0-20.0	1.053	180	10	7	52.4	F 180	F 155	L 26.7 F 45.4	0.284	F 6.25×10^{-4}
	HG-S-(S-11)	Ds^{n}	18.0-20.0	1.047	180	10	7	42.3	L 138 F 180	L 119 F 155	L 61.9 F 45.4	0.28	L 10.5×10^{-4} F 6.17×10^{-4}
SN-S-1	SN-S-1 (S-6)	Fill$^{\ell}$	1.0-2.0	0.827	20	5	11	1.9	L 121 F 100	L 181 F 149	L 61.9 F 41.7	0.35	L 5.65×10^{-4} F 8.39×10^{-4}
	SN-S-1 (S-10)	Ds^{n}	24.0-26.1	1.021	215	23	16	9	L 211 F 220	L 174 F 182	L 57.8 F 66.3	0.24	L 4.15×10^{-4} F 3.62×10^{-4}
SN-S-2	SN-S-2 (S-6)	As^{n}	13.0-14.0	0.837	115	26	24	5	L 209 F 220	L 202 F 182	L 76.3 F 84.8	0.23	L 3.01×10^{-4} F 2.71×10^{-4}
	SN-S-2 (S-7)	As^{n}	20.1-20.8	0.695	190	79	57	1.3	L 218 F 250	L 186 F 213	L 65.3 F 86.4	0.22	L 3.37×10^{-4} F 2.55×10^{-4}
	SN-S-2 (S-9)	As^{n}	20.8-21.8	1.073	198	79	57	5	L 134 F 250	L 113 F 211	L 24.1 F 84.0	0.2	L 8.30×10^{-4} F 2.38×10^{-4}

$N_1=1.7/(\sigma_v' +0.7)$

ℓ : Liquefied, n : non-liquefied, L : Laboratory, F : Field
As : Alluvial sand, Ds : Diluvial sand

6.2 Test Results on Samples from Ohya Site

The undisturbed samples from Kayagari tailings dam at Ohya site were tested in the laboratory of Kiso-Jiban Co., Ltd. using the triaxial test apparatus. Test procedure

was the same as that described in the section 4.3. The results of the tests are shown in Table 6.2 in the same fashion as in Table 6.1. In this laboratory test series, no measurement was made for the shear wave velocity. Thus, the V_S and V_{S1} values shown in Table 6.2 are only those monitored in-situ by the downhole method. As a result of the simple analysis, the near-surface deposits were identified to have liquefied to depths of about 10 m during the 2011 earthquake. Thus, the symbol "ℓ" is given for such liquefied samples in the second column in Table 6.2. The samples from deeper deposits without suffering liquefaction are indicated by the symbol "n" in Table 6.2.

Table 6.2: Tailings dam at Ohya mine (Miyagi Prefecture)

Site	Sample number	Age	Depth (m)	Void ratio (e)	σ_v' (kPa)	N-value	N1-value	FC (%)	Vs (m/s)	V5 (m/s)	G_{01} (MPa)	R_L	$\varepsilon_{ay} = R_L pa / G_{01}$
HG-S-1	HG-S-(S-1)	As^{ℓ}	2.0-3.0	0.967	25	4	6	11.8	L 127 F 110	L 180 F 156	L 59.5 F 47.6	0.23	L 3.86×10^{-4} F 4.83×10^{-4}
	HG-S-(S-4)	As^{ℓ}	4.0-5.0	1.02	60	6	8	12.1	L 115 F 115	L 131 F 131	L 31.5 F 31.5	0.3	L 9.52×10^{-4} F 9.52×10^{-4}
	HG-S-(S-1)	As^{n}	4.0-6.0	1.07	60	6	8	25.4	F 110	F 125	F 28.7	0.299	F 10.4×10^{-4}
	HG-S-(S-5)	As^{n}	7.0-10.0	0.653	87	18	19	26.2	F 170	F 176	F 45.4	0.281	F 4.80×10^{-4}
	HG-S-(S-11)	Ds^{n}	18.0-20.0	1.053	180	10	7	52.4	F 180	F 155	L 26.7 F 45.4	0.284	F 6.25×10^{-4}
	HG-S-(S-11)	Ds^{n}	18.0-20.0	1.047	180	10	7	42.3	L 138 F 180	L 119 F 155	L 61.9 F 45.4	0.28	L 10.5×10^{-4} F 6.17×10^{-4}
SN-S-1	SN-S-1(S-6)	$Fill^{\ell}$	1.0-2.0	0.827	20	5	11	1.9	L 121 F 100	L 181 F 149	L 61.9 F 41.7	0.35	L 5.65×10^{-4} F 8.39×10^{-4}
	SN-S-1(S-10)	Ds^{n}	24.0-26.1	1.021	215	23	16	9	L 211 F 220	L 174 F 182	L 57.8 F 66.3	0.24	L 4.15×10^{-4} F 3.62×10^{-4}
SN-S-2	SN-S-2(S-6)	As^{n}	13.0-14.0	0.837	115	26	24	5	L 209 F 220	L 202 F 182	L 76.3 F 84.8	0.23	L 3.01×10^{-4} F 2.71×10^{-4}
	SN-S-2(S-7)	As^{n}	20.1-20.8	0.695	190	79	57	1.3	L 218 F 250	L 186 F 213	L 65.3 F 86.4	0.22	L 3.37×10^{-4} F 2.55×10^{-4}
	SN-S-2(S-9)	As^{n}	20.8-21.8	1.073	198	79	57	5	L 134 F 250	L 113 F 211	L 24.1 F 84.0	0.2	L 8.30×10^{-4} F 2.38×10^{-4}

$N_1=1.7/(\sigma_v'+0.7)$

ℓ : Liquefied, n : non-liquefied, L : Laboratory, F : Field
As : Alluvial sand, Ds : Diluvial sand

6.3 Relation between the Cyclic Strength and Shear Wave Velocity for Undisturbed Samples

6.3.1 Plots of Cyclic Strength versus V_{S1} for Old Unliquefied Sands

As mentioned previously, it is considered likely that the relationship between the

cyclic strength, $R_L \cdot P_a$, and shear wave velocity, V_{S1}, for unliquefied old sand deposits would be different from that pertaining to new or liquefied sand deposits. Thus, plotting of the test data shown in Table 6.1 and Table 6.2 was made separately for each of these two types of sand deposits, that is, one for liquefied deposits as new sand deposits and the other for unliquefied deposits as old sand deposits.

The undisturbed samples from the old sand deposits denoted by As (Alluvial sand), and Ds (Diluvial sand) at Asahi site are from depths deeper than 5~7m as seen in the soil profiles in from Figure 4.3-4.5. As shown in Table 6.1, the cyclic stress ratio causing 2.5% single amplitude in 20 cycles of load applications, R_L, is of the order of 0.2 to 0.35. The shear wave velocity, V_{S1}, is seen to take relatively large values ranging between 120 and 250 m/s. Each of the data sets, R_L and V_{S1} is shown in the plot of Figure 6.1 by the open rectangle symbol, "⊡".

Regarding the values of V_{S1}, there appears no clearly discernible tendency of differentiating between the data from the field and those from the laboratory tests. Thus the data from these two sources are shown jointly by a horizontal line connecting two points in the diagram.

The data from Ohya site are plotted also in Figure 6.1 with the open reverse triangle symbol, "▽". Looking over the whole data, a curve in the form of $R_L = a\, V_{s1}^2$ is drawn so that it passes, as far as possible, through average points in the scattered plots of the data. As indicated before by the use of Equation 3.1, the value of the cyclic yield strain or reference strain is calculated by Equation 6.1. Thus, the value,

a, is implicitly given by $(\gamma_t.\varepsilon_{ay}/g.P_a)$.

$$\varepsilon_{ay} = \frac{R_L \cdot P_a}{G_{01}} = \frac{R_L \cdot P_a}{\gamma_t / g \cdot V_{s1}{}^2} \tag{6.1}$$

Note that the cyclic stress ratio is now expressed as the magnitude of cyclic stress at the atmospheric pressures, P_a, in order to make the cyclic yield strain, ε_{ay}, non-dimensional. Individual values of the coefficient, ε_{ay}, for each of the specimens tested are shown in the list of Table 6.1 and Table 6.2. It may be seen that the value of ε_{ay} varies in a wide range but an average value representative of all unliqufied old sand deposits may be obtained approximately as $\varepsilon_{ay} = 3.6\times10^{-4}$ as accordingly indicated in Figure 6.1. Thus, the curve of equal ε_{ay} established in the plot of R_L and V_{S1} is regarded as the correlation between the cyclic resistance R_L and V_{S1} for the old aged deposits, which is expressed as:

$$R_L = 0.68\times10^{-5} V_{s1}{}^2 \tag{6.2}$$

where γ_t/g is assumed equal to 18.5/9.8= 1.88 kN$\cdot$sec^2/m^4.

6.3.2 Plots of Cyclic Strength versus V_{S1} for Fresh Fills or Liquefied Deposits

The test data in Table 6.1 pertaining to the undisturbed samples from fresh artificial fills and liquefied deposits as new sand deposits are plotted in Figure 6.2 in the same fashion as in Figure 6.1. By drawing a curve through average data points, the relation between R_L and V_{S1} can be obtained as follows:

$$R_L = 0.9\times10^{-5} V_{s1}{}^2 \tag{6.3}$$

This relation is presented in Figure 6.2. In the some context as mentioned above, this curve is a line of constant cyclic yield strain of $\varepsilon_{ay} = 4.6\times10^{-4}$. It is to be noted that for the fresh or once-liquefied deposits as new sand deposits, the value of cyclic yield strain is found to be larger than $\varepsilon_{ay} = 3.6\times10^{-4}$ which is demonstrated in Figure 6.1 for

the old and unliquefied sand deposits. This is due to more ductile nature of the new sand deposits as compared to the old sand deposits.

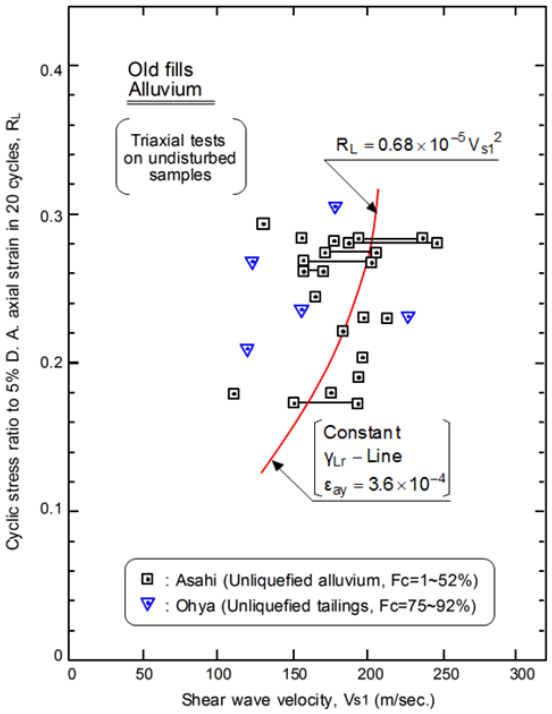

Figure 6.1: Relation between the cyclic resistance and shear wave velocity for old unliquefied deposits

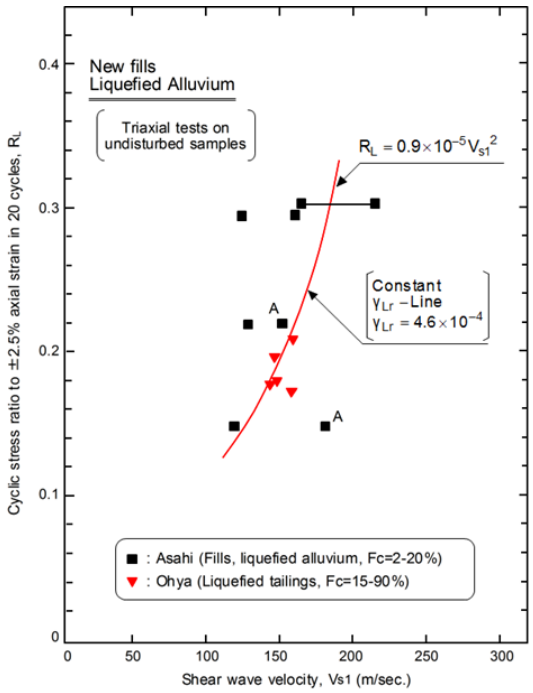

Figure 6.2: Relation between the cyclic resistance and shear wave velocity for undisturbed samples from new fills and liquefied alluvium

6.4 Cyclic Strength versus Shear Wave Velocity for Reconstituted Samples

6.4.1 Cyclic Strength versus V_{S1} for Reconstituted Samples from Asahi Sand

After the series of tests were finished for the undisturbed samples from Asahi, the same samples were mixed, air-dried and reconstituted to test specimens having approximately the same density by means of moist placement method. Five equal pre-weighed, dried portions of soil were mixed with de-aired water at a water content of the pertinent undisturbed specimen. After a rubber membrane is stretched taut to inside of a split mould, each portion of moist soil was totally strewed and gently tamped in order to reach a predetermined height.

In this case the tests were carried out only for the samples from HG-S-1, SN-S-1 and SN-S-2 sites. The V_S-measurements and cyclic loading tests were performed similarly on these reconstituted samples. The results of the tests are shown in Table 6.3 and the data are plotted in Figure 6.3 in terms of $R_L \cdot P_a$ versus V_{S1} with the open triangle symbol "△".The line of equal $\varepsilon_{ay} = 4.6 \times 10^{-4}$ established above in Figure 6.2 is quoted and displayed for comparison. Although there are some deviations, the cyclic yield strain for reconstituted samples appears to coincide approximately with that from the in-situ samples disturbed by liquefaction, which is considered as new sand deposits.

Table 6.3: Reconstituted specimens from Asahi sand

Specimens	Fc (%)	e	σ'_0 (kPa)	e_{max} / e_{min}	Dr (%)	V_{s1} (m/s)	G_{01} (MPa)	R_L	$\varepsilon_{ay} = \frac{R_L \cdot p_a}{G_{01}}$
HG-S-1 (2.0-3.0 m)	11.8	0.967	100	1.486 / 0.863	83.3	177	59.1	0.19	3.21×10^{-4}
HG-S-1 (4.0-5.0 m)	12.1	1.02	100	1.572 / 0.929	85.8	135	34.4	0.21	6.10×10^{-4}
HG-S-1 (18.0-19.0 m)	43.9	1.053	100	1.803 / 0.931	86	115	24.9	0.12	4.82×10^{-4}
HG-S-1 (19.0-20.0 m)	40.8	1.047	170	1.581 / 0.839	72	125	29.5	00:13	4.41×10^{-4}
SN-S-1 (24.0-24.6 m)	13.6	1.152	100	1.597 / 0.939	67.6	149	41.9	0.12	2.86×10^{-4}
SN -S-1 (25.3-26.1 m)	4.5	0.89	270	1.232 / 0.768	73.3	158	47.1	0.175	3.71×10^{-4}
SN-S-2 (13.0-14.0 m)	5.3	0.837	150	1.298 / 0.764	86.3	168	53.2	0.18	3.38×10^{-4}
SN-S-2 (20.1-20.8 m)	0.95	0.695	240	0.967 / 0.579	70.1	173	56.4	0.185	3.28×10^{-4}
SN-S-2 (20.8-21.8 m)	5	1.073	240	1.46 / 0.829	61.3	105	20.8	0.12	5.77×10^{-4}

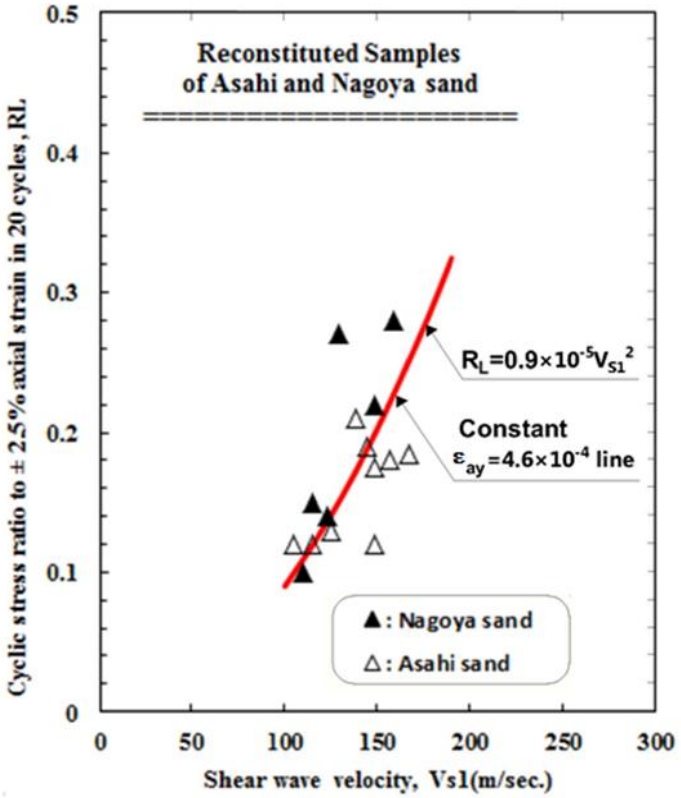

Figure 6.3: Relation between the cyclic resistance and shear wave velocity for disturbed or reconstituted samples

6.4.2 Cyclic Strength versus V_{S1} for Reconstituted Samples from Nagoya Sand

With an aim of examining effects of fines content, a sandy soil from a site in Nagoya was sorted out using the 74μ sieve to separate fines fraction from the silty sand. Then, the fines were mixed with sand fraction to produce silty sands having fines proportions of 10 and 30%. The artificial materials thus produced were used to prepare specimens with a relative density of 50 and 70% with 8% water content and tested in the same fashion using the same apparatus. The results of the tests are listed in Table 6.4 and plotted in Figure 6.3 with the solid triangle symbol "▲" in terms of R_L versus V_{S1}.

Table 6.4: Reconstituted samples of Nagoya sand with different fines contents

Specimens	Void ratio (e)	e_{max} e_{min}	σ'_0 (kPa)	Dr (%)	Vs_1 (m/s)	G_{01} (MPa)	R_L	$\varepsilon_{ay} = \frac{R_L \cdot p_a}{G_{01}}$
Fine content 0%	0.85	1.077 0.623	100	50	149	41.9	0.22	5.25×10^{-4}
	0.769	1.077 0.623	100	70	159	47.7	0.28	5.87×10^{-4}
Fine content 10%	0.867	1.118 0.616	100	50	123	28.5	0.14	4.91×10^{-4}
	0.767	1.118 0.616	100	70	129	31.4	0.27	8.60×10^{-4}
Fine content 30%	0.979	1.288 0.671	100	50	110	22.8	0.1	4.38×10^{-4}
	0.865	1.288 0.671	100	70	115	24.9	0.15	6.01×10^{-4}

In order to determine maximum and minimum void ratios of the specimens, the procedures stipulated by the Japanese Geotechnical Society (JIS A 1224:2009, JGS 0161-2009) were used. It is noted that with increasing relative density, both R_L and V_{S1} tend to increase, as seen from the measured values plotted in Figure 6.3. In addition, there appears no clearly discernible difference in the plot between samples with zero and 30% fines content. Thus, pending further detailed study, all the

samples reconstituted from Nagoya sand are likely, in the present study, to exhibit seemingly identical characteristics at least in terms of the relation between R_L and V_{S1}. For reference sake, the cuve of equal cyclic yield strain $\varepsilon_{ay} = 0.9\times10^{-4}$ is drawn in the plot of Figure 6.3. It is noted that the R_L-V_{S1} relation for the sand of Asahi is practically identical to that for the sand of Nagoya.

6.5 Summary of the R_L versus V_{S1} Relations for Undisturbed Samples from New Deposits and Reconstituted Samples

A comparison of the test data as shown in Figure 6.1 for undisturbed samples from liquefied deposits and those in Figure 6.2 for reconstituted samples shows that there is no appreciable difference, as a whole, between these two groups of data. In the light of the fact that new or once liquefied deposits of in-situ sandy soils still retain traces of disturbance, they are deemed to exhibit cyclic behaviour which is approximately identical to that of reconstituted samples in terms of the liquefaction resistance correlated with the shear wave velocity. Thus, it is reasonable to assume, at the present stage of the study, that they represent jointly the identical relationship between the liquefaction resistance, R_L, and shear wave velocity, V_{S1}, which might be usable for practical purposes. Based on the consideration as above, the equal cyclic yield strain-line of $\varepsilon_{ay} = 4.6\times10^{-4}$ displayed in Figure 6.2 and Figure 6.3 may be taken as being representative of the correlation between R_L versus V_{S1} for new sand deposits.

6.6 Discussion about the Cyclic Yield Strain as Related to the Liquefaction Resistance and Shear Wave Velocity

The yield strain or reference strain in cyclic loading, ε_{ay}, introduced in the present study appears to have some features in common with the volumetric threshold strain, γ_{tv}, proposed by Dobry et al. (1980). It was defined as the strain where dilatancy-

induced volume change begins to manifest itself in dry sand or pore water pressure starts to build up in saturated sand in undrained loading. This aspect was more thoroughly studied by Hsu and Vucetic (2004) who performed a comprehensive laboratory tests on various sandy soils using a cyclic simple shear tests device. They showed that the volumetric cyclic threshold strain tends to increase with plasticity index of the fines from about $(1\sim2)\times10^{-4}$ for clean sands up to $(4\sim10)\times10^{-4}$ for silty sands containing fines with a PI-value of 30. An overview of existing test data reported by 17 papers was made by Dobry and Abdoun (2011) who concluded that the value of γ_{tv} for normally consolidated sands lies in the range between $(0.5\sim2.0)\times10^{-4}$ with a representative value grouping closely around $\gamma_{tv}=1\times10^{-4}$.

The relationship between the pore water pressure build-up and the cyclic shear strain was studied Ladd et al. (1989) who performed a series of strain-controlled cyclic triaxial tests on saturated specimens of Monterey No. 0 sand. It was also shown that the pore water pressure begins to build up at the strain, γ_{tv}, amplitude of $\gamma = 1.5\varepsilon_a \fallingdotseq 1.0\times10^{-4}$ which is coincident with the threshold volumetric strain proposed by Dobry et al. (1980). The results of the data compilation made by Dobry and Abdoun (2011) for the pore water build-up are reproduced in Figure , together with the data obtained by Bhatia (1980) and Finn (1981) in similar vein. As indicated in Table 6.1 to Table 6.4, the range of cyclic yield strain, ε_{ay}, obtained in this study is $(2.0\sim10)\times10^{-4}$ and therefore the cyclic yield strain in simple shear mode, $\gamma_y=1.5\ \varepsilon_{ay}$, is $(3.0\sim15)\times10^{-4}$. This range is indicated in Figure .

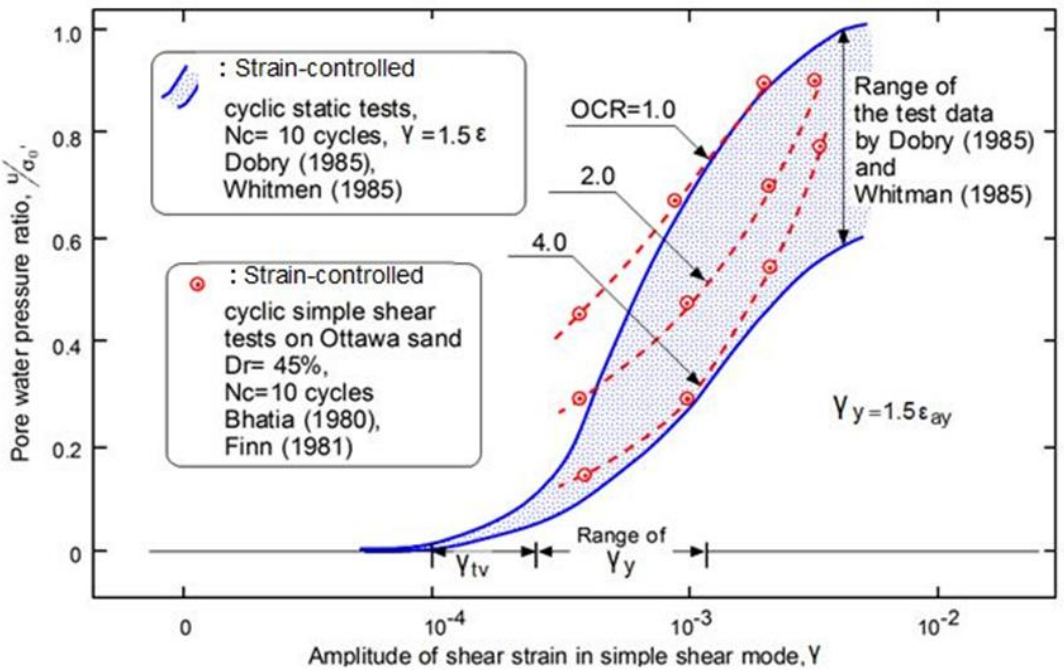

Figure 6.4: Amplitude of simple shear strain versus pore water pressure build-up (Reproduced from the figures by Dobry and Abdoun, 2011)

Looking over the data plots in Figure , one can realize that in the range of the cyclic yield strain, that is, $(3.0\sim15)\times10^{-4}$, the pore water pressure rises to values 10~70% of the initially applied confining pressure. Thus, this cyclic yield strain, γ_y, in simple shear mode is considered as being a benchmark level of strain at which pore water pressure has arisen substantially to a value 10~70% of the initial confining stress.

With the reported data as mentioned above, the threshold strains can mark the start of volumetric change and pore water pressure, the cyclic yield strain, $\gamma_y=1.5\ \varepsilon_{ay}$, defined in this study by Equation 3.2 may be considered to have the context similar to that proposed by Dobry (1980), but these are different in the aspects as follows:

1. The volumetric threshold strain γ_{tv} is an index property associated with the start of a residual volumetric strain or the start of the pore-water build-up resulting from application of cyclic strain. On the other hand, the cyclic yield strain is a threshold value conceptionally marking the beginning of significant amount of cyclic shear

strain before onset of liquefaction in sandy soils.

2. While the value of γ_{tv} takes typically a value of (0.5~2.0) $\times 10^{-4}$, the cyclic yield strain appears to take larger values. In fact, in terms of simple shear mode of deformation, the value of cyclic yield strain is given by $\gamma_y = 1.5\ \varepsilon_{ay}$ and thus takes values in a wider range most likely between $1.5\times(2.0\sim10)\times10^{-4} = (3.0\sim15)\times10^{-4}$ as presented in the test results shown in Table 6.1 to Table 6.4 and plotted in Figure 6.1 to Figure 6.3. In this range of amplitude of cyclic simple shear strain, a substantial amount of pore water pressure must be developing.

6.7 Discussions on the Relationship between Liquefaction Resistance and Shear Wave Velocity for Fresh and Old Deposits

The average curve in Figure 6.1 representative of old sand deposits is shown in Figure 6.5, together with the average curve pertaining to new man-made deposits or reconstituted samples (new sand deposits) which is quoted from Figure 6.2 and Figure 6.3.

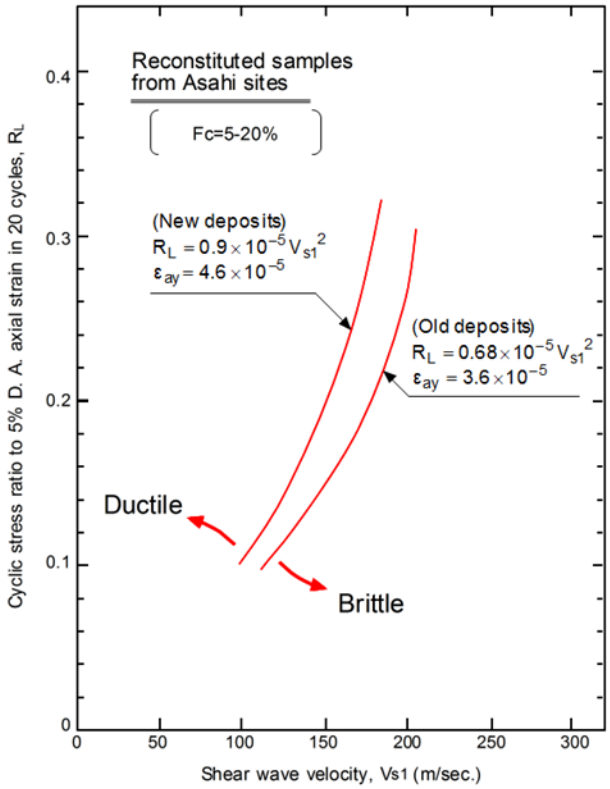

Figure 6.5: Summarized two curves for new and old deposits

It can be seen that the relation for old sand deposits is represented by the curve with a parameter of $\varepsilon_{ay} = 3.6\times10^{-4}$ which is smaller than the corresponding value of $\varepsilon_{ay} = 4.6\times10^{-4}$ for new sand deposits. This implies, as illustrated in Figure 3.2, that aged deposits are possessed more of brittle characteristics, as compared to ductile nature of newly placed or artificial deposits. Accordingly, it is suggested that multiple curves pertaining to the age of the deposit in question established separately can be used to estimate the resistance to liquefaction for each deposit in question when using the chart of R_L versus V_{S1} based on in-situ and laboratory measurements of shear wave velocity.

There are several charts proposed for the relationship between the cyclic strength and shear wave velocity V_{S1}. These are summarized by Andrus and Stokoe (2000) as reproduced in the diagram of Figure . The two curves proposed in the present study

are superimposed in Figure . It appears that the majority of the data sets complied hitherto are those from field observations and measurements.

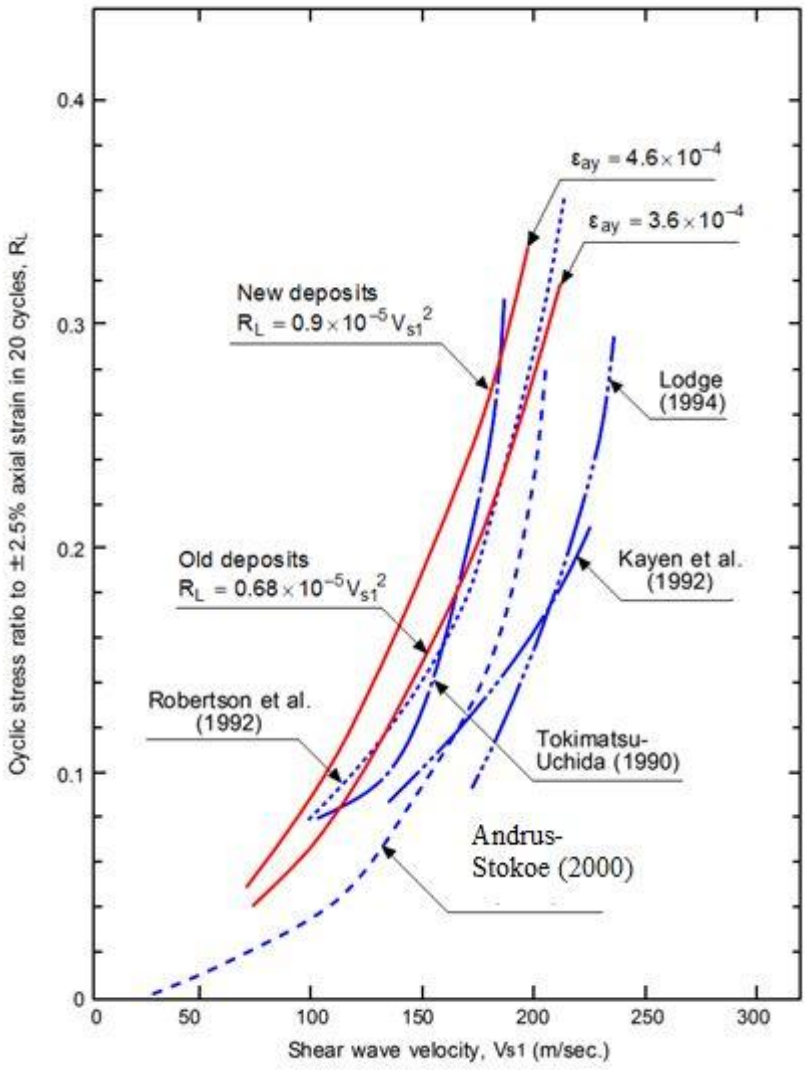

Figure 6.6: Summary curves of the liquefaction resistance versus shear wave velocity for newly deposited and old deposits of sandy soils (Reproduced from the figure by Andrus and Stokoe, 2000)

The curve with $\varepsilon_{ay} = 3.6\times10^{-4}$ seems to show a reasonable level of coincidence particularly with the relations proposed by Tokimatsu and Uchida (1990) and Robertson et al. (1992) as shown in Figure . Moreover, as shown in Figure 6.7, the trend of this curve is in good agreement with the results of intact samples obtained by Wang et al. (2006) from offshore platform sites in Bohai Bay, China. This figure

implies that the trend curve pertaining to the old sand deposits seems to be unique, though the V_S-based liquefaction curves of fresh sand deposits are soil dependent.

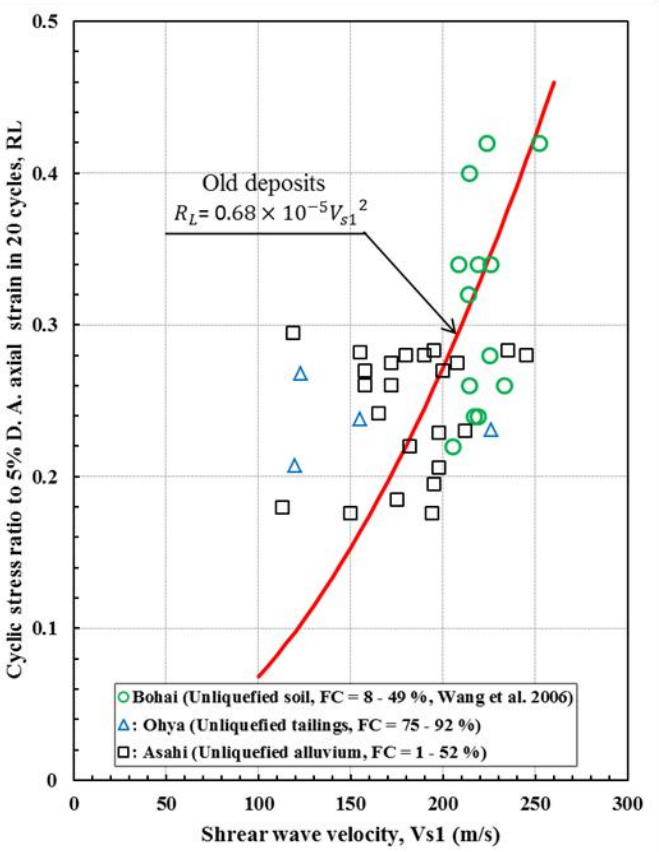

Figure 6.7: Results of undisturbed samples from Asahi, Ohya, and Bohai

Based on the procedure adopted in this study, since the curve pertaining to the new sand deposits obtained from the undisturbed specimens of shallow depths liquefied in the 2011 Great East Japan Earthquake, it can be the representative of the points in which liquefaction occurs in V_S-based liquefaction chart. Furthermore, by superimposing two curves proposed in this study on the contours proposed by Kayen et al. (2004) as shown in Figure , the probability (P_L = Liquefaction potential) of the curve pertaining to the new deposits is higher than 50% whereas the curve pertaining to old deposits is less than 50%, which can be consistent with the concept of old and new deposits. Thus, although these two curves are shown together on the identical

plot, they may not be comparable with each other because of their different characteristics, though the shear wave velocity of new deposits is slightly less than that of the old deposits.

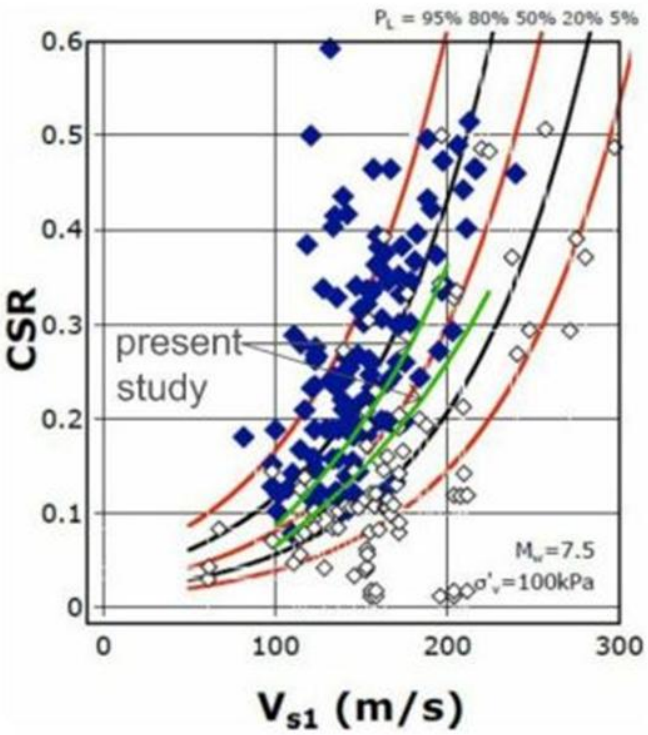

Figure 6.8: Preliminary probabilistic liquefaction triggering contours proposed by Kayen et al. (2004)

However, since the curve pertaining to aged deposits obtained from undisturbed specimens of medium to deep depths, not experienced the liquefaction at the moment of the 2011 earthquake, it may be considered as a boundary curve while assessing liquefaction susceptibility in old deposits. This is in good agreement with the curve proposed by Leon et al. (2006) based on strength gain factors, as shown in Figure 6.9. Given the fact that the shear wave velocities of SCCP (South Carolina coastal plain) greater than the upper limit of 215 m/s, as suggested by Andrus and Stokoe (2000), were not obtained for developing those curves, otherwise they could have shown a higher level of agreement with the old deposit curve.

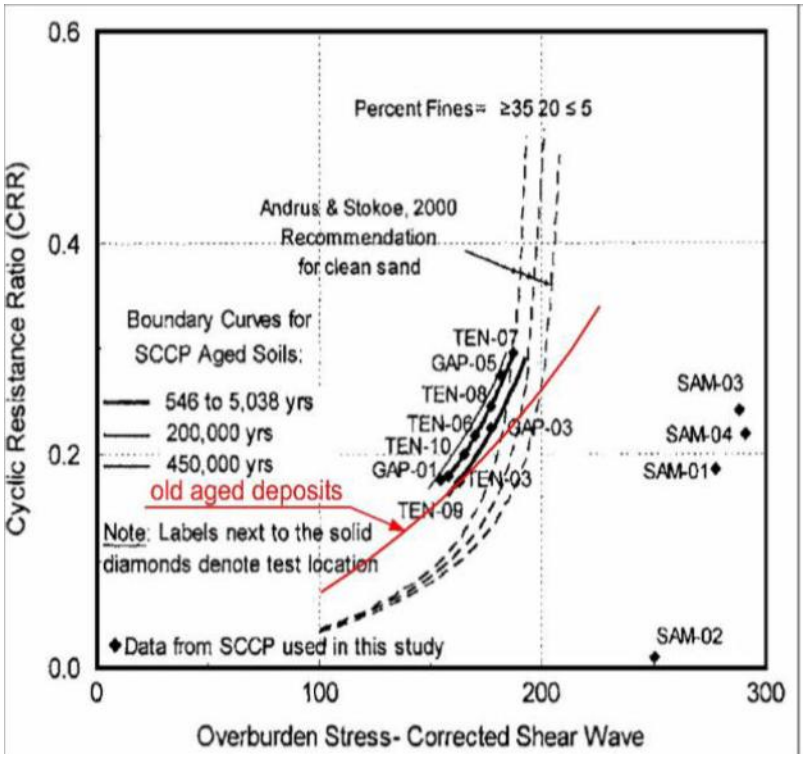

Figure 6.9: Curved lines proposed by Leon et al. (2006)

Moreover, Dobry et al. (2015) proposed the constant cyclic shear strain curve, corresponding to $\gamma_{cl} \sim (10\text{-}20)\times10^{-4}$, separating liquefaction occurrences from non-liquefaction occurrences in V_S-based liquefaction chart for preshaken natural sands of the Imperial Valley in California, as shown Figure 6.10.

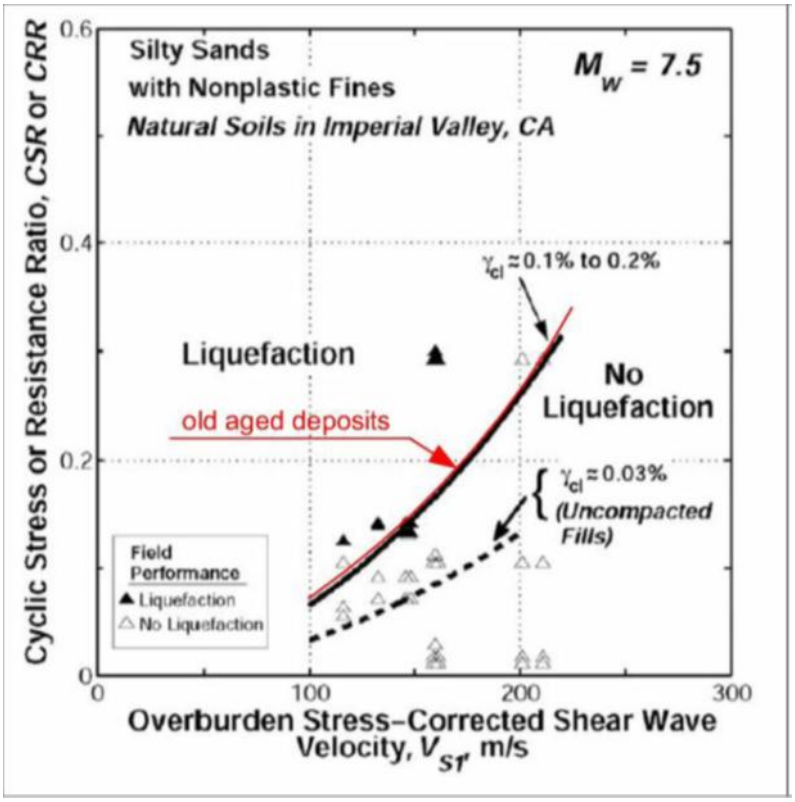

Figure 6.10: Curved line proposed by Dobry et al. (2015)

It was suggested that the increased cyclic strength in this area is not due to geologic age, but most likely due to preshaking of the natural sand sites because of being in high seismic activity region. Figure depicts that the curve proposed for aged deposits is highly consistent with the curve pertaining to the preshaken natural deposits. Although the boundary curve for preshaken natural silty sand in Imperial Valley based on the concept of constant cyclic shear strain, and the boundary curve proposed for old deposits utilizing the concept of cyclic yield strain in this study, the values of cyclic shear strain of both are somewhat in the same range.

Both peshaking by several earthquake occurrences and aging over a prolonged period of time can considerably increase the cyclic shear strength of sand (Seed et al. 1977, Seed 1979). Tokimatsu et al. (1986) indicated that a tube sample pre-sheared to recreate the in-situ density and initial shear modulus can show the liquefaction

characteristics similar to those of the sample obtained by freezing method. Wang et al. (2006) also stated that using pre-shearing along with over-consolidation can be an effective method to reproduce the shear wave velocity of undisturbed samples for the reconstituted samples. The liquefaction resistance of undisturbed samples is in good agreement with that of reconstituted ones, if the liquefaction is defined by double amplitude axial strain less than 6% and that their initial shear wave velocities are almost the same. Because of these reasons, it seems reasonable to compare aged deposits with pre-shaking of natural deposits in terms of liquefaction resistance versus shear wave velocity.

In order to indicate the effect of age on the liquefaction resistance of aged sand deposits, Hayati and Andrus (2009) and Andrus et al. (2009) developed updated correction factors (K_{DR}) with relevant reference age, and represented a relationship between those factors and measured to estimated shear wave velocity (MEVR). They also proposed the SPT-, CPT-, and V_S-based boundary curves for sands of different ages by means of various values of MEVR and K_{DR}. Since aged deposits from Asahi City are more than 10,000 years in age, it was conservatively assumed that the values of K_{DR} and MEVR are 1.51 and 1.26, respectively. Figure compares the CRR- V_{S1} curves for fresh and aged sand deposits proposed in this study with those proposed by Andrus et al. (2009). Although the trend of both groups of curves from fresh to aged sand deposits is mutually consistent with each other, the boundary curve of MEVR = 1.3 seems to be overly conservative in comparison with the curve of this study pertaining to old sand deposits.

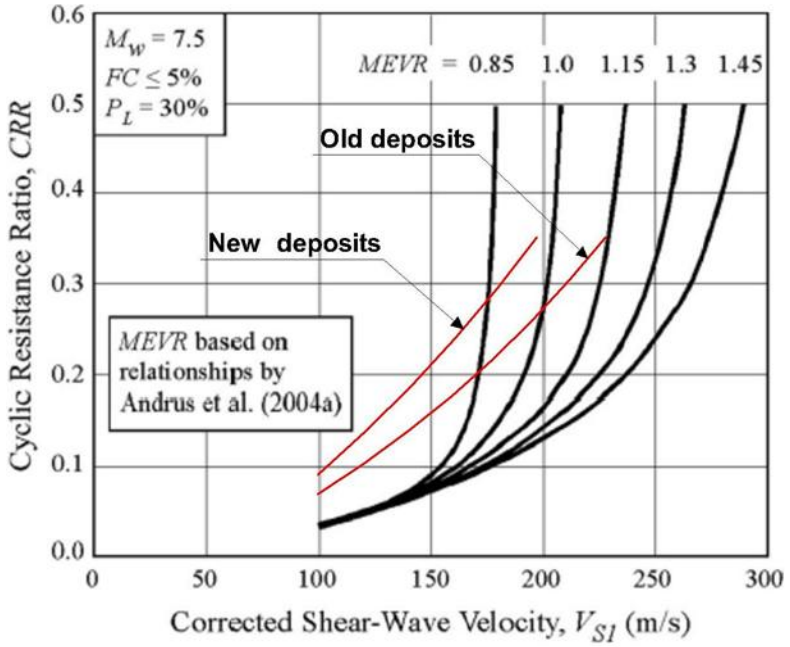

Figure 6.11: Comparison between the curves of the present study and those of Andrus et al. (2009)

Chapter 7

CONCLUSION AND RECOMMENDATION

7.1 Conclusion

It has been known that the cyclic resistance to liquefaction of sand deposits is influenced by a number of factors such as the number of cycles, content of fines, stress history and age of deposition. However, factors affecting the shear wave velocity or shear modulus at small strains have not been previously a target of detailed investigation. This trend appears to be due to relatively smaller degree of influence that the shear modulus has on the damage associated with large deformations of soils during earthquakes. In the light of this tendency, it is reasonable to believe that the relationship between the cyclic strength and shear wave velocity could emerge mainly from difference in the factors affecting the cyclic strength.

In the present study, an attempt is made to examine whether it is appropriate or not to make use of a single unique relationship for the cyclic strength of sand deposits as correlated with shear wave velocity. As one of the factors, effect of aging is investigated using the cyclic triaxial test apparatus equipped by V_S measurement system. The tests were performed on undisturbed samples recovered from in-situ deposits of known liquefaction and also on samples from deposits of known non-liquefaction at the time of the 2011 Great East Japan Earthquake. Similar series of tests were also carried out on reconstituted samples of several sandy soils. These

tests consisted of non-destructive type measurements of shear wave velocity first, followed by the cyclic loading to cause liquefaction. By taking the ratio of the cyclic resistance to cause liquefaction in 20 cycles to the square of the shear wave velocity, a new term, “cyclic yield strain” or “cyclic reference strain”, was defined.

It was shown that the higher the cyclic yield strain, the more ductile the soil is and the lower value indicates the more brittle nature of soils which seems to be due to the interlocked particles and filling related to old aged deposits. As a result of large numbers of tests, undisturbed samples from aged alluvial deposits (old sand deposits) were found to exhibit the cyclic yield strain which is lower than that from once-liquefied or artificially reclaimed soil deposits (new sand deposits). Similar results of tests were obtained for reconstituted samples. It is then suggested that two different curves pertaining to new and old sand deposits can be used to correlate the liquefaction resistance and the shear wave velocity in sites of natural deposits in order to consider the effect of aging or cementation. Thus, the relationship between these two quantities as determined via the relevant cyclic yield strain is considered to be a effective tool to assess the liquefaction resistance of in-situ deposits through measurements of the shear wave velocity.

The cyclic yield strain in simple shear mode is a kind of threshold shear strain at which the soils begin to deform and yield significantly in the cyclic stress-strain curve, conceptually marking the beginning of significant amount of cyclic yield strain before liquefaction triggering in sand deposits. Thus, a substantial amount of pore water pressure must be developing in the range of the value of cyclic yield strain in simple shear mode.

Last but not least, the tendency of the average curve pertaining to the old sand deposits seems to be unique, though the tendency of the curves representative of new sand deposits in the V_S-based liquefaction chart is soil or site-specific dependent.

7.2 Recommendation

1. For further studies, more data are required to refine and verify the suggested values of equal cyclic yield strain associated with new and old sand deposits, similar to what has been accomplished for Asahi sites.

2. Since the post-liquefaction volumetric strains were measured, along with determining shear-wave velocity and liquefaction resistance, the effects of aging on volumetric strains should be examined in both undisturbed and reconstituted samples with respect to different levels of cyclic shear strain.

3. It has been known that the value of volumetric strain is measured by the index properties such as relative density and SPT N-value. The shear-wave velocity as another index property may also be used to measure the volumetric strain using cyclic yield strain.

REFERENCES

Ahmadi, M., & Paydar, N. A. (2014). Requirements for soil-specific correlation between shear wave velocity and liquefaction resistance of sands. *Soil Dynamics and Earthquake Engineering, 57*, 152-163.

Andrianopoulos K. I., Bouckovalas, G. D., & Papadimitriou, A. G. (2001). A critical state evaluation of fines effect on liquefaction potential. Proceedings: Fourth International Conference on Recent Advances in Geotechnical Earthquake Engineering and Soil Dynamics and Symposium in Honor of Professor W.D. Liam Finn, San Diego, California, March 26-31.

Andrus, R. D., & Stokoe II, K. H. (2000). Liquefaction resistance of soils from shear-wave velocity. *Journal of Geotechnical and Geoenvironmental Engineering, 126*(11), 1015-1025.

Andrus, R. D., Piratheepan, P., Ellis, B. S., Zhang J., & Juang C. H. (2003). Comparing liquefaction evaluation methods using penetration-v_s relationships. *Soil Dynamics and Earthquake Engineering, 24* (9-10), 713-721.

Andrus, R. D., Stokoe, K. H., II, & Juang, C. H. (2004). Guide for shear wave-based liquefaction potential evaluation. *Earthquake Spectra, 20*(2), 285–308.

Andrus, R. D., Hayati, H., & Mohanan, N. P. (2009). Correcting liquefaction resistance for aged sands using measured to estimated velocity ratio. *Journal*

of Geotechnical and Geoenvironmental Engineering, 135(6), 735–744.

Arango, I., & Migues, R. E. (1996). Investigation of the seismic liquefaction of old sand deposits. Rep. on Research, Bechtel Corporation, National Science Foundation Grant No. CMS-94-16169, San Francisco.

Arango, I., Lewis, M. R., & Kramer, C. (2000). Updated liquefaction potential analysis eliminates foundation retrofitting of two critical structures. *Soil Dynamics and Earthquake Engineering, 20*, 17–25.

Baki, A. L., Lo, S. R. & Rahman, M. M. (2010). Effect of cyclic stress reversal on cyclic instability behavior of loose sand-silt mixtures. 11th IAEG Congress, 1649-1656.

Baxter, C. D. P., Bradshaw, A. S., Green, R. A., & Wang J. (2008). A new correlation between cyclic resistance and shear wave velocity for silts. *Journal of Geotechnical and Geoenvironmental Engineering, 134*(1), 37-46.

Belkhatir, M., Arab, A., & Della, N. (2010). Liquefaction resistance of Rhlef river silty sand, effect of low plastic fines and other parameters. *Acta Polytechnica Hungarica, 7*(2).

Bhatia, S. (1980). *The verification of relationships for effective stress method to evaluate liquefaction potential of saturated sands.* Ph.D. dissertation, University of British Columbia, Canada.

Bobe, D. C., Lo, S. R., Wanatowski, D., Gnanendran, C. T., & Rahman MM. (2009). Modified state parameter for characterizing static liquefaction of sand with fines. *Canadian Geotechnical Journal, 46*, 281–295.

Chang, N. Y., Yeh, S. T., & Kaufman L. P. (1982). Liquefaction Potential of Clean and Silty Sand. *Proceeding of third International Earthquake Microzonation Conference*, San Francisco, CA, USA.

Chang, N. Y. (1990). Influence of fines content and plasticity on earthquake-induced soil liquefaction. Contract No. DACW3988-C-O078, US Army WES, MS.

Cubrinovski, M., & Rees, S. (2008). Effects of fines on undrained behavior of sands. Sacramento, CA, USA: Geotechnical Earthquake Engineering and Soil Dynamics IV, 18-22.

Dash, H. K., & Sitharam, T. G. (2011). Undrained monotonic response of sand-silt mixtures: effect of nonplastic fines. *International Journal of Geomechanics and Geoengineering, 6*(1), 47–58.

Dobry, R., Powell, D. J., Yokel, F. Y., & Ladd, R. S. (1980). Liquefaction potential of saturated sand – the stiffness method. *Proceedings of 7th World Conference on Earthquake Engineering*, Istanbul, Turkey, 3, 25-32.

Dobry, R. (1985). Unpublished data files. Rensselaer Polytechnic Institute, Troy, NY.

Dobry, R., & Abdoun, T. (2011). An investigation into why liquefaction charts work: a necessary step towards integrating the states of art and practice. *Proceedings of 5th International Conference on Earthquake Geotechnical Engineering.* San Tiago, Chile, 13-44.

Dobry, R., Abdoun, T., Stokoe, K., II, Moss, R., Hatton, M., & El Ganainy, H. (2015). Liquefaction potential of recent fills versus natural sands located in high-seismicity regions using shear-wave velocity. *Journal of Geotechnical and Geoenvironmental Engineering, 141*(3), 0401411201-0401411213.

Erten, D., & Maher, M. H. (1995). Cyclic undrained behavior of silty sand. *Soil Dynamics and Earthquake Engineering, 14*(2), 115–123.

Fei, H. C. (1991). The characteristics of liquefaction of silt soil. Soil Dynamics and Earthquake Engineering V, Computational Mechanics Publications, South Hampton, 293-302.

Finn, W. D. L. (1981). Liquefaction potential: developments since 1976. *Proceedings of International Conference on Recent Advances in Geotechnical Earthquake Engineering and Soil Dynamics*, 2, 655-681.

Finn, W. D. L. (1991). Assessment of liquefaction potential and post liquefaction behavior of earth structures: developments 1981–1991. *In Proceedings of second international conference on recent advances in geotechnical earthquake engineering and soil dynamics,* St. Louis, 2, 11-15.

Garga, V., & McKay, L., (1984). Cyclic triaxial strength of mines tailings. *Journal of Geotechnical and Geoenvironmental Engineering, 110*(8), 1091- 1105.

Georgiannou, V. N. (2006). The Undrained Response of Sands with Additions of Particles of Various Shapes and Sizes. *Géotechnique, 56*(9), 639–649.

Hardin, B. O., & Richart, F. E. (1963). Elastic wave velocities in granular soils. *Journal of Soil Mechanics and Foundations, 89*, 33-65.

Hayati, H., & Andrus, R. D. (2008). Liquefaction potential map of Charleston, South Carolina based on the 1886 earthquake. *Journal of Geotechnical and Geoenvironmental Engineering, 134*(6), 815–828.

Hayati, H., & Andrus, R. D. (2009). Updated liquefaction resistance correction factors for aged sands. *Journal of Geotechnical and Geoenvironmental Engineering, 135*(11), 1683–1692.

Hazirbaba, K., & Rathje, E. M. (2009). Pore pressure generation of silty sands due to induced cyclic shear strains. *Journal of Geotechnical and Geoenvironmental Engineering, 135*(12).

Heidari, T., & Andrus, R. D. (2010). Mapping liquefaction potential of aged soil deposits in Mount Pleasant, South Carolina. *Engineering Geology, 112*(1-4), 1-12.

Hsu, C. C., & Vucetic, M. (2004). Volumetric threshold shear strain for cyclic

settlement. *Journal of Geotechnical and Geoenvironmental Engineering, 130* (1), 58-70.

Ishihara, K., Silver, M. L., & Kitagawa, H. (1979). Cyclic strength of undisturbed sands obtained by a piston sampler. *Soils and Foundations, 19*(3), 61-76.

Ishihara, K. (1993). Liquefaction and flow failure during earthquakes. *Geotechnique, 43*(3), 351-415.

Ishihara, K., Ueno, K., Yamada, S., Yasuda, S., & Yoneoka, T. (2015). Breach of tailings dam in the 2011 earthquake in Japan. *International Journal of Soil Dynamics and Earthquake Engineering, 68*, 3-22.

Jamiolkowski, M., & Lo Presti, D. C. F. (1990). Correlation between liquefaction resistance and shear wave velocity. *Soils and Foundations, 32*(2), 145–148.

Kayen, R. E., Mitchell, J. K., Seed, R. B., Lodge, A., Nishio, S., & Coutinho, R. (1992). Evaluation of SPT-, CPT- and Shear wave-based method for liquefaction potential assessment using Loma Prieta data. *Proceedings of 4th Japan-U. S. Workshop on Earthquake Resistant Design of Lifeline Facilities and Coutermeasures for Soil Liquefaction,* Technical Report NCEER-92-0019, by M. Hamada and T. D. O'Rounke, 177-204.

Kayen, R. E., Seed, R. B., Moss, R. E., Çetin, K. O., Tanaka, Y., & Tokimatsu, K. (2004). Global shear wave velocity database for probabilistic assessment of the initiation of seismic-soil liquefaction. 11th International Conference on

Soil Dynamics & Earthquake Engineering, Berkeley, CA.

Kayen, R., Moss, R. E. S, Thompson, E. M, Seed, R. B., Cetin, K. O., Der Kiureghian, A., Tanaka, Y., & Tokimatsu, K. (2013). Shear-wave velocity–based probabilistic and deterministic assessment of seismic soil liquefaction potential. *Journal of Geotechnical and Geoenvironmental Engineering, 139*(3), 407–419.

Koester, J. P. (1994). The influence of fines type and content on cyclic strength. In Ground Failures under Seismic Conditions, ASCE publication No.44, 17-33.

Kokusho, T., Yoshida, Y., Nishi, K., & Esashi, Y. (1983). Evaluation of seismic stability of sand layer (part 1). Report 383025, Electric Power Central Research Institute (In Japanese).

Kramer, C. & Arango, I. (1998). Aging effects on the liquefaction resistance of sand deposits: a review and update. *Proceedings of Eleventh European Conference on Earthquake Engineering*, A.A. Balkema, CD-ROM, Bisch Philippe, Pierre Labbe, and Alain Pecker, eds., Paris.

Kuerbis, R., Negussey, D., & Vaid, V. P. (1988). Effect of gradation and fines content on the undrained response of sand. *Proceedings of Hydraulic Fill Structures*, Fort Collins, USA, 330-345.

Kulhawy, F. H., & Mayne, P. W. (1990). Manual on estimating soil properties for foundation design. Final Rep. 1493-6, EL-6800, Electric Power Research

Institute, Palo Alto, CA.

Lade, P. V., & Yamamuro, J. A. (1997). Effects of nonplastic fines on static liquefaction of sands. *Canadian Geotechnical Journal, 34*(6), 918–928.

Ladd, R. S., Dobry, R., Dutko, P., Yokel, F. Y., & Chung, R. M. (1989). Pore water pressure buildup in clean sands because of cyclic straining. *ASTM Geotechnical Testing Journal, 12*(1), 77-86.

Lee, K. L., & Seed, H. B. (1967). Drained strength characteristics of sands. *Journal of the Soil Mechanics and Foundations Division, 93*(6), 117–141.

Lee, K. L., & Fitton, J. A., (1968). Factors affecting the cyclic loading strength of soil. ASTM STP 450, American Society for Testing and Materials, 71-95.

Lee, W. F., Chen, C., Chen, J., & Ishihara, K. (2013). Liquefaction potential of non-plastic silty sands. *Journal of Marine Science and Technology*, DOI: 10.6119/JMST-013-0117-3.

Leon, E., Gassman, S. L., & Talwani, P. (2006). Accounting for soil aging when assessing liquefaction potential. *Journal of Geotechnical and Geoenvironmental Engineering, 132*(3), 363-377.

Lewis, M. R., Arango, I., Kimball, J. K., & Ross, T. E. (1999). Liquefaction resistance of old sand deposits. *Proceedings of 11th Panamerican Conference on Soil Mechanics and Geotechnical Engineering,* ABMS, San Paulo, Brazil,

821–829.

Lewis, M. R., McHood, M. D., & Arango, I. (2004). Liquefaction evaluations at the Savannah river site, a case history. *Proceedings of Fifth International Conference on Case Histories in Geotechnical Engineering*, Paper No.3.21.

Lewis, M. R., Arango, I., & McHood, M. D. (2008). Site characterization philosophy and liquefaction evaluation of aged sands–A Savannah river site and Bechtel perspective. From Research to Practice in Geotechnical Engineering, Geotechnical Special Publication No.180, I. E. Laier, D. K. Grapps, M. H. Hussein, eds.

Liu, N., & Mitchell, J. K. (2006). Influence of nonplastic fines on shear wave velocity-based assessment of liquefaction. *Journal of Geotechnical and Geoenvironmental Engineering, 132*(8), 1091–1097.

Monkul, M. M., & Yamamuro, J. A. (2011). Influence of silt size and content on liquefaction behavior of sands. *Canadian Geotechnical Journal, 48*(6), 931-942.

Monkul, M. M. (2012). On some of the factors influencing the fines' role on liquefaction of silty sands. Geotechnical Special Publication No: 225; GeoCongress: State of the Art and Practice in Geotechnical Engineering, ASCE, 799-808.

Mori, K., Seed, H. B., & Chan, C. K. (1978). Influence of sample disturbance on

sand liquefaction characteristics. *Journal of Soil Mechanics and Foundations, 104*(3), 323-339.

Muir Wood, D., & Maeda, K. (2008). Changing grading of soil: effect on critical states. *Acta Geotechnica, 3*(1), 3–14.

Murthy, T. G., Loukidis D., Carraro, J. A. H., Prezzi M., & Salgado R. (2007). Undrained monotonic response of clean and silty sands. *Geotechnique, 57*(3), 273–288.

Naeini, S. A., & Baziar, M. H. (2004). Effect of fines content on steady state strength of mixed and layered samples of sand. *Journal of Soil Dynamics and Earthquake Engineering, 24*, 181-187.

Ni, Q., Tan, T. S., Dasari, G. R., & Hight, D. W. (2004). Contribution of fines to the compressive strength of mixed soils. *Géotechnique, 54*(9), 561–569.

Ohsaki, Y. (1970). Effects of sand compaction on liquefaction during Tokachioki earthquake. *Soils and Foundations, 10*(2), 112-128.

Okusa, S., Anma, S., & Maikuma, H. (1980). Liquefaction of mine tailings in the 1978 Izu-Oshima-Kinkai earthquake, central Japan. *Proceedings of the Seventh World Conference on Earthquake Engineering*, Istanbul, Turkey, 3, 89-96.

Papadimitriou A. G., Bouckovalas G. D., & Dafalias Y. F. (2001). Plasticity model

for sand under small and large cyclic strains. *Journal of Geotechnical and Geoenvironmental Engineering, 127*(11), 973 – 983.

Papadopoulou, A., & Tika, T. (2008). The effect of fines on critical state and liquefaction resistance characteristics of non-plastic silty sands. *Soils and Foundations, 48*(5), 713–725.

Pitman, T. D., Robertson, P. K., & Sego, D. C. (1994). Influence of fines on the collapse of loose sands. *Canadian Geotechnical Journal, 31*(5), 728–739.

Polito, C. P. (1999). *The effects of non-plastic and plastic fines on the liquefaction of sandy soils.* Ph.D. Dissertation, Virginia Polytechnic Institute and State University, USA.

Polito, C. P., & Martin II, J. R. (2001). Effects of nonplastic fines on the liquefaction resistance of sands. *Journal of Geotechnical and Geoenvironmental Engineering, 127*(5), 408-415.

Pradhan, T. B. S., Kiku, H., & Sato, K. (1995). Effect of fines content on behavior of sand during the process to liquefaction. *Proceedings of First International Conference on Earthquake Geotechnical Engineering,* Tokyo, 14-16 November.

Rahman, M. M., & Lo, S. R. (2007). Equivalent granular void ratio and state parameters for loose clean sand with small amount of fines. Brisbane, Australia: 10th Australia New Zealand Conference on Geomechanics:

Common Ground, 2, 674-679.

Rahman, M. M., Baki, M. A. L., & Lo, S. R. (2013). Prediction of undrained monotonic and cyclic liquefaction behavior of sand with fines based on equivalent granular state parameter. *International Journal of Geomechanics, 14*(2), 254-266.

Rahman, M. M., Baki, M., & Lo, S. (2014). Prediction of undrained monotonic and cyclic liquefaction behavior of sand with fines based on the equivalent granular state parameter. *International Journal of Geomechanics*, 10.1061/(ASCE)GM.1943-5622.0000316, 254-266.

Rees SD. (2010). *Effects of fines on the undrained behavior of Christchurch sandy soils.* Ph.D dissertation, University of Canterbury, Christchurch, New Zealand.

Robertson, P. K., Woeller, D. J., & Finn, W. D. L. (1992). Seismic cone penetration test for evaluating liquefaction potential under cyclic loading. *Canadian Geotechnical Journal, 29*, 686-695.

Roy, D., Campanella, R. G., Byrne, P. M., & Hughes, J. M. O. (1996). Uncertainty in the geologic environment: From theory to practice. In C. D. Shackelford, P. P. Nelson, and M. J. S. Roth (Eds.), *Strain level and uncertainty of liquefaction related index Tests* (pp. 1149-1169). Geotech. Spec. Publ. No. 58, New York.

Seed, H. B., & Idriss, I. M. (1971). Simplified procedure for evaluating soil liquefaction potential. *Journal of Soil Mechanics and Foundation Division, 97*(9), 1249–1273.

Seed, H. B., Mori, K., & Chan, C. K. (1977). Influence of seismic history on liquefaction of sands. *Journal of the Geotechnical Engineering Division, 103*(4), 257-270.

Seed, H. B. (1979). Soil liquefaction and cyclic mobility evaluation for level ground during earthquakes. *Journal of the Geotechnical Engineering Division, 105*(2), 201–255.

Seed, H. B., Tokimatsu, K., Harder, L., & Chung, R. (1985). Influence of SPT procedures in soil liquefaction resistance evaluations. *Journal of Geotechnical and Geoenvironmental Engineering, 111*(12), 1425-1445.

Shapiro, S. & Yamamuro, J. (2003). Effects of silt on three-dimensional stress–strain behavior of loose sand. *Journal of Geotechnical and Geoenvironmental Engineering, 129*(1), 1–11.

Shen, C. K., Vrymoed, J. L., & Uyeno, C. K. (1977). The effect of fines on liquefaction of sands. *Proceedings of the 9th International Conference on Soil Mechanics and Foundation Engineering,* Tokyo, Japan. 2, 381–385.

Singh, S. (1994). Liquefaction characteristics of silt. Ground Failures Under Seismic Conditions, Geotechnical Special Publication No. 44, ASCE, 105-116.

Sitharam, T. G., GovindaRaju, L., & Murthy, B. R. S. (2004). Evaluation of liquefaction potential and dynamic properties of silty sand using cyclic triaxial testing. *Geotechnical Testing Journal, 27*(5).

Sitharam, T. G., & Dash, H. K. (2008). Effect of non-plastic fines on cyclic behavior of sandy soils. In GeoCongress: The Challenge of Sustainability in the Geoenvironment, New Orleans.

Skempton, A. W. (1986). Standard penetration test procedures and the effects in sands of overburden pressure, relative density, particle size, aging, and overconsolidation. *Geotechnique, 36*(3), 425–447.

Stamatopoulous, C. A. (2010). An experimental study of the liquefaction strength of silty sands in terms of the state parameter. *Soil Dynamics and Earthquake Engineering, 30*, 662–678.

Stamatopoulos, C. A. (2011). The liquefaction strength of silty sands in terms of the state parameter. 5th International Conference on Earthquake Geotechnical Engineering, Santiago, Chile.

Stokoe, L. H. II, Roesset, J. M., Biershwale, J. G., & Aouad, M. (1988). Liquefaction potential of sands from shear wave velocity. *Proceedings of 9th World Conference on Earthquake Engineering*, 3, 213-218.

Teachavorasinskun, S., Tatsuoka, F., & Lo Presti, D. C. F. (1994). Effects of the cyclic prestaining on dilatancy characteristics and liquefaction strength of

sand. Pre-failure deformation of geomaterials, S. Shibuya, T. Mitachi, and S. Miura, eds., Balkema, Rotterdam, The Netherlands, 75–80.

Thevanayagam, S. (1998). Effect of fines and confining stress on undrained shear strength of silty sands. *Journal of Geotechnical and Geoenvironmental Engineering, 124*(6), 479–491.

Thevanayagam, S., & Mohan, S. (2000). Intergranular state variables and stress-strain behaviour of silty sands. *Géotechnique, 50*(1): 1–23.

Thevanayagam, S., Fiorillo, M., & Liang, J. (2000). Soil dynamics and liquefaction. In R. Y. S. Pak & J. Yamamura (Eds.), *Effect of non-plastic fines on undrained cyclic strength of silty sands* (pp 77-91). Geotechnical Special Publication No.107, ASCE.

Thevanayagam, S. & Martin, G. R. (2002). Liquefaction in silty soils-screening and remediation issues. *Soil Dynamics and Earthquake Engineering, 22*(9–12), 1035–1042.

Thevanayagam, S., Shenthan, T., Mohan, S., & Liang, J. (2002). Undrained fragility of clean sands, silty sands, and sandy silts. *Journal of Geotechnical and Geoenvironmental Engineering, 128*(10), 849–859.

Tokimatsu, K. & Yoshimi, Y., (1983). Empirical correlation of soil liquefaction based on SPT N-value and fines content. *Soils and Foundations, 23*(4), 56-74.

Tokimatsu, K., Yamazaki, T., & Yoshimi, Y. (1986). Soil liquefaction evaluations by elastic shear moduli. *Soils and Foundations, 26*(1), 25-35.

Tokimatsu, K., & Uchida, A. (1990). Correlation between liquefaction resistance and shear wave velocity. *Soils and Foundations, 30*(2), 33-42.

Troncoso, J. H., & Verdugo, R. (1985). Silt content and dynamic behavior of tailing sands. *Proceedings of Twelfth International Conference on Soil Mechanics and Foundation Engineering,* San Francisco, USA, 1311-1314.

Troncoso, J., Ishihara, K., & Verdugo, R. (1988). Aging effects on cyclic shear strength of tailings materials. *Proceedings of Ninth World Conference on earthquake Engineering,* Tokyo-Kyoto, Japan.

Wang, J. H., Moran, K., & Baxter, C. D. P. (2006). Correlation between cyclic resistance ratios of intact and reconstituted offshore saturated sands and silts with the same shear wave velocity. *Journal of Geotechnical and Geoenvironmental Engineering, 132*(12), 1574-1580.

Whitman, R. V. Ed. (1985). Liquefaction of soils during earthquakes. Committee on Earthquake Engineering, National Research Council, National Academy Press, Washington, D. C.

Xenaki, V. C., & Athanasopoulos, G. A. (2003). Liquefaction resistance of sand-silt mixtures: an experimental investigation of the effect of fines. *Soil Dynamics and Earthquake Engineering, 23,* 183-194.

Yamamuro, J. A., & Lade, P. V. (1997). Static liquefaction of very loose sands. *Canadian Geotechnical Journal, 34*, 905–917.

Yamamuro, J. A., & Lade, P. V. (1998). Steady state concepts and static liquefaction of silty sands. *Journal of Geotechnical and Geoenvironmental Engineering, 124*(9), 868-877.

Yamamuro, J. A., & Covert, K. M. (2001). Monotonic and cyclic liquefaction of very loose sands with high silt content. *Journal of Geotechnical and Geoenvironmental Engineering, 127*(4), 314-324.

Yamamuro, J. A., & Wood, F. M. (2004). Effect of depositional method on the undrained behavior and microstructure of sand with silt. *Soil Dynamics and Earthquake Engineering, 24*(9–10), 751–760.

Yang, S. L., Sandven, R., & Grande, L. (2006). Instability of sand silt mixtures. *Soil Dynamics and Earthquake Engineering, 26*,183–190.

Youd, T. L., & Hoose, S. N. (1977). Liquefaction susceptibility and geologic setting. *Proceedings of 6th World Conf. on Earthquake Engineering*, New Delhi, India, 6, 37–42.

Youd, T. L., & Perkins, D. M. (1978). Mapping liquefaction-induced ground failure potential. *Journal of Geotechnical Engineering Division, 104*, 433–446.

Youd, T., Idriss, I., Andrus, R., Arango, I., Castro, G., Christian, J., Dobry, R., Finn,

W., Harder, L., Jr., Hynes, M., Ishihara, K., Koester, J., Liao, S., Marcuson, W., III, Martin, G., Mitchell, J., Moriwaki, Y., Power, M., Robertson, P., Seed, R., & Stokoe, K., II (2001). Liquefaction resistance of soils: summary report from the 1996 NCEER and 1998 NCEER/NSF workshops on evaluation of liquefaction resistance of Soils. *Journal of Geotechnical and Geoenvironmental Engineering,* 10.1061/(ASCE)1090-0241(2001)127:10(817), 817-833.

Zhou, T. G., & Chen, T. M. (2007). Laboratory investigation on assessing liquefaction resistance of sandy soils by shear wave velocity. *Journal of Geotechnical and Geoenvironmental Engineering, 133*(8), 959–972.

Zhou, Y., Chen, Y., & Shamoto, Y. (2010). Verification of the soil type specific correlation between liquefaction resistance and shear-wave velocity of sand by dynamic centrifuge test. *Journal of Geotechnical and Geoenvironmental Engineering, 136*(1), 165–177.

Zlatovic, S., & Ishihara, K. (1995). On the influence of non-plastic fines on residual strength. *Proceedings of First International Conference on Earthquake Geotechnical Engineering,* 1, 239–244.

Zlatovic, S., & Ishihara, K. (1997). Normalized behavior of very loose non-plastic soils: effects of fabric. *Soils and foundations, 37* (4), 47–56.

APPENDICES

Appendix A: Axial and Deviator Stress, Stress Path and Pore Water Pressure of Undisturbed and Reconstituted Samples

1. Undisturbed Specimens

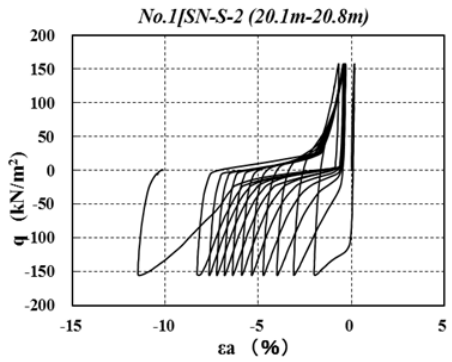

Figure A.1.1 Deviator stress versus axial strain

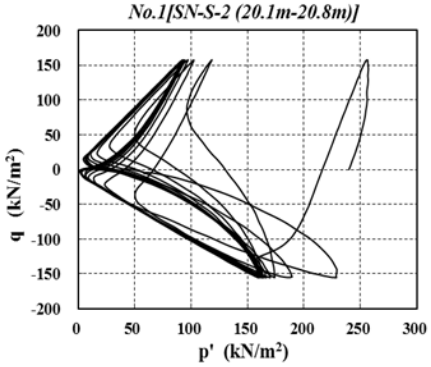

Figure A.1.2 Stress path during the undrained condition

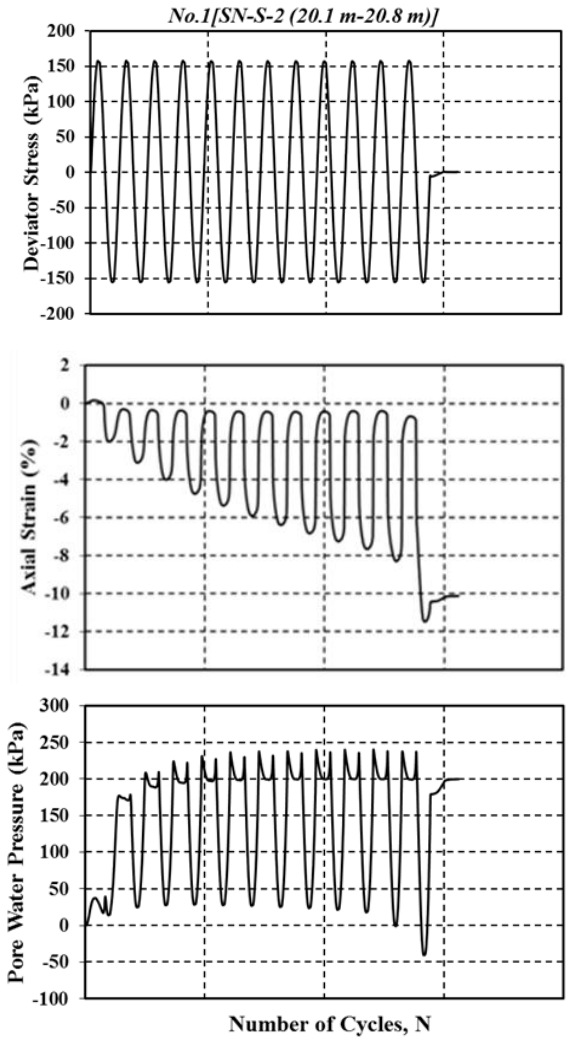

Figure A.1.3 Pore water pressure, axial strain, devaitor stress versus number of

cycles

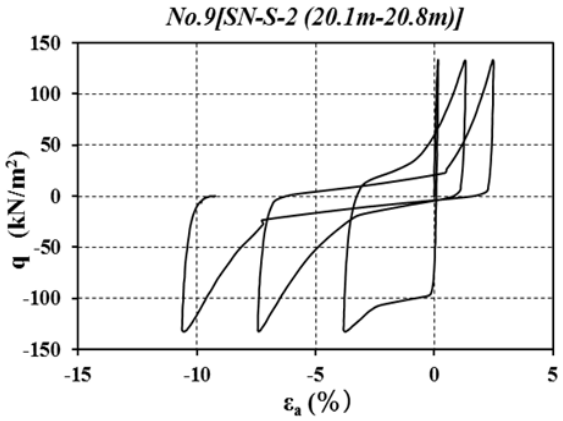

Figure A.1.4 Deviator stress versus axial strain

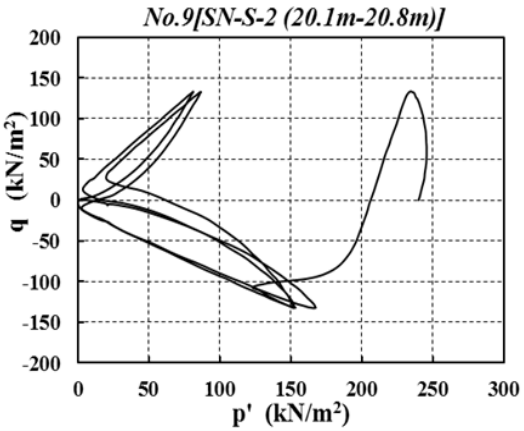

Figure A.1.5 Stress path during the undrained condition

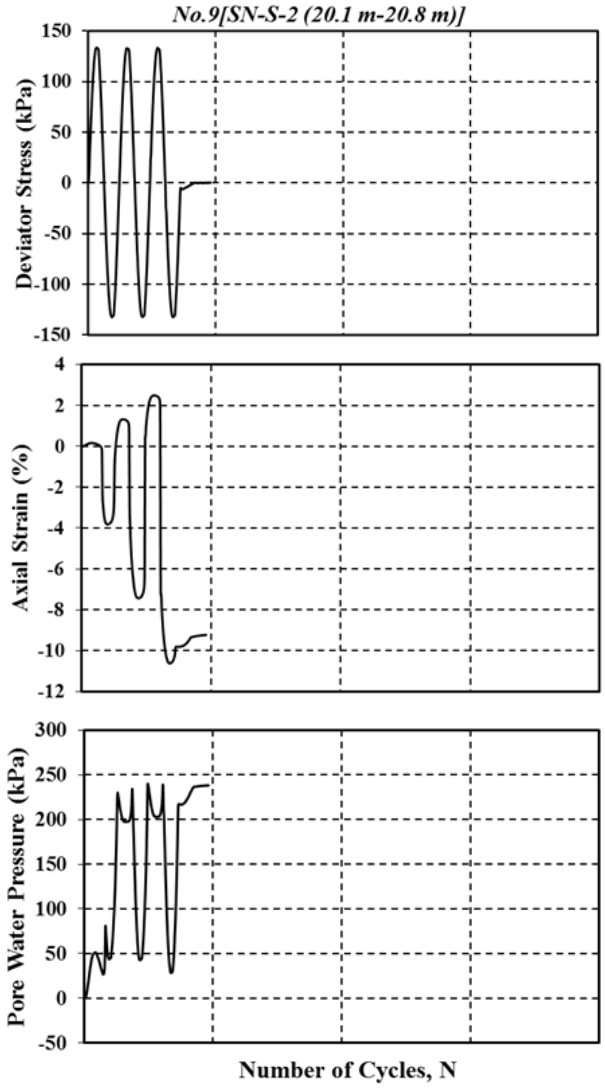

Figure A.1.6 Pore water pressure, axial strain, devaitor stress versus number of cycles

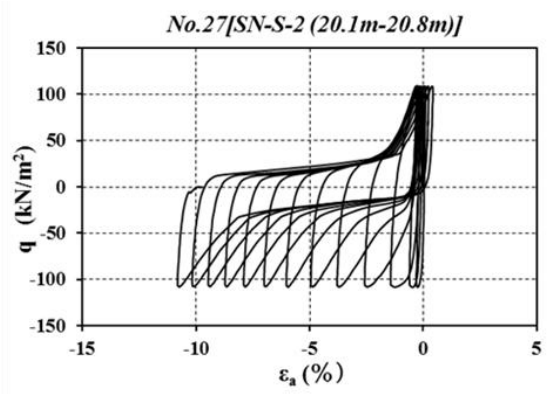

Figure A.1.7 Deviator stress versus axial strain

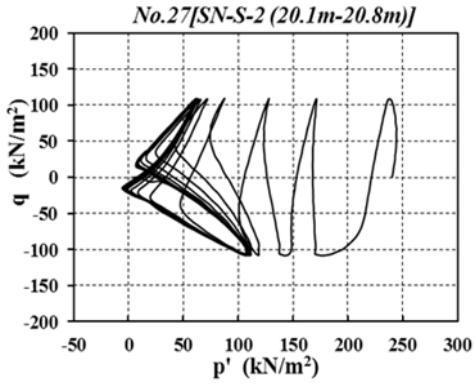

Figure A.1.8 Stress path during the undrained condition

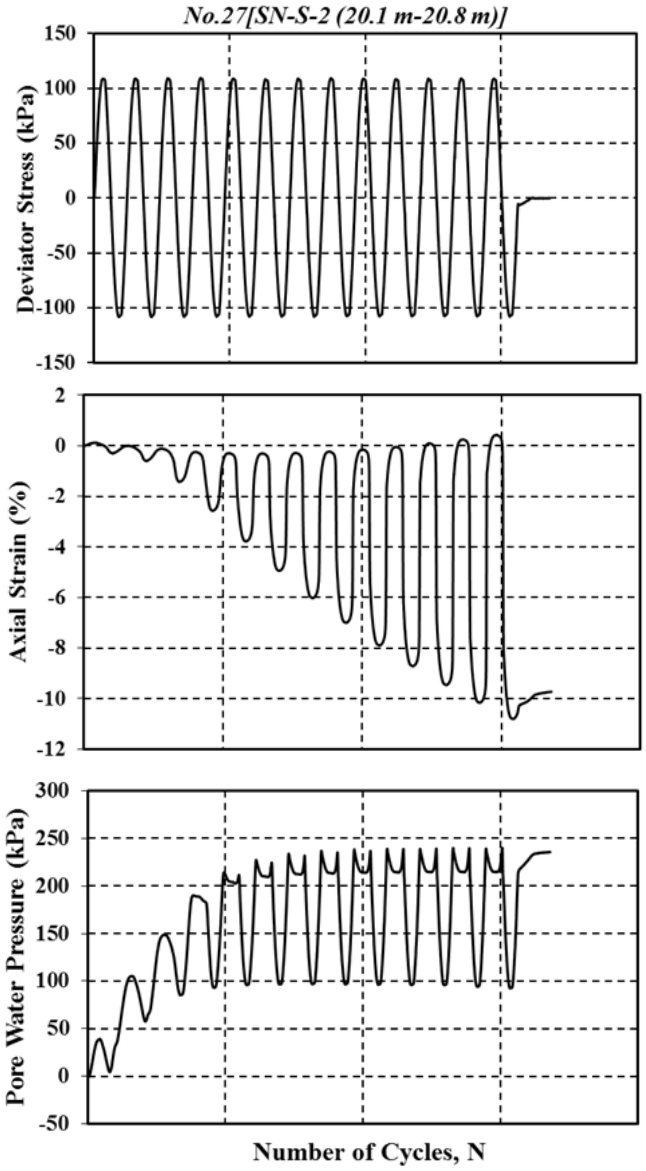

Figure A.1.9 Pore water pressure, axial strain, devaitor stress versus number of cycles

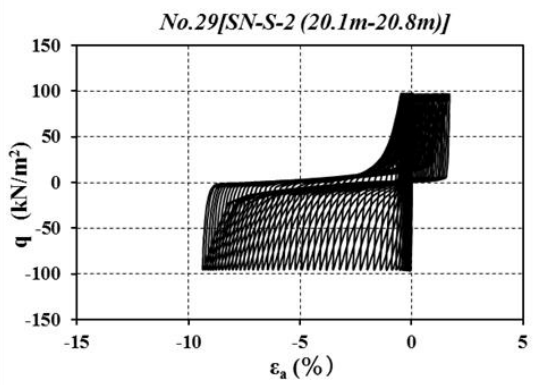

Figure A.1.10 Deviator stress versus axial strain

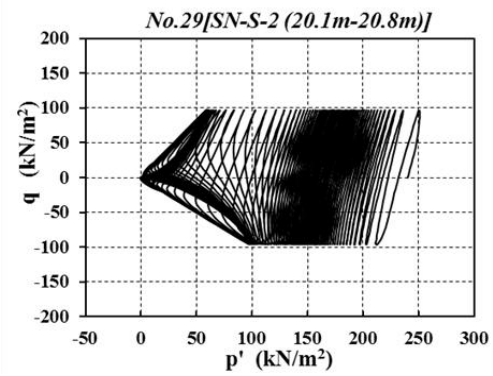

Figure A.1.11 Stress path during the undrained condition

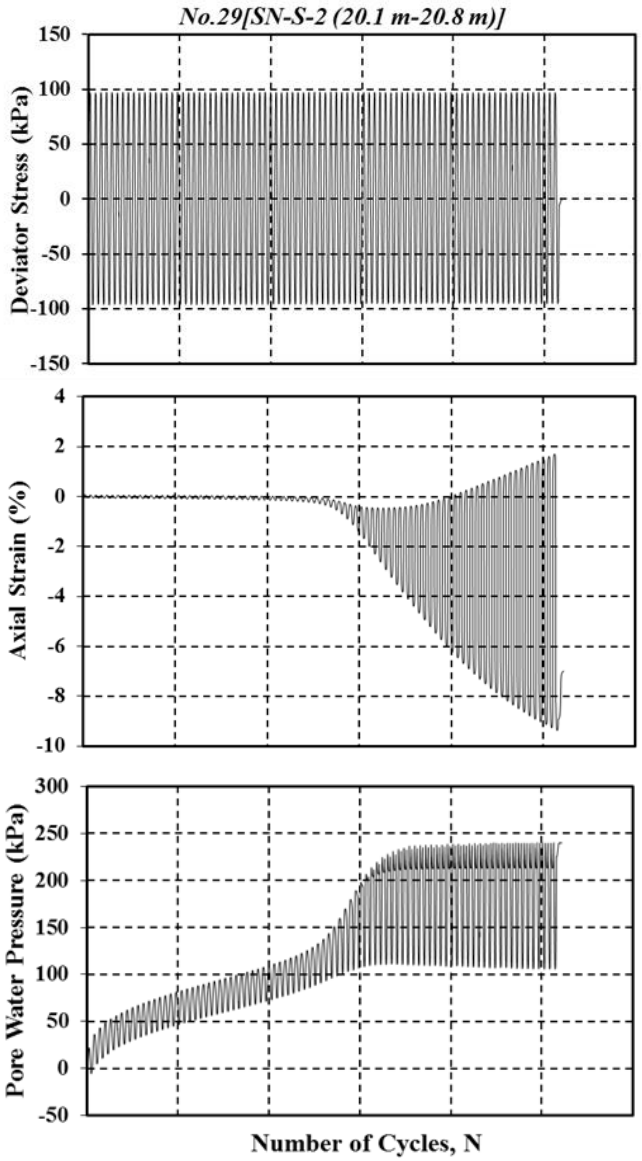

Figure A.1.12 Pore water pressure, axial strain, devaitor stress versus number of cycles

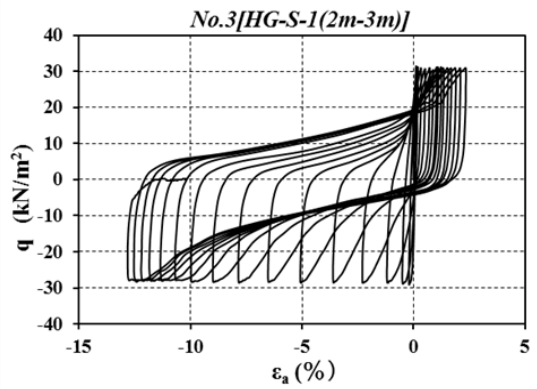

Figure A.1.13 Deviator stress versus axial strain

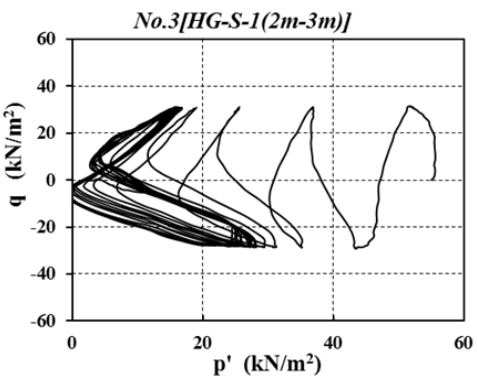

Figure A.1.14 Stress path during the undrained condition

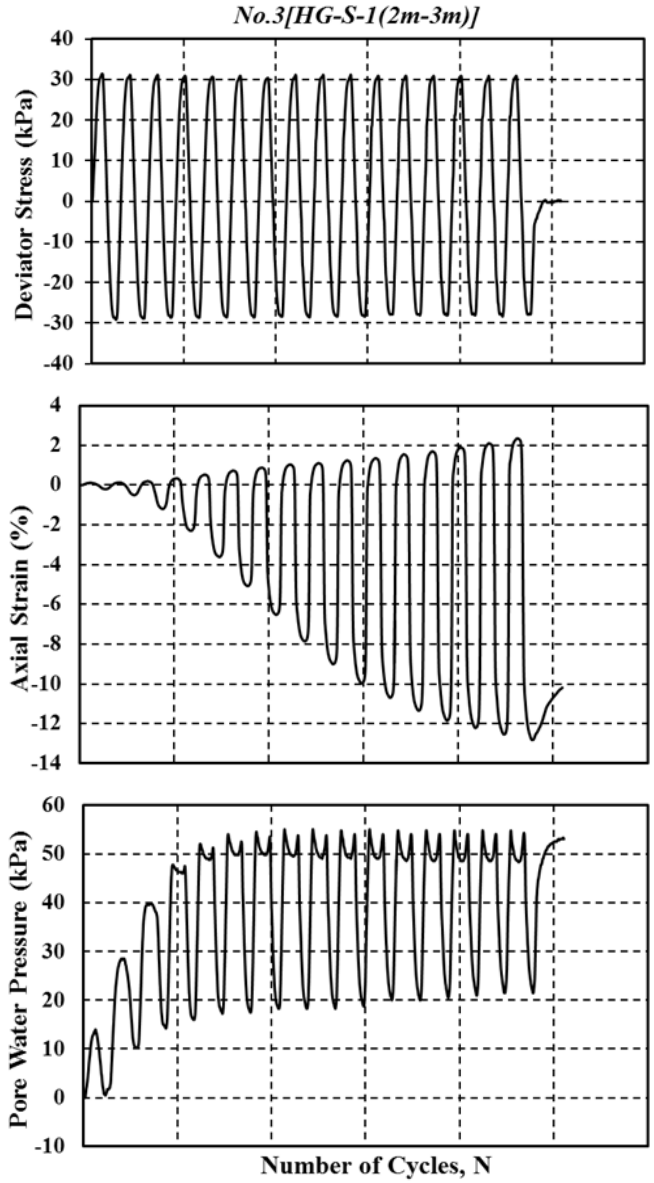

Figure A.1.15 Pore water pressure, axial strain, devaitor stress versus number of cycles

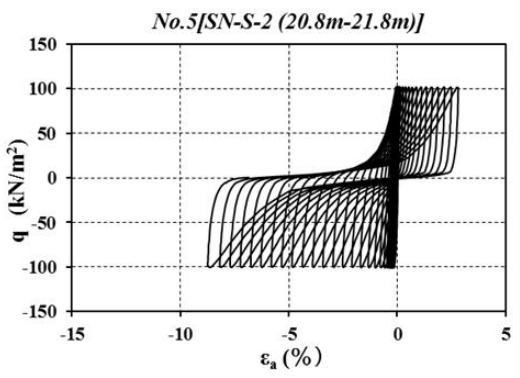

Figure A.1.16 Deviator stress versus axial strain

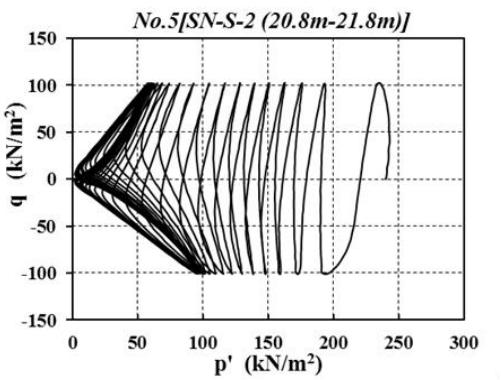

Figure A.1.17 Stress path during the undrained condition

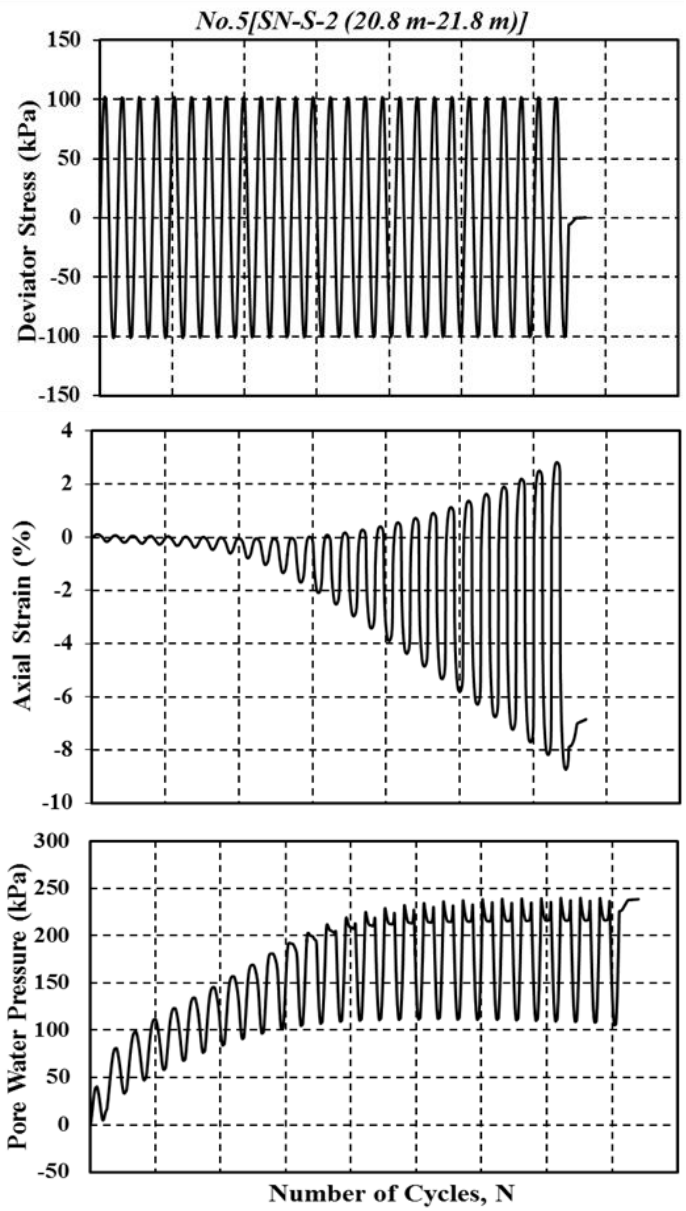

Figure A.1.18 Pore water pressure, axial strain, devaitor stress versus number of cycles

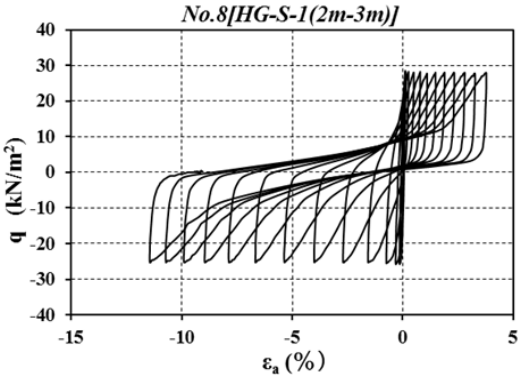

Figure A.1.19 Deviator stress versus axial strain

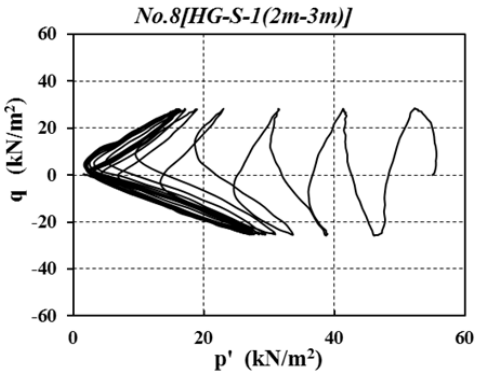

Figure A.1.20 Stress path during the undrained condition

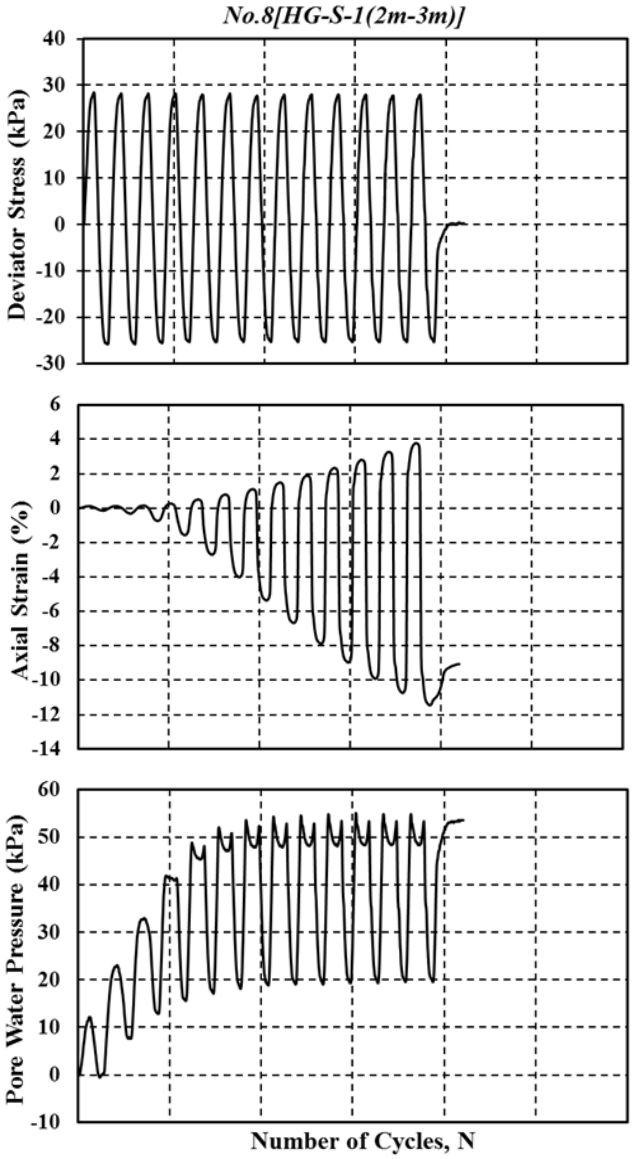

Figure A.1.21 Pore water pressure, axial strain, devaitor stress versus number of cycles

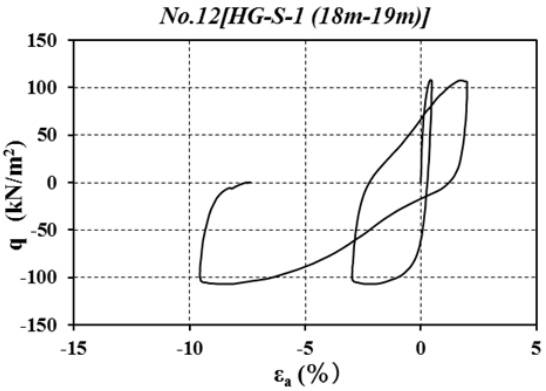

Figure A.1.22 Deviator stress versus axial strain

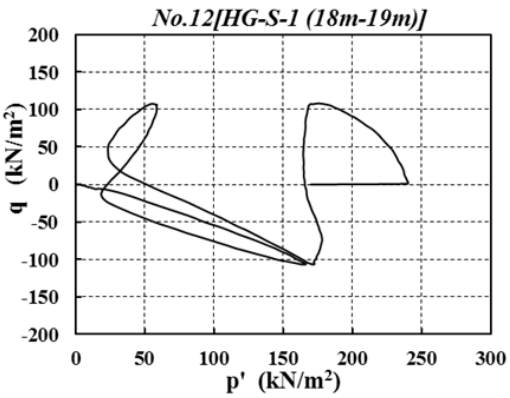

Figure A.1.23 Stress path during the undrained condition

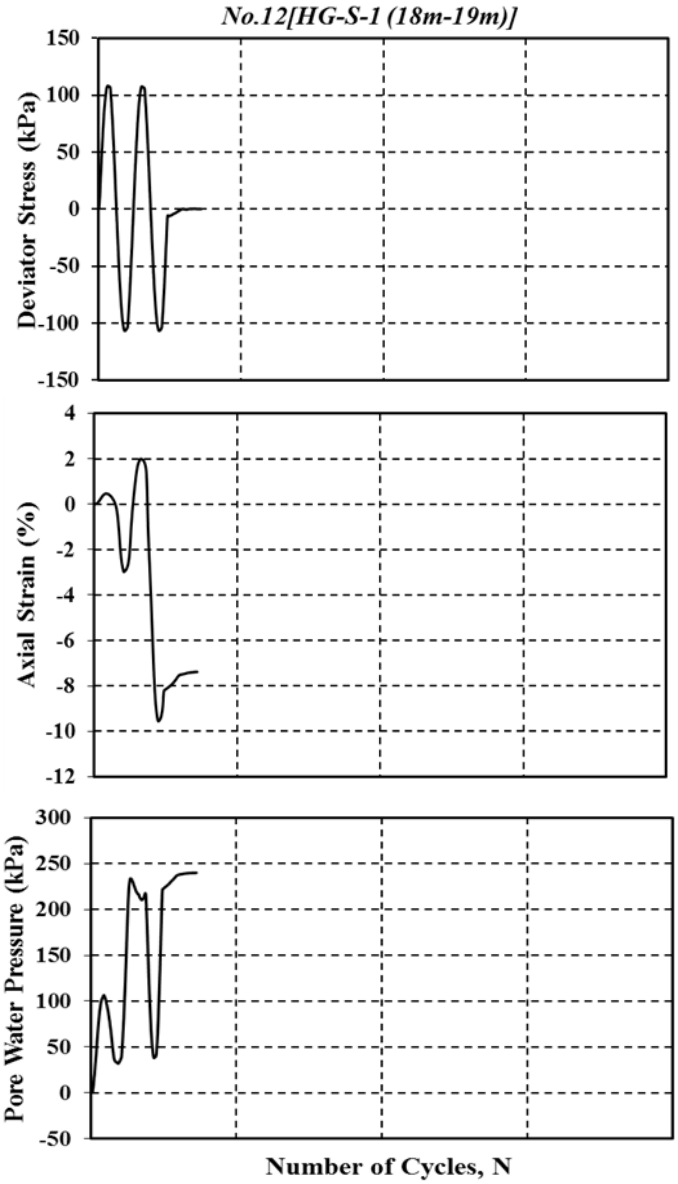

Figure A.1.24 Pore water pressure, axial strain, devaitor stress versus number of cycles

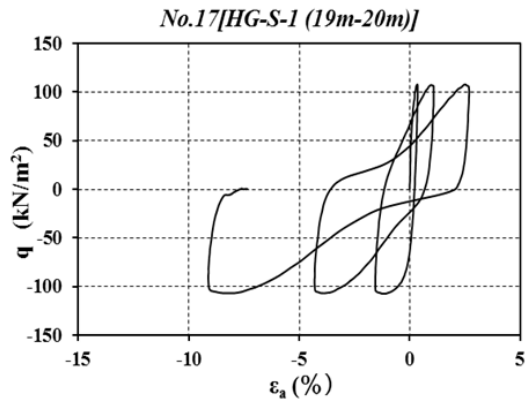

Figure A.1.25 Deviator stress versus axial strain

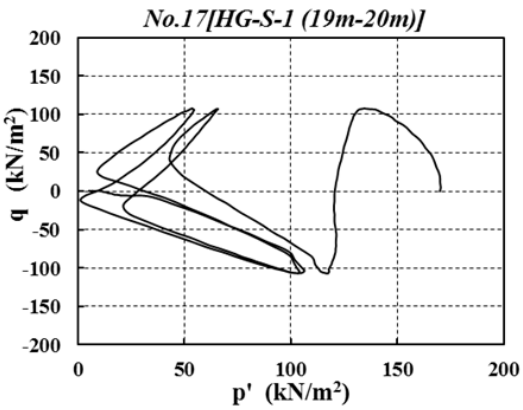

Figure A.1.26 Stress path during the undrained condition

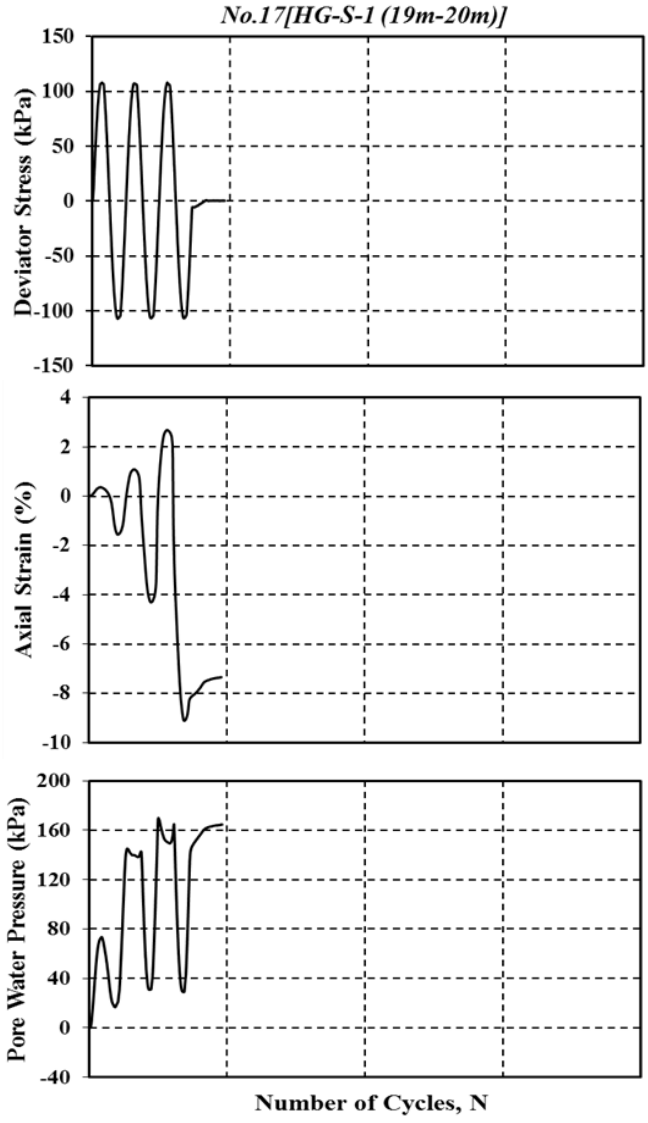

Figure A.1.27 Pore water pressure, axial strain, devaitor stress versus number of cycles

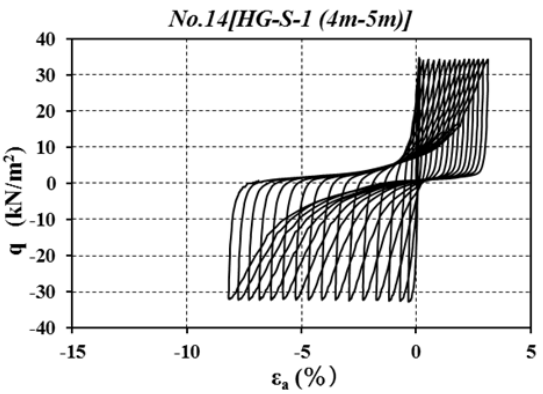

Figure A.1.28 Deviator stress versus axial strain

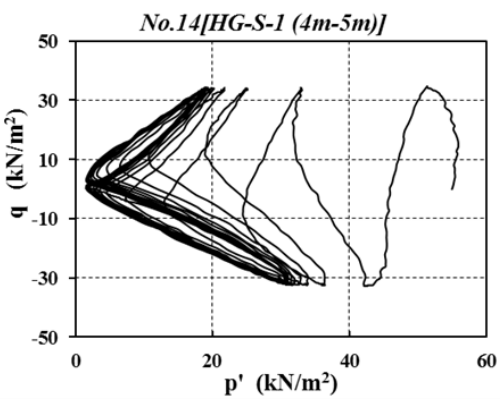

Figure A.1.29 Stress path during the undrained condition

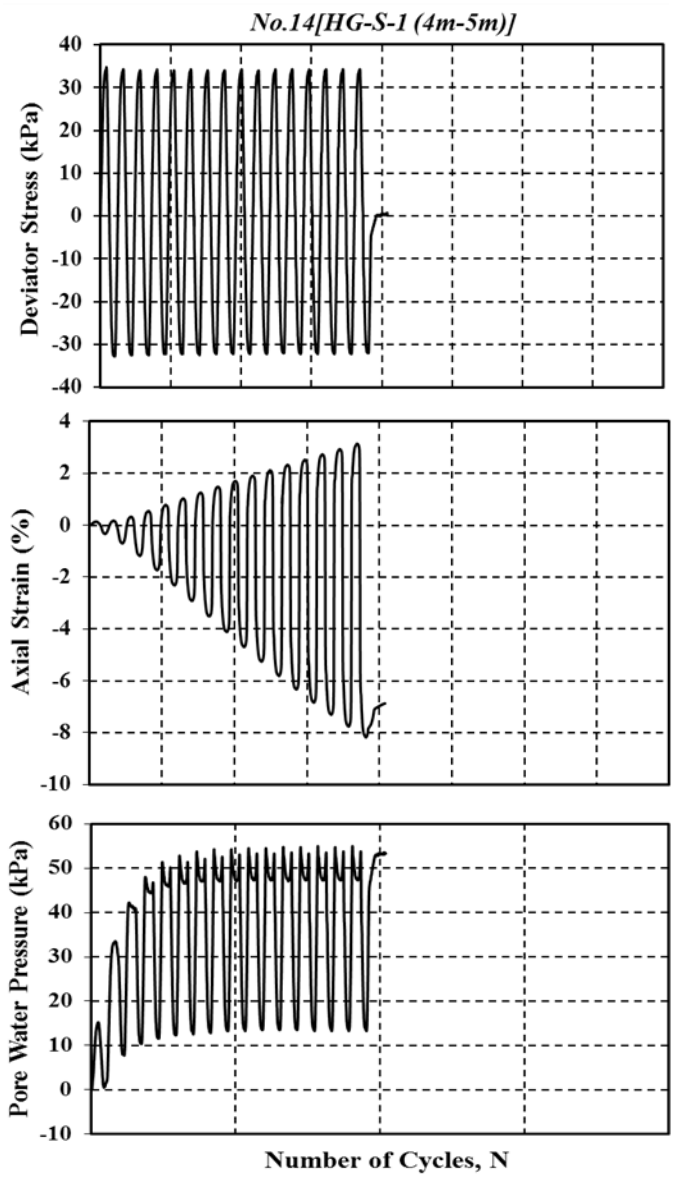

Figure A.1.30 Pore water pressure, axial strain, devaitor stress versus number of cycles

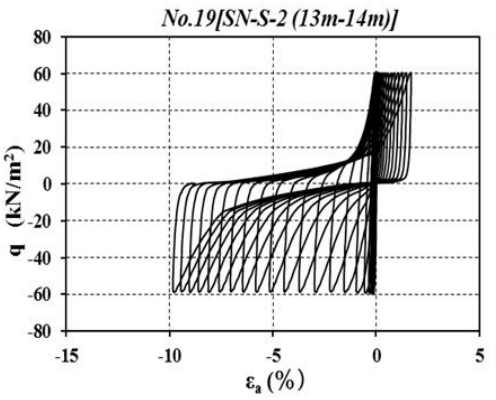

Figure A.1.31 Deviator stress versus axial strain

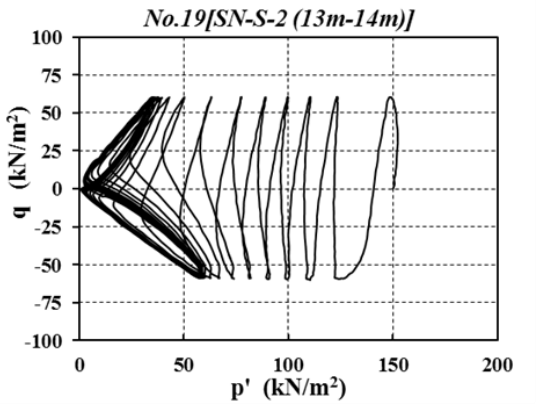

Figure A.1.32 Stress path during the undrained condition

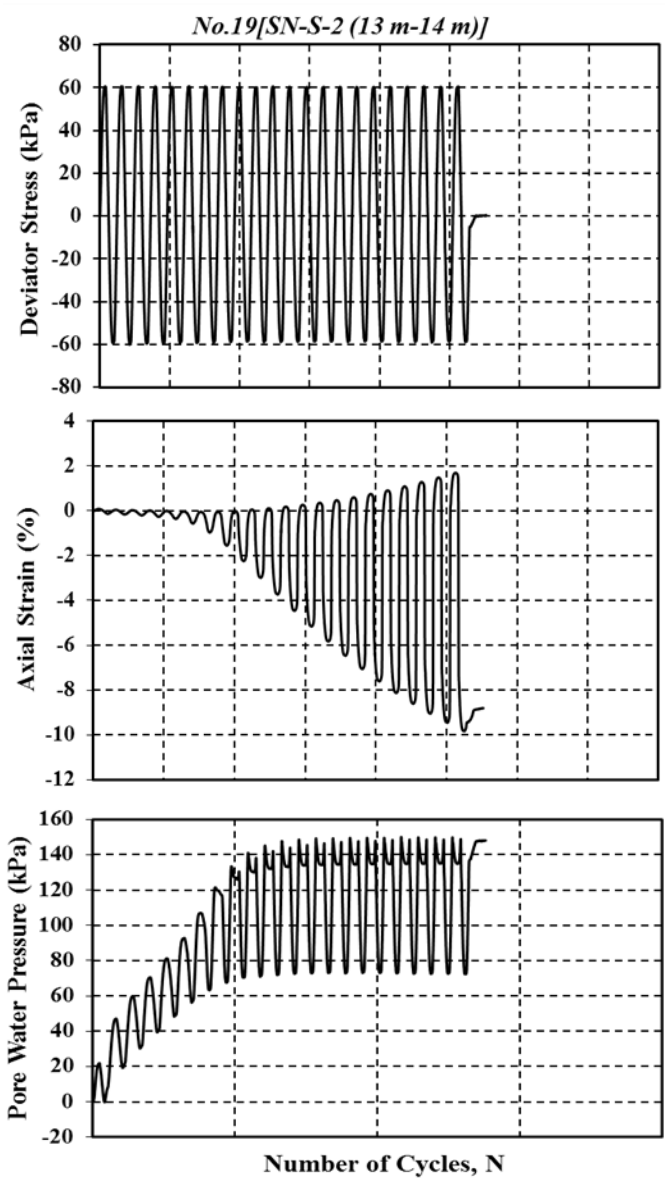

Figure A.1.33 Pore water pressure, axial strain, devaitor stress versus number of cycles

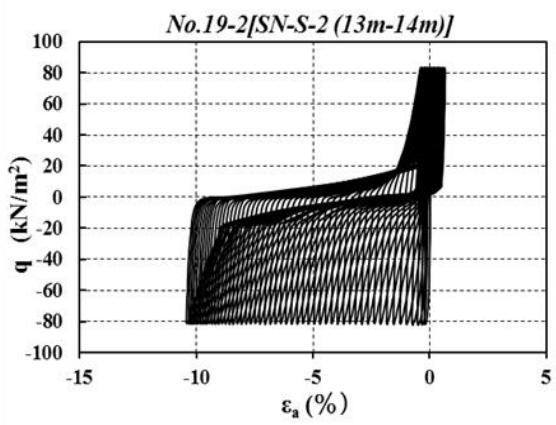

Figure A.1.34 Deviator stress versus axial strain

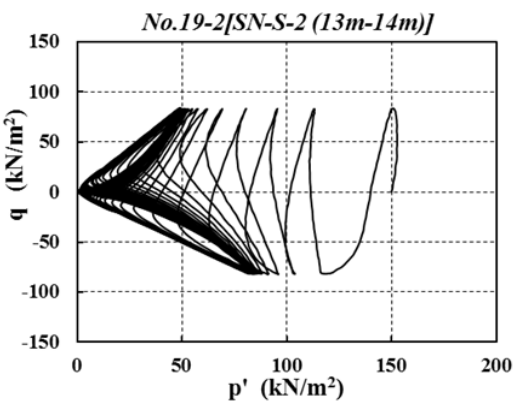

Figure A.1.35 Stress path during the undrained condition

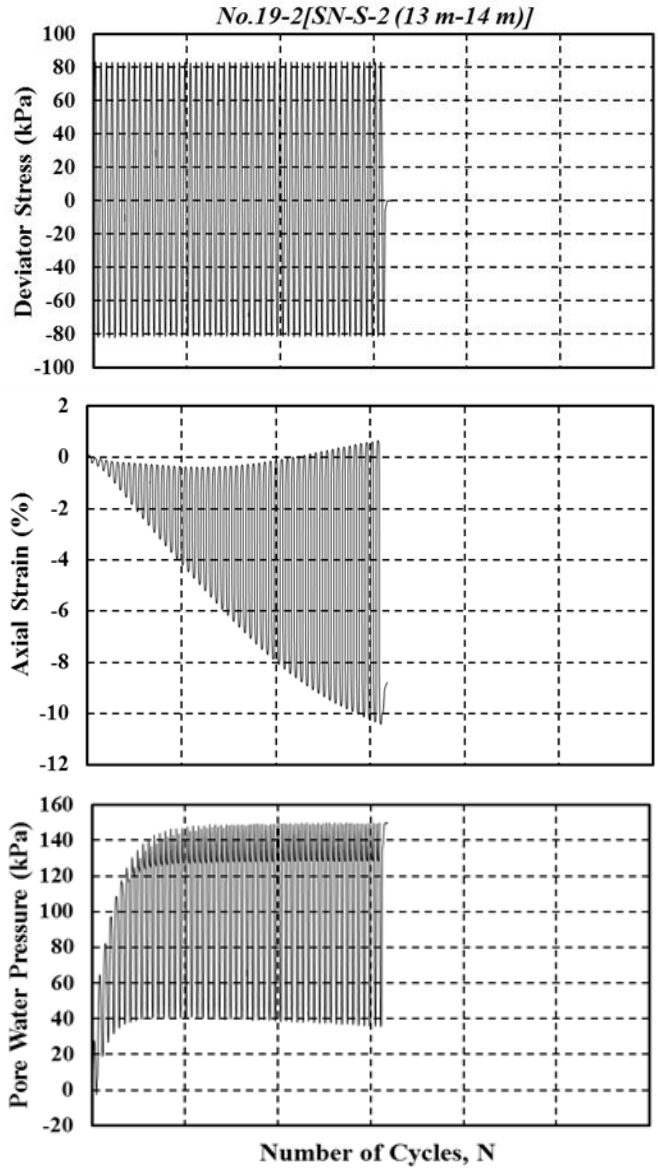

Figure A.1.36 Pore water pressure, axial strain, devaitor stress versus number of cycles

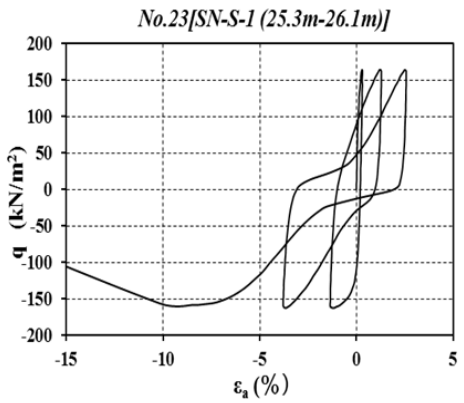

Figure A.1.37 Deviator stress versus axial strain

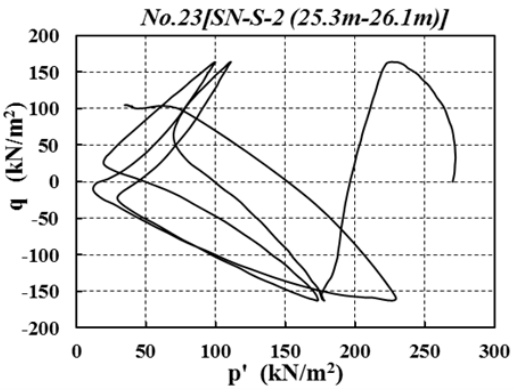

Figure A.1.38 Stress path during the undrained condition

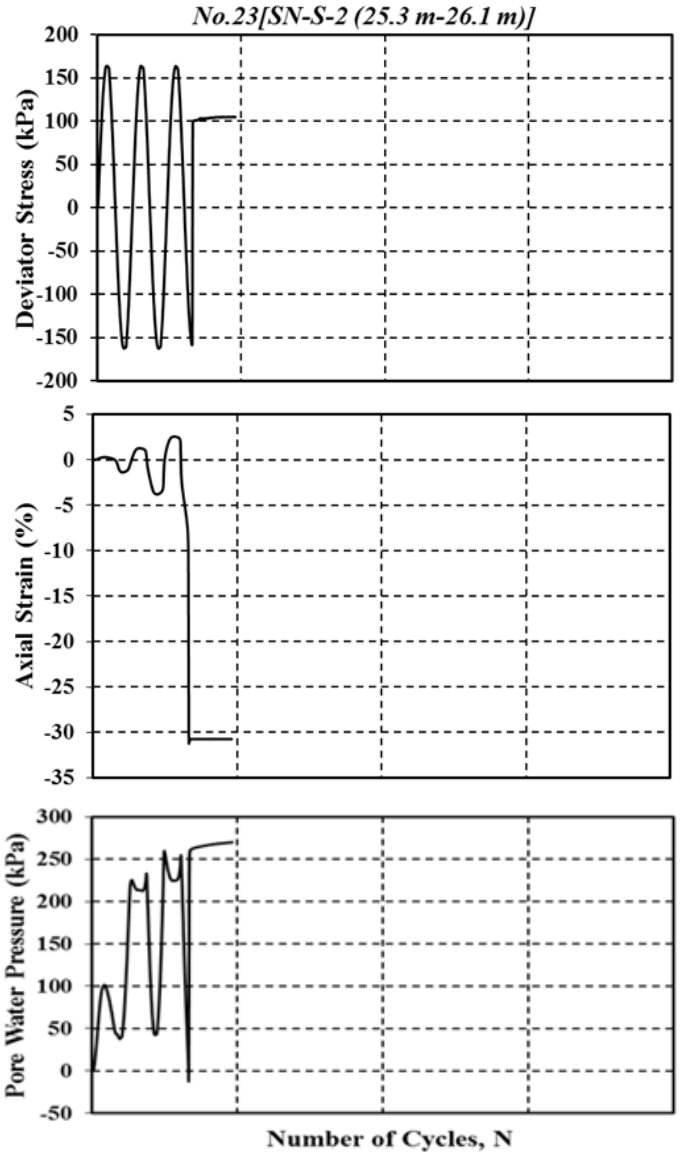

Figure A.1.39 Pore water pressure, axial strain, devaitor stress versus number of cycles

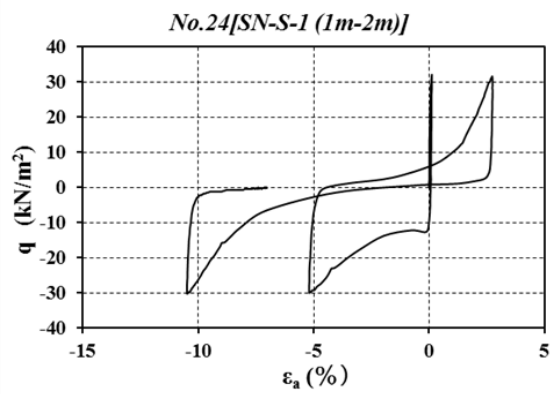

Figure A.1.40 Deviator stress versus axial strain

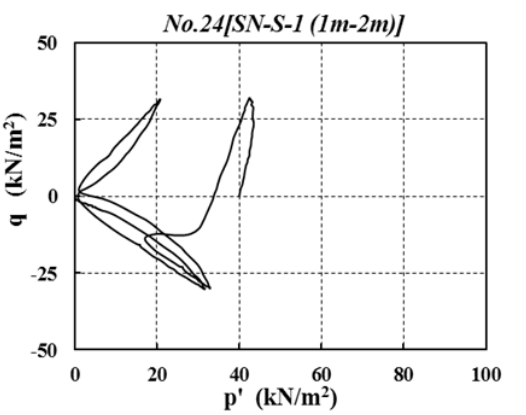

Figure A.1.41 Stress path during the undrained condition

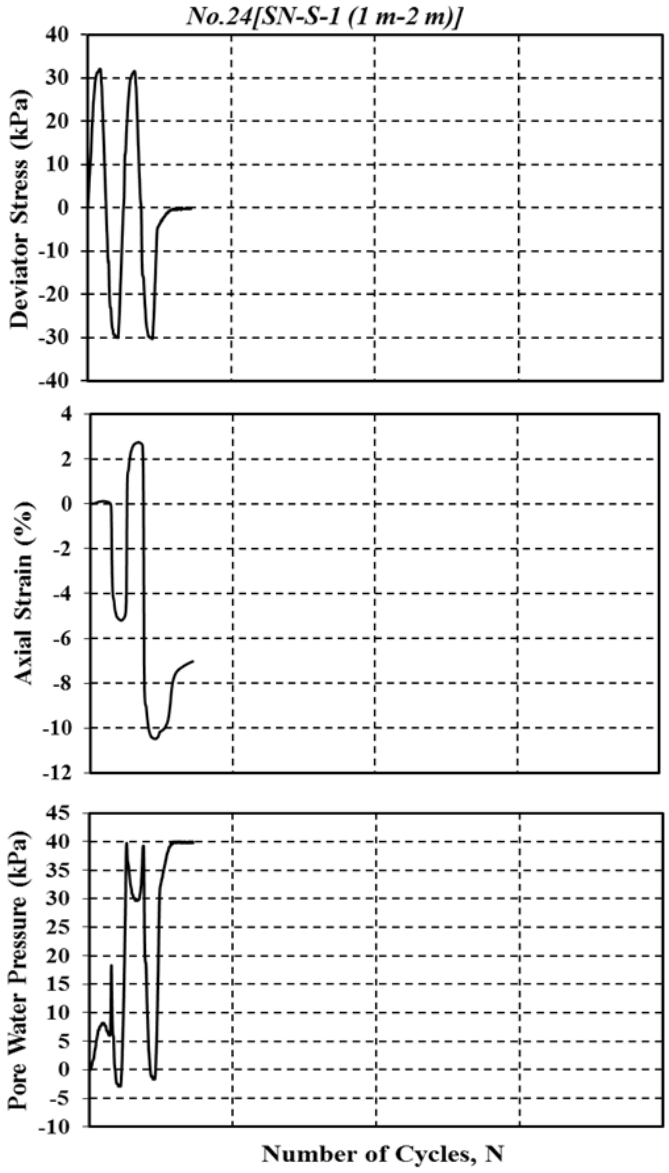

Figure A.1.42 Pore water pressure, axial strain, devaitor stress versus number of cycles

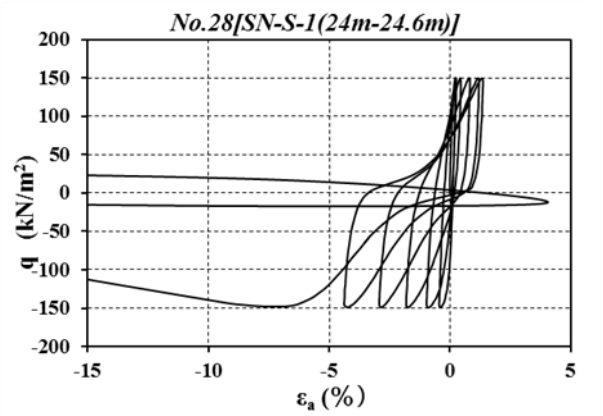

Figure A.1.43 Deviator stress versus axial strain

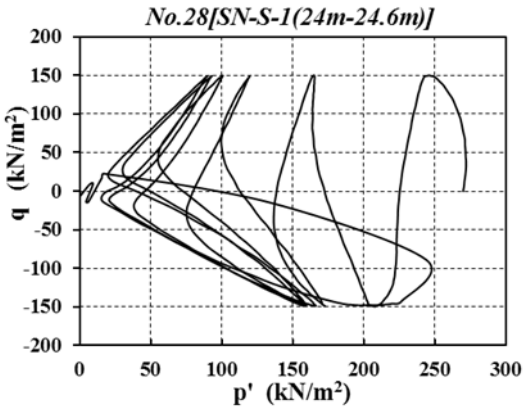

Figure A.1.44 Stress path during the undrained condition

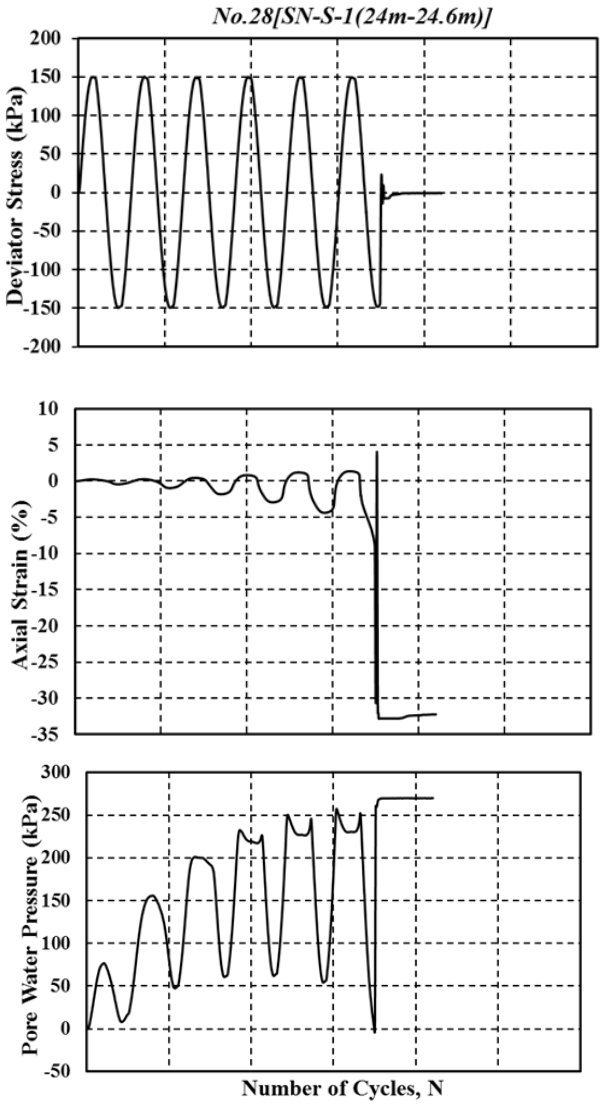

Figure A.1.45 Pore water pressure, axial strain, devaitor stress versus number of cycles

2. Reconstituted Specimens

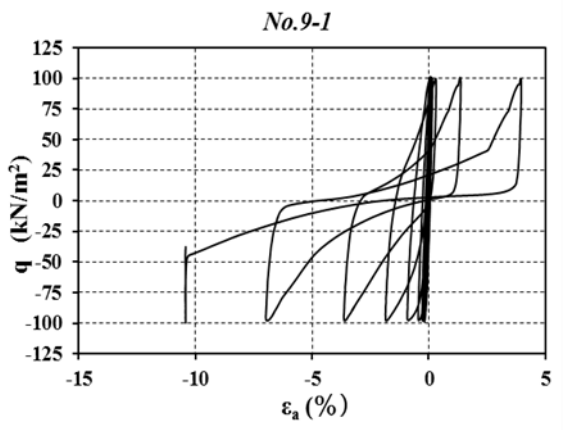

Figure A.2.46 Deviator stress versus axial strain

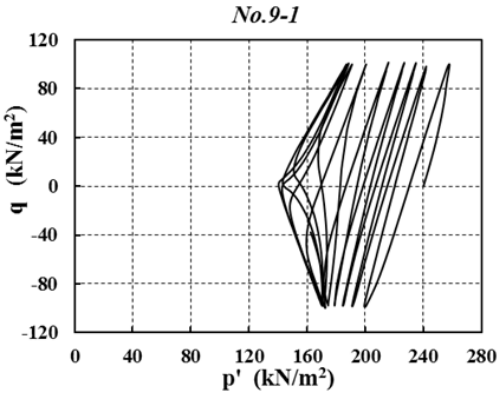

Figure A.2.47 Stress path during the undrained condition

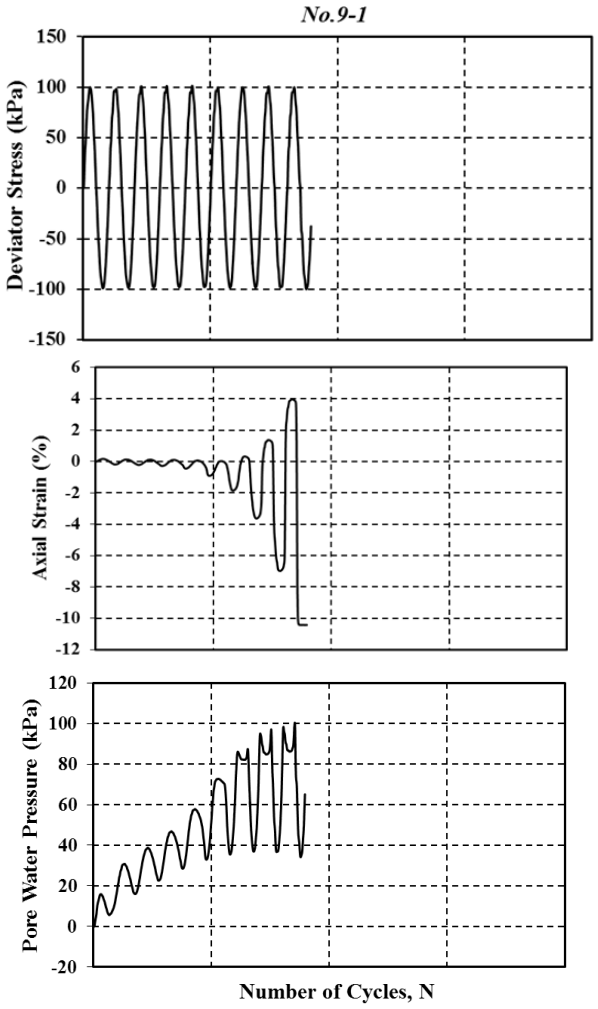

Figure A.2.48 Pore water pressure, axial strain, devaitor stress versus number of cycles

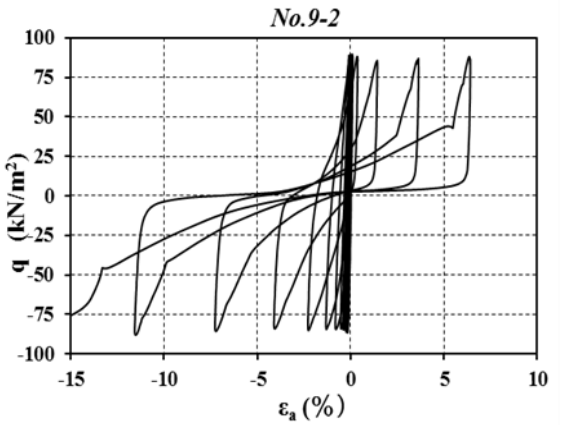

Figure A.2.49 Deviator stress versus axial strain

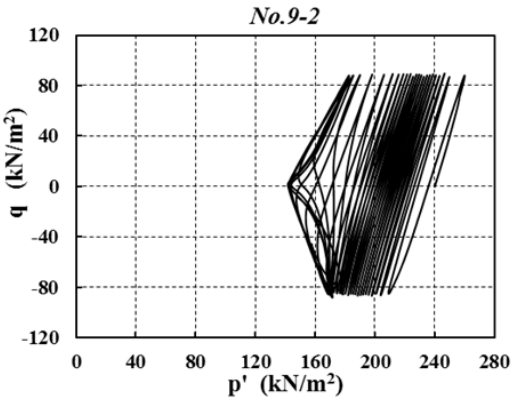

Figure A.2.50 Stress path during the undrained condition

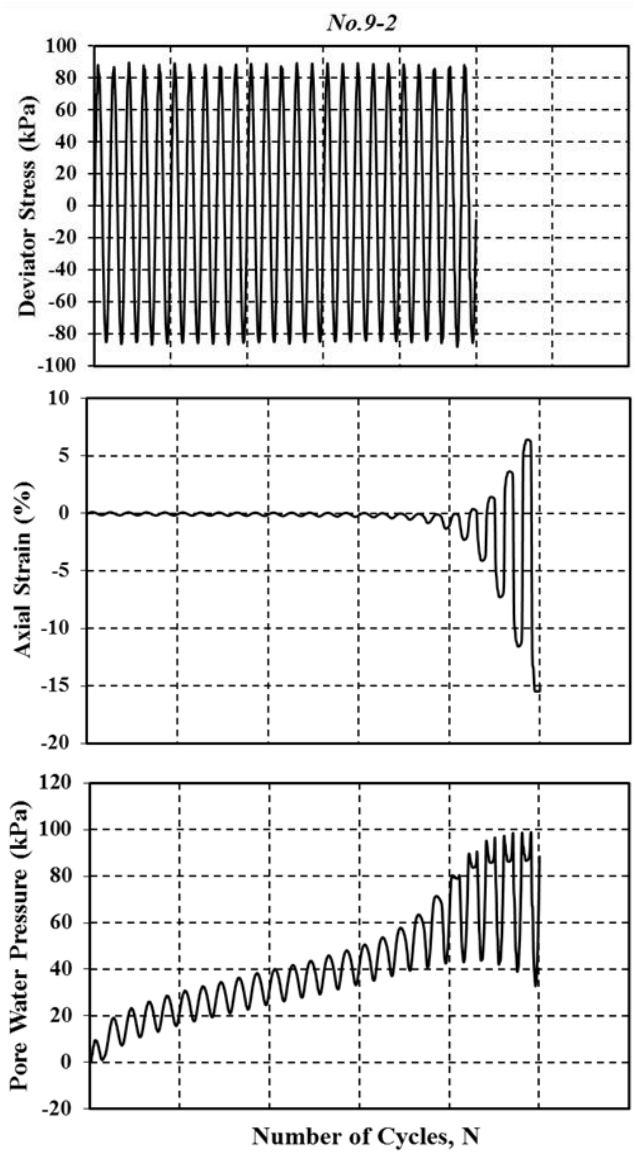

Figure A.2.51 Pore water pressure, axial strain, devaitor stress versus number of cycles

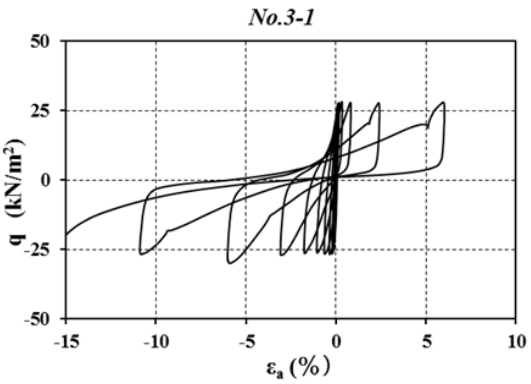

Figure A.2.52 Deviator stress versus axial strain

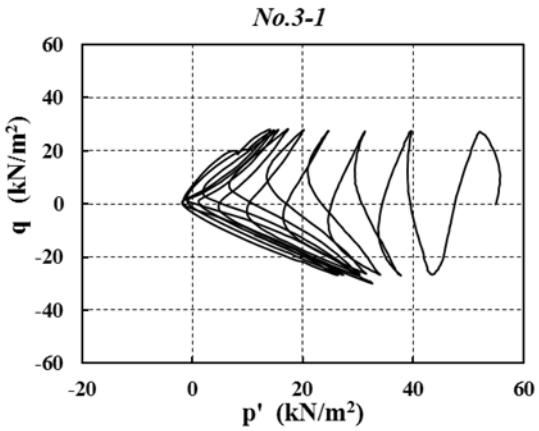

Figure A.2.53 Stress path during the undrained condition

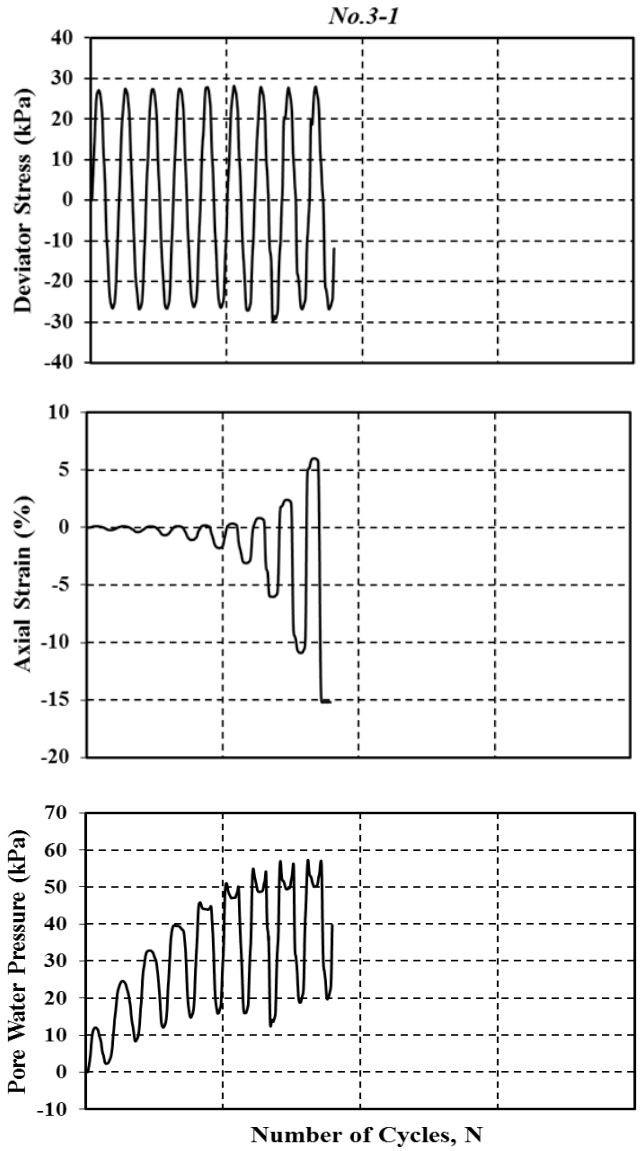

Figure A.2.54 Pore water pressure, axial strain, devaitor stress versus number of cycles

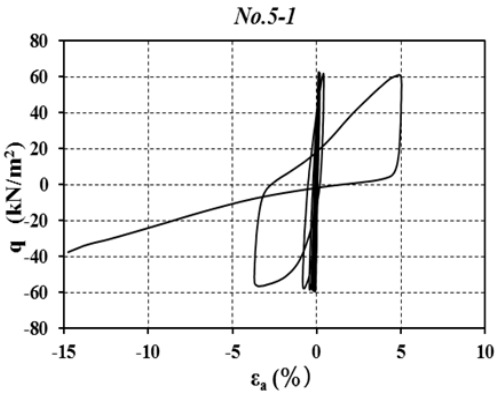

Figure A.2.55 Deviator stress versus axial strain

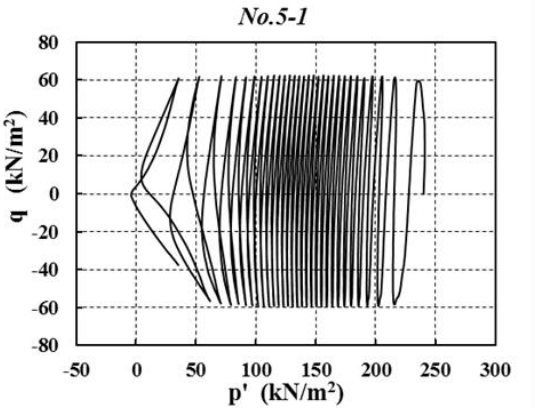

Figure A.2.56 Stress path during the undrained condition

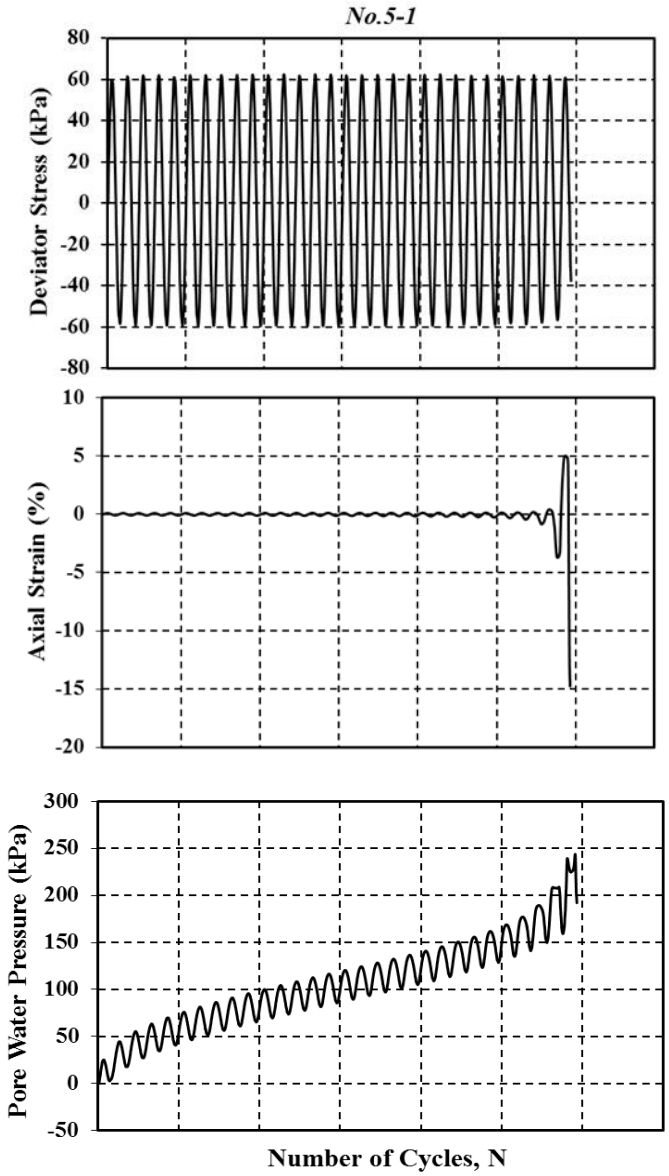

Figure A.2.57 Pore water pressure, axial strain, devaitor stress versus number of cycles

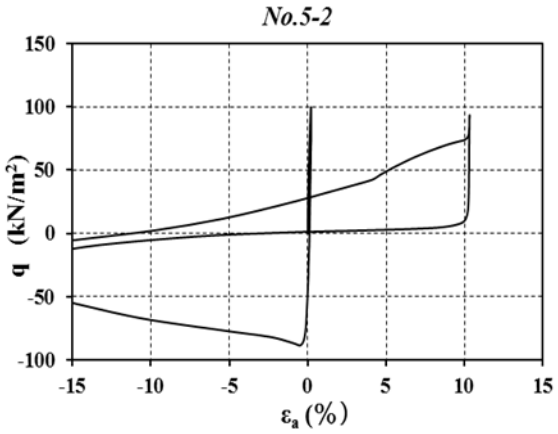

Figure A.2.58 Deviator stress versus axial strain

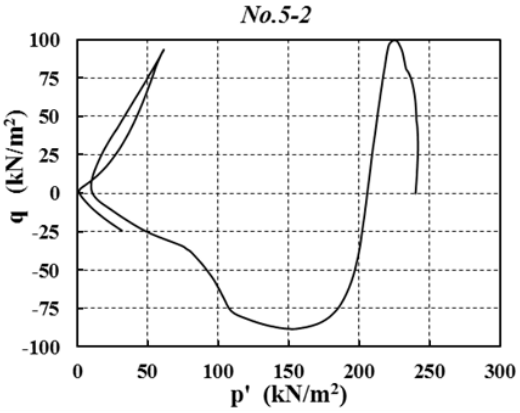

Figure A.2.59 Stress path during the undrained condition

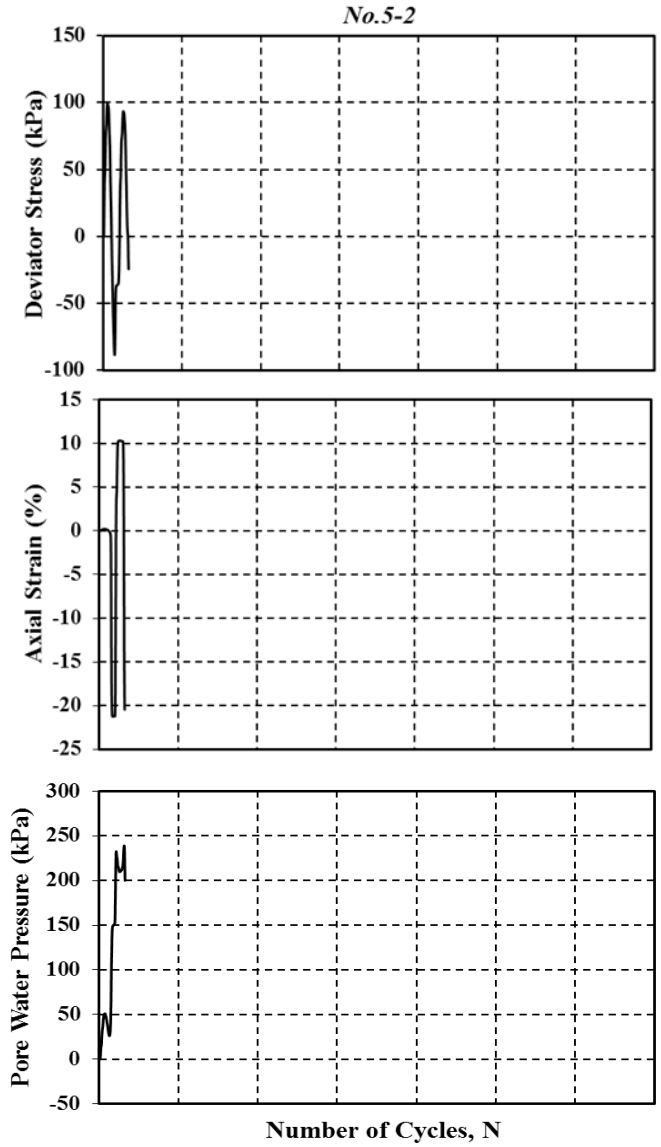

Figure A.2.60 Pore water pressure, axial strain, devaitor stress versus number of cycles

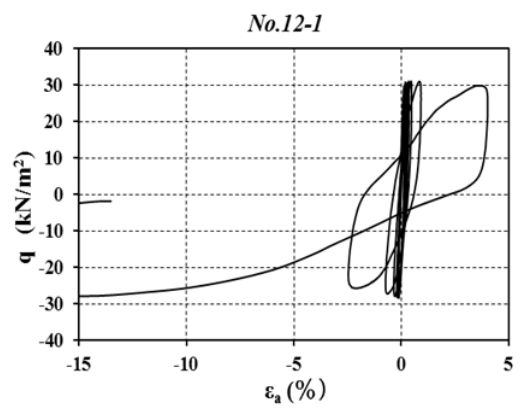

Figure A.2.61 Deviator stress versus axial strain

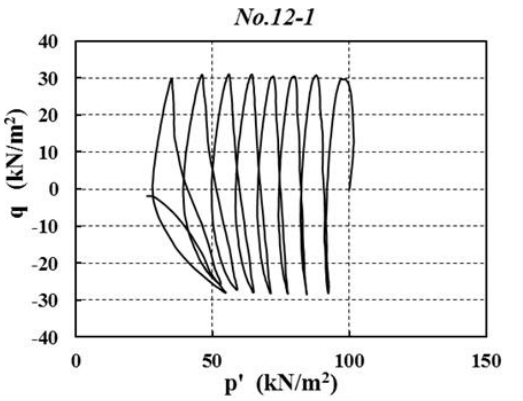

Figure A.2.62 Stress path during the undrained condition

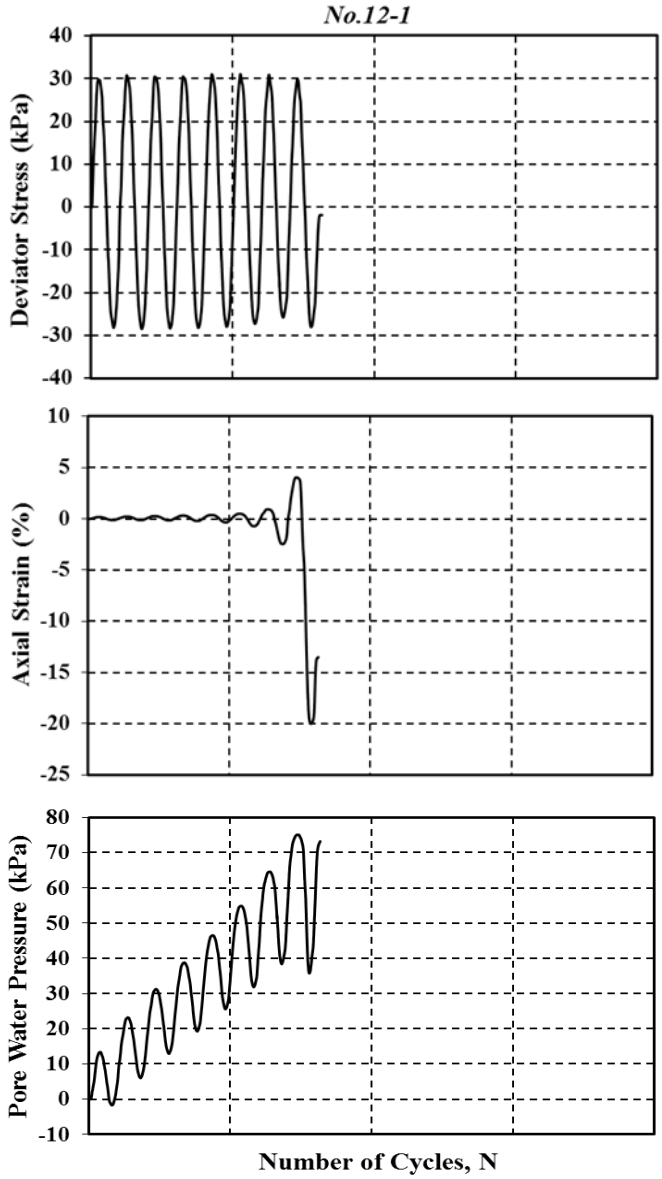

Figure A.2.63 Pore water pressure, axial strain, devaitor stress versus number of cycles

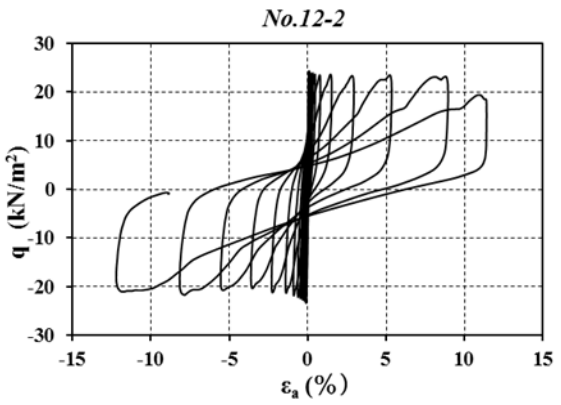

Figure A.2.64 Deviator stress versus axial strain

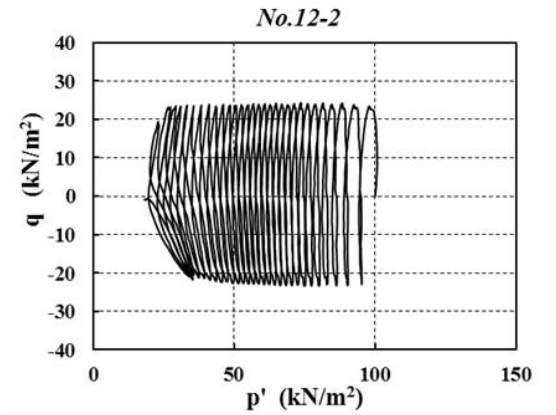

Figure A.2.65 Stress path during the undrained condition

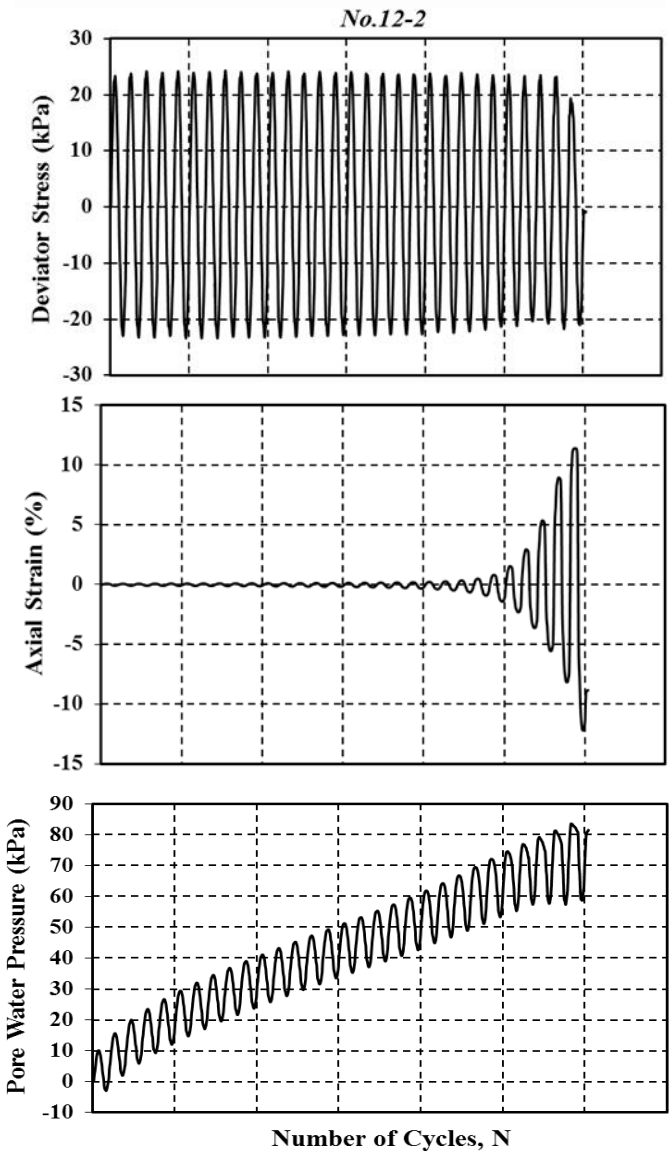

Figure A.2.66 Pore water pressure, axial strain, devaitor stress versus number of cycles

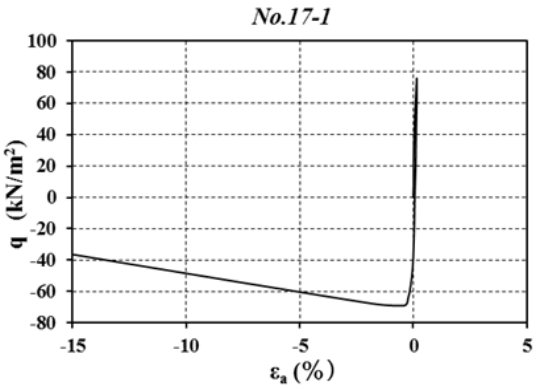

Figure A.2.67 Deviator stress versus axial strain

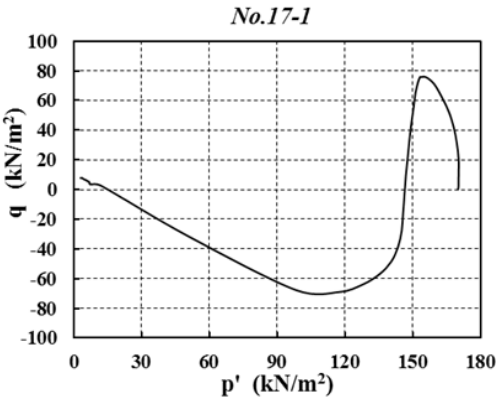

Figure A.2.68 Stress path during the undrained condition

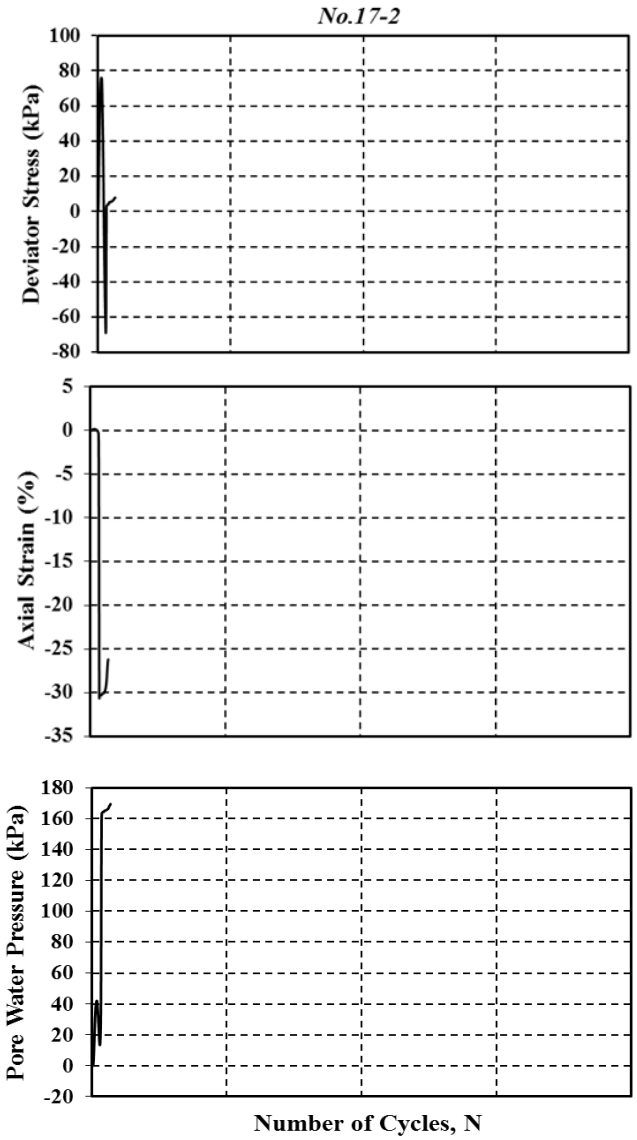

Figure A.2.69 Pore water pressure, axial strain, devaitor stress versus number of cycles

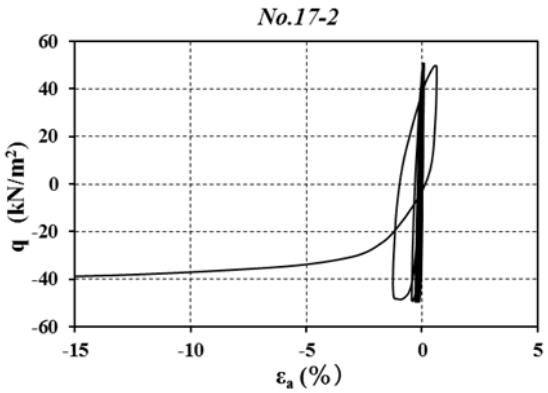

Figure A.2.70 Deviator stress versus axial strain

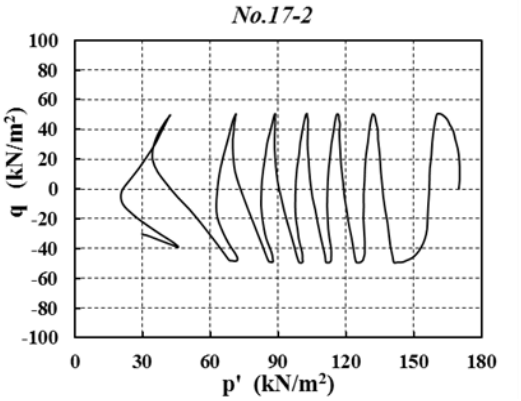

Figure A.2.71 Stress path during the undrained condition

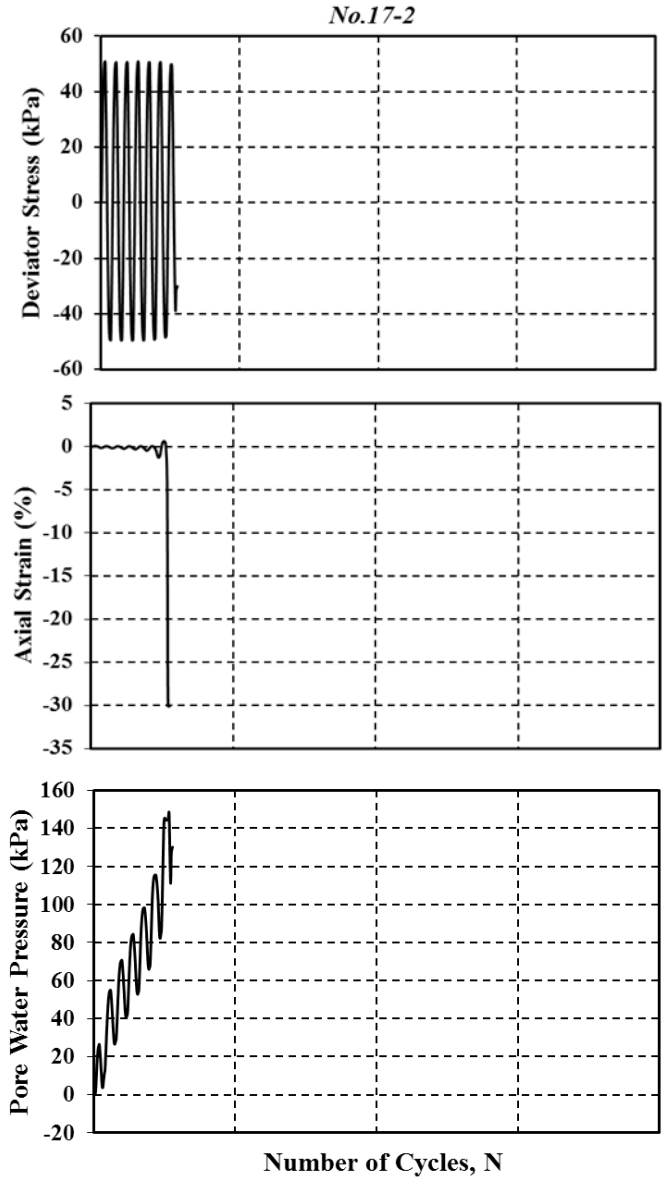

Figure A.2.72 Pore water pressure, axial strain, devaitor stress versus number of cycles

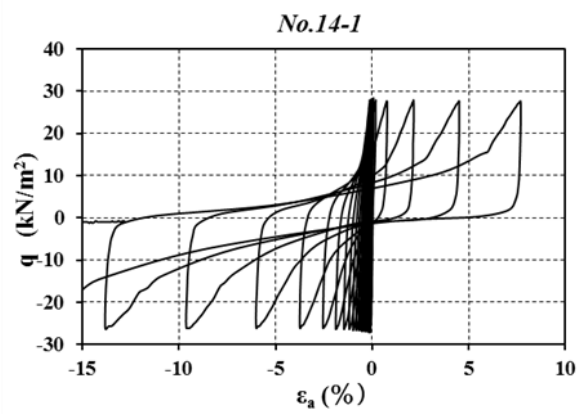

Figure A.2.73 Deviator stress versus axial strain

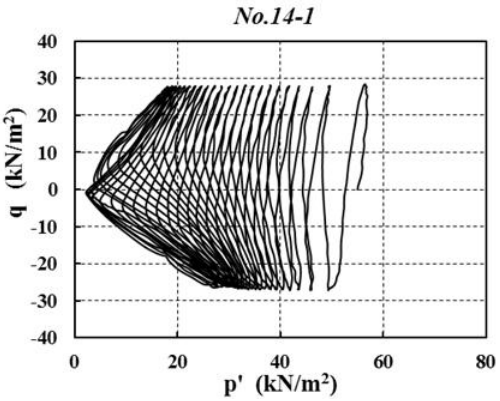

Figure A.2.74 Stress path during the undrained condition

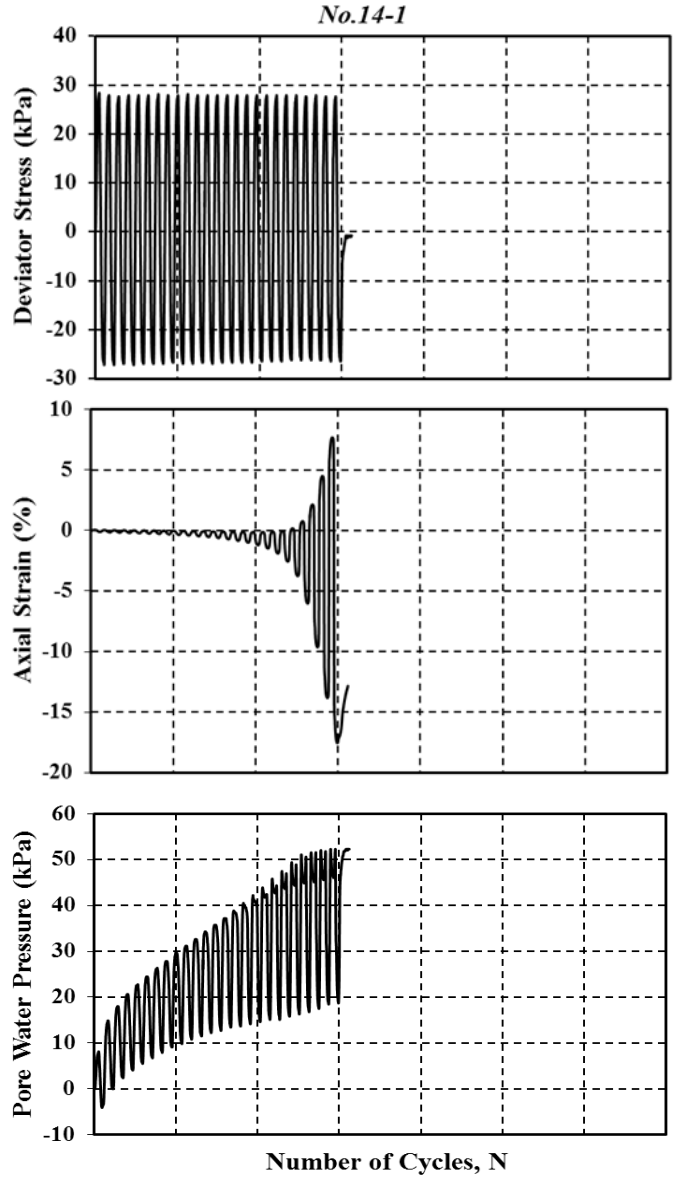

Figure A.2.75 Pore water pressure, axial strain, devaitor stress versus number of cycles

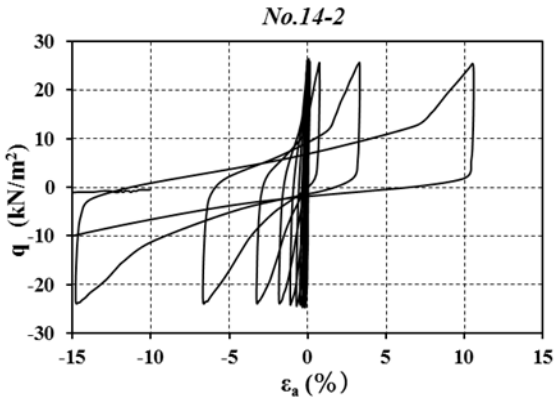

Figure A.2.76 Deviator stress versus axial strain

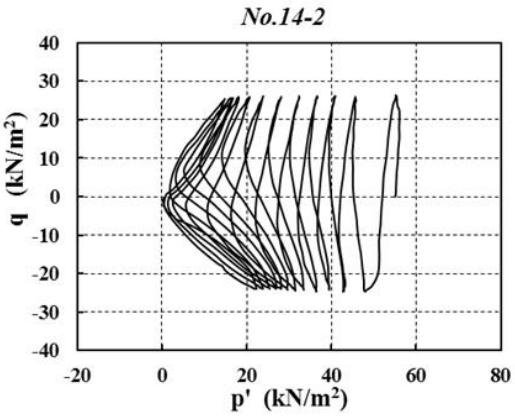

Figure A.2.77 Stress path during the undrained condition

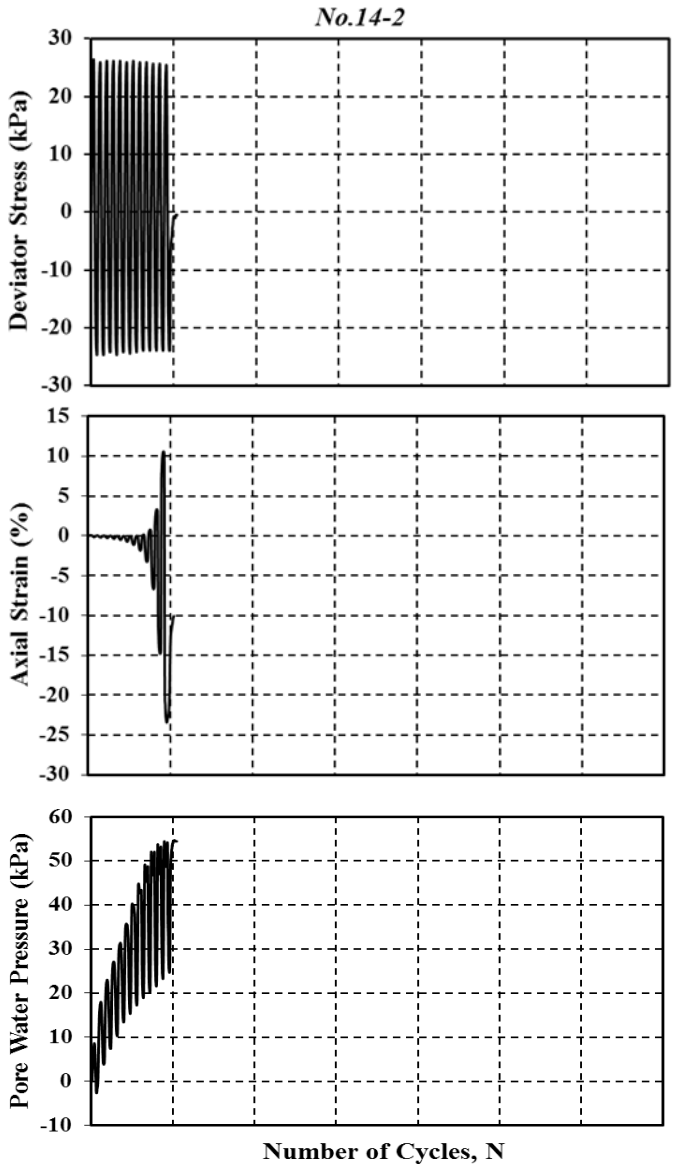

Figure A.2.78 Pore water pressure, axial strain, devaitor stress versus number of cycles

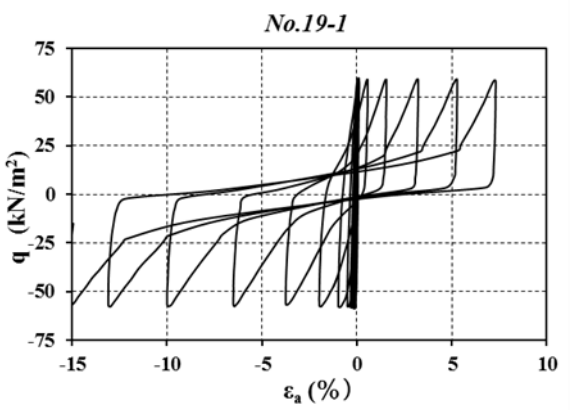

Figure A.2.79 Deviator stress versus axial strain

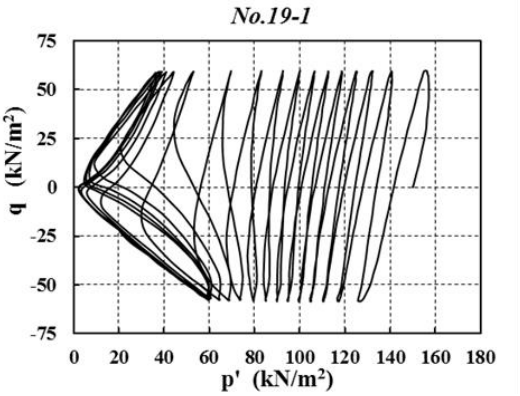

Figure A.2.80 Stress path during the undrained condition

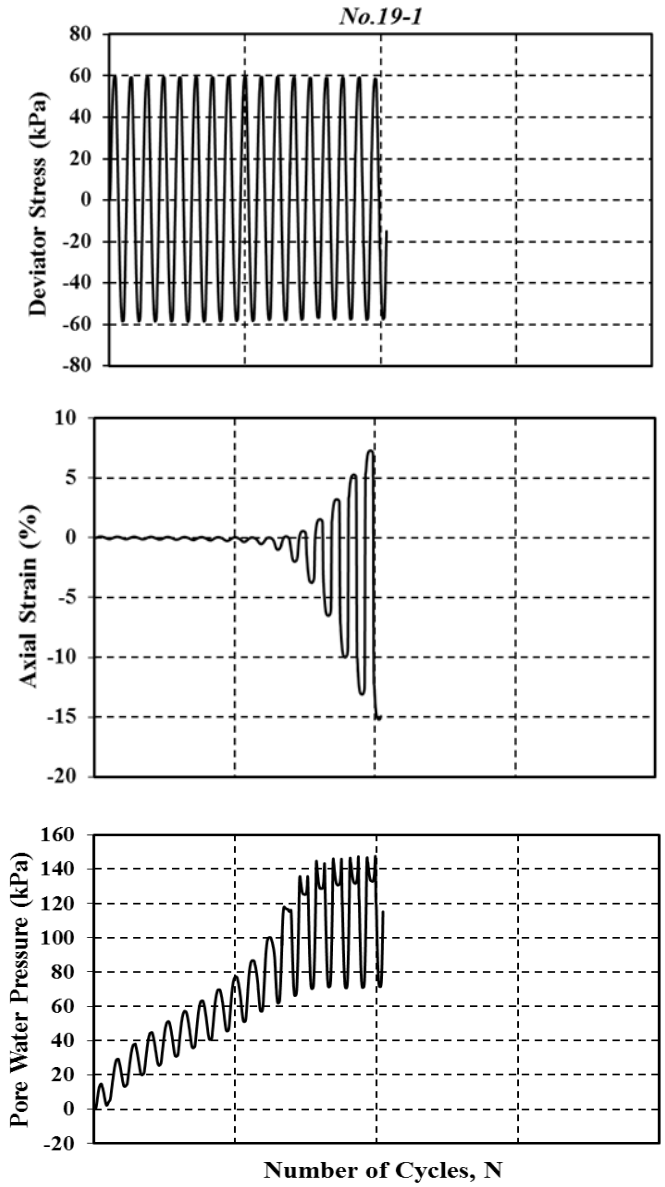

Figure A.2.81 Pore water pressure, axial strain, devaitor stress versus number of cycles

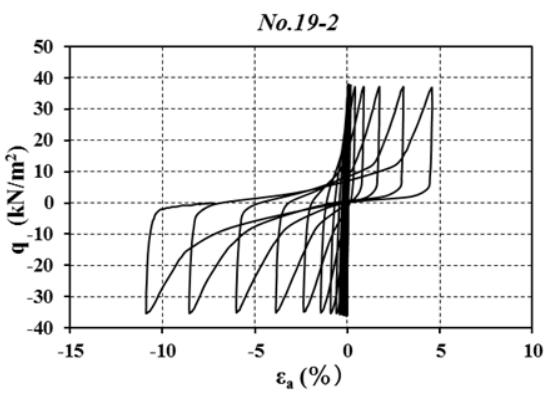

Figure A.2.82 Deviator stress versus axial strain

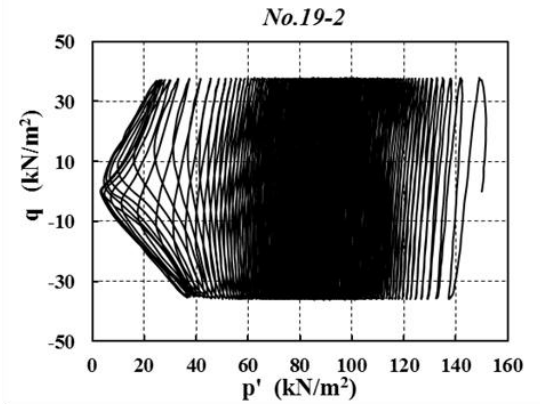

Figure A.2.83 Stress path during the undrained condition

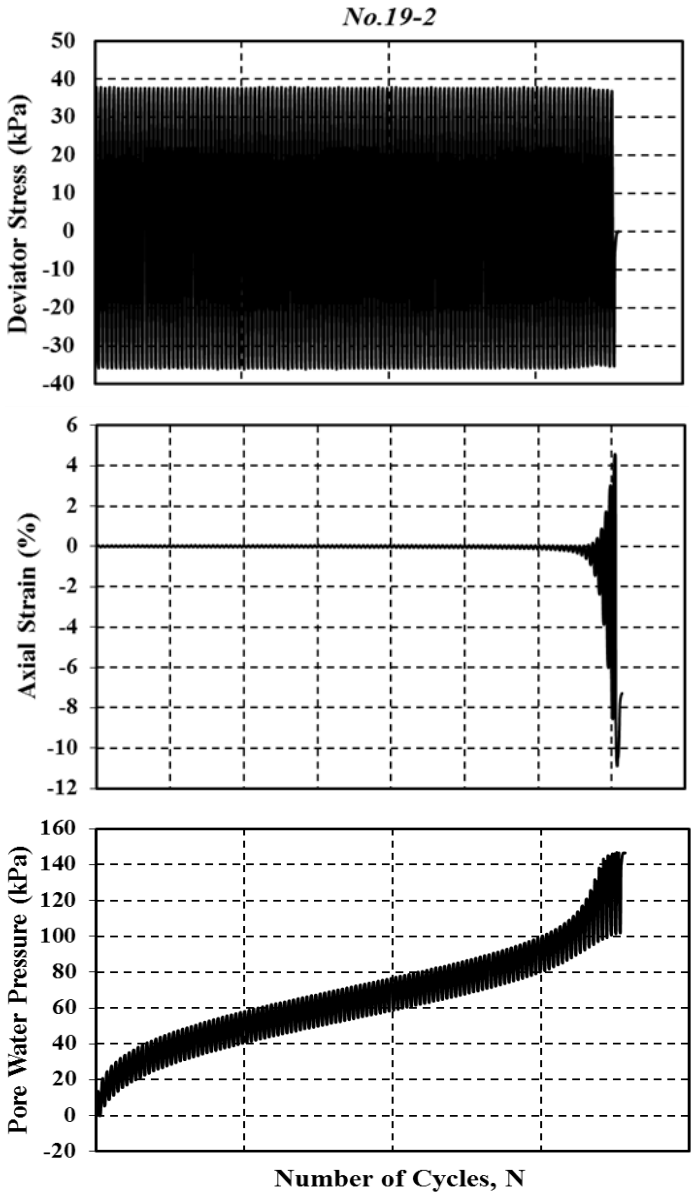

Figure A.2.84 Pore water pressure, axial strain, devaitor stress versus number of cycles

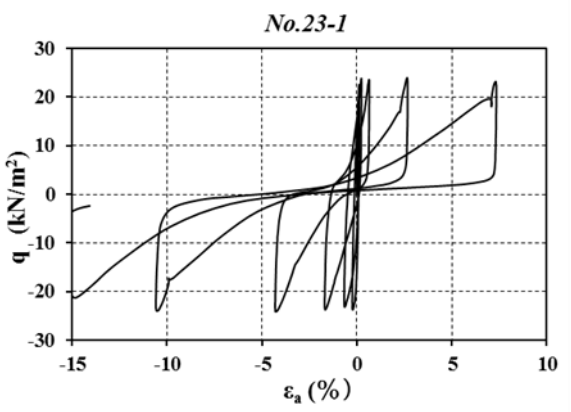

Figure A.2.85 Deviator stress versus axial strain

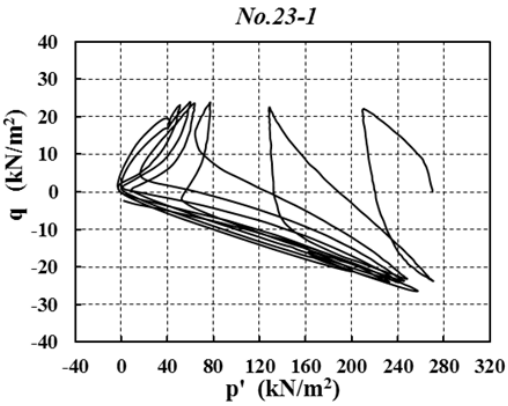

Figure A.2.86 Stress path during the undrained condition

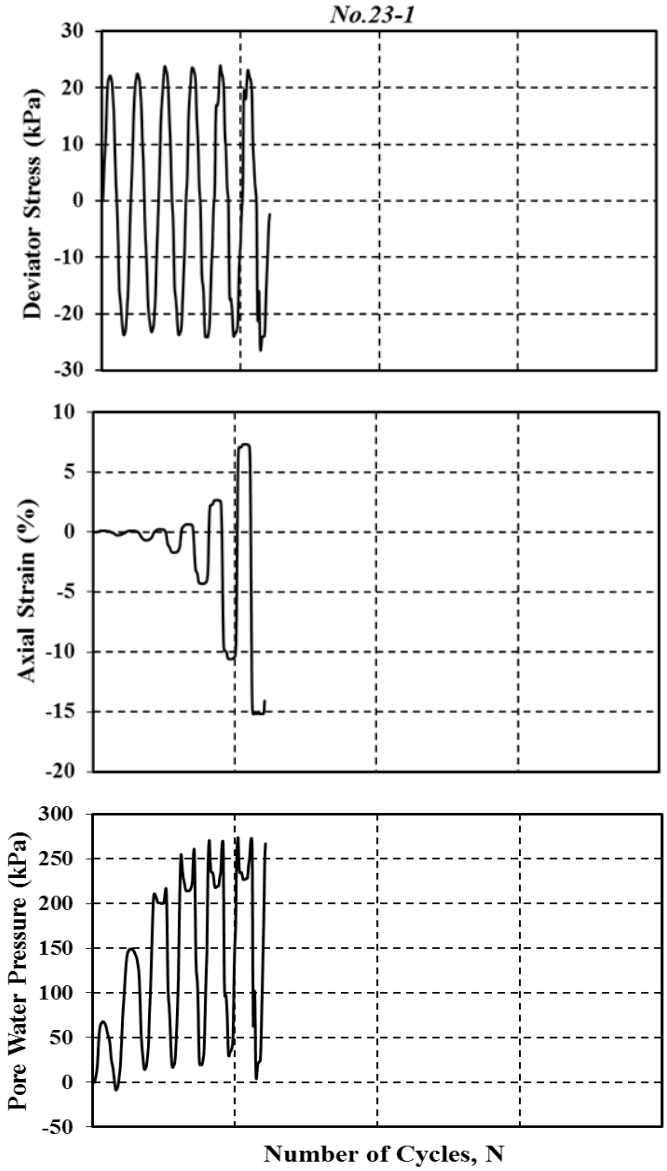

Figure A.2.87 Pore water pressure, axial strain, devaitor stress versus number of cycles

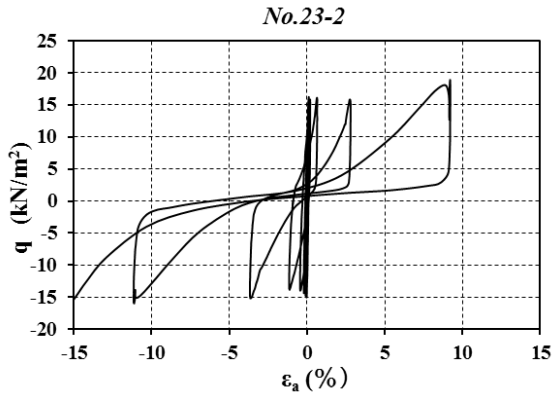

Figure A.2.88 Deviator stress versus axial strain

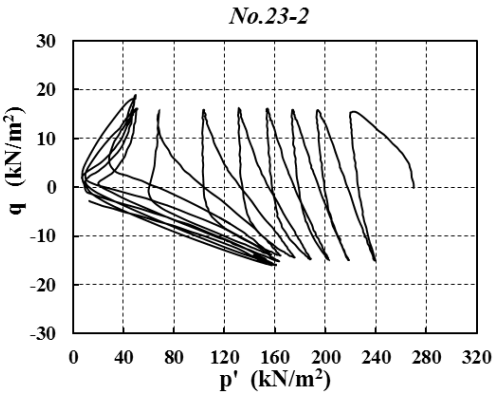

Figure A.2.89 Stress path during the undrained condition

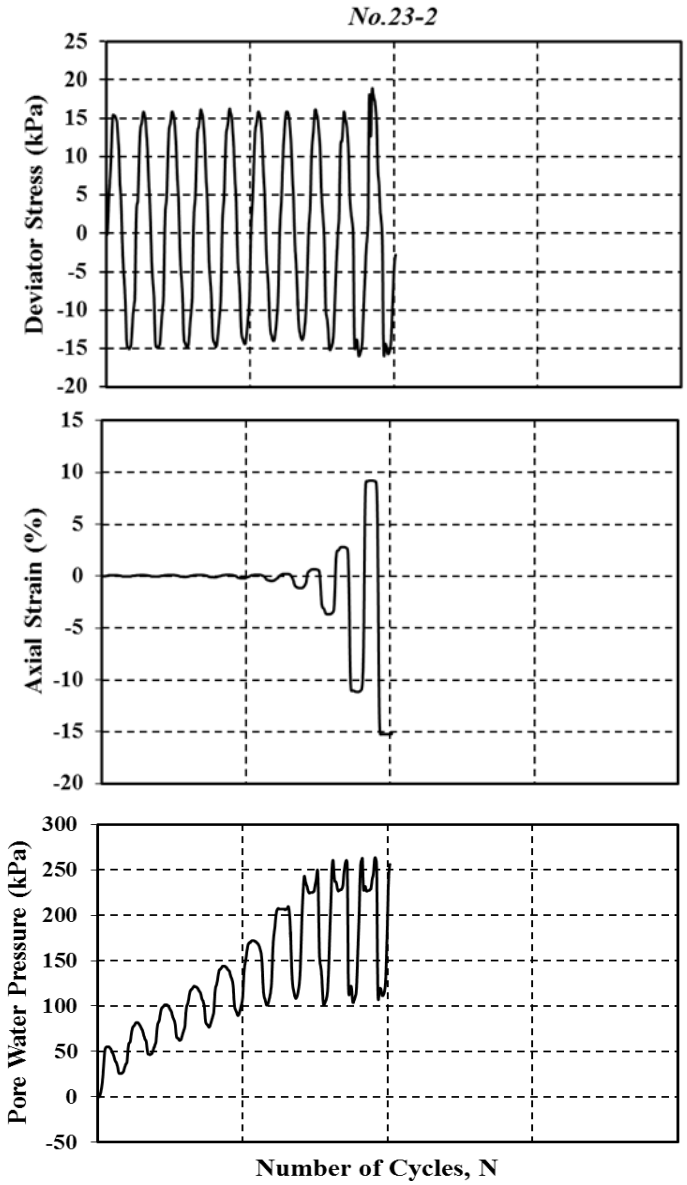

Figure A.2.90 Pore water pressure, axial strain, devaitor stress versus number of cycles

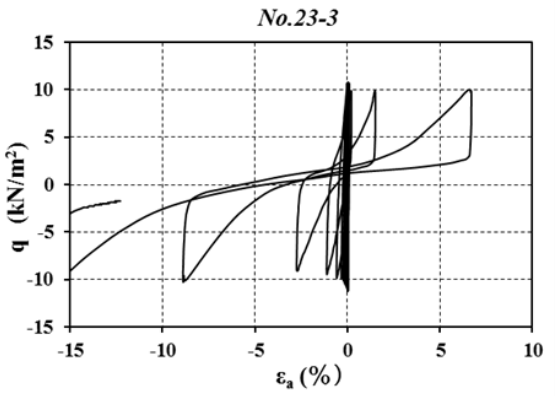

Figure A.2.91 Deviator stress versus axial strain

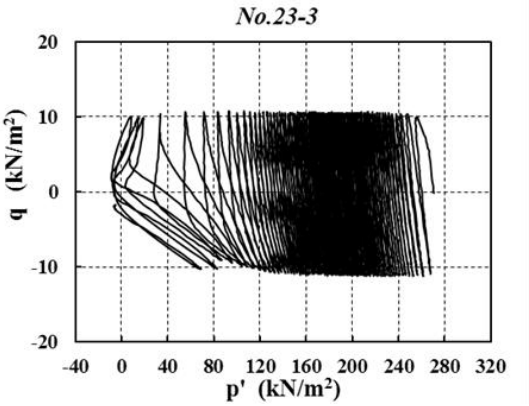

Figure A.2.92 Stress path during the undrained condition

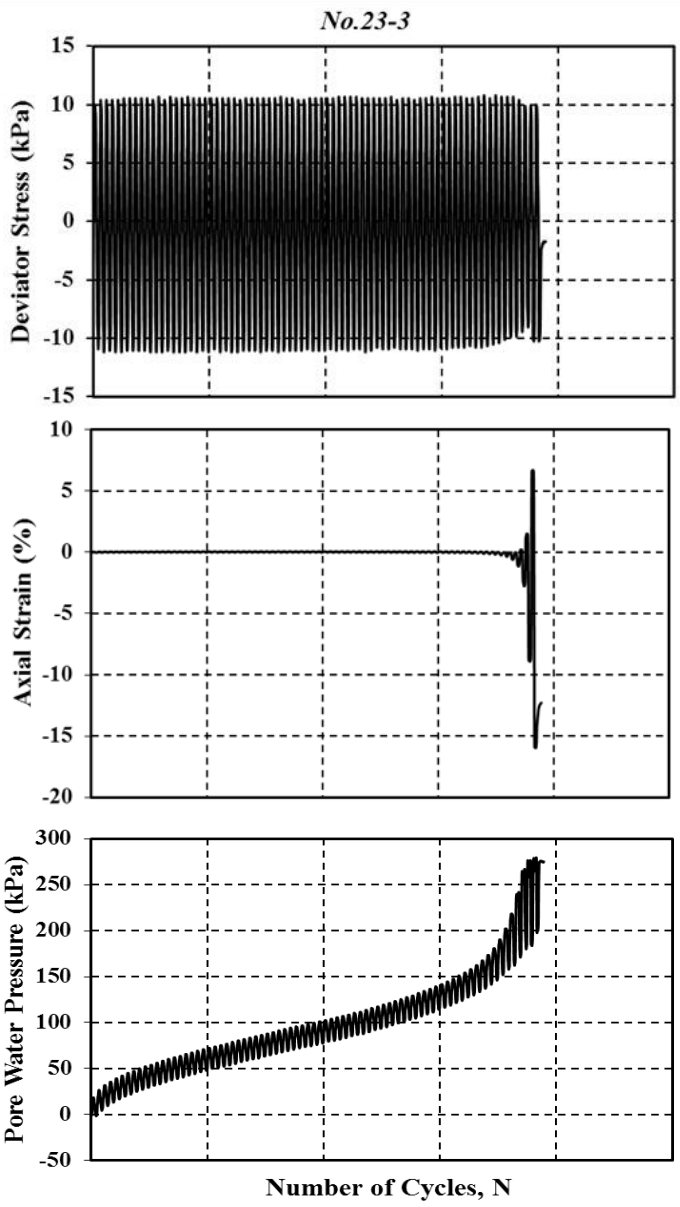

Figure A.2.93 Pore water pressure, axial strain, devaitor stress versus number of cycles

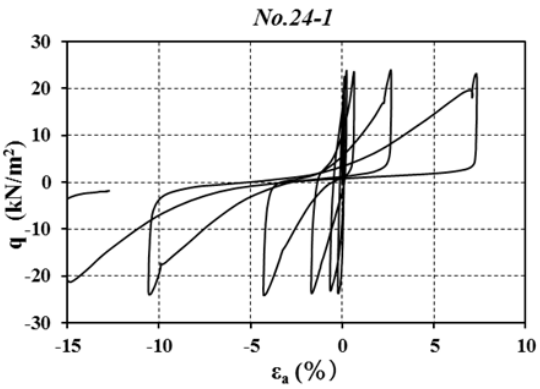

Figure A.2.94 Deviator stress versus axial strain

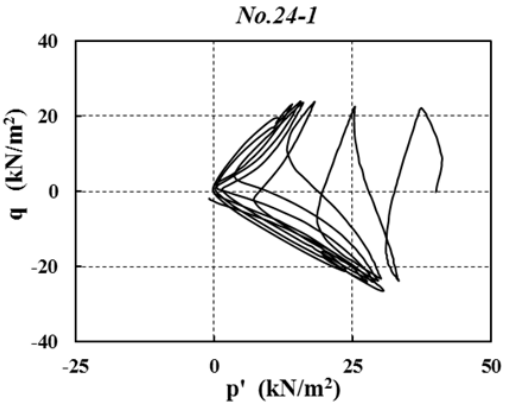

Figure A.2.95 Stress path during the undrained condition

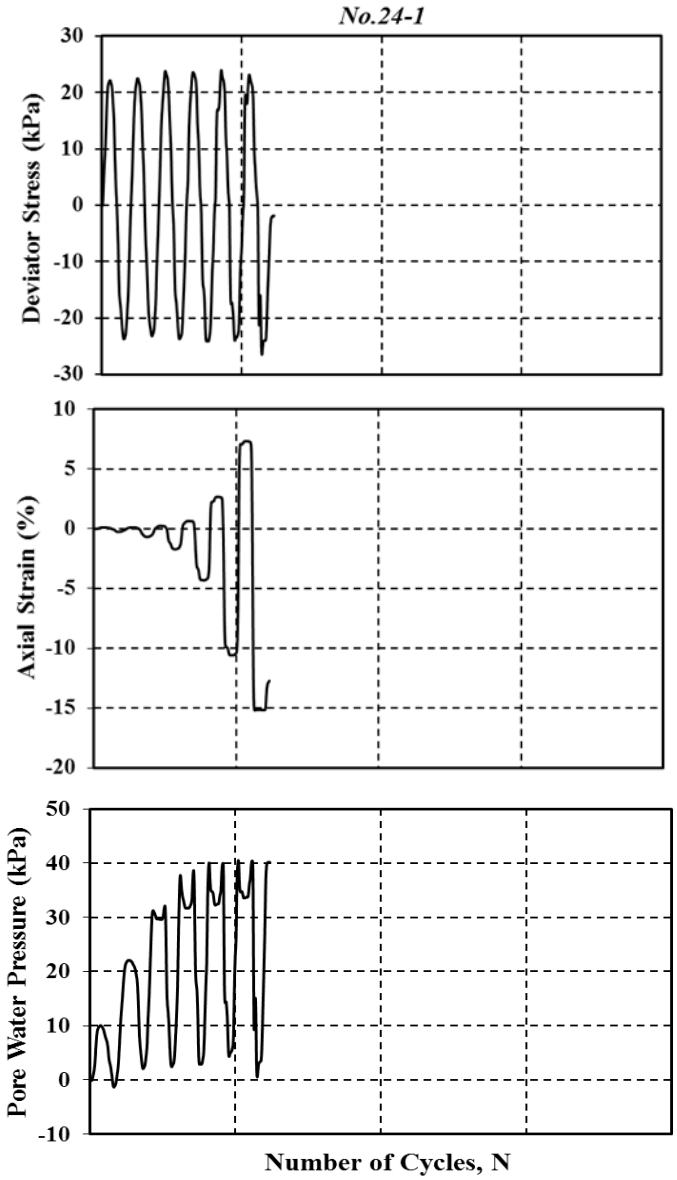

Figure A.2.96 Pore water pressure, axial strain, devaitor stress versus number of cycles

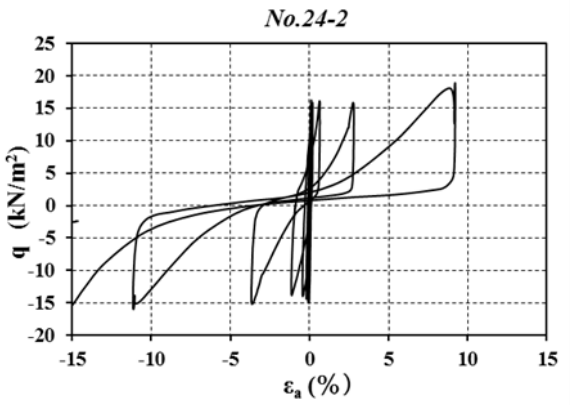

Figure A.2.97 Deviator stress versus axial strain

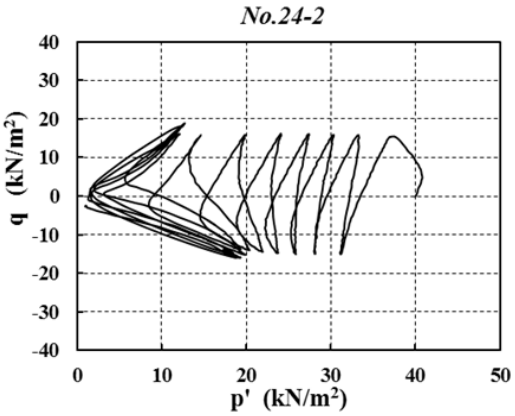

Figure A.2.98 Stress path during the undrained condition

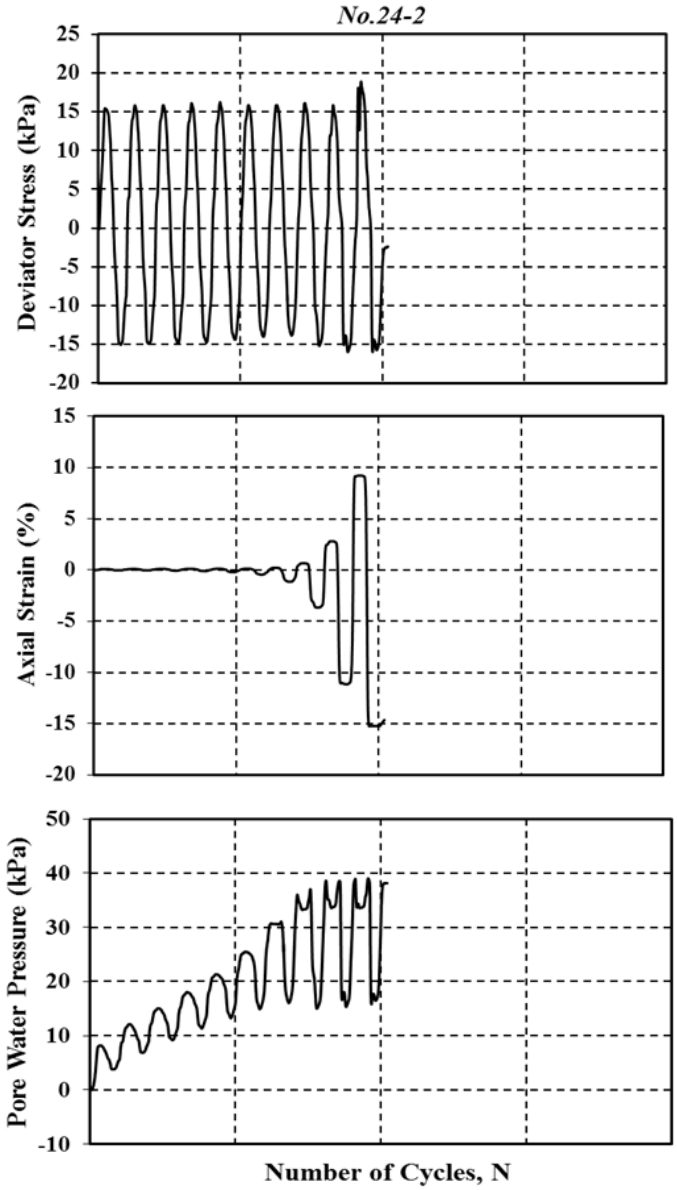

Figure A.2.99 Pore water pressure, axial strain, devaitor stress versus number of cycles

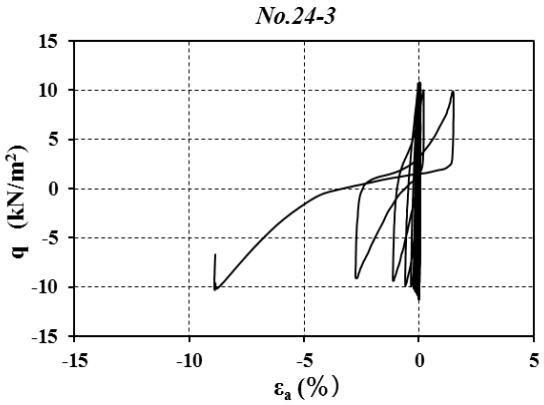

Figure A.2.100 Deviator stress versus axial strain

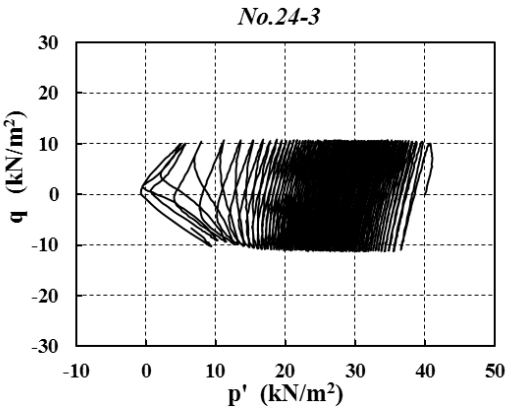

Figure A.2.101 Stress path during the undrained condition

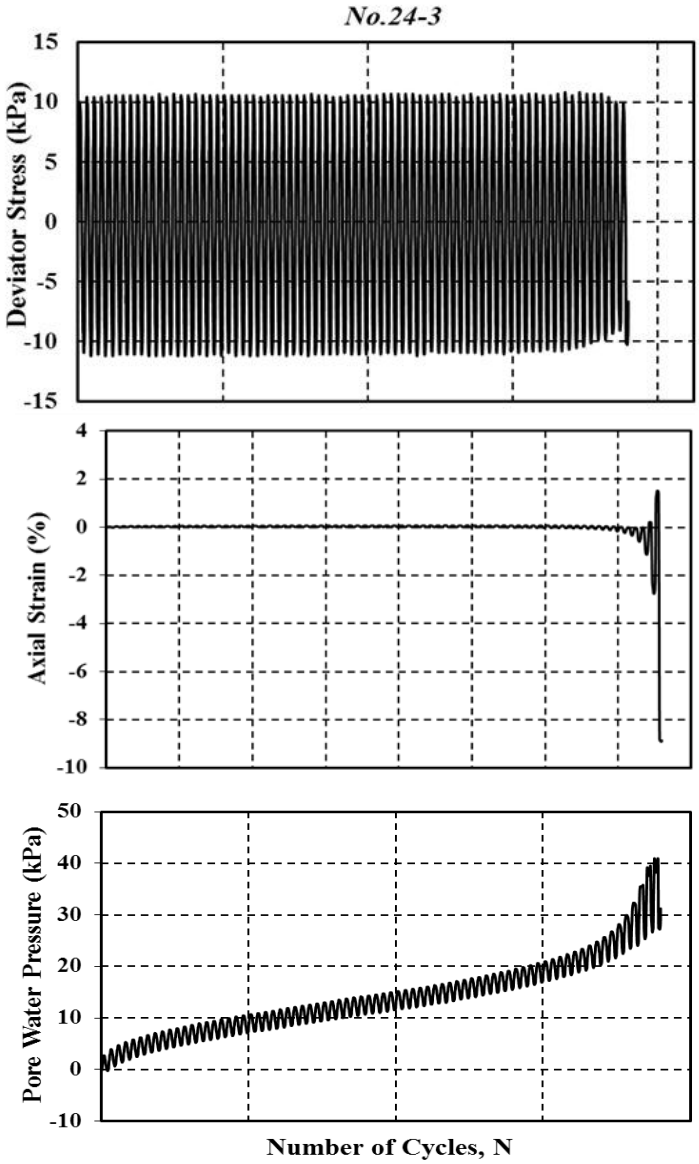

Figure A.2.102 Pore water pressure, axial strain, devaitor stress versus number of cycles

3. Nagoya Sand

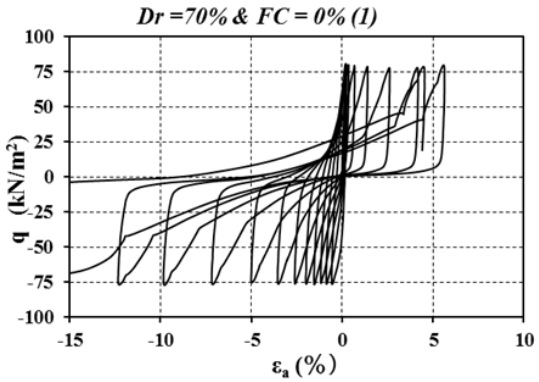

Figure A.3.103 Deviator stress versus axial strain

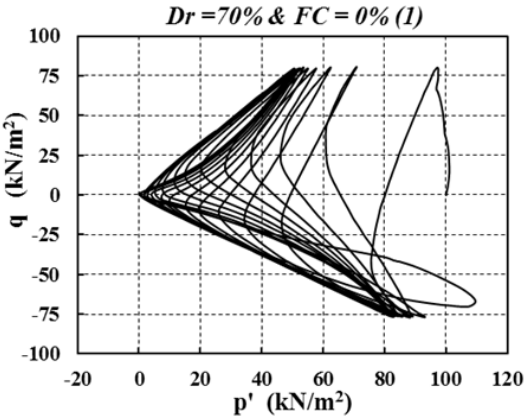

Figure A.3.104 Stress path during the undrained condition

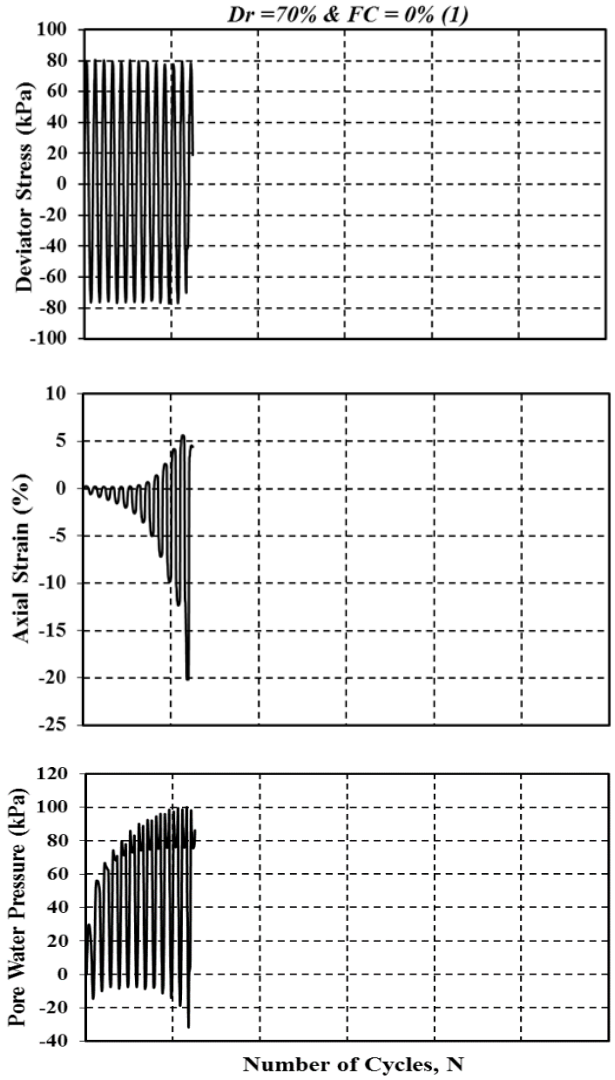

Figure A.3.105 Pore water pressure, axial strain, devaitor stress versus number of cycles

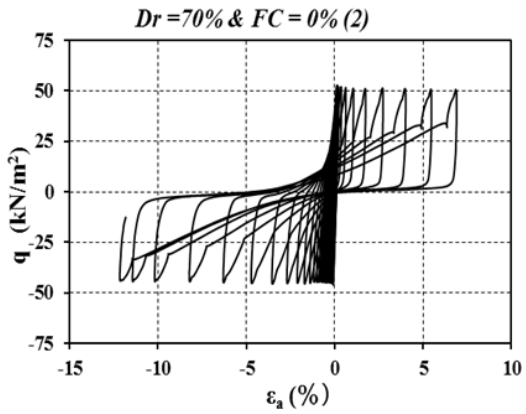

Figure A.3.106 Deviator stress versus axial strain

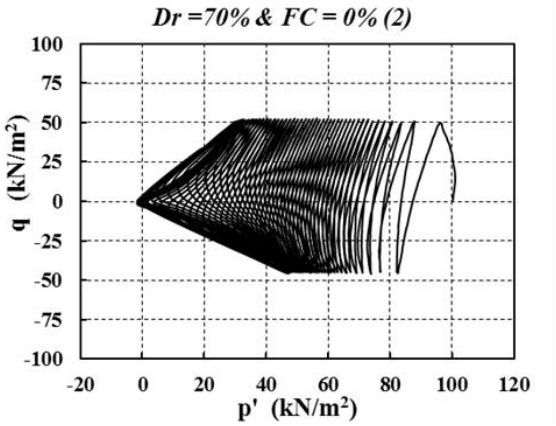

Figure A.3.107 Stress path during the undrained condition

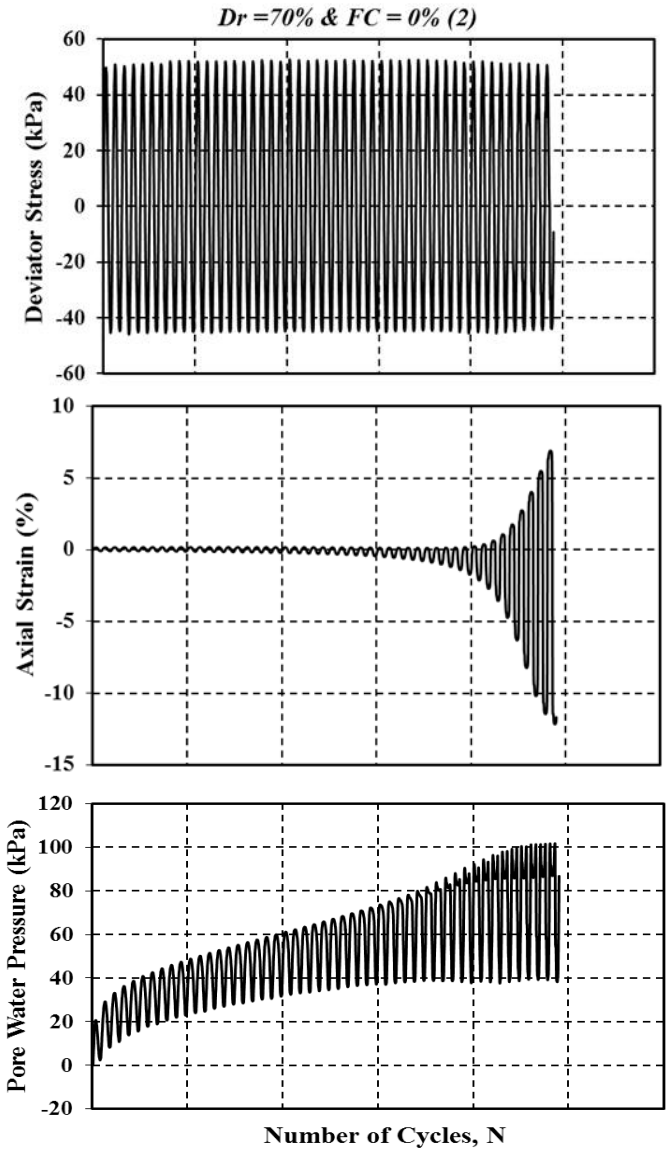

Figure A.3.108 Pore water pressure, axial strain, devaitor stress versus number of cycles

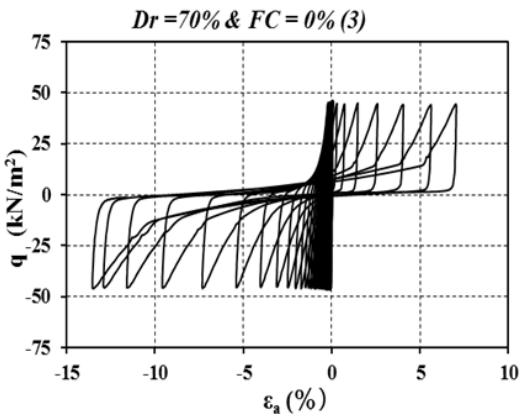

Figure A.3.109 Deviator stress versus axial strain

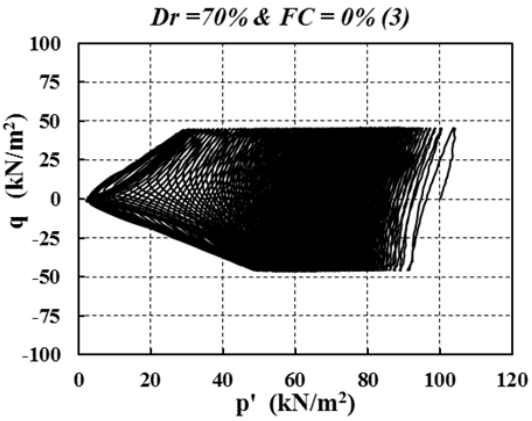

Figure A.3.110 Stress path during the undrained condition

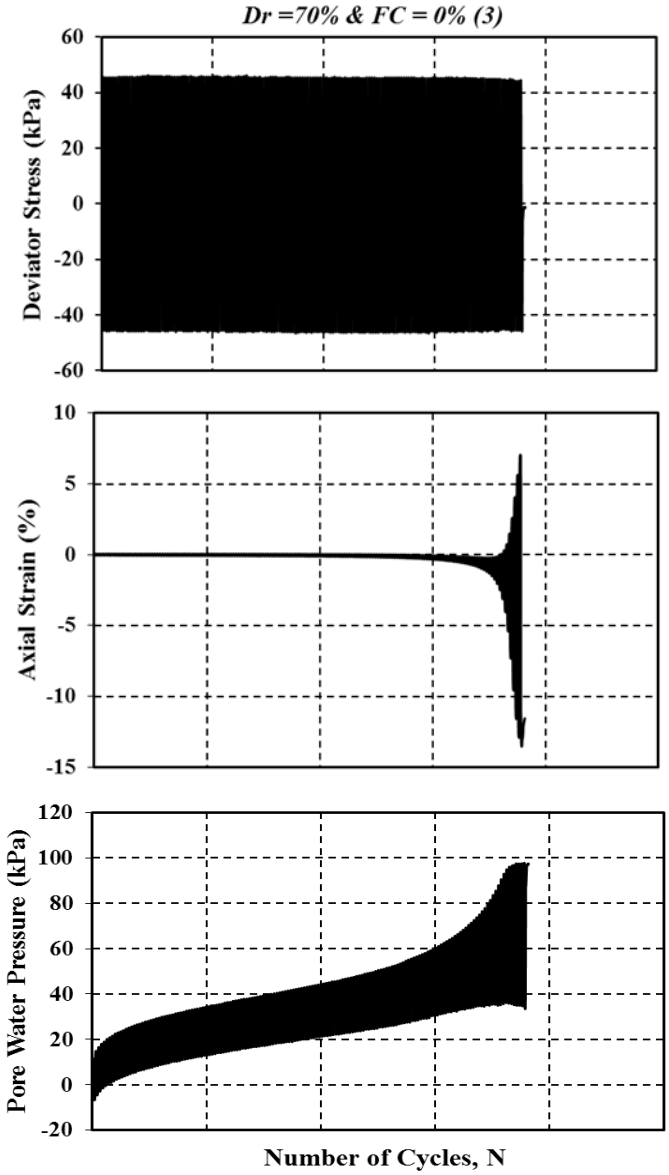

Figure A.3.111 Pore water pressure, axial strain, devaitor stress versus number of cycles

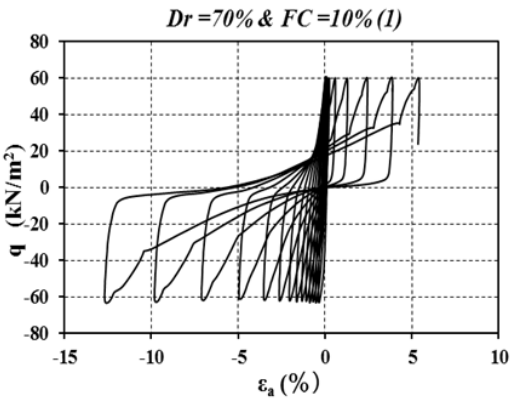

Figure A.3.112 Deviator stress versus axial strain

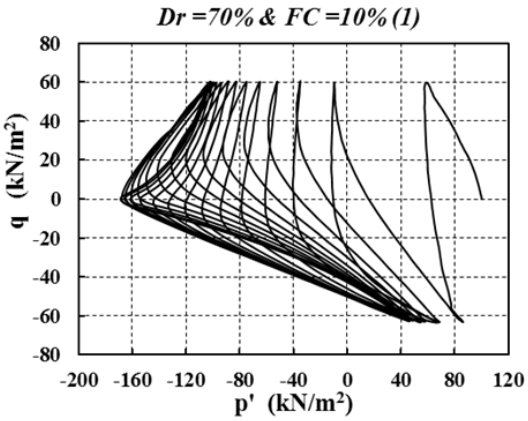

Figure A.3.113 Stress path during the undrained condition

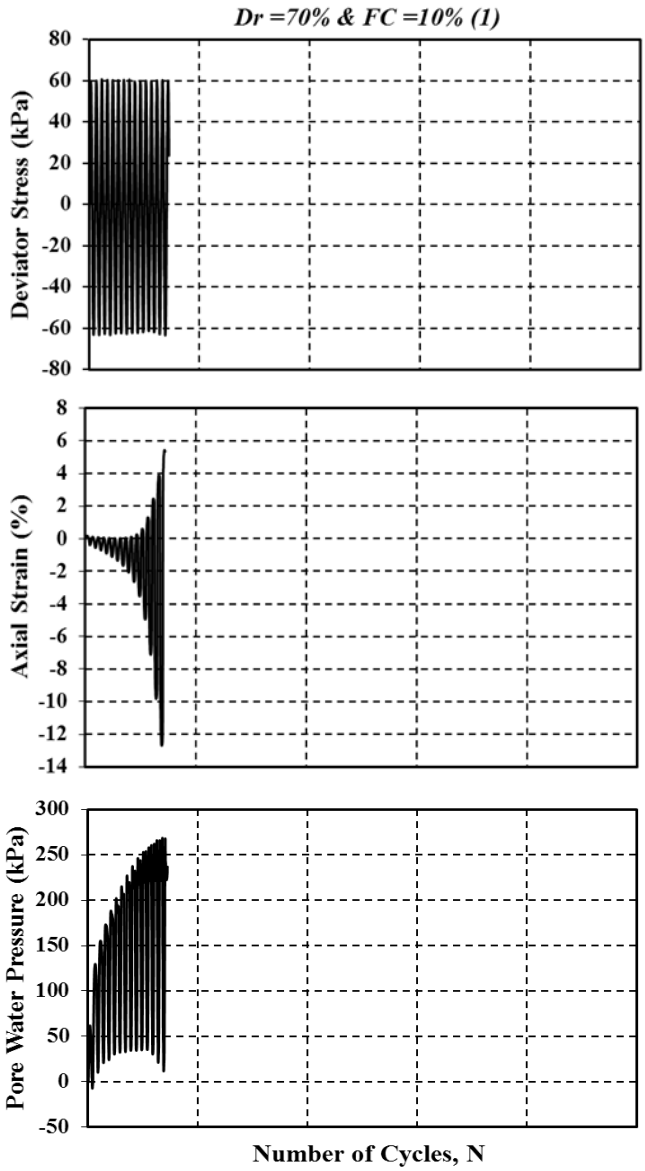

Figure A.3.114 Pore water pressure, axial strain, devaitor stress versus number of cycles

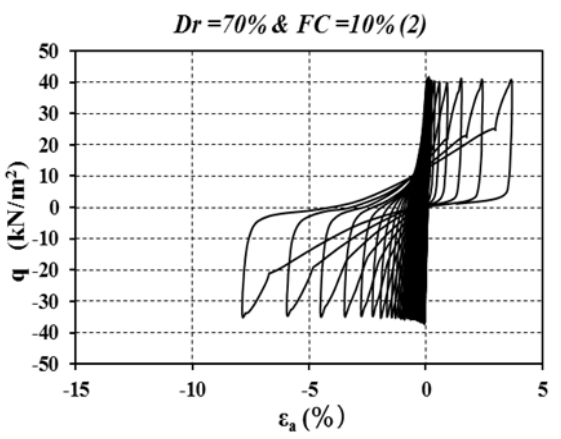

Figure A.3.115 Deviator stress versus axial strain

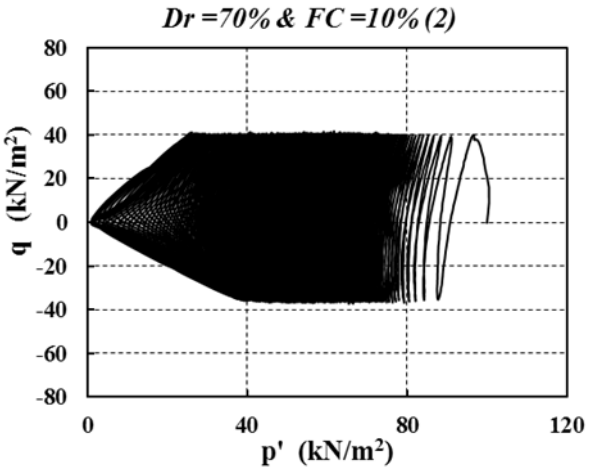

Figure A.3.116 Stress path during the undrained condition

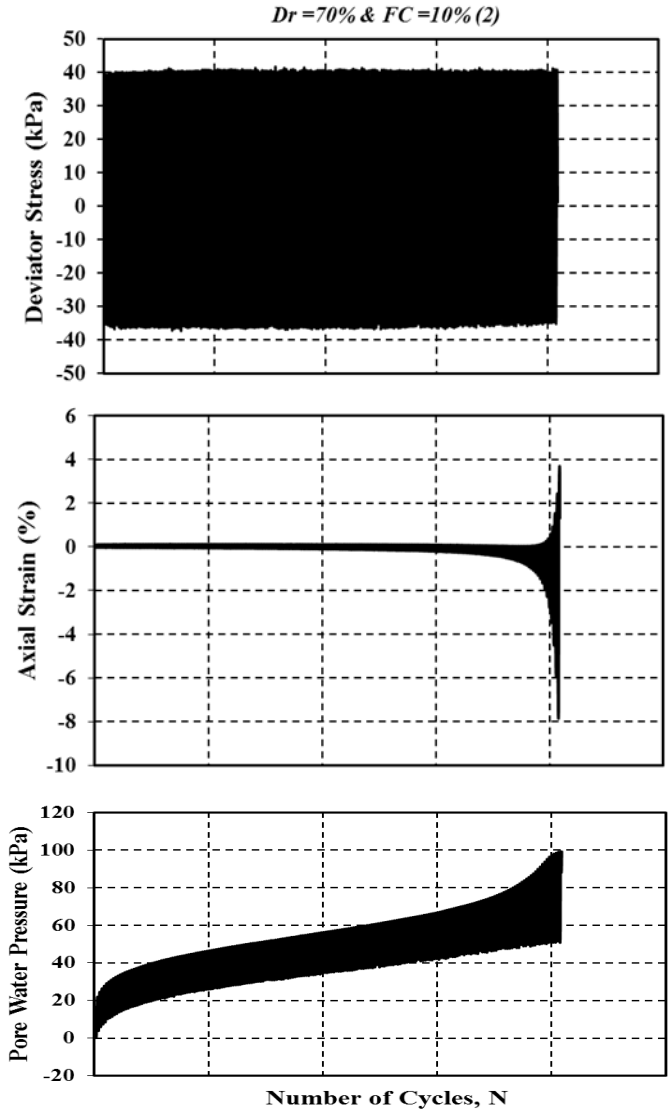

Figure A.3.117 Pore water pressure, axial strain, devaitor stress versus number of cycles

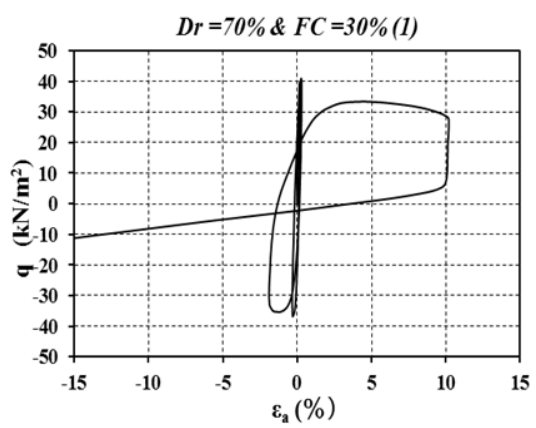

Figure A.3.118 Deviator stress versus axial strain

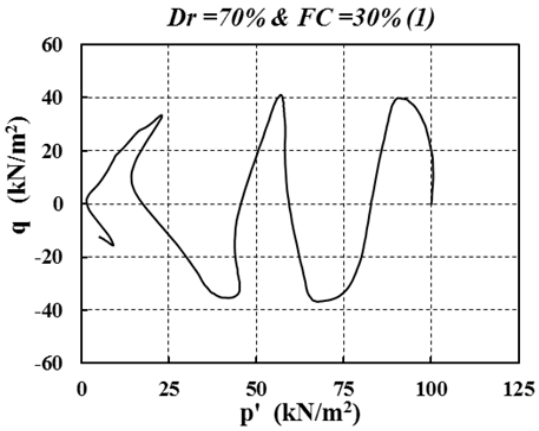

Figure A.3.119 Stress path during the undrained condition

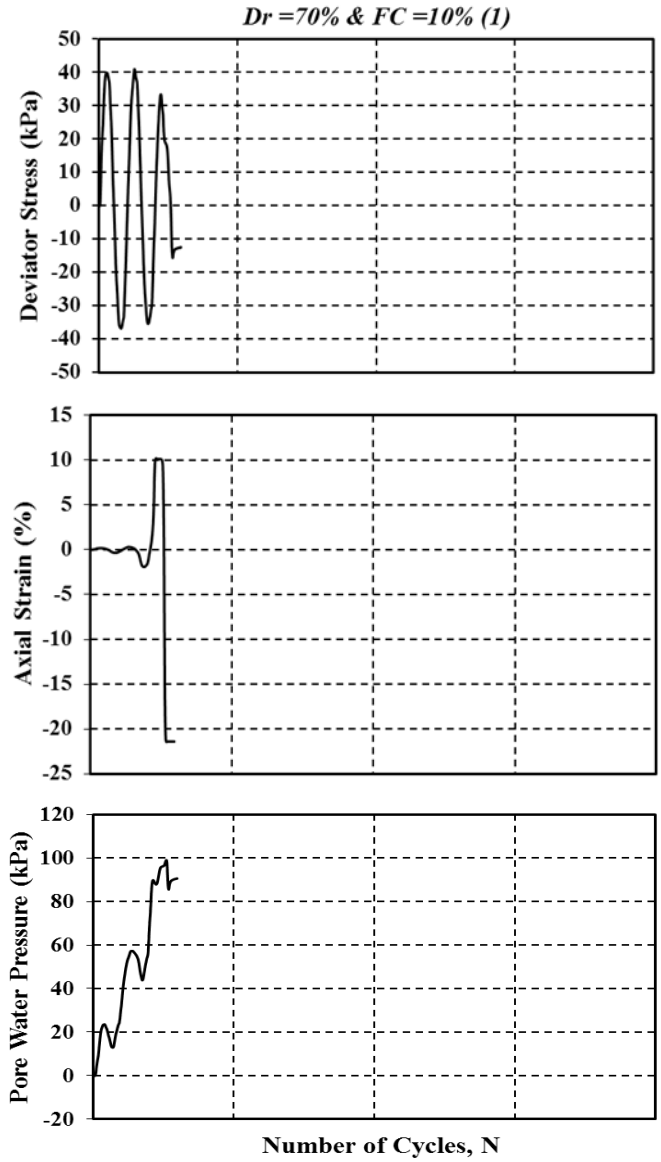

Figure A.3.120 Pore water pressure, axial strain, devaitor stress versus number of cycles

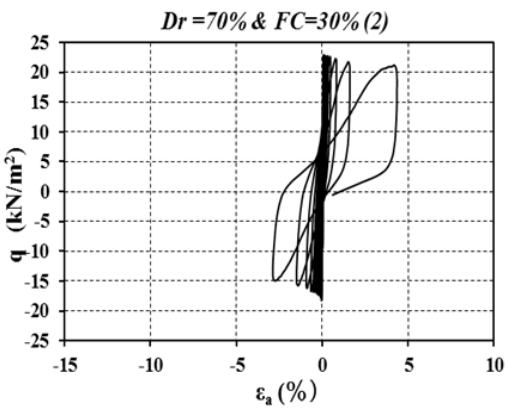

Figure A.3.121 Deviator stress versus axial strain

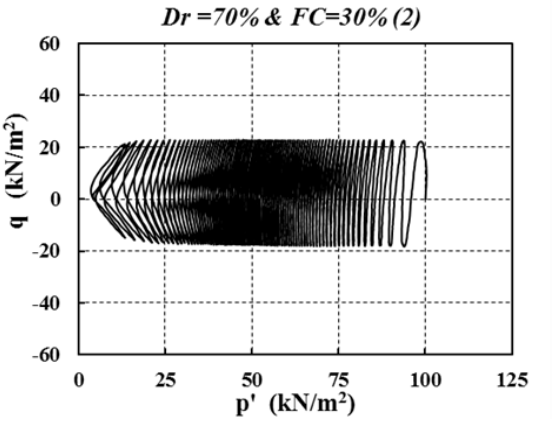

Figure A.3.122 Stress path during the undrained condition

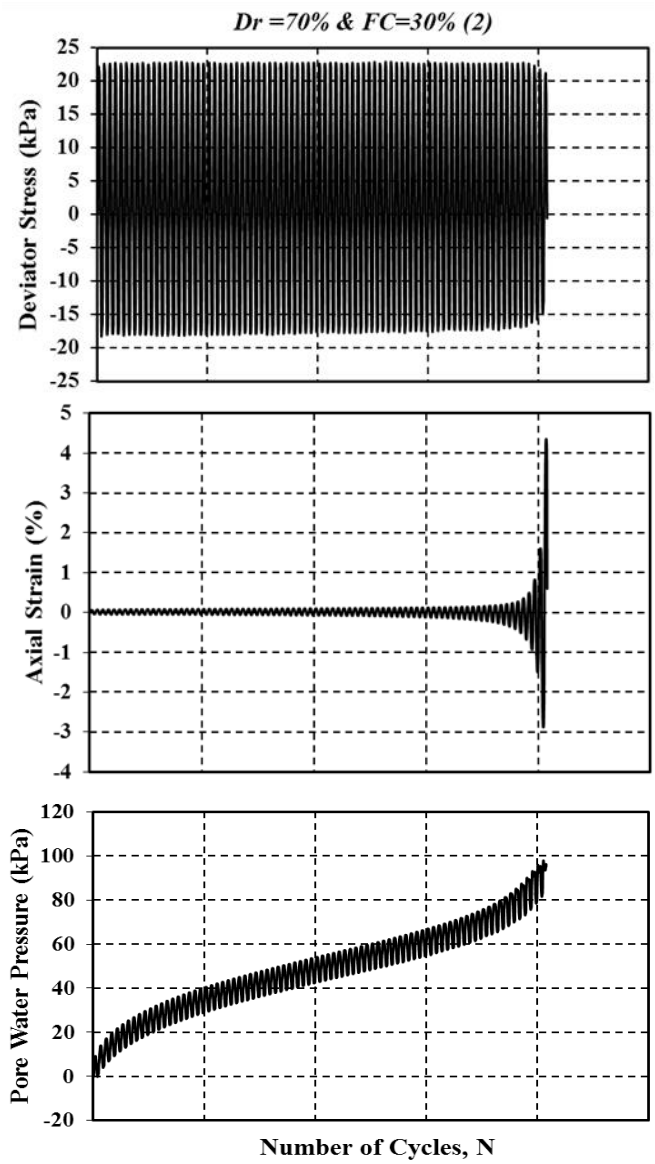

Figure A.3.123 Pore water pressure, axial strain, devaitor stress versus number of cycles

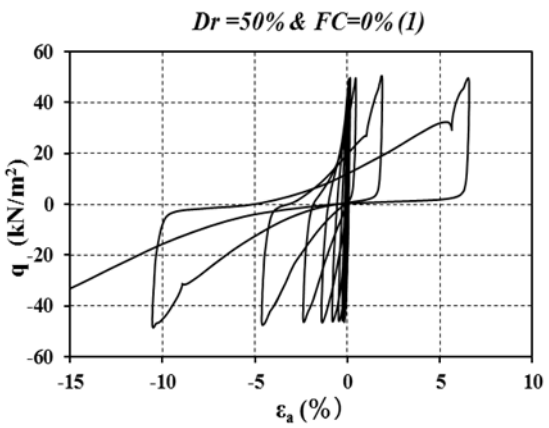

Figure A.3.124 Deviator stress versus axial strain

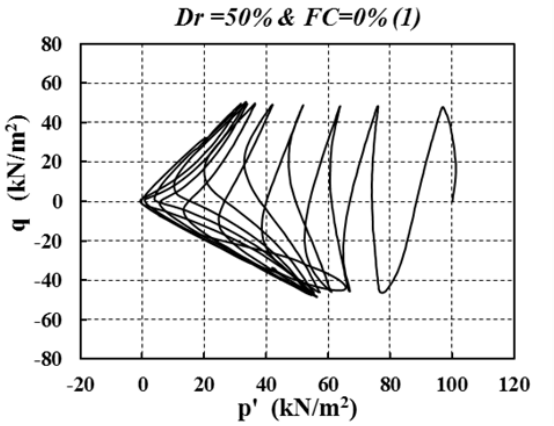

Figure A.3.125 Stress path during the undrained condition

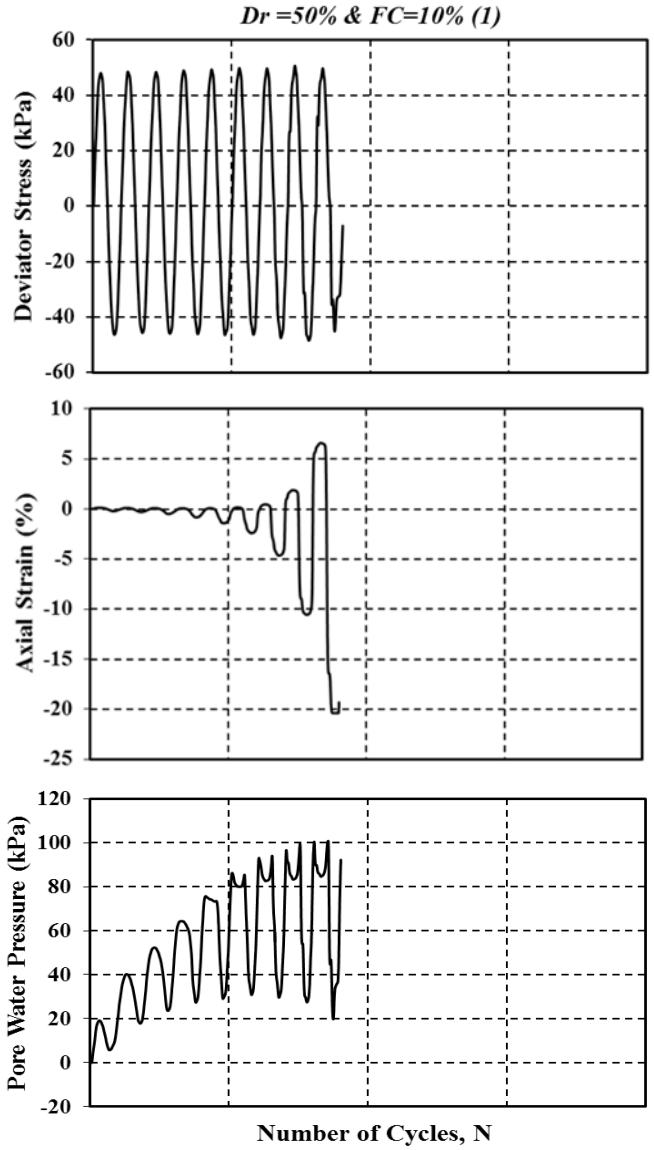

Figure A.3.126 Pore water pressure, axial strain, devaitor stress versus number of cycles

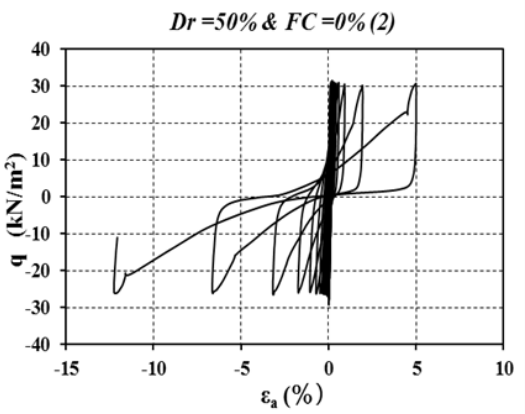

Figure A.3.127 Deviator stress versus axial strain

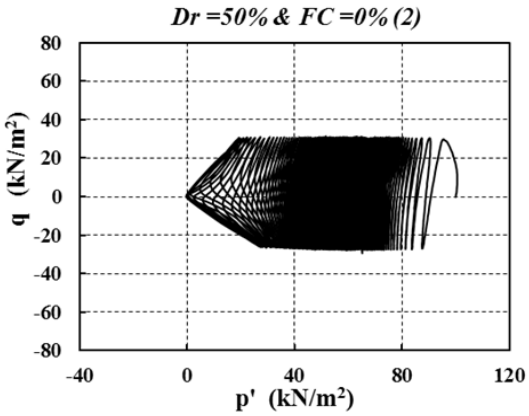

Figure A.3.128 Stress path during the undrained condition

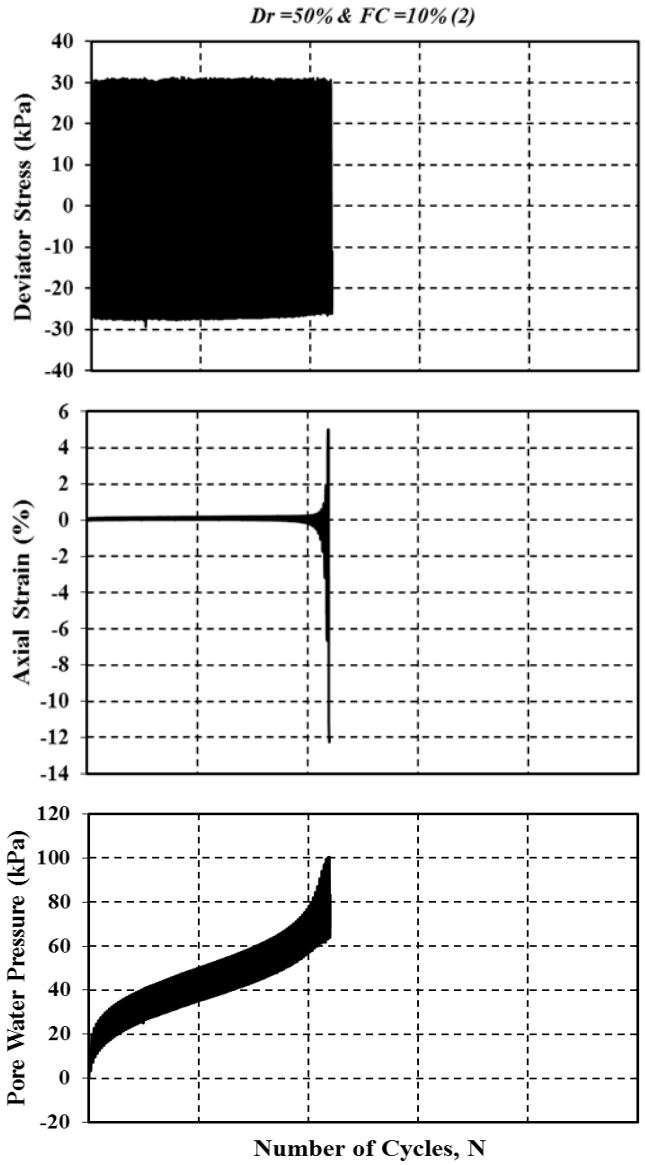

Figure A.3.129 Pore water pressure, axial strain, devaitor stress versus number of cycles

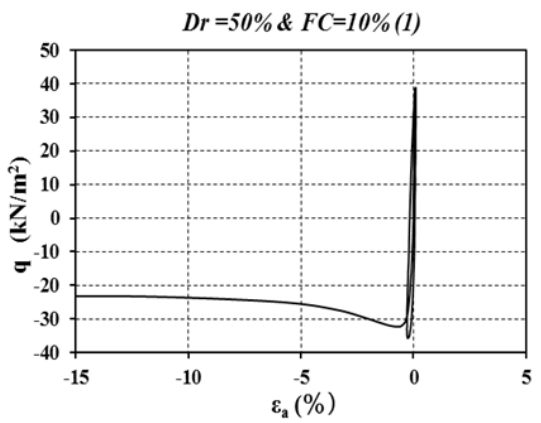

Figure A.3.130 Deviator stress versus axial strain

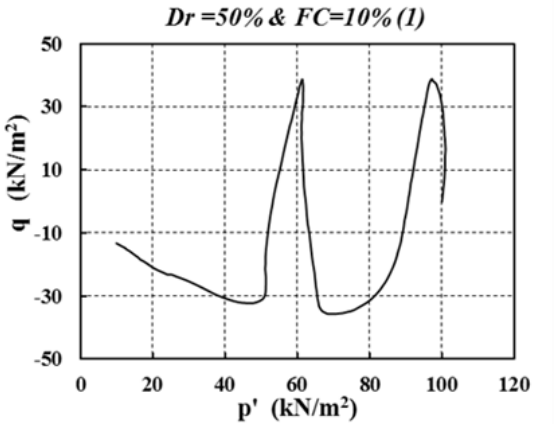

Figure A.3.131 Stress path during the undrained condition

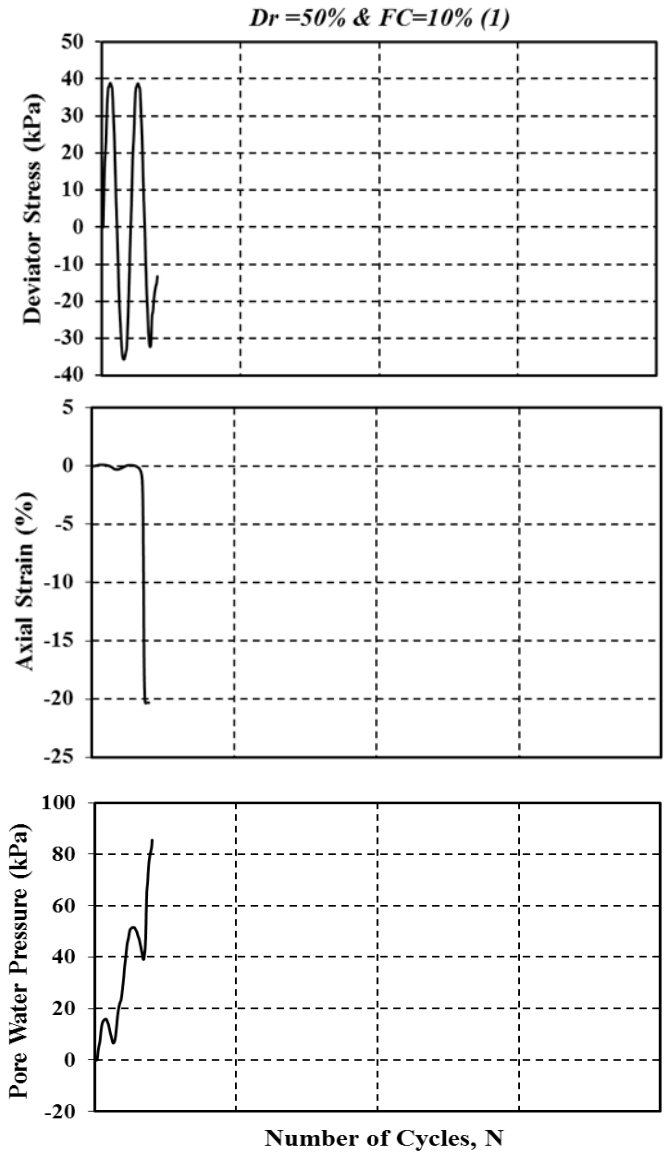

Figure A.3.132 Pore water pressure, axial strain, devaitor stress versus number of cycles

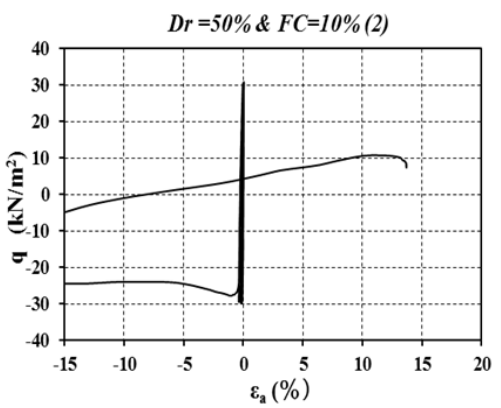

Figure A.3.133 Deviator stress versus axial strain

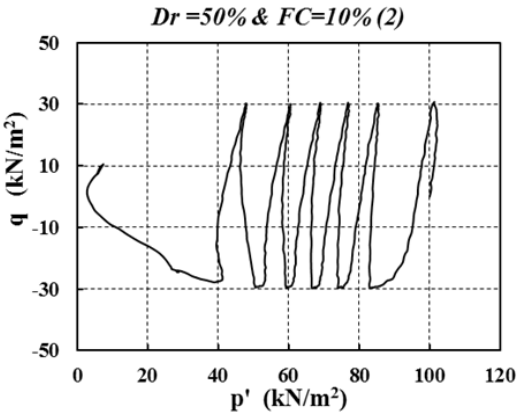

Figure A.3.134 Stress path during the undrained condition

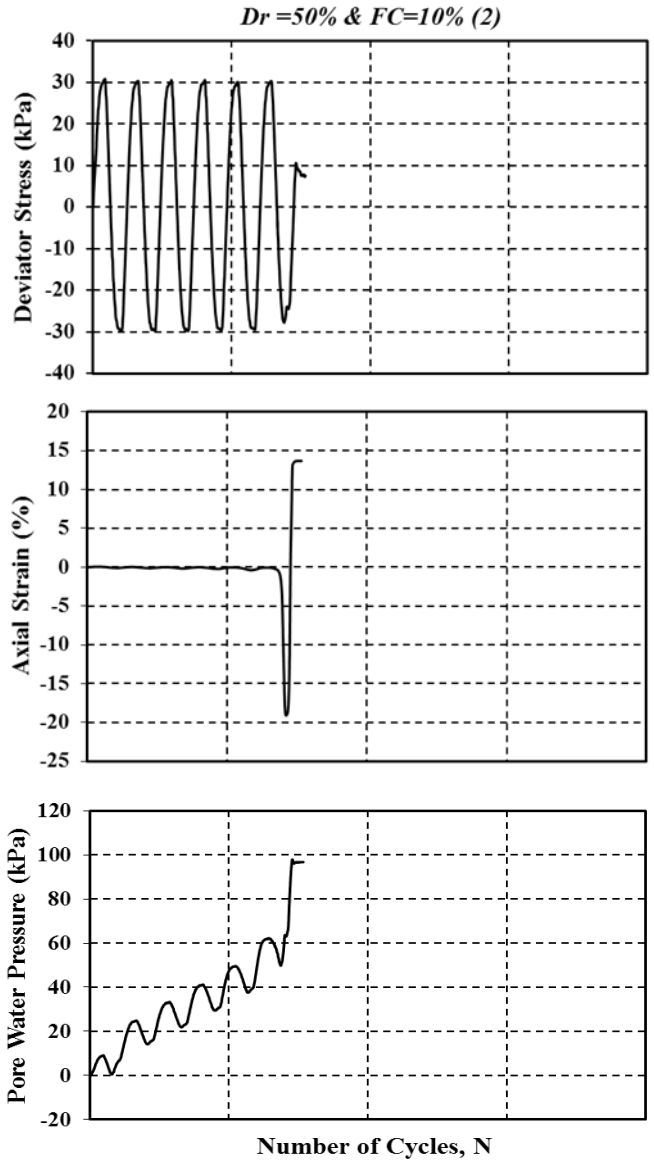

Figure A.3.135 Pore water pressure, axial strain, devaitor stress versus number of cycles

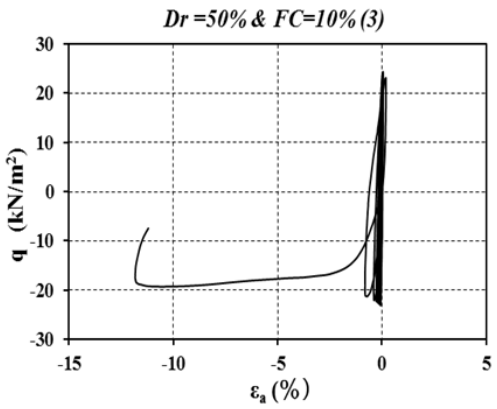

Figure A.3.136 Deviator stress versus axial strain

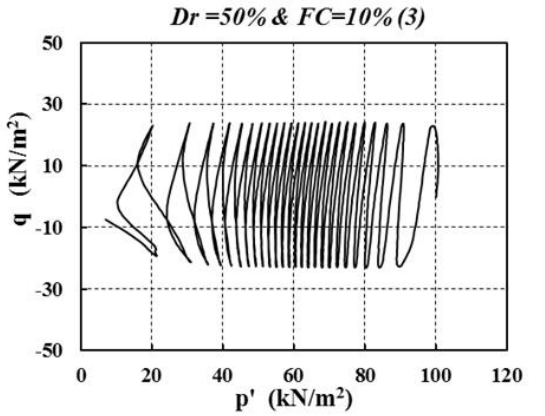

Figure A.3.137 Stress path during the undrained condition

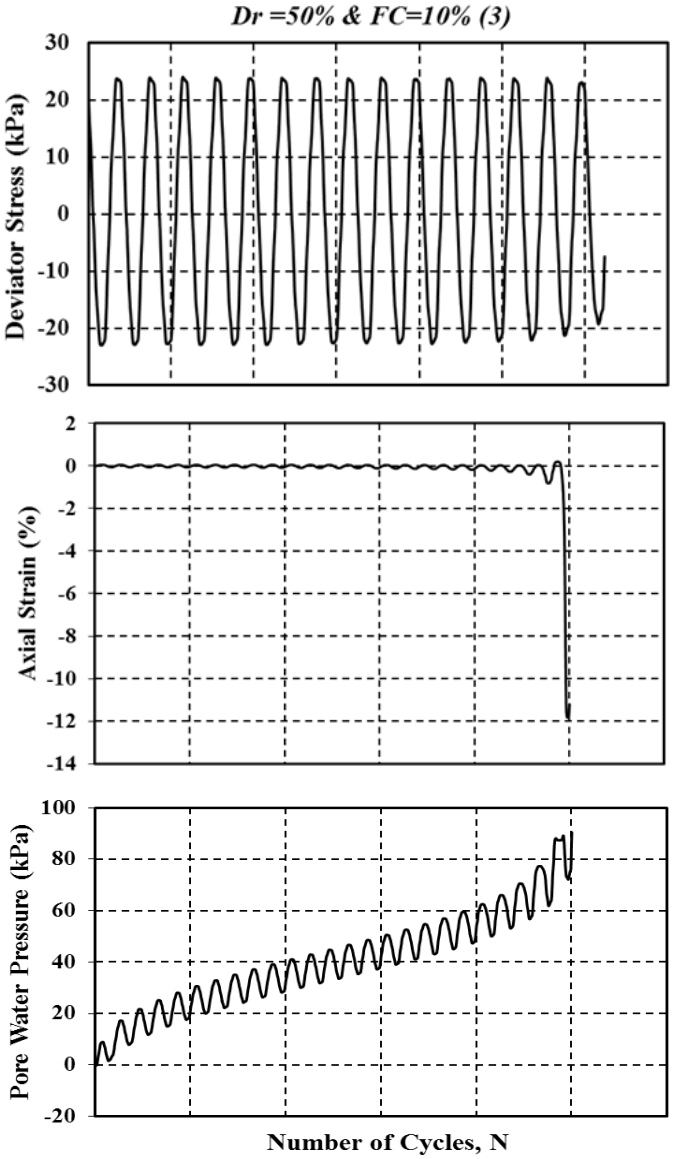

Figure A.3.138 Pore water pressure, axial strain, devaitor stress versus number of cycles.

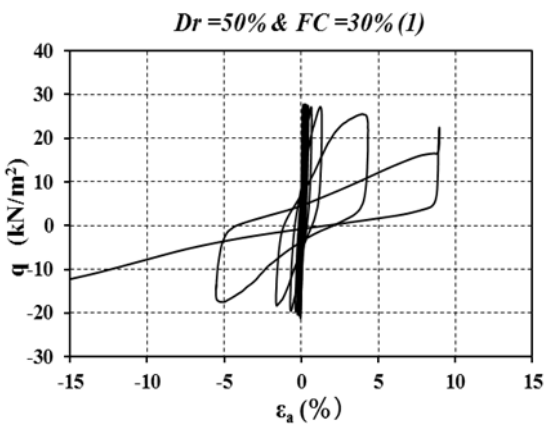

Figure A.3.139 Deviator stress versus axial strain

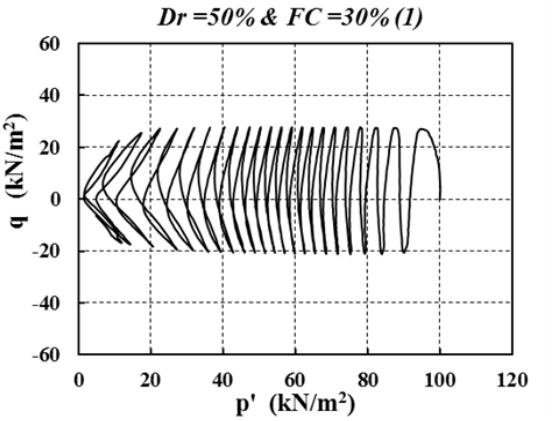

Figure A.3.140 Stress path during the undrained condition

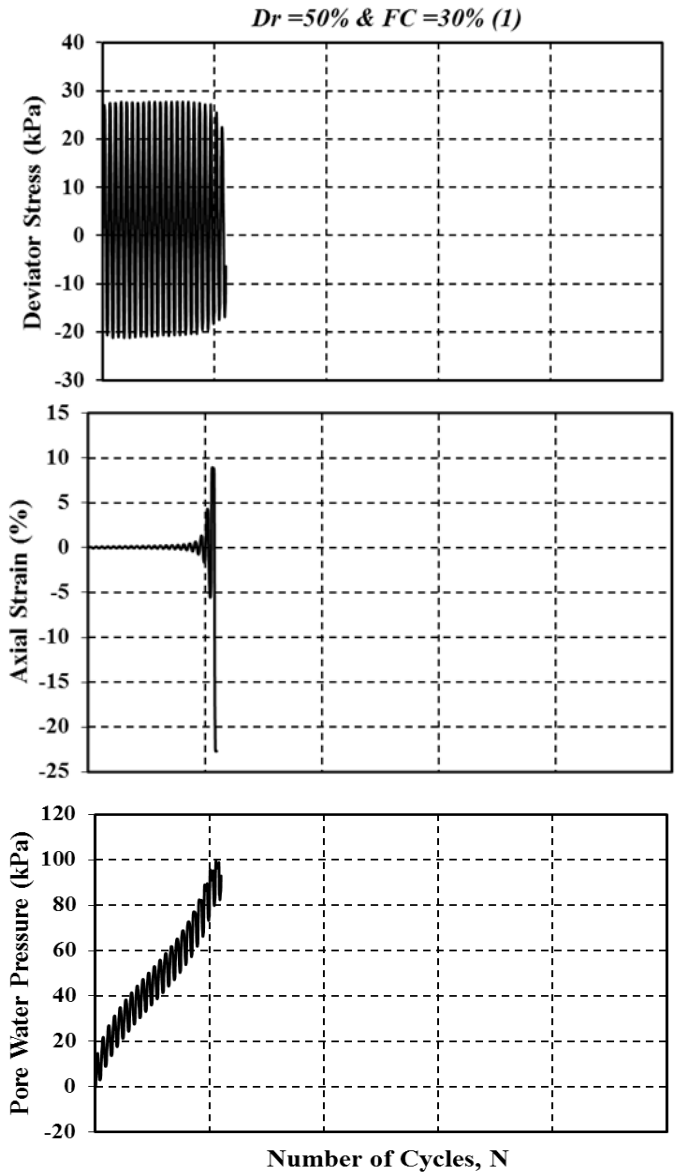

Figure A.3.141 Pore water pressure, axial strain, devaitor stress versus number of cycles

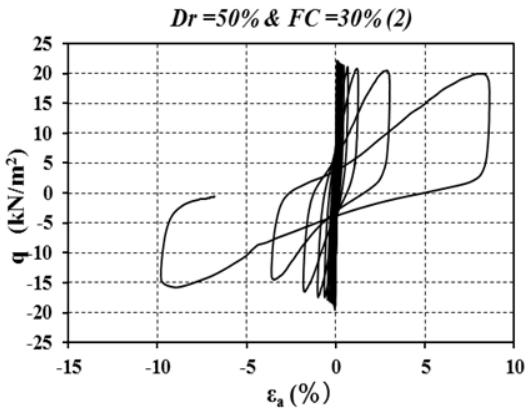

Figure A.3.142 Deviator stress versus axial strain

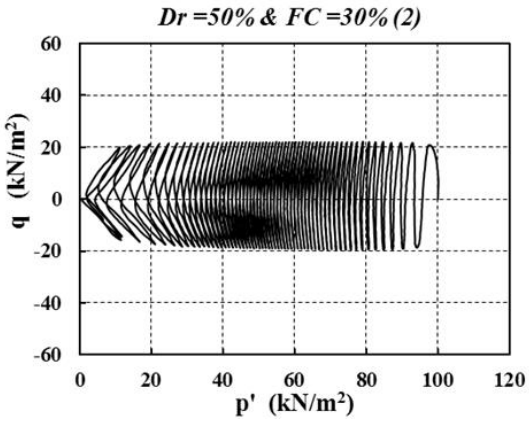

Figure A.3.143 Stress path during the undrained condition

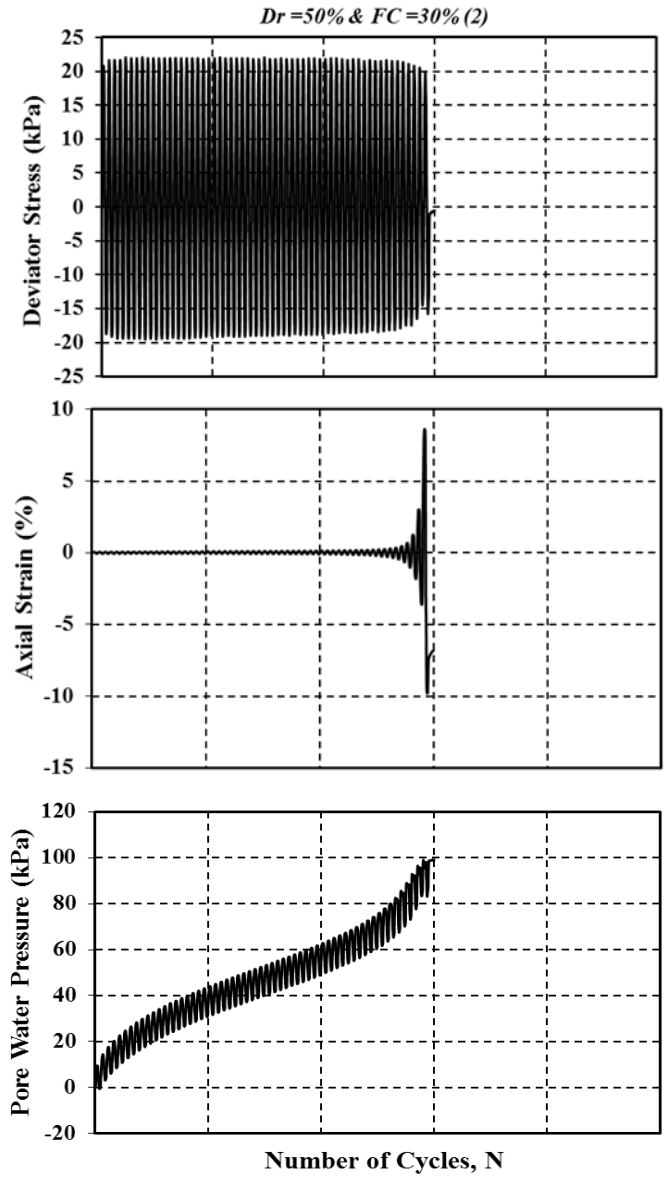

Figure A.3.144 Pore water pressure, axial strain, devaitor stress versus number of cycles

Appendix B: V_S and V_P Measurements

Vs	σh kN/m²	t1(▲) msec	t2(△) msec	δt msec	Vs m/sec
test 1	240.0	0.345	0.795	0.45	221
test 2	240.0	0.345	0.815	0.47	212
Average					216

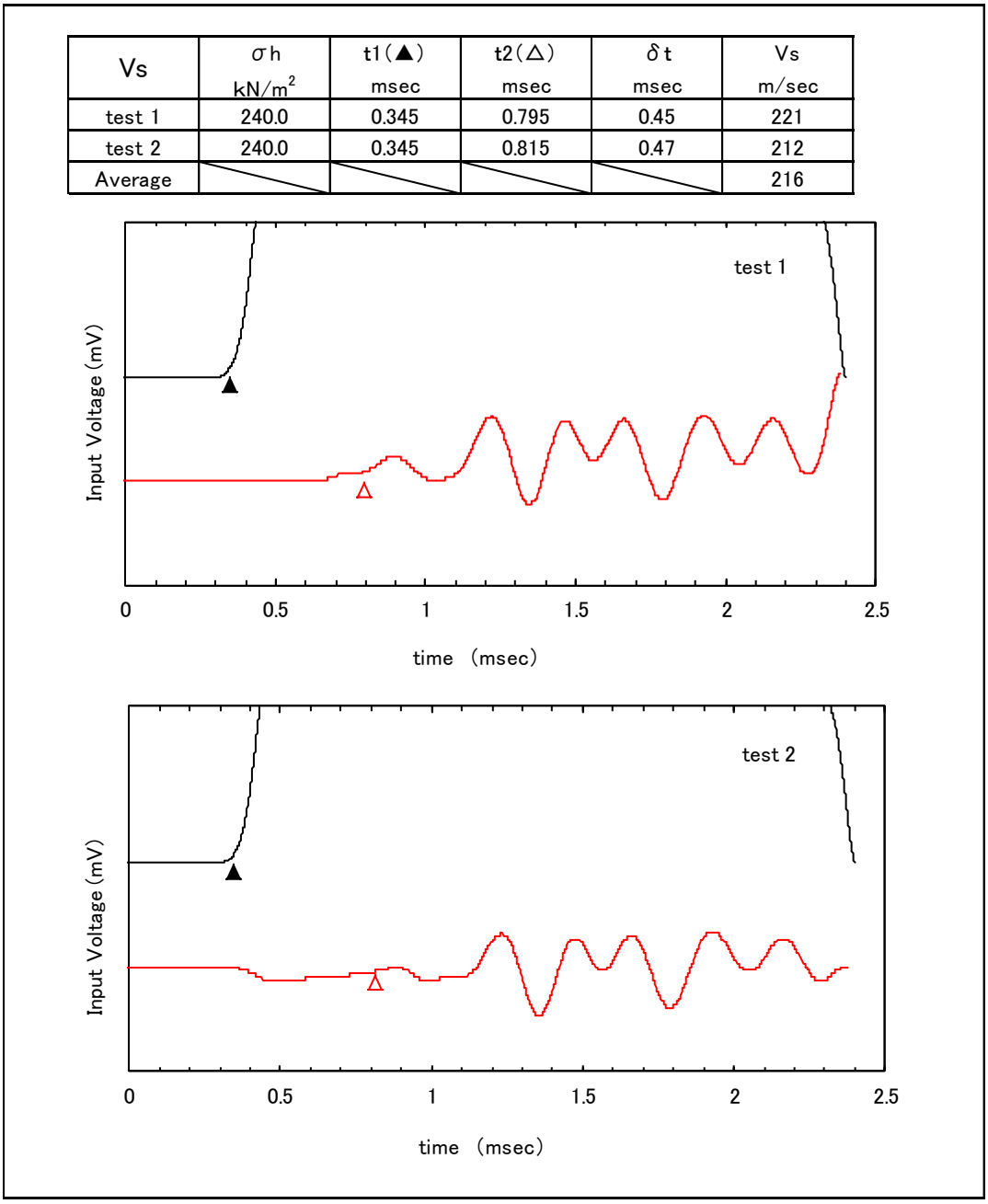

Figure B.1 V_S measurements of the sample No.1 [SN-S-2 (20.1-20.8m)]

Vp	σh kN/m^2	t1(▲) msec	t2(△) msec	δt msec	Vp m/sec
test 1	240.0	0.205	0.260	0.055	1809
test 2	240.0	0.205	0.260	0.055	1809
Average					1809

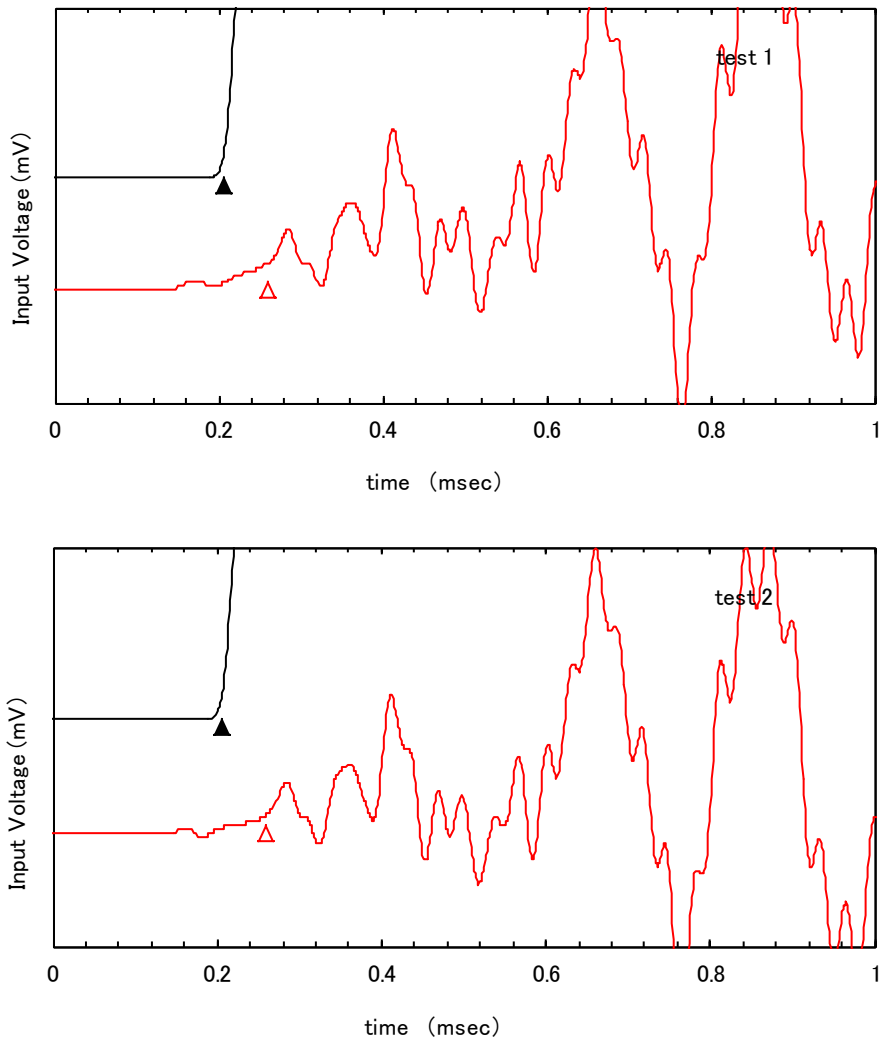

Figure B.2 V_P measurements of the sample No.1 [SN-S-2 (20.1-20.8 m)]

Vs	σh kN/m^2	t1(▲) msec	t2(△) msec	δt msec	Vs m/sec
test 1	55.0	0.335	1.030	0.695	139
test 2	55.0	0.335	1.035	0.7	138
Average					139

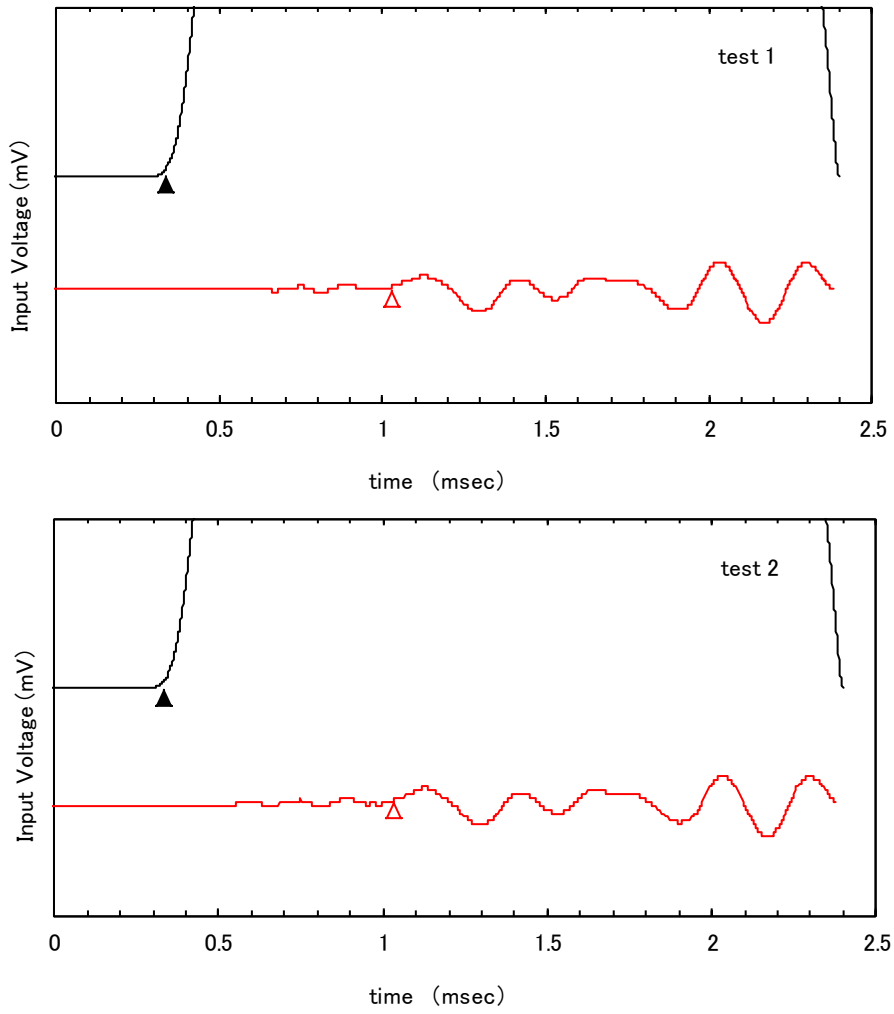

Figure B.3 V_S measurements of the sample No.3 [HG-S-1 (2.0-3.0m)]

Vp	σh kN/m²	t1(▲) msec	t2(△) msec	δt msec	Vp m/sec
test 1	55.0	0.198	0.246	0.048	2019
test 2	55.0	0.198	0.246	0.048	2019
Average					2019

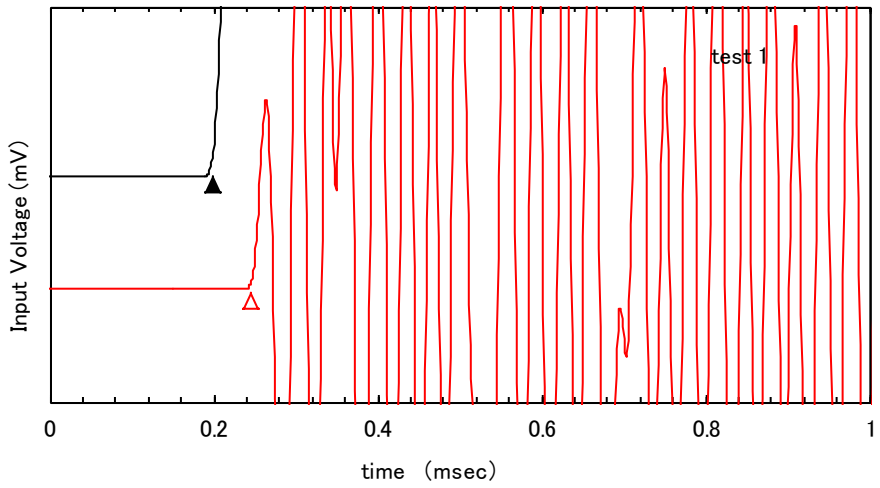

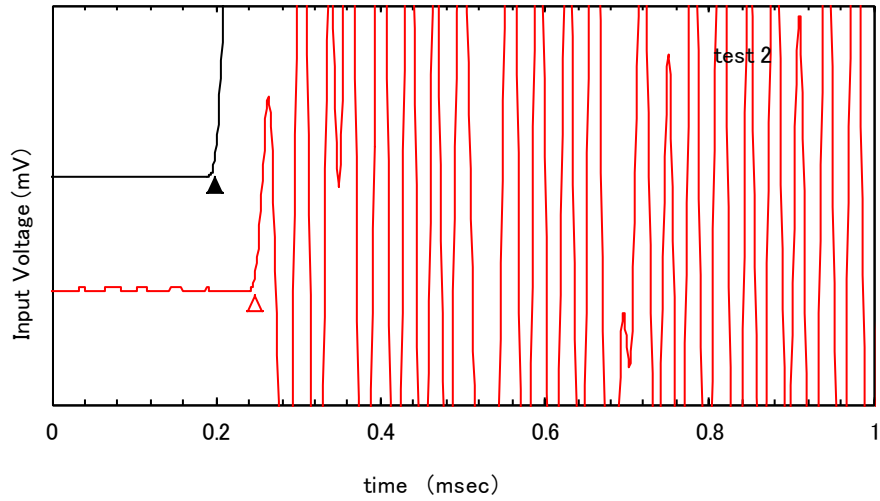

Figure B.4 V_P measurements of the sample No.3 [HG-S-1 (2.0-3.0m)]

Vs	σh kN/m^2	t1(▲) msec	t2(△) msec	δt msec	Vs m/sec
test 1	240.0	0.345	1.090	0.745	134
test 2	240.0	0.345	1.085	0.74	134
Average					134

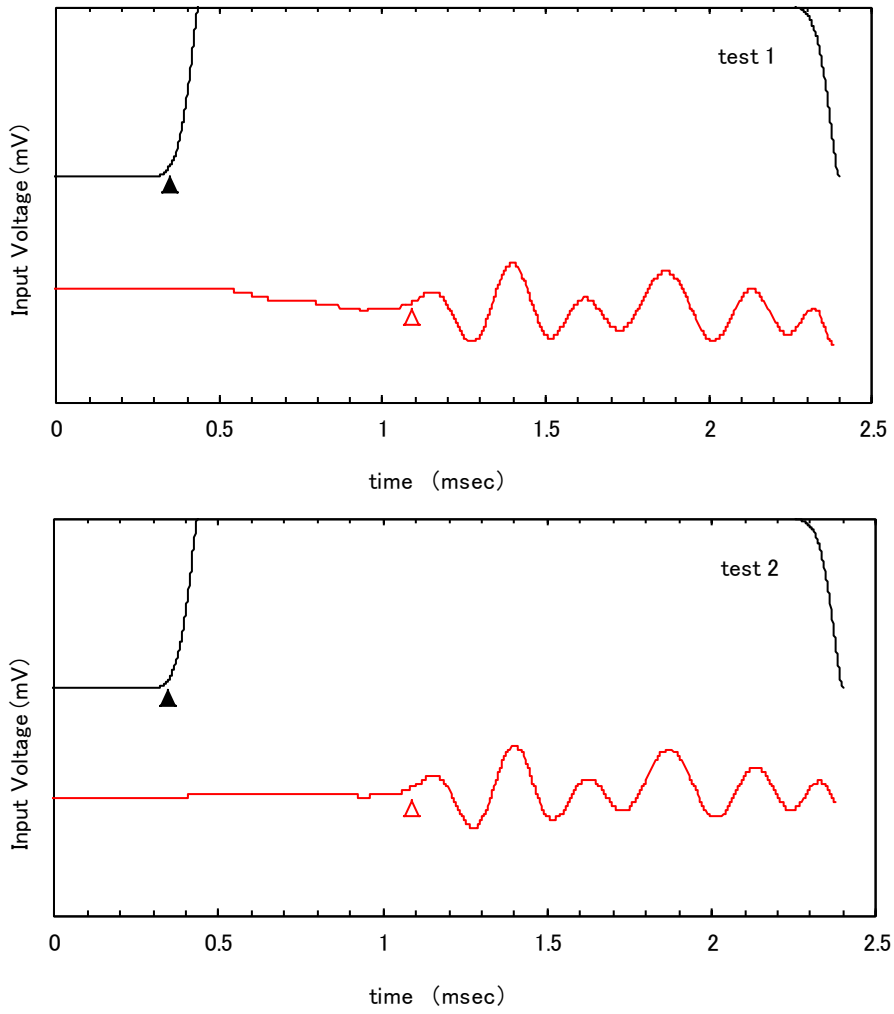

Figure B.5 V_S measurements of the sample No.5 [SN-S-2 (20.8-21.8m)]

Vp	σh kN/m^2	t1(▲) msec	t2(△) msec	δt msec	Vp m/sec
test 1	240.0	0.200	0.255	0.055	1809
test 2	240.0	0.200	0.255	0.055	1809
Average					1809

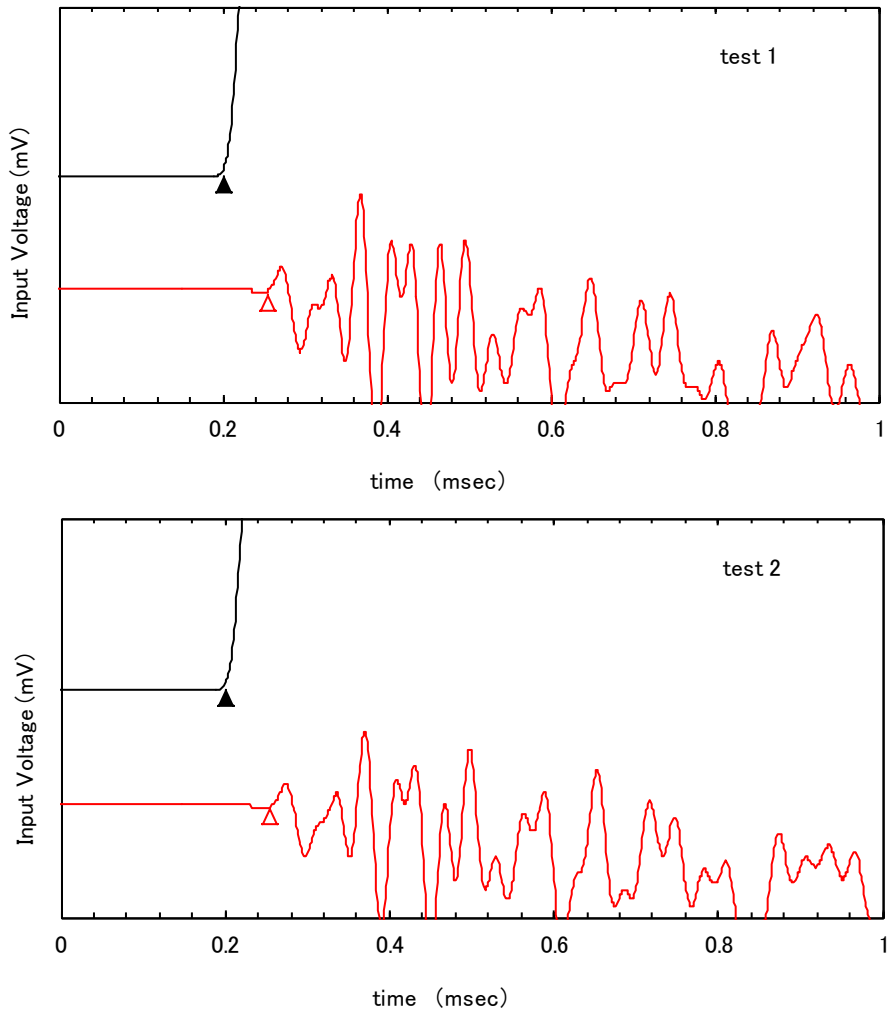

Figure B.6 V_P measurements of the sample No.5 [SN-S-2 (20.8-21.8m)]

Vs	σh kN/m^2	t1(▲) msec	t2(△) msec	δt msec	Vs m/sec
test 1	55.0	0.335	1.150	0.815	119
test 2	55.0	0.335	1.145	0.81	120
Average					120

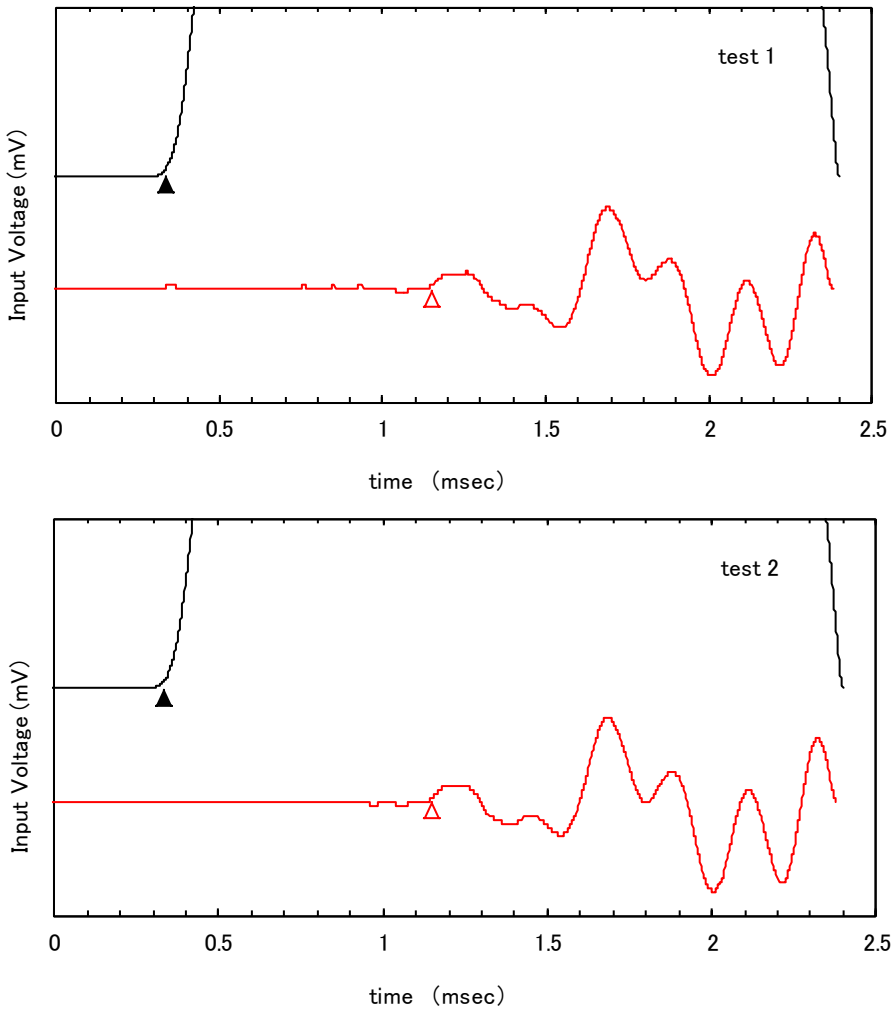

Figure B.7 V_S measurements of the sample No.8 [HG-S-1 (2.0-3.0m)]

Vp	σh kN/m²	t1(▲) msec	t2(△) msec	δt msec	Vp m/sec
test 1	55.0	0.198	0.245	0.047	2067
test 2	55.0	0.198	0.245	0.047	2067
Average					2067

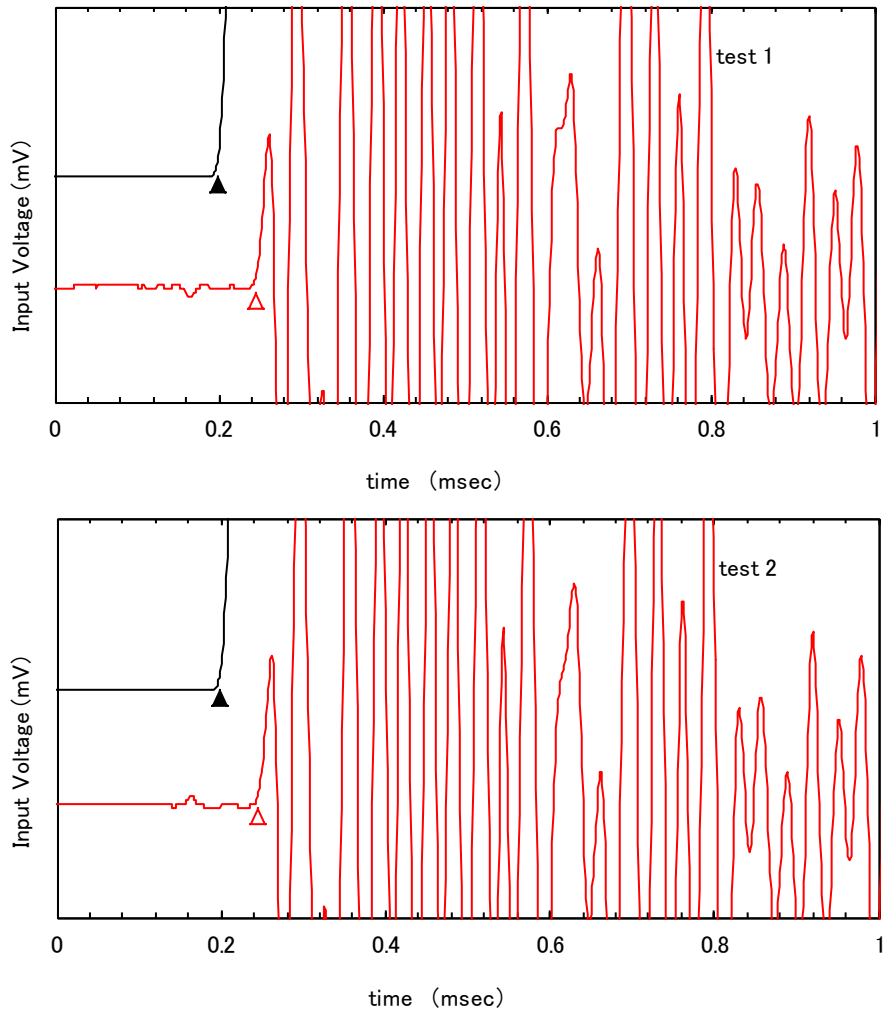

Figure B.8 V_P measurements of the sample No.8 [HG-S-1 (2.0-3.0m)]

Vs	σh kN/m^2	t1(▲) msec	t2(△) msec	δt msec	Vs m/sec
test 1	240.0	0.345	0.790	0.445	224
test 2	240.0	0.345	0.785	0.44	226
Average					225

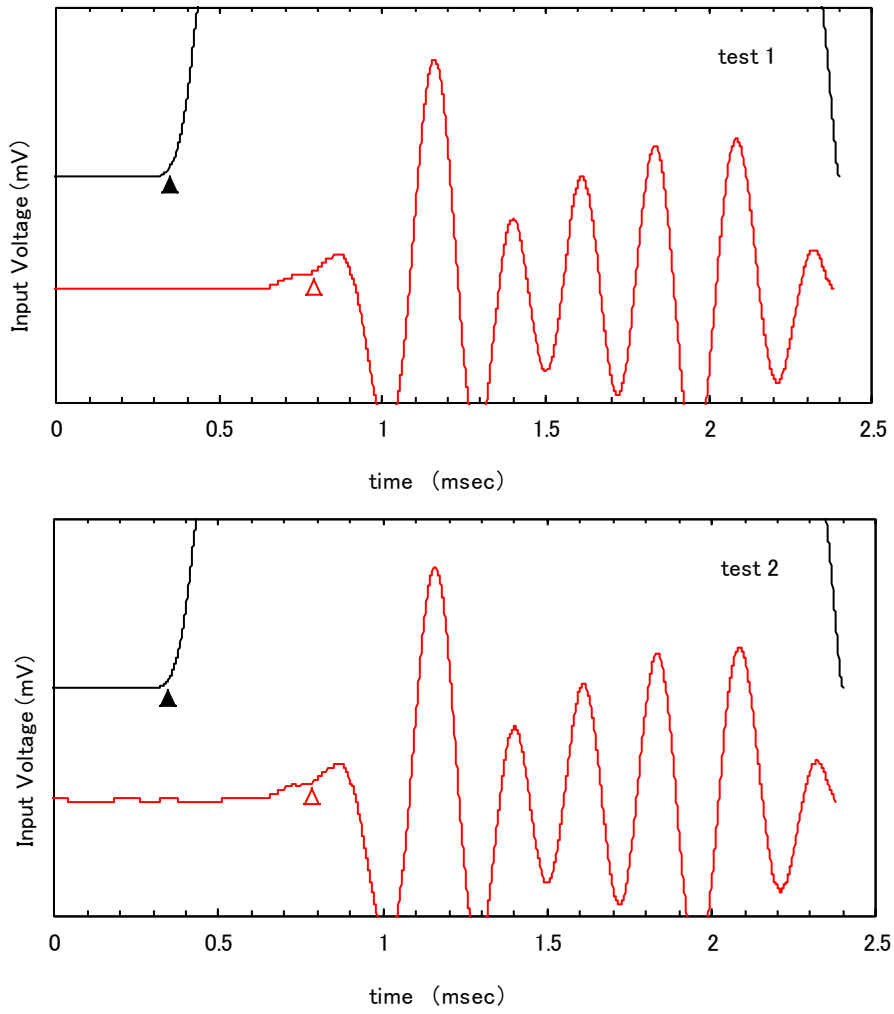

Figure B.9 V_S measurements of the sample No.9 [SN-S-2 (20.1-20.8m)]

Vp	σh kN/m²	t1(▲) msec	t2(△) msec	δt msec	Vp m/sec
test 1	240.0	0.200	0.250	0.05	1991
test 2	240.0	0.200	0.250	0.05	1991
Average					1991

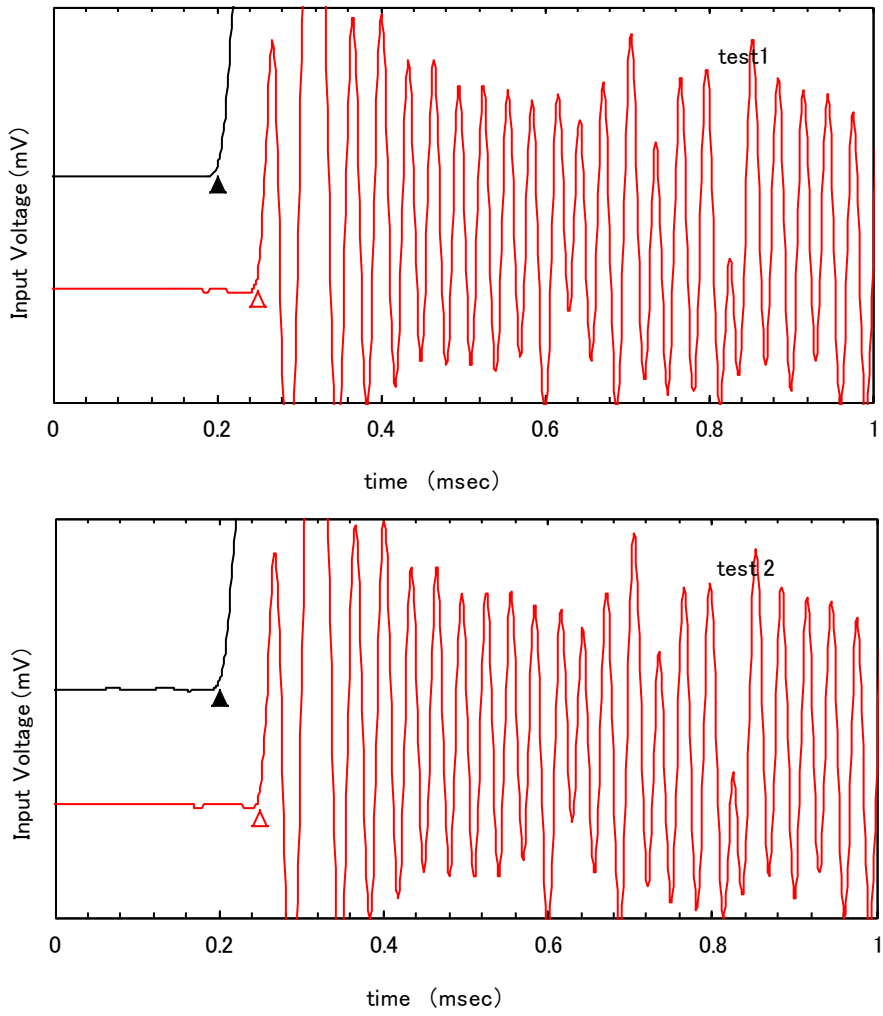

Figure B.10 V_P measurements of the sample No.9 [SN-S-2 (20.1-20.8m)]

Vs	σh kN/m^2	t1(▲) msec	t2(△) msec	δt msec	Vs m/sec
test 1	170.0	0.345	1.165	0.82	119
test 2	170.0	0.345	1.185	0.84	116
Average					118

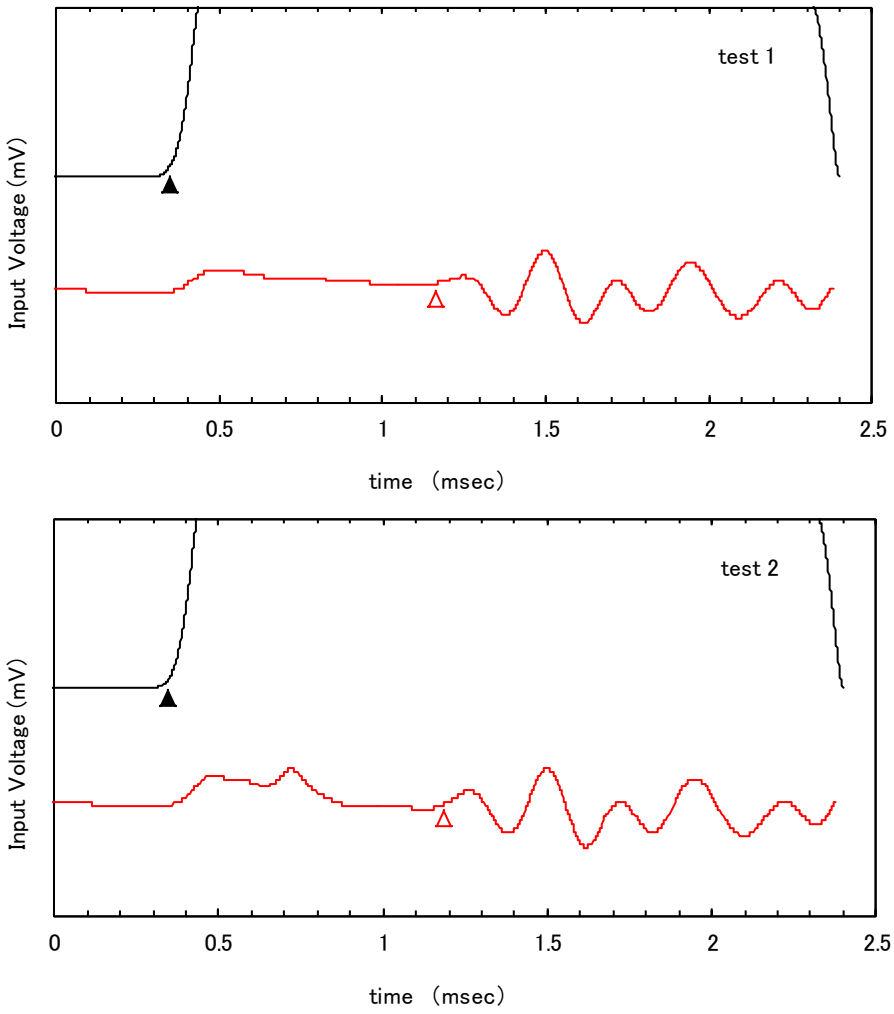

Figure B.11 V_S measurements of the sample No.12 [HG-S-1 (18.0-19.0m)]

Vp	σh kN/m²	t1(▲) msec	t2(△) msec	δt msec	Vp m/sec
test 1	170.0	0.205	0.255	0.05	1953
test 2	170.0	0.205	0.255	0.05	1953
Average					1953

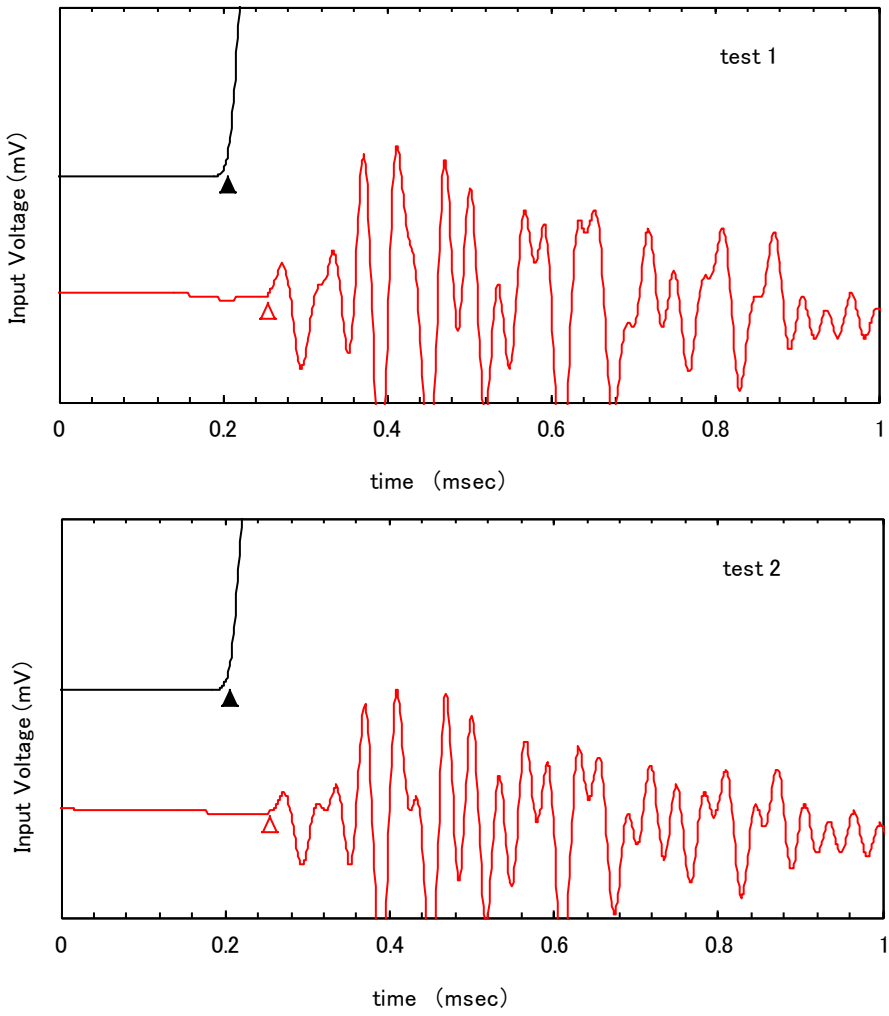

Figure B.12 V_P measurements of the sample No.12 [HG-S-1 (18.0-19.0m)]

Vs	σh kN/m^2	t1(▲) msec	t2(△) msec	δt msec	Vs m/sec
test 1	55.0	0.345	1.210	0.865	115
test 2	55.0	0.345	1.210	0.865	115
Average					115

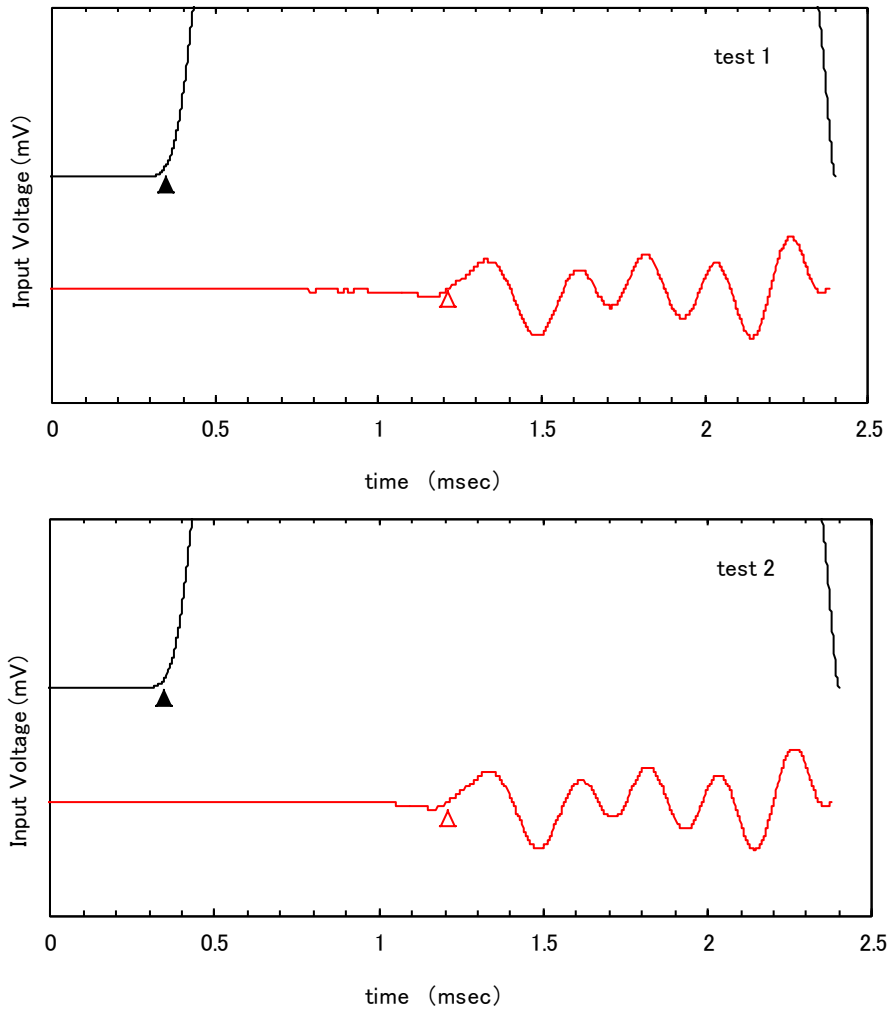

Figure B.13 V_S measurements of the sample No.14 [HG-S-1 (4.0-5.0m)]

Vp	σh kN/m²	t1(▲) msec	t2(△) msec	δt msec	Vp m/sec
test 1	55.0	0.200	0.250	0.05	1981
test 2	55.0	0.200	0.250	0.05	1981
Average					1981

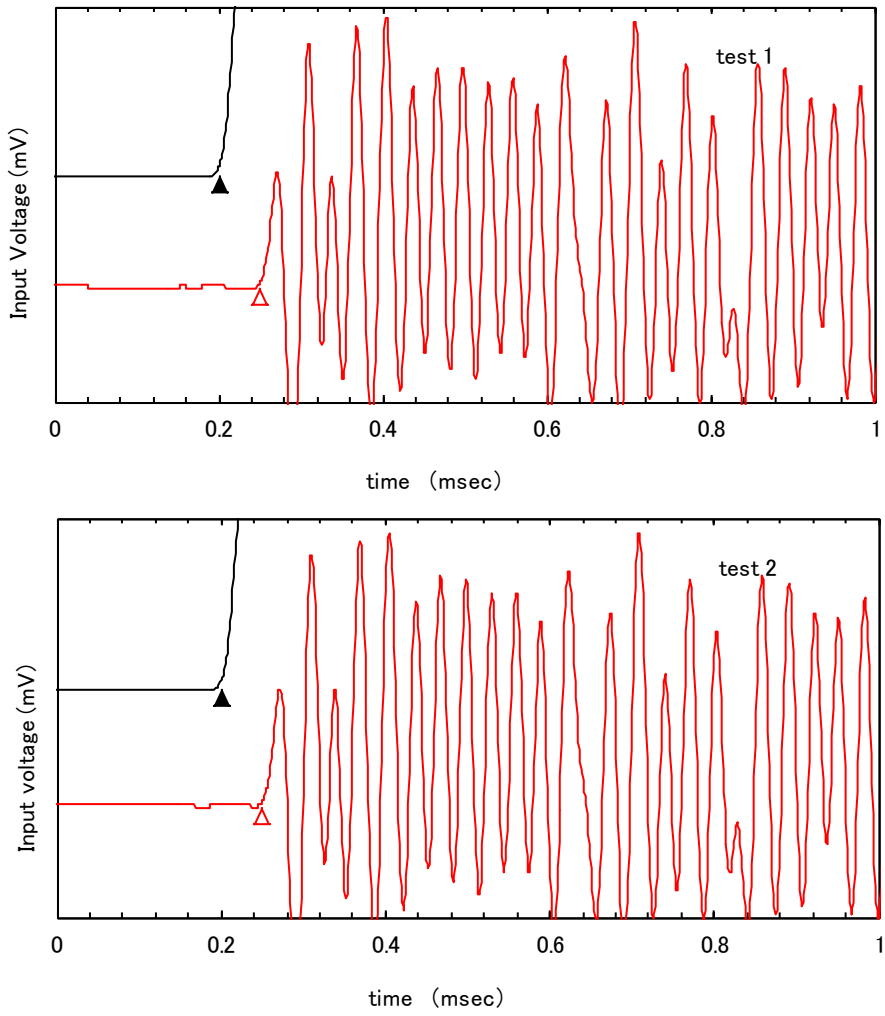

Figure B.14 V_P measurements of the sample No.14 [HG-S-1 (4.0-5.0m)]

Vs	σh kN/m²	t1(▲) msec	t2(△) msec	δt msec	Vs m/sec
test 1	170.0	0.345	0.960	0.615	159
test 2	170.0	0.345	0.960	0.615	159
Average					159

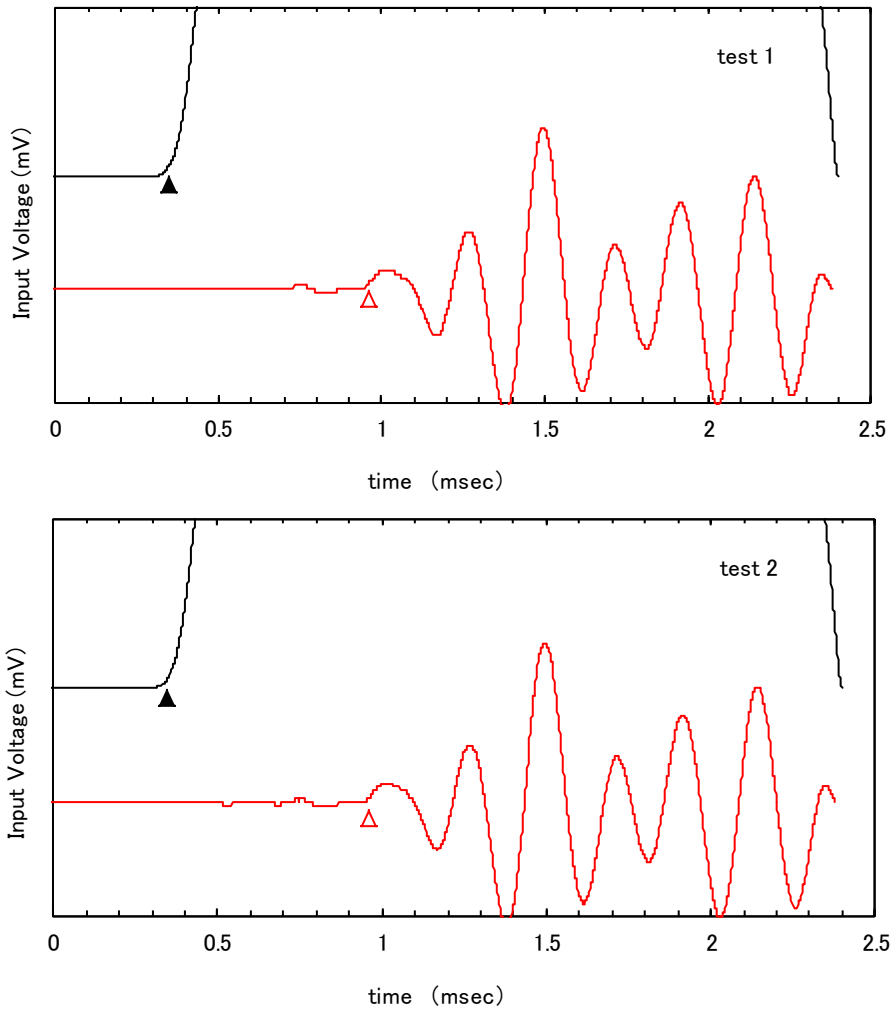

Figure B.15 V_S measurements of the sample No.17 [HG-S-1 (19.0-20.0m)]

Vp	σh kN/m²	t1(▲) msec	t2(△) msec	δt msec	Vp m/sec
test 1	170.0	0.200	0.250	0.05	1960
test 2	170.0	0.200	0.250	0.05	1960
Average					1960

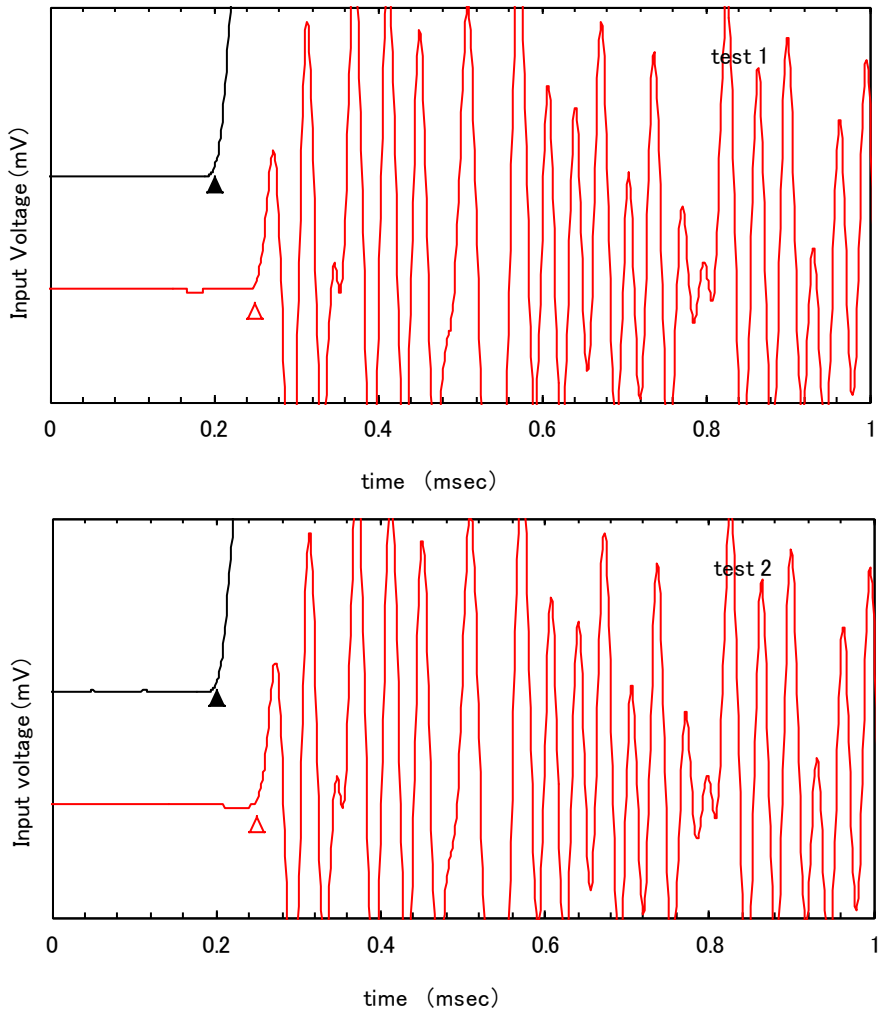

Figure B.16 V_P measurements of the sample No.17 [HG-S-1 (19.0-20.0m)]

Vs	σh kN/m²	t1(▲) msec	t2(△) msec	δt msec	Vs m/sec
test 1	150.0	0.345	0.845	0.5	199
test 2	150.0	0.345	0.850	0.505	197
Average					198

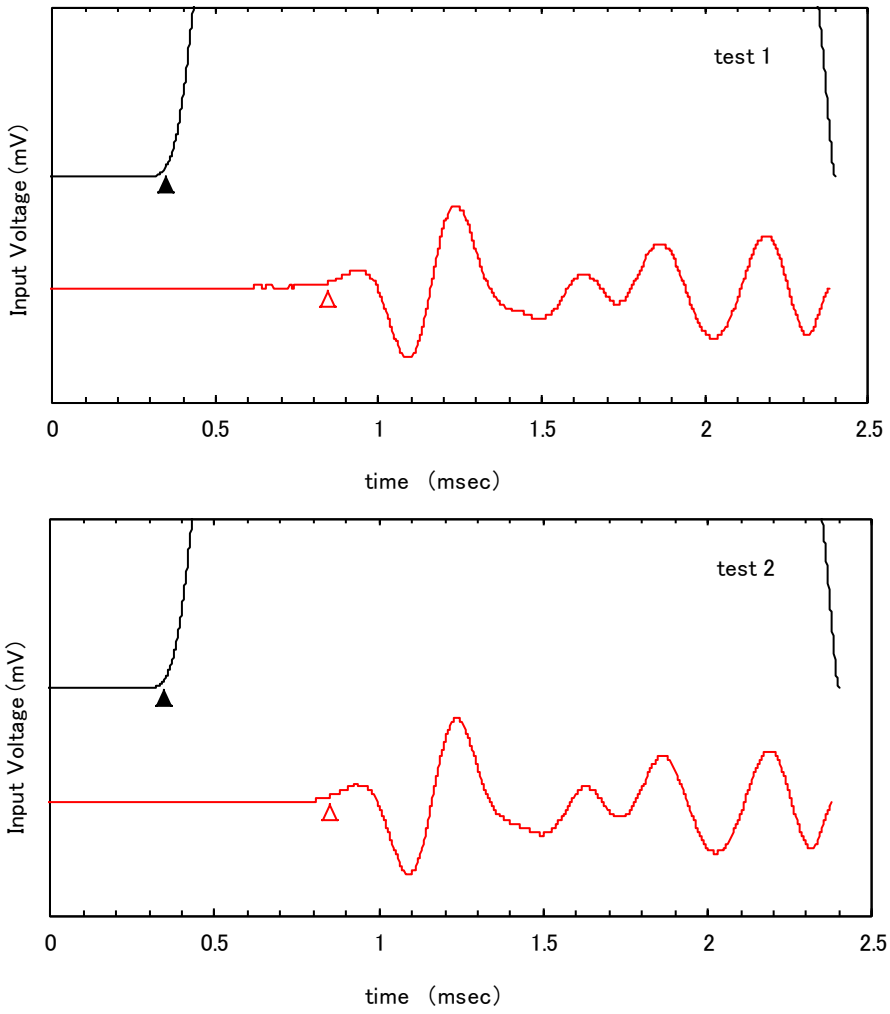

Figure B.17 V_S measurements of the sample No.19 [SN-S-2 (13.0-14.0m)]

Vp	σh kN/m²	t1(▲) msec	t2(△) msec	δt msec	Vp m/sec
test 1	150.0	0.203	0.252	0.049	2026
test 2	150.0	0.203	0.252	0.049	2026
Average					2026

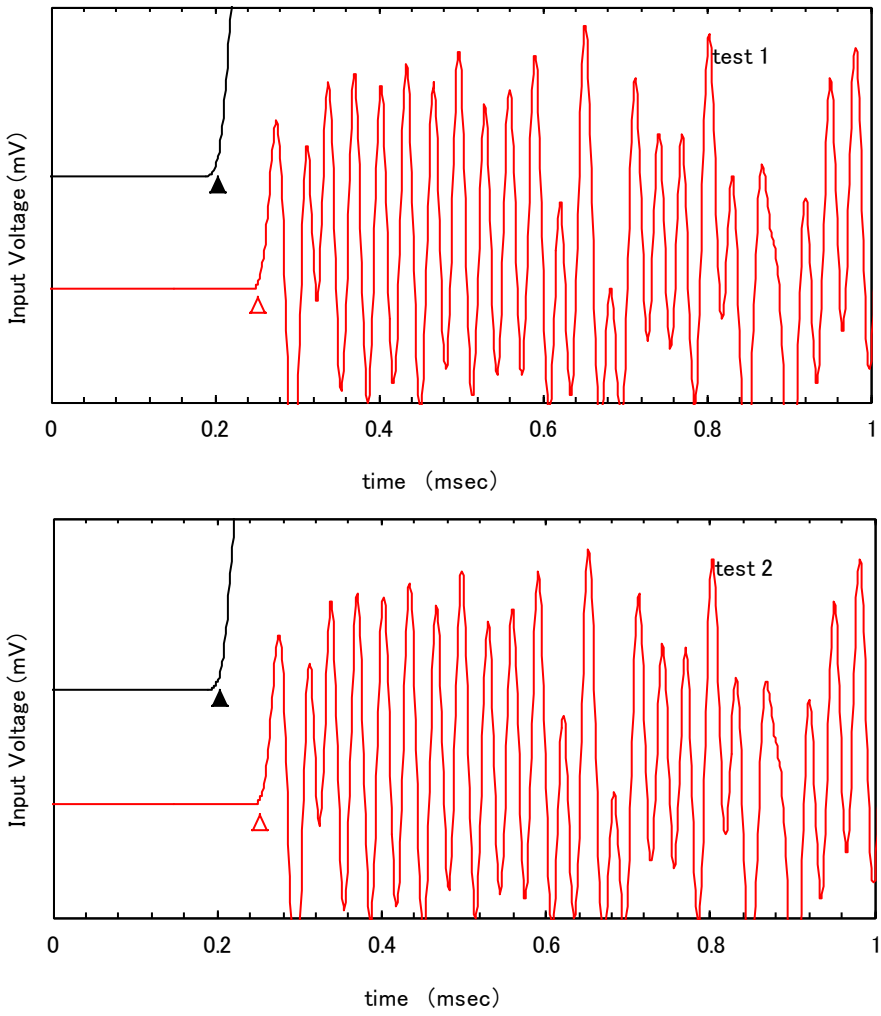

Figure B.18 V_P measurements of the sample No.19 [SN-S-2 (13.0-14.0m)]

Vs	σh kN/m^2	t1(▲) msec	t2(△) msec	δt msec	Vs m/sec
test 1	150.0	0.345	0.800	0.455	220
test 2	150.0	0.345	0.805	0.46	218
Average					219

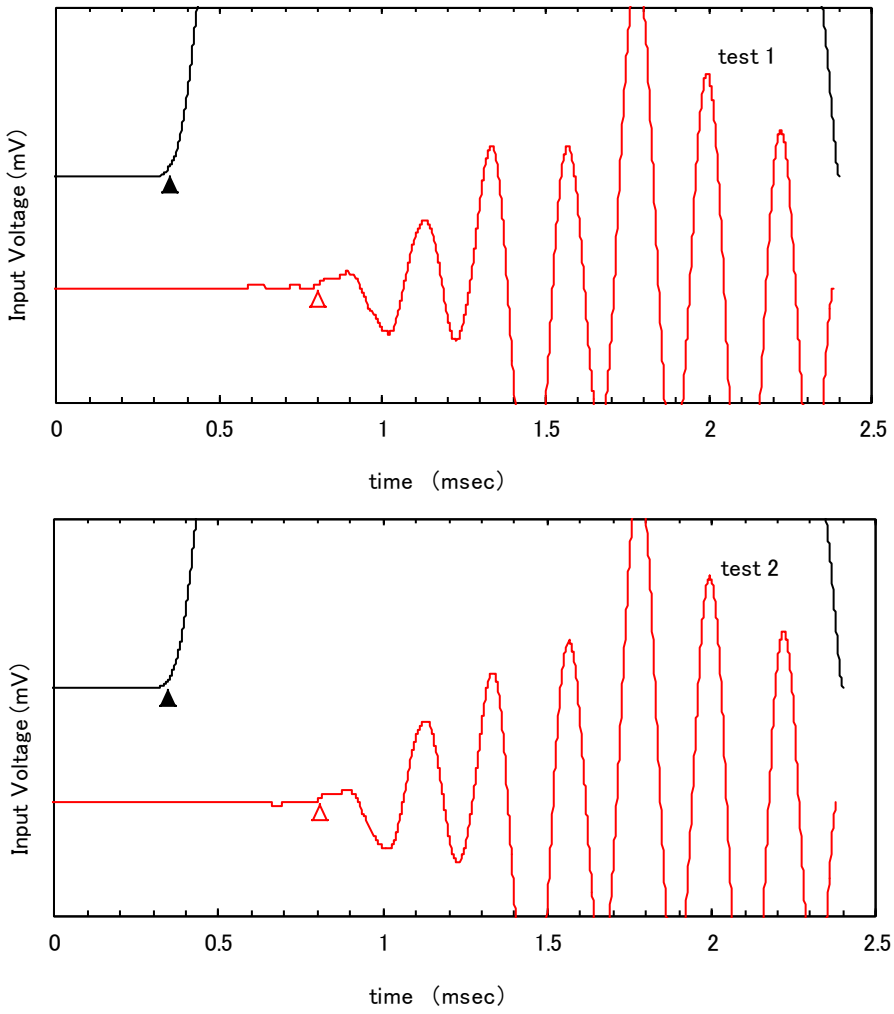

Figure B.19 V_S measurements of the sample No.19-2 [SN-S-2 (13.0-14.0m)]

Vp	σh kN/m²	t1(▲) msec	t2(△) msec	δt msec	Vp m/sec
test 1	150.0	0.200	0.245	0.045	2226
test 2	150.0	0.200	0.245	0.045	2226
Average					2226

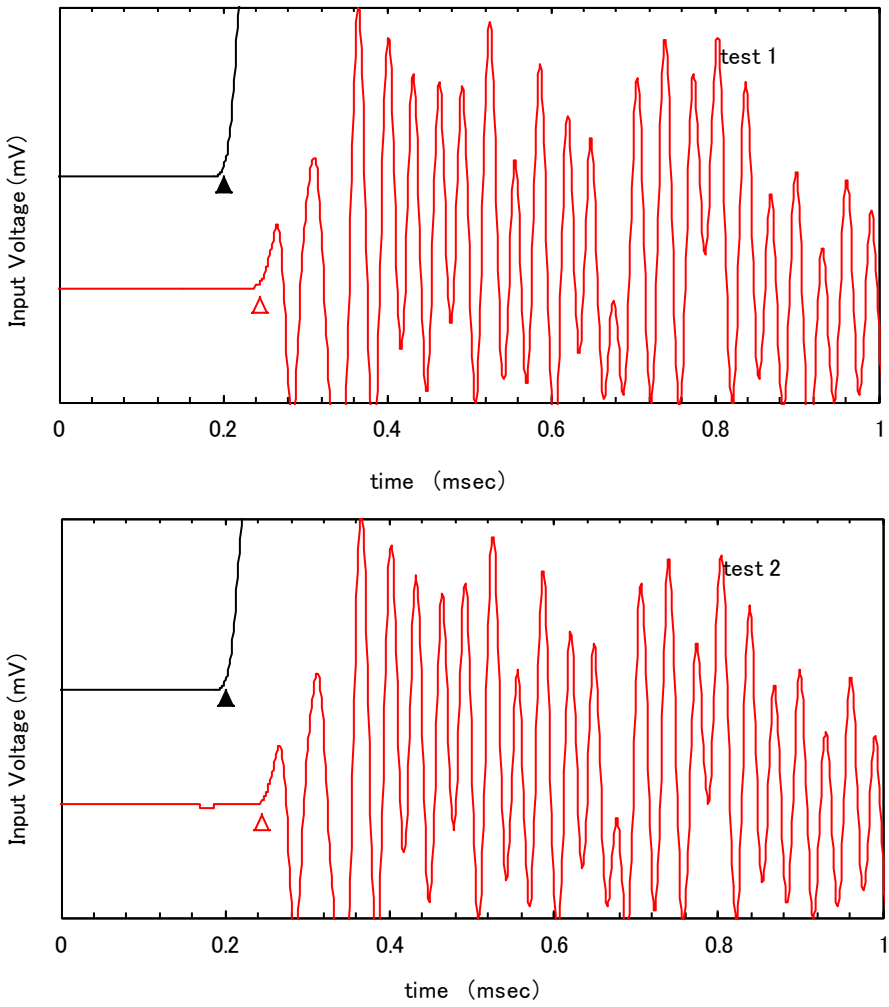

Figure B.20 V_P measurements of the sample No.19-2 [SN-S-2 (13.0-14.0m)]

Vs	σh kN/m^2	t1(▲) msec	t2(△) msec	δt msec	Vs m/sec
test 1	270.0	0.445	0.925	0.48	205
test 2	270.0	0.445	0.925	0.48	205
Average					205

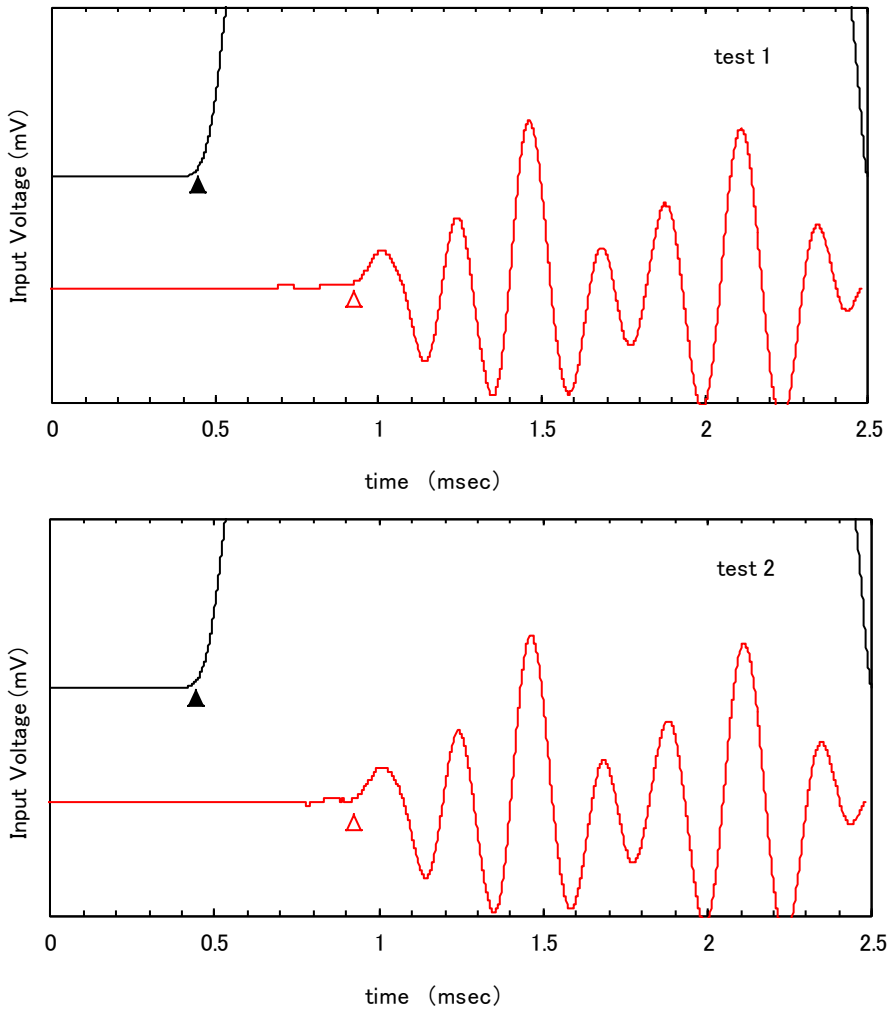

Figure B.21 V_S measurements of the sample No.23 [SN-S-1 (25.3-26.1m)]

Vp	σh kN/m²	t1(▲) msec	t2(△) msec	δt msec	Vp m/sec
test 1	270.0	0.200	0.245	0.045	2192
test 2	270.0	0.200	0.245	0.045	2192
Average					2192

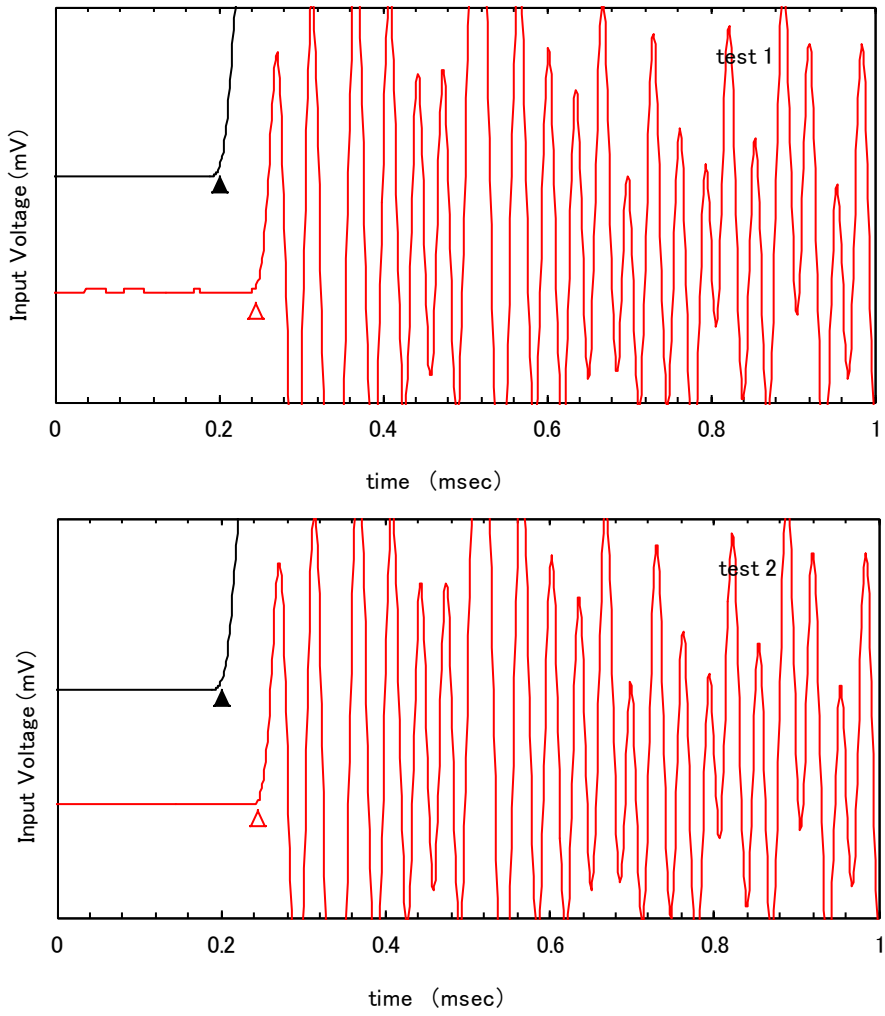

Figure B.22 V_P measurements of the sample No.23 [SN-S-1 (25.3-26.1m)]

Vs	σh kN/m^2	t1(▲) msec	t2(△) msec	δt msec	Vs m/sec
test 1	40.0	0.345	1.170	0.825	121
test 2	40.0	0.345	1.170	0.825	121
Average					121

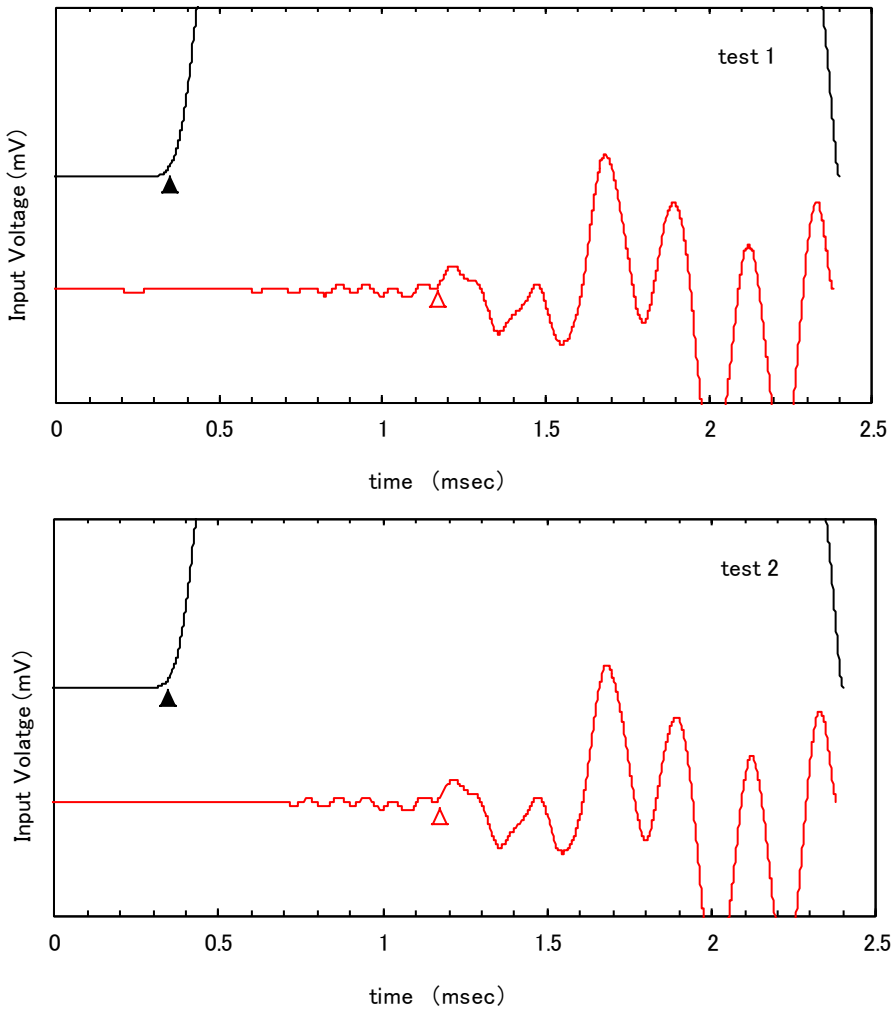

Figure B.23 V_S measurements of the sample No.24 [SN-S-1 (1.0-2.0m)]

Vp	σh kN/m²	t1(▲) msec	t2(△) msec	δt msec	Vp m/sec
test 1	40.0	0.200	0.245	0.045	2218
test 2	40.0	0.200	0.245	0.045	2218
Average					2218

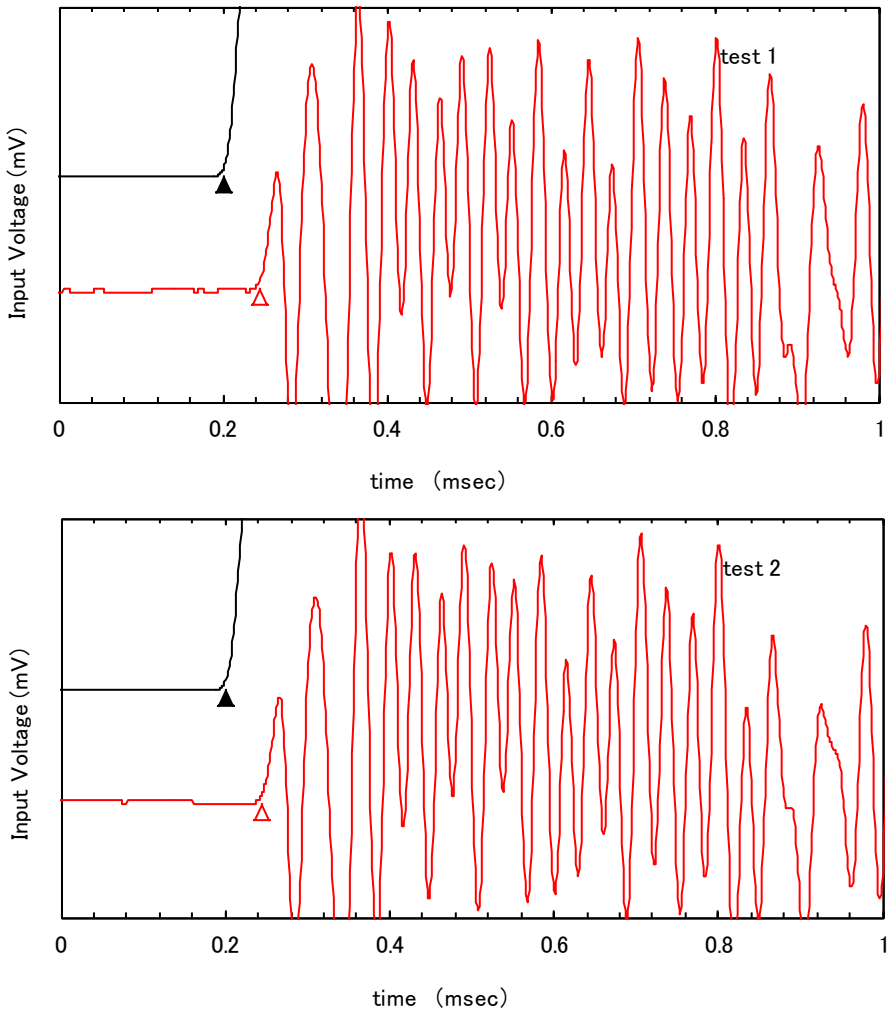

Figure B.24 V_P measurements of the sample No.24 [SN-S-1 (1.0-2.0m)]

Vs	σh kN/m^2	t1(▲) msec	t2(△) msec	δt msec	Vs m/sec
test 1	240.0	0.445	0.945	0.5	200
test 2	240.0	0.445	0.945	0.5	200
Average					200

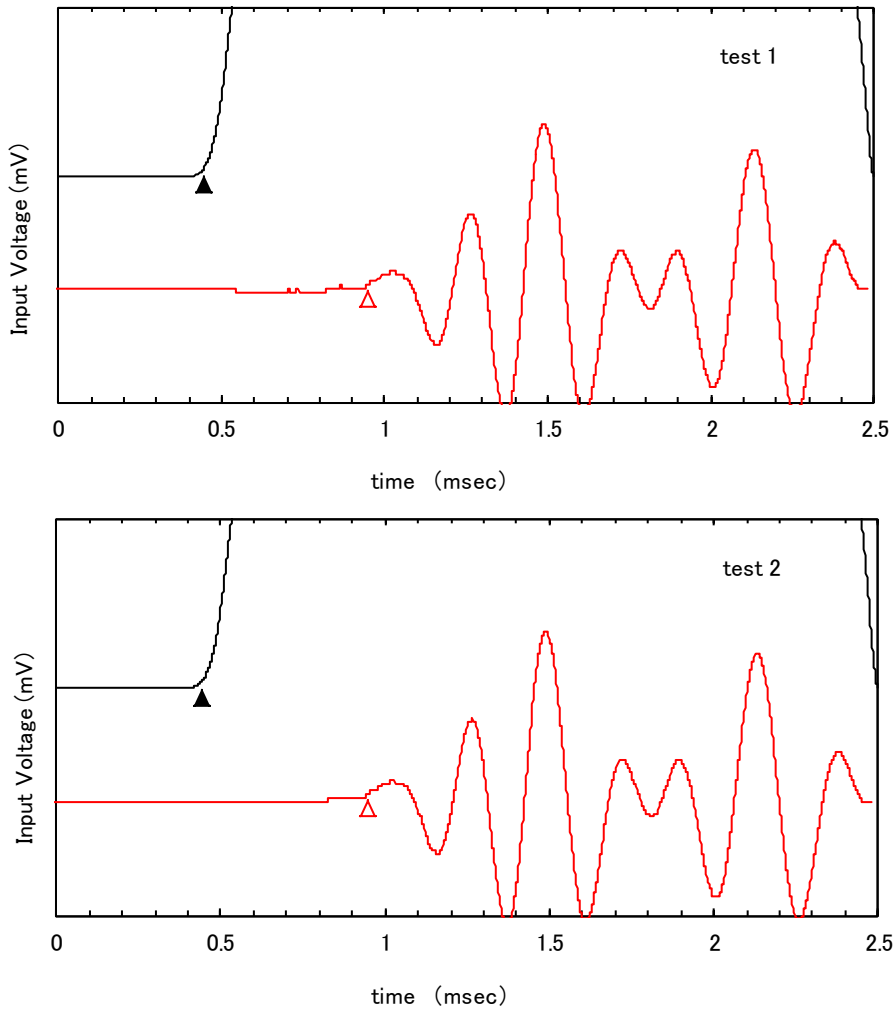

Figure B.25 V_S measurements of the sample No.27 [SN-S-2 (20.1-20.8m)]

Vp	σh kN/m²	t1(▲) msec	t2(△) msec	δt msec	Vp m/sec
test 1	240.0	0.200	0.250	0.05	1999
test 2	240.0	0.200	0.250	0.05	1999
Average					1999

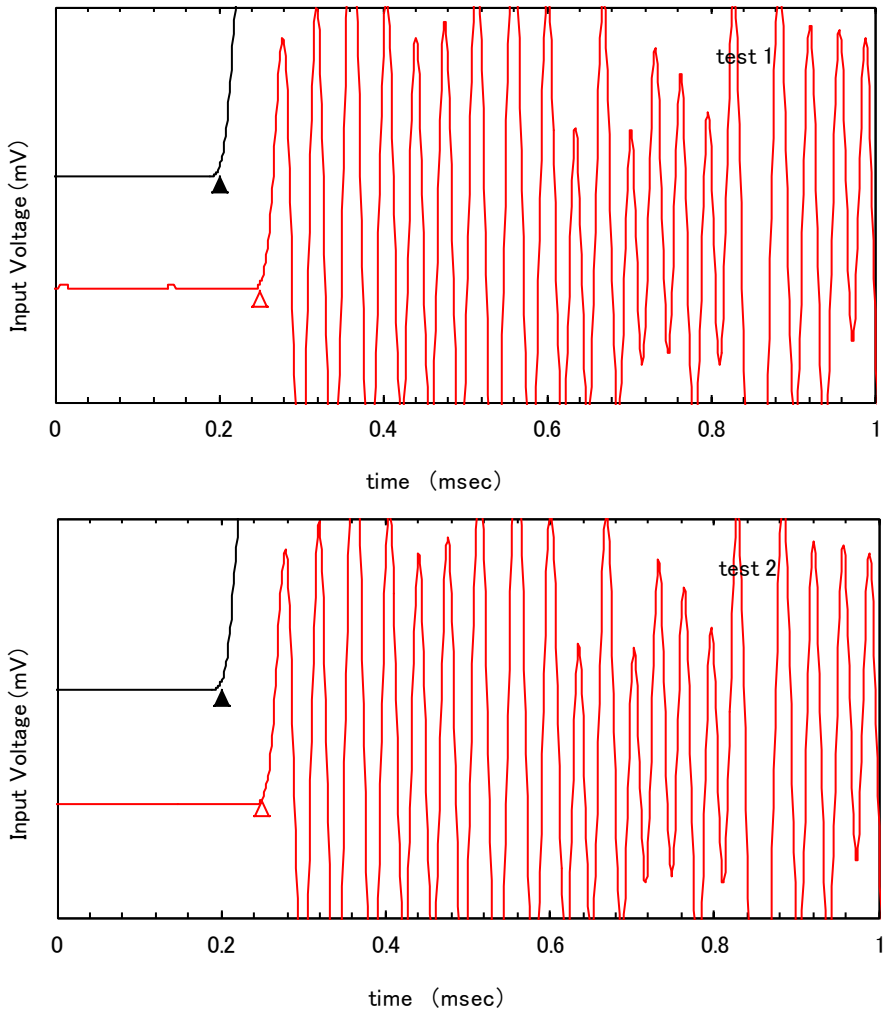

Figure B.26 V_P measurements of the sample No.27 [SN-S-2 (20.1-20.8m)]

Vs	σh kN/m²	t1(▲) msec	t2(△) msec	δt msec	Vs m/sec
test 1	270.0	0.445	0.897	0.452	215
test 2	270.0	0.445	0.890	0.445	218
Average					217

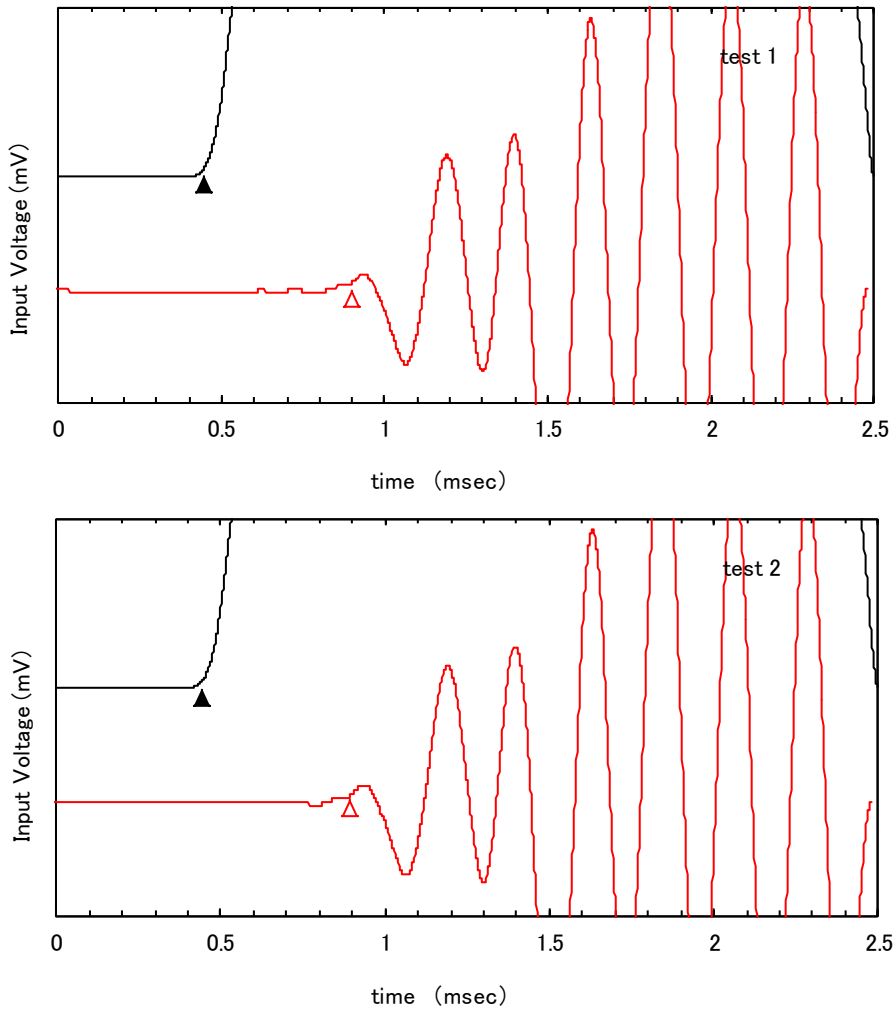

Figure B.27 V_S measurements of the sample No.28 [SN-S-2 (24.0-24.6m)]

Vp	σh kN/m²	t1(▲) msec	t2(△) msec	δt msec	Vp m/sec
test 1	270.0	0.200	0.248	0.048	2024
test 2	270.0	0.200	0.248	0.048	2024
Average					2024

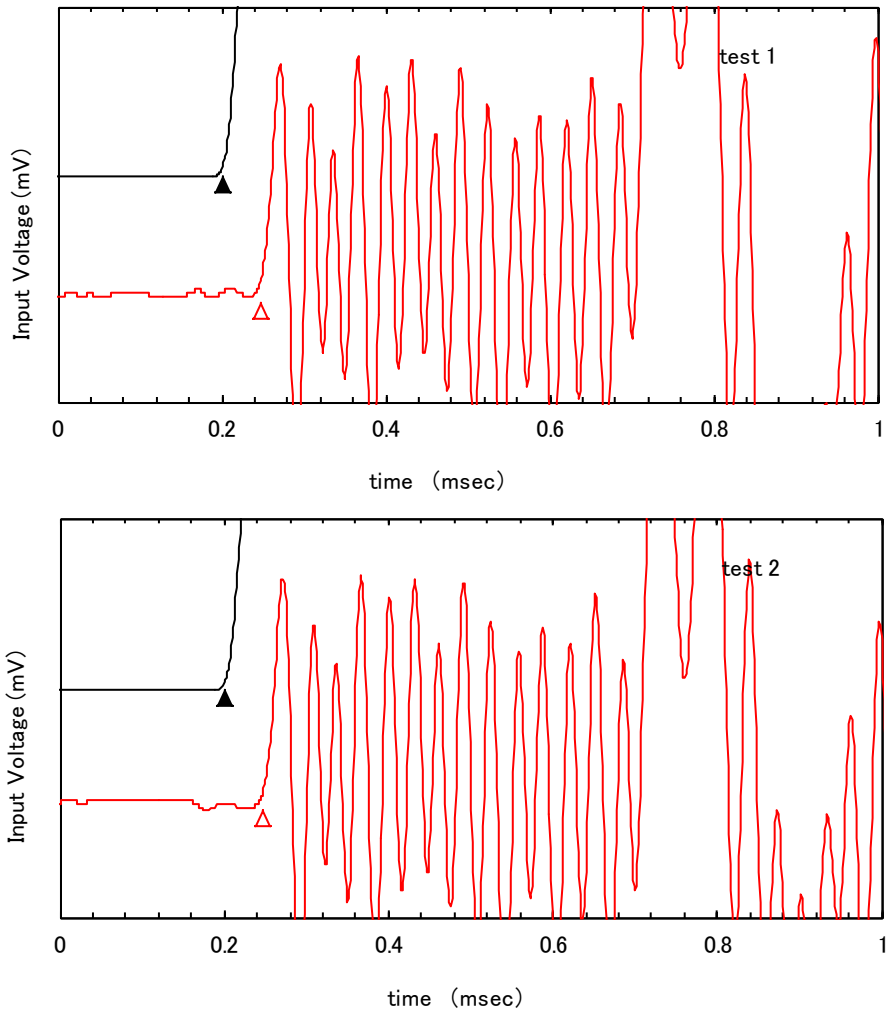

Figure B.28 V_P measurements of the sample No.28 [SN-S-2 (24.0-24.6m)]

Vs	σh kN/m²	t1(▲) msec	t2(△) msec	δt msec	Vs m/sec
test 1	240.0	0.445	0.868	0.423	232
test 2	240.0	0.445	0.868	0.423	232
Average					232

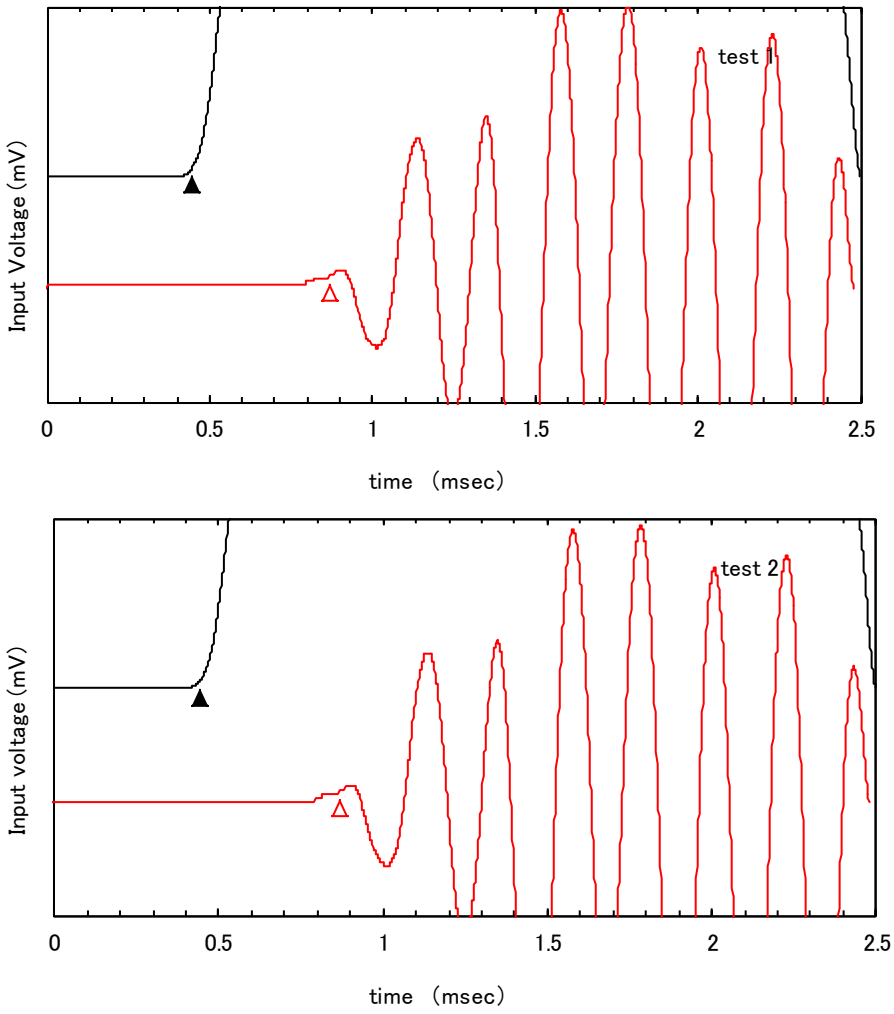

Figure B.29 V_S measurements of the sample No.29 [SN-S-2 (20.1-20.8m)]

Vp	σh kN/m²	t1(▲) msec	t2(△) msec	δt msec	Vp m/sec
test 1	240.0	0.200	0.245	0.045	2180
test 2	240.0	0.200	0.245	0.045	2180
Average					2180

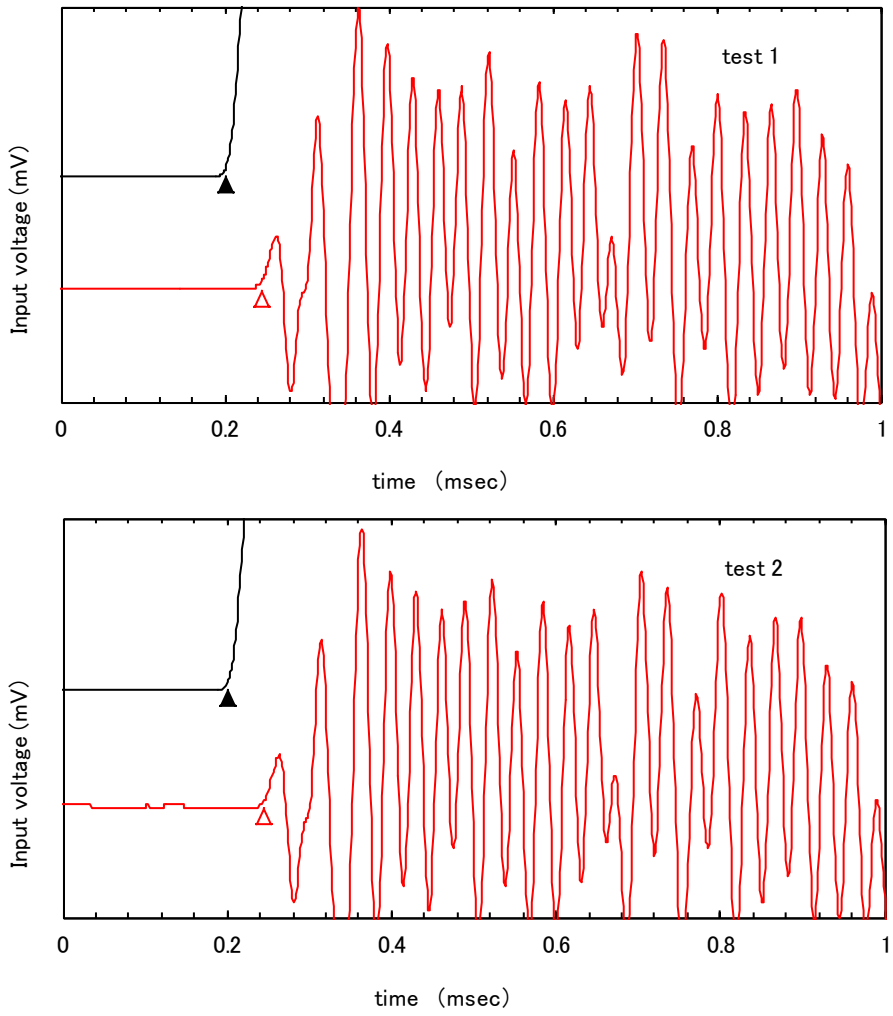

Figure B.30 V_P measurements of the sample No.29 [SN-S-2 (20.1-20.8m)]

Appendix C: Post-liquefaction Volume Change

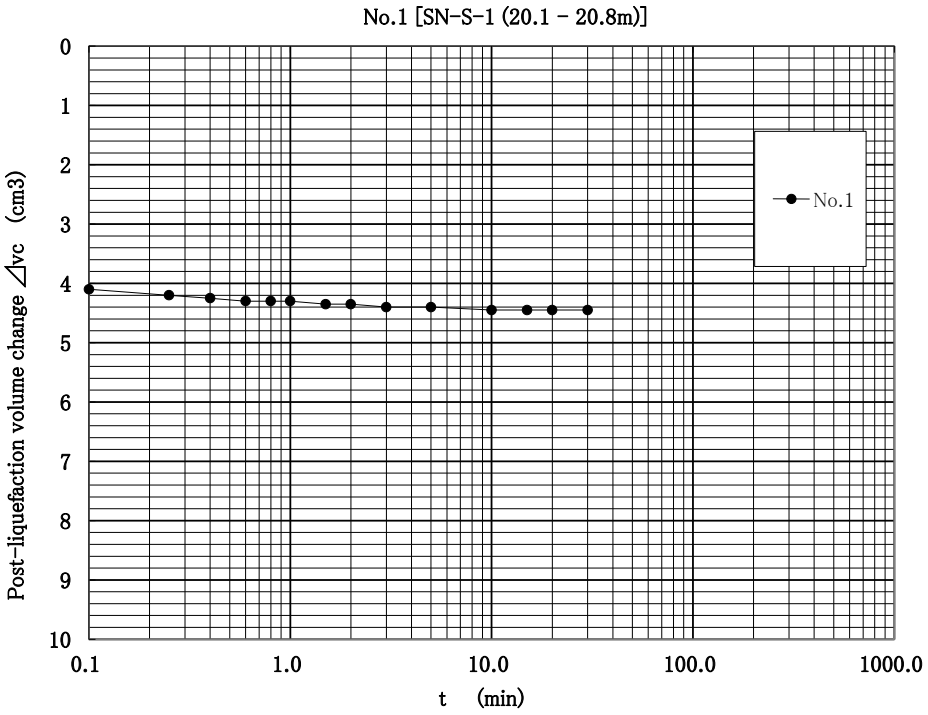

Figure C.1 Post-liquefaction Volume change versus time

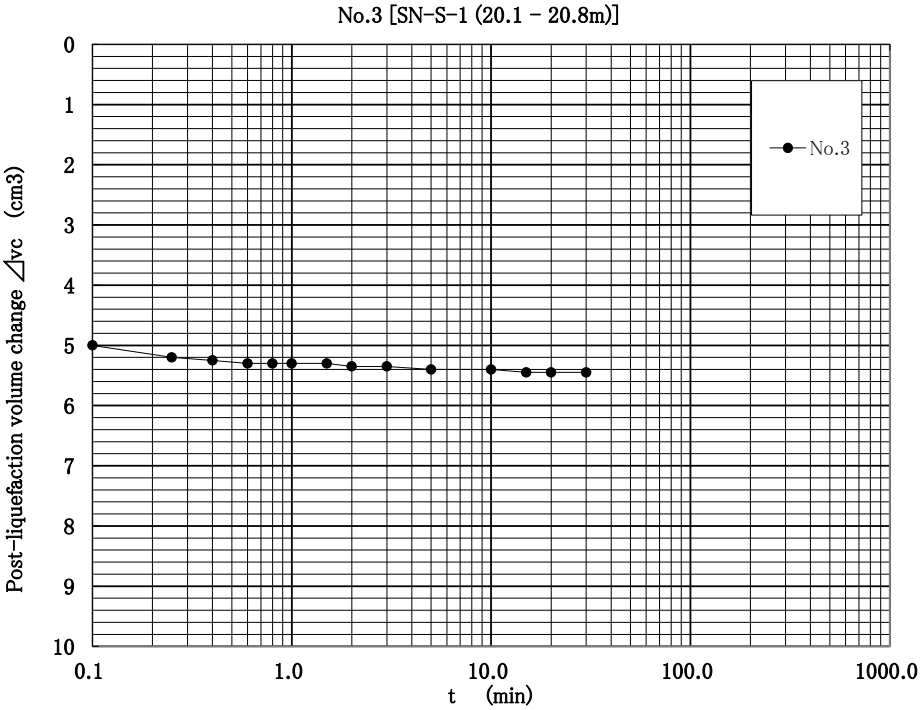

Figure C.2 Post-liquefaction Volume change versus time

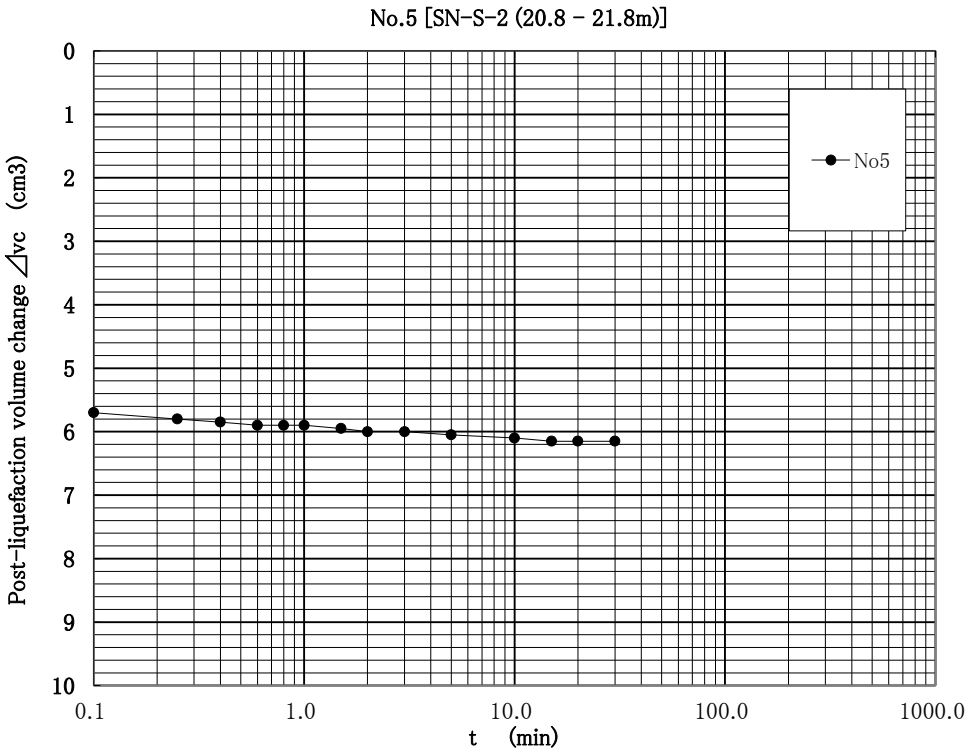

Figure C.3 Post-liquefaction Volume change versus time

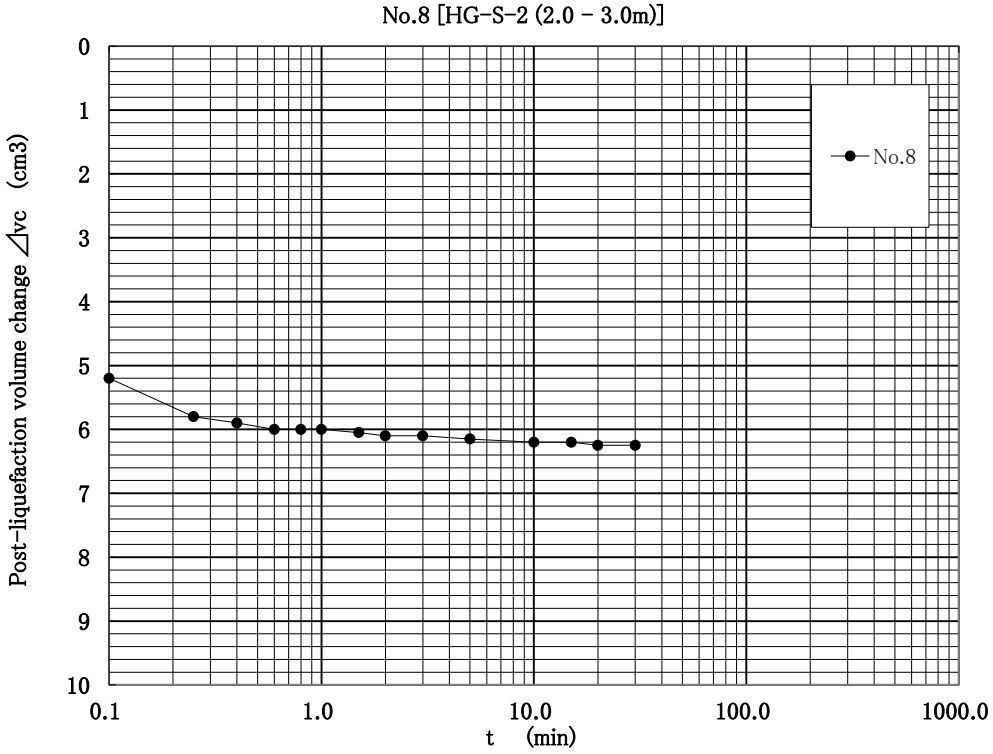

Figure C.4 Post-liquefaction Volume change versus time

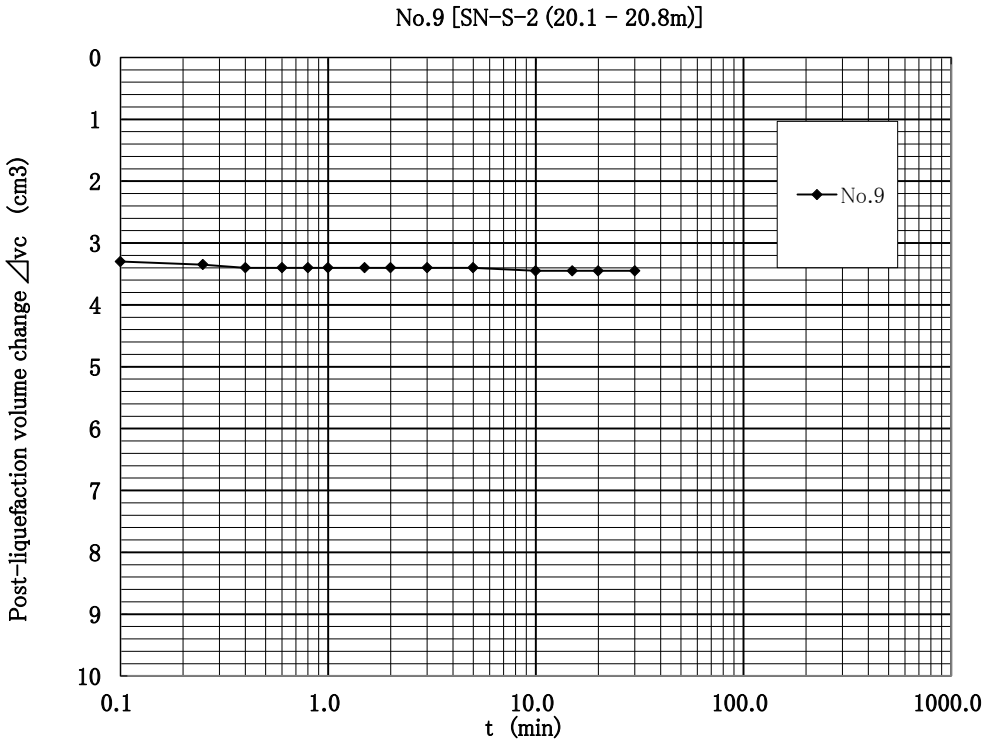

Figure C.5 Post-liquefaction Volume change versus time

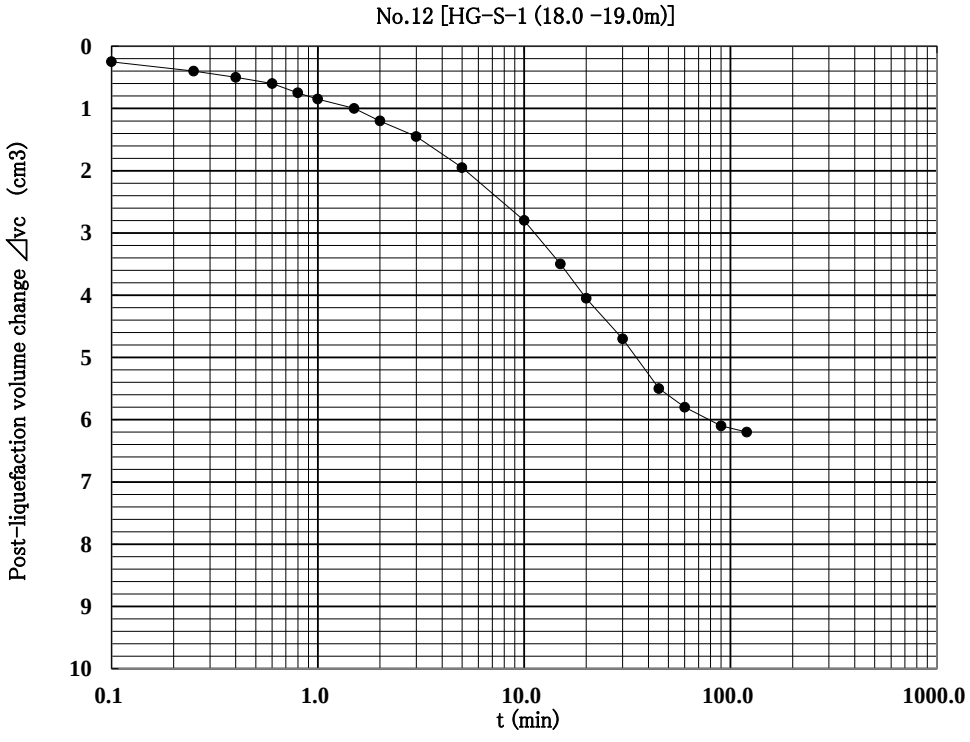

Figure C.6 Post-liquefaction Volume change versus time

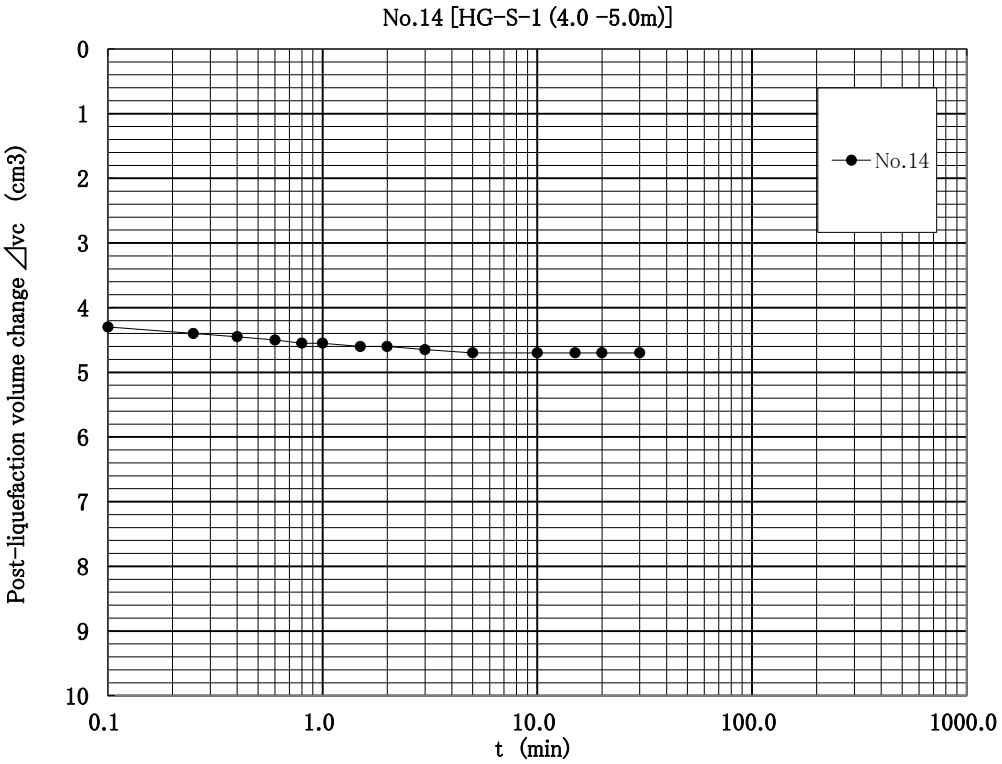

Figure C.7 Post-liquefaction Volume change versus time

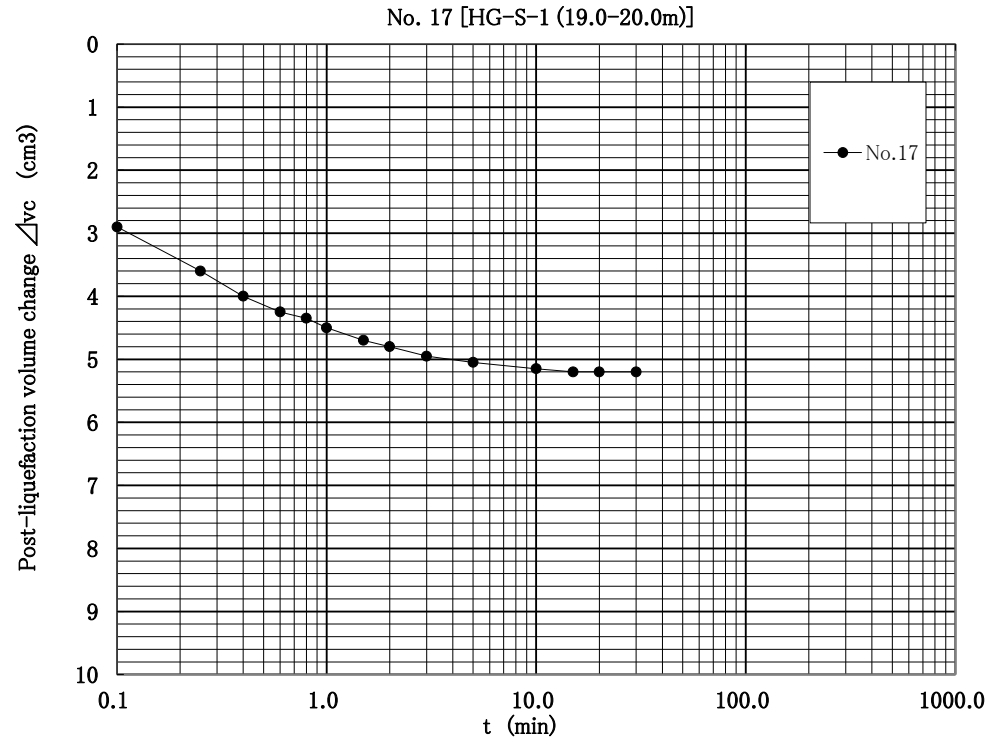

Figure C.8 Post-liquefaction Volume change versus time

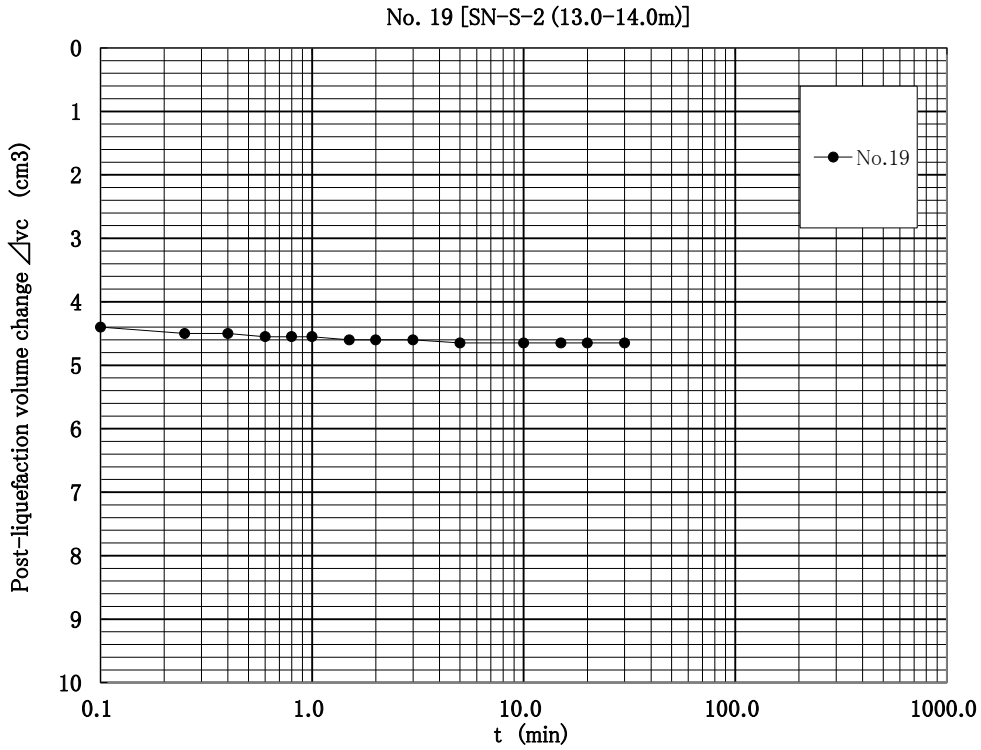

Figure C.9 Post-liquefaction Volume change versus time

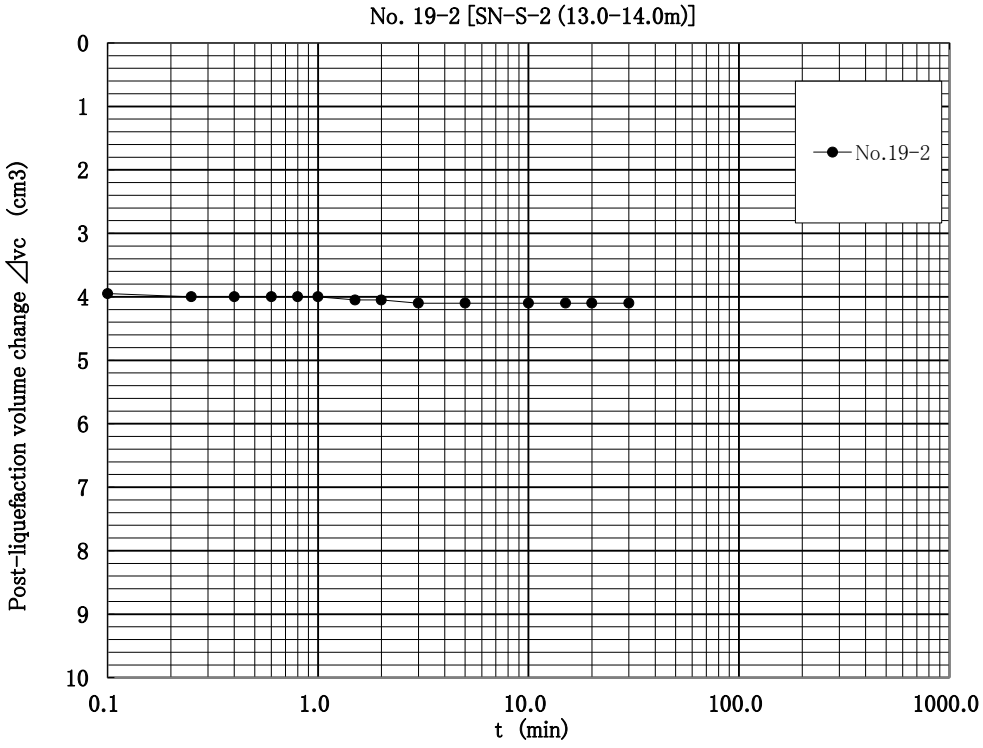

Figure C.10 Post-liquefaction Volume change versus time

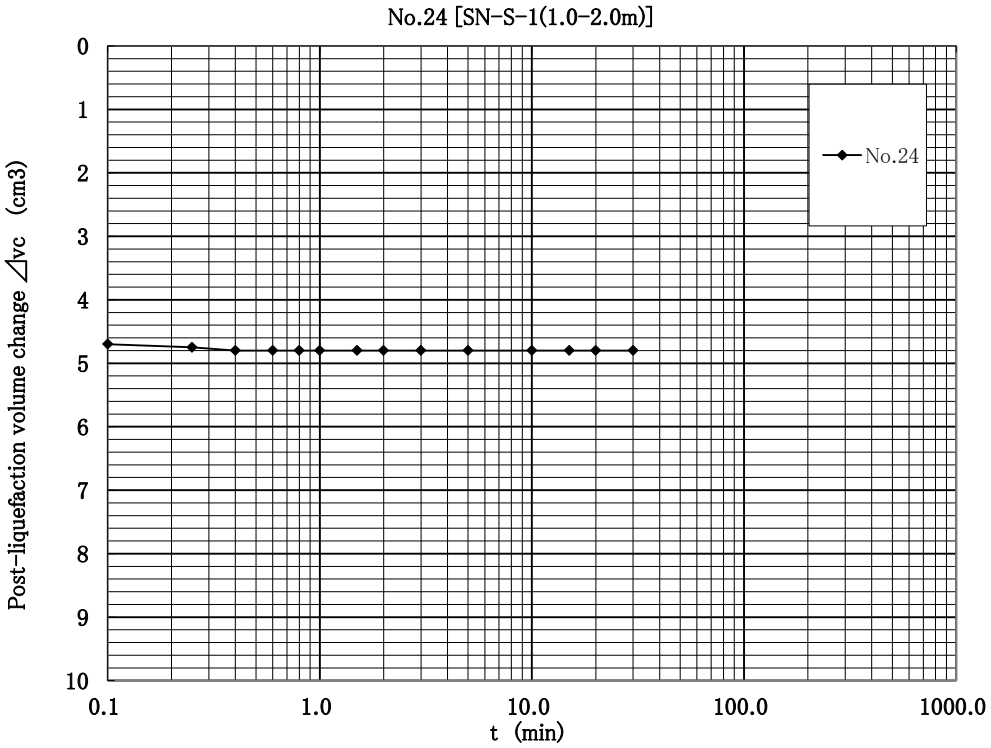

Figure C.11 Post-liquefaction Volume change versus time

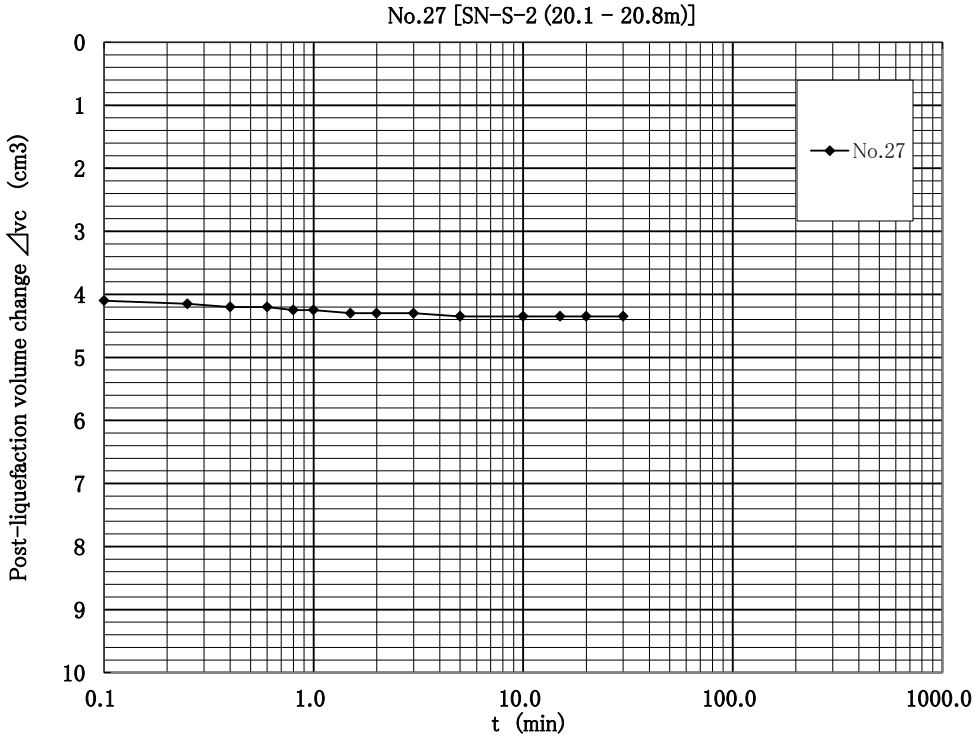

Figure C.12 Post-liquefaction Volume change versus time

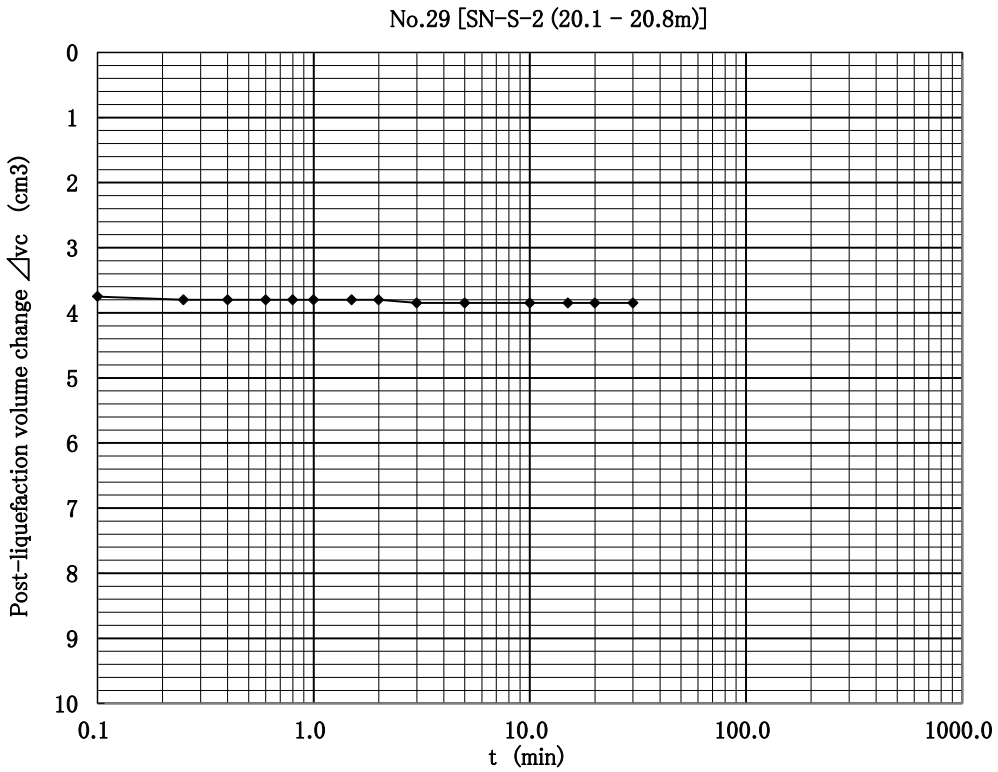

Figure C.13 Post-liquefaction Volume change versus time